# PhD Thesis

## The role of Endo180 in prostate cancer cell migration and metastasis

Julian Hendrik Gronau

Supervisor: Dr Justin Sturge
Co-supervisor: Dr Nick Dibb

Division of Cancer, Department of Surgery & Cancer,
Imperial College London

# Table of Contents

**Table of Contents** ..... 2
**Acknowledgements** ..... 6
**Declaration of Originality** ..... 7
**Copyright Declaration** ..... 7
**Abbreviations** ..... 8
**Abstract** ..... 11
**1 Introduction** ..... 13
**1.1 The prostate and prostate cancer** ..... 13
1.1.1 Function, anatomy and histology of the prostate ..... 13
1.1.2 Prostate cancer overview ..... 16
1.1.3 Prostate cancer disease staging and grading ..... 18
1.1.4 Course of disease and treatment ..... 21
1.1.5 Cell-line models available for prostate cancer research ..... 22
1.1.6 The search for prostate cancer biomarkers ..... 23
**1.2 Cancer Metastasis** ..... 25
**1.3 Epithelial-to-mesenchymal transition - EMT** ..... 27
1.3.1 Overview ..... 27
1.3.2 EMT in development ..... 28
1.3.3 EMT in prostate development ..... 29
1.3.4 Potential role for EMT-like processes in carcinoma progression ..... 31
1.3.5 EMT in prostate cancer progression ..... 32
**1.4 Endo180 and its interaction partners** ..... 34
1.4.1 Synonyms ..... 34
1.4.2 Historical background ..... 34
1.4.3 Endo180 gene locus, alternative splicing and regulation of expression ..... 35
1.4.4 Endo180 partial knockout mice and Endo180 in development ..... 39
1.4.4.1 Engelholm mouse ..... 39
1.4.4.2 Isacke/East mouse ..... 40
1.4.5 Endo180 structure ..... 42
1.4.6 Post-translational modification and phosphorylation of Endo180 ..... 43
1.4.7 Endo180 subcellular localisation and receptor recycling ..... 45
1.4.8 Endo180 ligands ..... 46
1.4.8.1 MMP-13 and MMP-14/MT1-MMP ..... 46
1.4.8.2 uPA and uPAR ..... 46
1.4.8.3 Carbohydrates ..... 48
1.4.8.4 Extracellular matrix - collagen ..... 49
1.4.8.5 Fibronectin ..... 50
1.4.9 Endo180 signalling ..... 51
1.4.9.1 Small GTPases and the regulation of the Actin cytoskeleton ..... 52
1.4.9.2 Endo180 and small GTPase signalling ..... 54
1.4.9.3 Endo180-dependent activation of Cdc42 ..... 54
1.4.9.4 Endo180-dependent activation of Rac ..... 55
1.4.9.5 Endo180-dependent activation of Rho-ROCK-MLC2 ..... 55
1.4.10 Potential role of Endo180 in disease ..... 56

1.4.10.1 Osteoarthritis ..... 56
1.4.10.2 Fibrosis ..... 56
1.4.10.3 Crooked tail syndrome ..... 57
1.4.10.4 Wound healing ..... 57
1.4.10.5 Cancer ..... 57
1.4.11 Summary ..... 59
**1.5 Project aims and overview ..... 60**
1.5.1 Major aim ..... 60
1.5.2 Specific objectives ..... 60
1.5.3 Experimental approaches proposed at the outset of this project ..... 60
**2 Materials and Methods ..... 61**
**2.1 Materials ..... 61**
2.1.1 SDS-PAGE - 1-D ..... 61
2.1.2 SDS-PAGE - 1-D - Phos-Tag ..... 62
2.1.3 Gel electrophoresis -2-D ..... 63
2.1.4 Western Blot ..... 65
2.1.5 Immunprecipitation ..... 65
2.1.6 Immunocytometry ..... 65
2.1.7 Immunofluorescence ..... 66
2.1.8 Tissue staining ..... 66
2.1.9 Invasion sssay ..... 66
2.1.10 Dunn chamber ..... 66
2.1.11 Growth factors ..... 67
2.1.12 Molecular Cloning ..... 67
**2.2 Methods ..... 68**
2.2.1 Cell culture ..... 68
2.2.2 Preparation of cell lysates for SDS-PAGE ..... 68
2.2.2.1 RIPA buffer ..... 68
2.2.2.2 Direct lysis in SDS-PAGE loading buffer ..... 69
2.2.3 Preparation of cell lysates - 2D SDS-PAGE – urea based ..... 70
2.2.4 Immunoprecipitation ..... 70
2.2.4.1 Protein-G coupled magnetic beads ..... 70
2.2.4.2 Cross-linking of Protein-G coupled magnetic beads with $BS^3$ ..... 71
2.2.4.3 Epoxy activated magnetic beads ..... 71
2.2.5 2-D Gel Electrophoresis ..... 71
2.2.6 SDS-PAGE -1-D ..... 72
2.2.7 Phos-Tag ..... 73
2.2.7.1 Standard assay - 100 µM Phos-Tag ..... 73
2.2.7.2 Agarose-acrylamide-hybrid gels - 20 µM Phos-Tag ..... 75
2.2.7.3 Low current assay - 3.5 µM Phos-Tag ..... 77
2.2.8 Western Blot ..... 77
2.2.9 Immunofluorescent staining and analysis using ImageXpress$^{MICRO}$ ..... 81
2.2.10 Immunofluorescence and confocal microscopy ..... 82
2.2.11 Cell motility ..... 84
2.2.12 Dunn chamber chemotaxis ..... 84
2.2.13 Organotypic invasion assay ..... 85
2.2.13.1 Preparation of organotypic gels - day 1 ..... 85
2.2.13.2 Addition of cancer cells - day 2 ..... 87
2.2.13.3 Preparation of nylon sheets - day 2 ..... 87

2.2.13.4 Raising gels to grids - day 3-5 ... 88
2.2.13.5 Harvesting gels - day 3-5 + 14 (17-19) ... 88
2.2.14 Paraffin embedded tissue staining ... 89
2.2.14.1 De-paraffinisation ... 89
2.2.14.2 Antigen retrieval ... 89
2.2.14.2.1 Antigen retrieval - proteinase K ... 89
2.2.14.2.2 Antigen retrieval - citrate buffer ... 91
2.2.14.3 DAB staining ... 91
2.2.14.4 DAB staining controls ... 92
2.2.14.5 Eosin Y and haematoxylin staining ... 93
2.2.15 Molecular Cloning ... 94

**3. Structural analysis of Endo180 ... 95**
**3.1 Introduction ... 95**
**3.2 Evolutionary conservation of Endo180 ... 96**
**3.3 Evolutionary conservation of the cytoplasmic tail of Endo180 ... 96**
**3.4 Evolutionary conservation of ectodomains in the mannose receptor family ... 99**
3.4.1 Ricin B – cysteine rich domain - CRD ... 101
3.4.2 Fibronectin type II domain - FNII ... 101
3.4.3 C-type lectin-like domains - CTLDs ... 101
**3.5 interaction of Endo180 with uPA ... 102**
**3.6 Mutation of KxxSSxR motif in human Endo180 ... 110**
**3.7 Discussion ... 113**

**4. Functional studies of Endo180 ... 117**
**4.1 Introduction ... 117**
**4.2 2-D gel electrophoresis ... 118**
**4.3 Immunoprecipitation - Protein-G magnetic beads ... 121**
**4.4 Covalent binding of antibody to Protein-G magnetic beads ... 124**
**4.5 Covalent coupling of antibodies to Epoxy activated magnetic beads ... 126**
**4.6 Phosphorylation shift assay - Phos-Tag system ... 129**
**4.7 Usage of Epoxy-beads to identify proteins interacting with Endo180 ... 134**
**4.8 Sub-cellular localisation of Endo180 in DU145 cells ... 140**
**4.9 Sub-cellular localisation in DU145 cells overexpressing Endo180-hmKO2 fluorescent fusion protein ... 146**
**4.10 Sub-cellular localisation in DU145 cells overexpressing Endo180 ... 158**
**4.11 Preliminary results: Overexpression of Endo180 in PC3 cells (PC3 Endo180) ... 169**
4.11.1 Myosin light chain phosphorylation in PC3 Endo180 cells ... 169
4.11.2 Chemotaxis of PC3 Endo180 cells towards uPA gradients ... 169
**4.12 Discussion ... 174**

**5. The role of Endo180 in prostate cancer progression ... 176**
**5.1 Validation of antibodies on an FDA approved multi-tissue array ... 177**
5.1.1 Antigen retrieval by proteinase K - 39:10 mAb staining ... 177
5.1.2 Antigen retrieval by boiling in citrate buffer - 39:10/A5:158 mAb staining ... 177
5.1.2.1 Endo180 expression and localisation - 39:10 ... 192
5.1.2.2 Endo180 expression and localisation - A5:158 ... 192
5.1.3 Discussion ... 195
5.1.3.1 Comparison to other studies ... 195
5.1.3.2 Discussion - multi tissue array ... 198

**5.2 Endo180 expression in prostate cancer ..... 202**
5.2.1 The PR208 TMA ..... 208
5.2.1.1 Endo180 - 39:10 mAb - staining ..... 208
5.2.1.2 Collagen I and collagen IV staining ..... 208
5.2.2 Newcastle arrays - Endo180 staining ..... 209
5.2.3 Discussion ..... 219
**5.3 A cell line model for prostate cancer progression ..... 222**
5.3.1 Introduction ..... 222
5.3.2 Androgen-receptor expression during prostate cancer EMT ..... 223
5.3.3 Changes in cell morphology during prostate cancer EMT ..... 224
5.3.4 Expression profile of epithelial- and mesenchymal-associated cytoskeletal markers during prostate cancer EMT ..... 229
5.3.5 Endo180 expression during prostate cancer EMT ..... 230
5.3.6 uPAR and uPA expression during prostate cancer EMT ..... 233
5.3.7 Differential modes of migration & invasion during prostate cancer EMT ..... 234
5.3.8 Discussion ..... 244
**6 Final Discussion ..... 246**
**6.1 Structural analysis of Endo180 *in silico* ..... 246**
**6.2 Functional studies of Endo180 ..... 248**
**6.3 Endo180 as biomarker and prostate cancer model ..... 251**
**6.4 Final remarks ..... 253**
**7 Bibliography ..... 254**
**8 Appendix ..... 271**
**8.1 Evolutionary conservation of Endo180 ecto-domains (non-modified figure) . 271**

## Acknowledgements

This work would not have been possible without the support and advice of my supervisor Dr Justin Sturge, who always offered me a great deal of support. Additionally, Dr Justin Sturge gave me the opportunity to listen to the experts in the field on numerous conferences and presentations. I want to thank the entire Sturge and Pshezhetskiy lab for a great 4 years! Especially, Dr Matthew Caley, Dr Mercedes Rodriguez-Teja, Dr Ana Violeta Fonseca, Dr Giolanta Kogianni Dr Dmitry Pshezhetskiy, Lysann Sauer and Joao Nunes Farinha. I am grateful for all the advice and help from Prof Jonathan Waxman who always reminded me not to forget the bigger picture when I got lost in tiny little details.

I would like to thank Aleksandra Filipovic, Luke Gaughan and Steven Darby for a great collaboration. Many thanks go to Dr Francesco Mauri and Dr Jayson Wang from the histopathology department. I would like to acknowledge Dr John Marshall and his co-workers for teaching me how to perform the organotypic invasion assays! The proteomics assays would not have been possible without the support of Dr Paul Hitchen. Many thanks go to Prof Graham Dunn for the Mathematica notebook.

It was great to supervise all my students: Dennis Zhang, Fionola Fogarty, Fiona Kogera and Silvia Ottaviani. Some of Dennis's and Fiona's work is shown in this thesis (2D electrophoresis, chemotaxis and cloning).

Very special thanks go to my parents and my sister for all the support over the years.

I thank the Prostate Cancer Charity for funding my project.

## Declaration of Originality

All work in this thesis has been carried out by the author with the following exceptions:

- 2D Gel electrophoresis (BSc student Dennis Zhang under day-to-day direct supervision by the author)
- Dunn Chamber chemotaxis assays (MSc student Fiona Kogera under day-to-day direct supervision by the author)
- Side directed mutagenesis of pcDNA3 Endo180 expression vector (MSc student Fiona Kogera under day-to-day direct supervision by the author)
- Tissue micro array – scoring of Endo180/Collagen expression level (Dr Francesco Mauri, Hammersmith Hospital)
- Tissue micro array – Staining of the Newcastle array (Prof Craig Robson, Dr Luke Gaughan, Dr Steven Darby – University of Newcastle)
- Paraffin embedding of organotypic invasion assays (Paul Nya, Histophathology, Hammersmith Hospital)
- Mass spectroscopy (Dr Paul Hitchen, Division of Molecular Biosciences, Imperial College, South Kensington)
- FACS sorting (MRC Flow Cytometry Centre, Hammersmith Hospital Campus)

## Copyright Declaration

The copyright of this thesis rests with the author and is made available under a Creative Commons Attribution Non-Commercial No Derivatives licence. Researchers are free to copy, distribute or transmit the thesis on the condition that they attribute it, that they do not use it for commercial purposes and that they do not alter, transform or build upon it. For any reuse or redistribution, researchers must make clear to others the licence terms of this work

## Abbreviations

| | |
|---|---|
| AR | androgen receptor |
| bFGF | basic fibroblastic growth factor |
| BPH | benign prostatic hyperplasia |
| BSA | bovine serum albumin |
| Ck | cytokeratin |
| Conc. | concentrated |
| CR | cysteine-rich domain |
| CRD | cysteine-rich domain |
| CSF-1 | colony stimulating factor 1 |
| Cdc42 | cell division cycle 42 |
| CTLD | C-type lectin-like domain |
| Cy5 | cyanine-5 |
| DAPI | 4',6-diamidino-2-phenylindole |
| DMEM | Dulbecco's modified essential medium |
| EAT | epithelial to amoeboid transition |
| ECL | enhanced chemiluminescence |
| ECM | extracellular matrix |
| ECPA2 | early prostate cancer antigen-2 |
| EMA | ethidium monoazide bromide |
| EMT | epithelial to mesenchymal transition |
| Endo180 | endocytic receptor 180 (see uPARAP) |
| ERK | extracellular signal-regulated kinase |
| ERM | Ezrin, Radixin and Moesin |

| | |
|---|---|
| FCS | fetal calf serum |
| FNII | fibronectin type II |
| FRET | fluorescence resonance energy transfer |
| FSC | forward scatter |
| GAP | GTPase activating protein |
| GDI | Guanine nucleotide dissociation inhibitor |
| GEF | Guanine nucleotide exchange factor |
| H&E | hematoxylin and eosin |
| HGF | hepatocyte growth factor |
| hOB | human osteoblasts |
| IFB | immunofluorescent buffer |
| IFF | immunofluorescent staining buffer |
| IGF-II | insulin-like growth factor 2 |
| K-SFM | keratinocyte serum-free medium |
| LIMK1 | LIM Domain Kinase 1 |
| MAT | mesenchymal to amoeboid transition |
| MET | mesenchymal to epithelial transition |
| MLC | myosin light chain |
| MLC2 | myosin light chain-2 |
| MT1-MMP | membrane-type 1 matrix metalloproteinase |
| MYPT1 | myosin phosphatase target subunit 1 |
| $NaN_3$ | sodium azide |
| PAK | p21 activated kinase |
| PBS | phosphate buffered saline |

| | |
|---|---|
| PDGF | platelet-derived growth factor |
| PDGF-BB | platelet-derived growth factor-BB isoform |
| PE | phycoerythrin |
| PerCP | peridinin-chlorophyll-protein Complex |
| PFA | paraformaldehyde |
| PI | propidium-iodide |
| POR1 | Porin 1 |
| PSA | prostate specific antigen |
| PVDF | polyvinylidene fluoride |
| qPCR | quantitative real time polymerase chain reaction |
| ROCK | rho kinase |
| RPMI | Roswell Park Memorial Institute medium |
| SSC | side scatter |
| TBS-T | tris-buffered saline-Tween-20 |
| TfR | transferrin receptor |
| TG | tris glycine buffer |
| TGF-$\beta_1$ | transforming growth factor-β1 |
| TMA | tissue micro array |
| TMPRSS2 | transmembrane protease, serine 2 |
| uPA | urokinase-type plasminogen activator |
| uPAR | uPA receptor |
| uPARAP | uPAR associated protein |

## Abstract

Expression of the transmembrane type I receptor Endo180 (CD280, *MRC*2, uPARAP) has been associated with fibrosis, breast cancer, glioma and head and neck cancer. In this thesis I have evaluated the role of Endo180 in prostate cancer pathology with a particular focus on its link to increased tumour cell migration and metastasis. The aims of my project were as follows: (a) to ascertain the co-evolution of Endo180, its interaction partners and domain function *in silico*; (b) to design a non-radioactive assay to enable the study of Endo180 phosphorylation *in vitro*; (c) to establish of a multi-cell line model as a clinically relevant experimental tool to investigate the relevance of Endo180 expression with prostate cancer progression; and (d) to conduct the first full clinicopathological evaluation of Endo180 in prostate cancer patients.

The findings presented confirm that the *MRC*2 gene, which encodes Endo180, is conserved throughout all known vertebrate genomes and that functional amino acid residues within the receptor are conserved across a wide range of species. A putative urokinase-plasminogen activator uPA-binding motif located in the C-type lectin domain-4 (CTLD-4) of the receptor was present in all mammals but no other species. Three-dimensional modelling revealed that the motif is accessible for predicted high-affinity binding between the two molecules. To investigate the biological consequence of the interaction between Endo180 and uPA, site directed mutagenesis was used to generate Endo180 lacking uPA-binding capacity.

2-D SDS-PAGE, immunoprecipitation and band-shift assays failed to detect Endo180 phosphorylation in fibroblasts; a finding that may reflect redundancy of this post-translational modification in stromal versus epithelial cells.

A high-throughput screening approach was taken to identify factors that promote epithelial-to-mesenchymal transition (EMT) like responses in prostate cell lines derived from normal prostate epithelium (RWPE-1), benign hyperplasia (RCN170, RCN165), primary prostate cancer (RC92a, RC58T) and secondary metastatic prostate cancer (LNCaP, DU145 and PC3). With the exception of LNCaP cells all lines

expressed low to intermediate levels of Endo180. The Endo180-transcriptional regulatory factor, TGF-$\beta_1$, increased Vimentin expression in RC92a cells. The invasive properties of this panel of cell lines were assessed using a modified organotypic invasion assay in the absence and presence of TGF-$\beta_1$.

Multiple tissue microarray analysis revealed an increase of 26% in the five-year survival rate of patients with negative Endo180 expression ($p = 0.02$) and 46% in patients with negative Endo180 expression and low Gleason grade ($p = 0.015$). This data is the first to confirm a major clinical impact of Endo180 expression in any disease state.

Future work should now be focused on the mechanisms through which Endo180 can promote prostate cancer progression and its application as a biomarker. The mechanistic studies will benefit from the clinically relevant *in vitro* models established as part of this thesis; and will help pinpoint the precise molecular interactions that could be potential therapeutic targets.

# 1 Introduction

## 1.1 The prostate and prostate cancer

### 1.1.1 Function, anatomy and histology of the prostate

The prostate is a fibro-muscular gland, which produces components of the seminal fluids in male mammals (Standring and Gray, 2008). The human prostate can be described as "walnut or doughnut shaped" (Lee et al., 2011; Thibodeau and Patton, 1999; Thomson and Marker, 2006), has dimensions of approximately 2x3x4cm and approximately weighs 8g in young males. It grows with age and usually weighs between 40g and 150g by the age of 50 (Standring and Gray, 2008). The organ surrounds the urethra from the bladder base to the membranous urethra and is palpable through the rectal ampulla (Lee et al., 2011; Standring and Gray, 2008).

The internal urethral sphincter is compound of smooth muscle and surrounds the urethra distal to the prostate (Standring and Gray, 2008). It prevents retrograde ejaculation (Drake et al., 2005). The external urethral sphincter is composed of skeletal muscle and maintains continence. It surrounds the urethra proximal to the prostate (Standring and Gray, 2008). The innervation of the prostate and the external sphincter are essential to erectile function and continence (Standring and Gray, 2008; Walz et al., 2011). However, both functions can be maintained after transurethral resection of the prostate, TURP, by sparing the innervating nerves (Alsaid et al., 2010; Walsh and Donker, 1982; Walz et al., 2011). TURP is a procedure used in the treatment of prostate cancer.

The ejaculatory ducts pass through the prostate and open into the prostatic urethra (Standring and Gray, 2008) (figure 1.1.1). The follicles of the glandular part of the prostate open into canals, which merge into 15-20 ducts opening into the prostatic urethra (Fine et al., 2007; Fine and Reuter, 2012; McNeal, 1981; Standring and Gray, 2008). The follicles are embedded into fibromuscular stroma (Standring and Gray, 2008). The follicular epithelium is described as predominantly columnar and pseudo-stratified or single layered (Standring and Gray, 2008). A pseudo-capsule of

smooth muscle and collagen encloses the glandular tissue of the prostate (Fine and Reuter, 2012; Lee et al., 2011; McNeal, 1981).

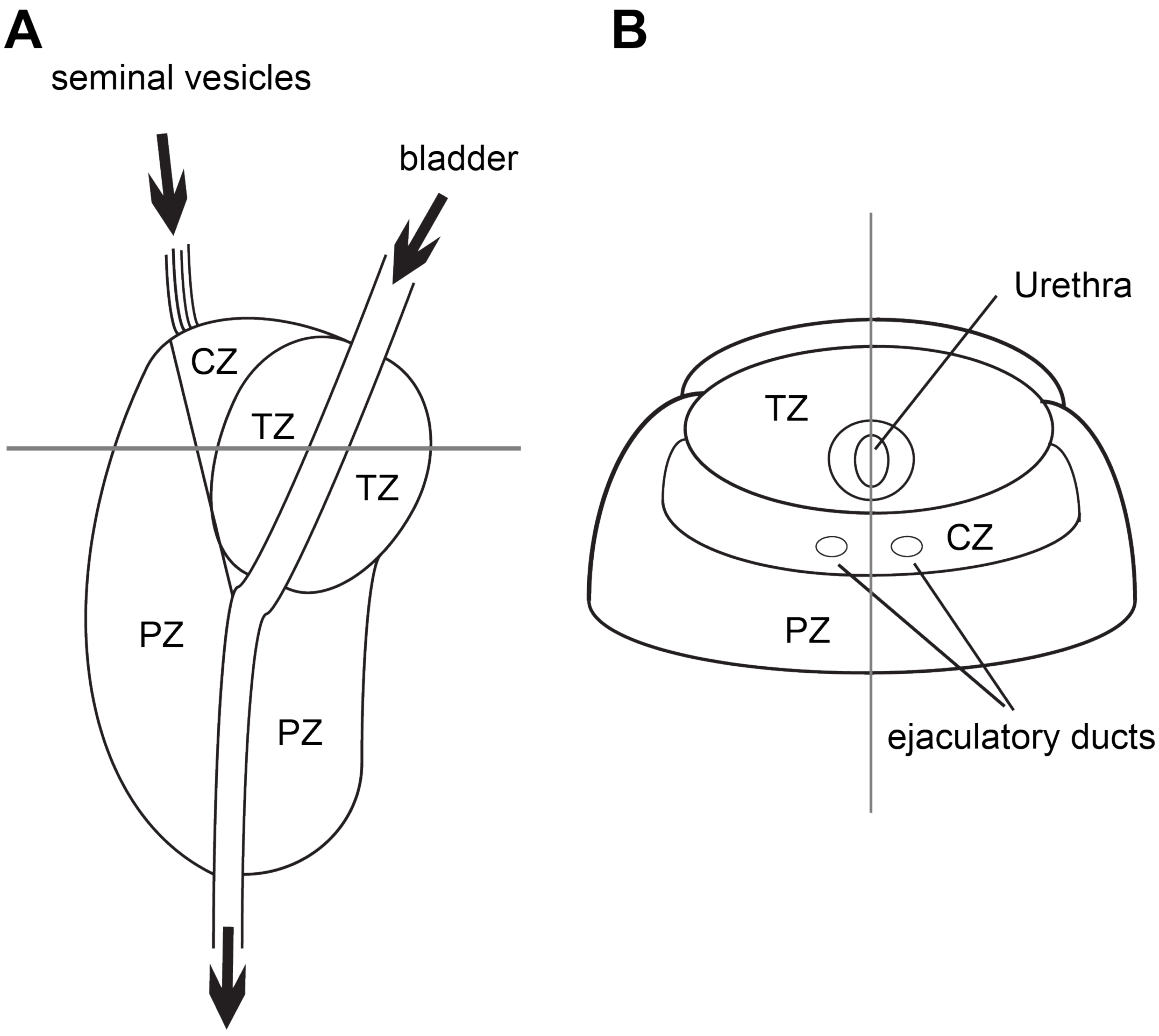



**Figure 1.1.1:** Sagital (A) and transverse (B) schematic of the different zones of the prostate: (CZ) central zone, (TZ) transition zone and (PZ) peripheral zone. Adapted and modified based on (Choi et al., 2007).

In humans approximately 20-30% of the seminal fluids are secreted by the prostate (Martini and Ober, 2006; Thibodeau and Patton, 1999). The secrete of the prostate is emptied into the urethra by smooth muscle contraction during the emission phase but before the expulsion phase (Sherwood, 2013). The prostate contributes several components to the seminal plasma, mainly zinc, citric acid, spermine, seminin, acid

phosphatase, prostatic acid phosphatase and prostatic specific antigen (Frick and Aulitzky, 1991; Kumar and Majumder, 1995). The biological importance of seminal plasma is mainly investigated in the context of sperm storage for the breeding of cattle and to a lesser extent in the context of human fertility (Caballero et al., 2012; Juyena and Stelletta, 2012; Kareskoski and Katila, 2008; Muino-Blanco et al., 2008; Rodriguez-Martinez et al., 2011). In humans, the slightly basic fluid of the prostate is believed to improve sperm viability (Sherwood, 2013; Thibodeau and Patton, 1999). Furthermore, prostatic clotting enzymes produce fibrin from fibrinogen, which leads to clotting of the semen, thus keeping it within the female reproductive tract upon withdrawal of the penis. Subsequently, prostate-specific antigen, PSA, degrades fibrin to release sperm (Sherwood, 2013).

The organ is usually categorised into a central, transition and peripheral zone (**figure 1.1.1**) (McNeal, 1981; Standring and Gray, 2008). The transition zone (approximately 5% of the volume) surrounds the prostatic urethra distal of the openings of the ejaculatory ducts (figure 1.1.1 TZ) (Fine and Reuter, 2012; Standring and Gray, 2008). The central zone (approximately 25-30% of the volume) surrounds the ejaculatory ducts but does not surround the urethra (figure 1.1.1 CZ) (Fine and Reuter, 2012; Standring and Gray, 2008). Both are embedded into the peripheral zone (approximately 65-70% of the volume) (figure 1.1.1 CZ). However, anteriorly, both, the peripheral zone and the transition zone are in contact with non-glandular, pure fibromuscular stroma (Fine and Reuter, 2012; Standring and Gray, 2008).

These three zones differ in their developmental origins and are anatomically and histologically distinguishable. Initial observations by McNeal between region of origin and aggressiveness of prostate cancer have been refined over the years (Fine et al., 2007; Fine and Reuter, 2012; McNeal, 1981). Benign prostate hyperplasia, BPH, commonly arises from the transition zone which usually only represents 5% of the volume of the organ but can grow to become the largest part of the organ (Standring and Gray, 2008). Most carcinomas arise from the peripheral zone while the central zone is rarely associated with malignancy (Standring and Gray, 2008). Interestingly, the central zone is believed to arise from the Wolffian ducts during

development while in contrast, both, the transition and peripheral zone are believed to originate from the urogenital sinus (Standring and Gray, 2008).

Histologically, the prostate epithelium appears to consist of two distinct cell layers, a basal layer that is in direct contact with the basal lamina and luminal cells that produce the secrete of the prostate. The luminal cell layer is in contact with the basal cell layer on one side and the cavity of the ducts on the other side. Furthermore, single neuroendocrine cells are present throughout the epithelium (Long et al., 2005).

Experiments in mice and rats have demonstrated that androgen deprivation leads to apoptosis and loss of the luminal cell layer. Restoration of androgen levels leads to a regeneration of the luminal cell layer (Sinha and Bentley, 1984; Verhagen et al., 1988). Therefore, the stem cell population of the self-renewing epithelium is believed to be located within the basal cell layer (Robinson et al., 1998; Sinha and Bentley, 1984; Verhagen et al., 1988).

Basal and luminal cells express different patterns of keratins, which can be exploited for differentiation in immunohistochemistry. In addition to basal and luminal cells, at least two intermediate cell types have been identified based on their keratin expression patterns *in vivo* (Hudson et al., 2001; Long et al., 2005; van Leenders et al., 2000; van Leenders and Schalken, 2003; Verhagen et al., 1988; Walker et al., 2008).

### 1.1.2 Prostate cancer overview

Prostate cancer is a common disease of men older than 50 years of age. In most cases prostate cancer is asymptomatic during the early stages of the disease and is usually detected as part of a preventative medicine programme following the measurement of serum-prostate specific antigen (PSA) levels and rectal examination. The symptoms of prostate cancer usually become apparent once the disease has metastasised to other parts of the body, at which stage a cure is very unlikely. Prostate cancer primarily metastasises to the bone (especially to the pelvis

and spinal column), rectum, bladder and lymph nodes. For these reasons alternative biomarkers to help indicate progression of the disease and new therapies to delay onset of metastasis are needed (Miller et al., 2003; van der Cruijsen-Koeter et al., 2005).

Basal cell carcinoma of the prostate is an extremely rare diagnosis (Begnami et al., 2007; Komura et al., 2010; Montironi et al., 2005). It was originally believed that prostate cancer originates from luminal cells. However, there is an increasing amount of evidence supporting the theory that luminal-like prostate cancer originates from progenitor or intermediate cells that are not yet fully differentiated into luminal cells (Hudson, 2004; Long et al., 2005; van Leenders and Schalken, 2003; Walker et al., 2008). This theory is based on the high susceptibility of fully differentiated luminal cells to apoptosis as well as the expression patterns of keratins and cadherins. The expression patterns of early stage prostate cancer resemble those of intermediate rather than fully differentiated luminal cells (Hudson, 2004; Long et al., 2005; van Leenders and Schalken, 2003; Walker et al., 2008).

### 1.1.3 Prostate cancer disease staging and grading

Clinical staging describes the 'extent' of the local disease and the status of lymph nodes and metastasis (the 'spread'), whereas the histological grading reflects the differentiation of the tissue.

The "tumour, node, metastasis" (TNM) system has been developed in 1944 (Denoix, 1946; Menoret, 2002). It describes the local status/extent of the disease (T), the status of the lymph nodes (N) and presence or absence of metastatic disease (M). Currently, the TNM guidelines are being published and updated by the "Union For International Cancer Control" (UICC). In the latest edition (7$^{th}$), prostate cancer clinical staging is defined as (Sobin et al., 2009):

- T1 Not palpable or visible
    - T1a <5% or less
    - T1b >5%
    - T1c Detected by needle biopsy
- T2 Confined within prostate
    - T2a < half of one lobe
    - T2b > half of one lobe
    - T2c Both lobes
- T3 Through prostate capsule
    - T3a Extracapsular
    - T3b Seminal vesicle(s)
- T4 Fixed or invades adjacent structures
- N lymph node status
    - N0 Not detectable
    - N1 Present in lymph nodes
- M1 metastasis
    - M0 No metastasis detectable
    - M1 Presence of metastatic disease

It has been demonstrated that the 'T-categories' correlate with disease outcome and patient survival (Ohori et al., 1994). Sometimes, prostate cancer was staged in the Whitmore-Jewett system. However, it has been demonstrated that the TNM system has superior prognostic value (Zagars et al., 1994).

The Gleason grading system (named after its inventor) is specific for the prostate and reflects the histological differentiation of the tissue (Gleason, 1966). The system increases the predictability of disease outcome in combination with clinical staging (Gleason and Mellinger, 1974). The inventor updated and reviewed his system (Gleason, 1992). Overall, the system ranks the histological presentation of the tissue on a scale from 1 to 5. Tissues of grade 1 look closest to healthy tissue whereas tissues of grade 5 are most distinct from healthy tissue. The Gleason system lays out the rules by which the pathologist assigns the different categories. The article that summarises the standardisation attempt of the ISUP conference in 2005 describes that there is no unanimity amongst pathologist regarding the definition of the 5 Gleason grades (Epstein et al., 2005; Osunkoya, 2012). The conference suggested the following definition with at least 75% of the attendants agreeing:

- Pattern 1:
    - Circumscribed nodule of closely packed but separate, uniform, rounded to oval, medium-sized acini (larger glands than pattern 3)
- Pattern 2:
    - Like pattern 1, fairly circumscribed, yet at the edge of the tumor nodule there may be minimal infiltration
    - Glands are more loosely arranged and not quite as uniform as Gleason pattern 1
- Pattern 3:
    - Discrete glandular units
    - Typically smaller glands than seen in Gleason pattern 1 or 2 Infiltrates in and amongst nonneoplastic prostate acini
    - Marked variation in size and shape
    - Smoothly circumscribed small cribriform nodules of tumor
- Pattern 4:
    - Fused microacinar glands
    - Ill-defined glands with poorly formed glandular lumina
    - Large cribriform glands
    - Cribriform glands with an irregular border
    - Hypernephromatoid
- Pattern 5:
    - Essentially no glandular differentiation, composed of solid sheets, cords, orvsingle cells
    - Comedocarcinoma with central necrosis surrounded by papillary, cribriform, or solid masses

The conference proceedings were accompanied by an illustration of the histological patterns (**figure 1.1.3**). This illustration is an adaption of the original drawings by the inventor of the Gleason system (Epstein et al., 2005).

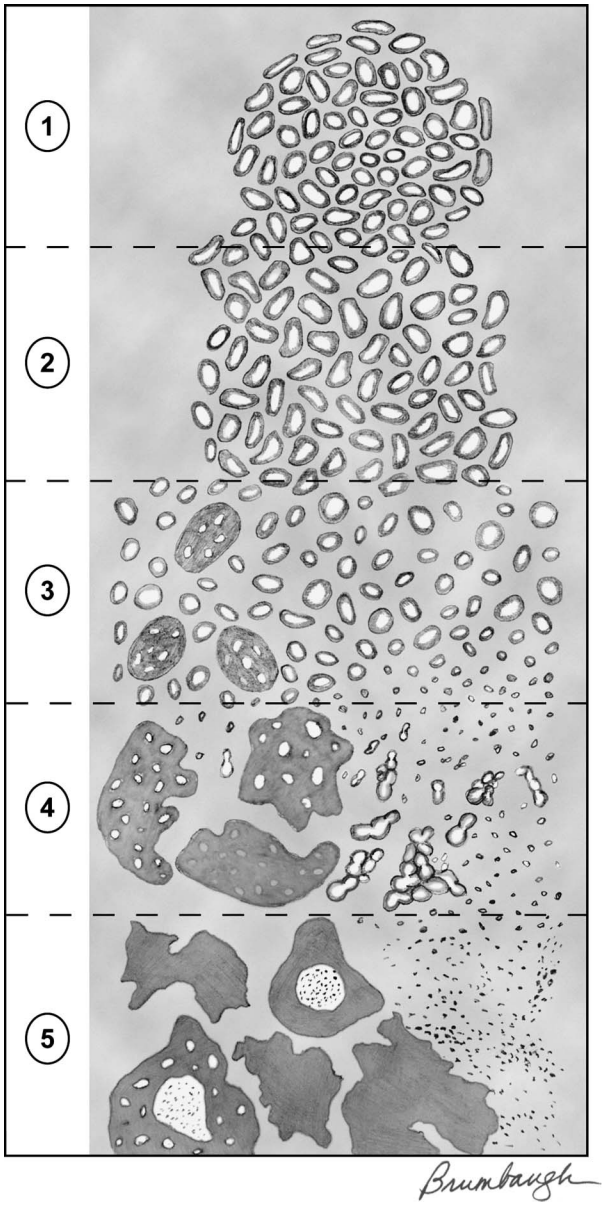



**Figure 1.1.3:** Gleason system, as presented in the ISUP proceedings in 2005 (Epstein et al., 2005).

In addition to defining the five different patterns, the Gleason system gives guidance to the pathologist on how to categorise tumours that display more than one pattern.

The pathologist has to report grades in the format Y+Z where Y is the dominant pattern and Z is the minor pattern. A Gleason grade of 4+5 would indicate a histological sample that is dominated by pattern 4 with some pattern 5 present. The proceedings of the ISUP in 2005 provide guidelines for the pathologist on how to report an overall Gleason grade in cases where very small proportions of a minor pattern are present. Additionally, the grading of samples with more than two patterns is defined. Furthermore, there are instructions on the applicability of the Gleason system onto tissues that deviate from the 5 patterns such as small cell carcinomas (Epstein et al., 2005; Osunkoya, 2012).

### 1.1.4 Course of disease and treatment

Patients diagnosed with prostate cancer that has not yet broken out of the capsule surrounding the prostate gland (T1-2 N0/X M0/X) will either be treated with radiotherapy or undergo surgery to remove the cancerous lobe. In the case of a very early stage of the disease (T1–2a, Gleason <6, PSA <10 mg/l) active monitoring until treatment is common practice and justifiable since this approach is associated with a 99% disease-specific 8 year survival rate (Horwich and Parker, 2007).

If the disease breaks out of the capsule (T3–4 N0/X M0/X) long-term hormone therapy becomes a standard treatment. However, once the disease has metastasised a cure is impossible. At this stage the disease can be managed by hormone therapy, which normally remains effective until insensitivity to this treatment develops. Hormone independent disease is currently treated with taxane-based chemotherapy or radiotherapy (Horwich and Parker, 2007).

The unique responsiveness of prostate cancer to hormone therapy has been studied extensively since its discovery in 1941 (Taplin, 2007) and this has led to the development of successful strategies for the treatment of the hormone-responsive stage of the disease (Singer et al., 2008). The new focus and major challenge facing prostate cancer research is to improve the treatment and management of advanced hormone-independent prostate cancer.

### 1.1.5 Cell-line models available for prostate cancer research

The LNCaP cell line was isolated from a lymph node metastasis of a patient with advanced prostate carcinoma (Horoszewicz et al., 1980). Three years later the cell line was characterised for its androgen dependent growth. In these studies, the depletion of steroids from fetal bovine serum (FBS) by charcoal filtration added to culture medium reduced the proliferation of LNCaP cells and addition of dihydrotestosterone (DHT) to steroid-depleted culture medium restored their normal capacity for growth (Horoszewicz et al., 1983). The failure of earlier as well as later attempts to isolate androgen sensitive cell lines from malignant prostate tissue established the LNCaP cell line as the leading cell line model for prostate cancer research (Fizazi and Navone, 2005).

A PubMed search: prostate AND "name of cell line"; carried out on 27$^{th}$ of September 2011 revealed 4944 studies using LNCaP cells and 1818 and 1815 respective studies of the PC3 and DU145 androgen-independent cell lines, which were generated at a similar time (Kaighn et al., 1979; Mickey et al., 1980). More than half of all studies using the LNCaP cell line in the same time period appear to have either a specific or general focus on the role of androgen in prostate cancer (PubMed search: "prostate" AND "LNCaP AND androgen = 2442 studies).

PC3 cells were isolated from a metastatic bone lesion in the lumbar vertebra of a prostate cancer patient; and DU145 cells were isolated from a rare visceral metastatic lesion located in the parieto-occipital fissure of the cerebrum of another prostate cancer patient who had the added complication of lymphocytic leukaemia (Kaighn et al., 1979; Mickey et al., 1980). In contrast to LNCaP cells, PC3 and DU145 cell lines can be employed to model advanced androgen-insensitive prostate cancer. To date no other cell line, representing the early, non-invasive state of the disease, has been widely used for prostate cancer research.

In 1997 Bello et al. immortalised cells derived from healthy prostates using HPV18 virus and established the RWPE-1 cell line (Bello et al., 1997). A PubMed search on 27$^{th}$ September 2011 revealed that this cell line has been used in a total of 127

studies, mainly in the capacity as a negative control representing normal prostate epithelium. The same group went on to create cell lines from patients with benign hyperplasia (BPH) and early/intermediate prostate cancer using hTert, which is considered to be a superior immortalisation technique compared to HPV18. These cell lines have been characterised by the group for their androgen responsiveness and growth profiles and a collaborative studies have been reported (Gu et al., 2006; Li et al., 2007; Li et al., 2008; Miki et al., 2007). Further characterisation of these cell lines for their pro-migratory and invasive properties has been included in this thesis (see **Section 5**).

### 1.1.6 The search for prostate cancer biomarkers

Although prostate cancer remains a major cause of death in the developed world most men diagnosed with the disease will present with a low-risk status (Gleason score 4-6). This has been achieved, at least in part, by the widespread use of serum PSA as a screening biomarker. Unfortunately, the PSA-test detects a high rate of false-positives and false-negatives (Polascik et al., 1999; Thompson et al., 2004). For this reason several improvements to the PSA-test and the search for new prostate cancer biomarkers has become a rapidly developing area of research. The major healthcare aims are to reduce the amount of unnecessary biopsies, to detect cancer associated with low serum PSA and to improve diagnosis and prognosis based on the analysis of needle core biopsies, serum or urine (Makarov et al., 2009).

Several antigens have been under investigation with the potential to become prostate cancer biomarkers. DD3PCA3/UPM-3 is a pseudo gene with an mRNA level that is positively correlated with and specific for prostate cancer. mRNA levels can be measured via real-time quantitative reverse transcription-PCR (Bussemakers et al., 1999; de Kok et al., 2002; Makarov et al., 2009). The marker is now under consideration for its suitability as a diagnostic and/or prognostic urine test (Deras et al., 2008; Groskopf et al., 2006; Hessels et al., 2003; Makarov et al., 2009; Sokoll et al., 2008; van Gils et al., 2007). Early prostate cancer antigen-2 (ECPA-2), which can be detected in serum, discriminates between the different stages of prostate cancer

with a significantly higher sensitivity than PSA (Leman et al., 2007). Another promising approach is to monitor for chromosomal gene rearrangements (Barry et al., 2007; Demichelis et al., 2007; Demichelis and Rubin, 2007), with the rearrangement of the TMPRSS2 gene locus having significant promise in this area (Soller et al., 2006; Tomlins et al., 2005). Work recently carried out in the laboratory of Dr Justin Sturge at Imperial College London has identified a strong positive correlation between the expression of tumour-cell associated Endo180 and Gleason sum score, which suggests it has the potential to be used as a diagnostic measure of prostate cancer disease status (Kogianni et al., 2009). This thesis reports on the first investigation of Endo180 expression as a biomarker in prostate tissue for the prediction of patient survival (see **Section 5**).

## 1.2 Cancer Metastasis

Approximately 10% of tumour related deaths are attributed to the primary tumour. The remaining 90% are caused by the development of secondary tumours at adjacent or more distant tissue sites. Metastasis involves tumour cell dissemination from the primary tumour and intravasation into lymphatic or blood vessels followed by subsequent extravasation of circulating tumour cells (CTCs) at a distant tissue site where they form micrometastasis (Weinberg, 2007). The selection of a new host tissue is not random. The most common metastastic site in prostate cancer is bone. Bone metastasis will occur in 40% of all men diagnosed with prostate cancer.

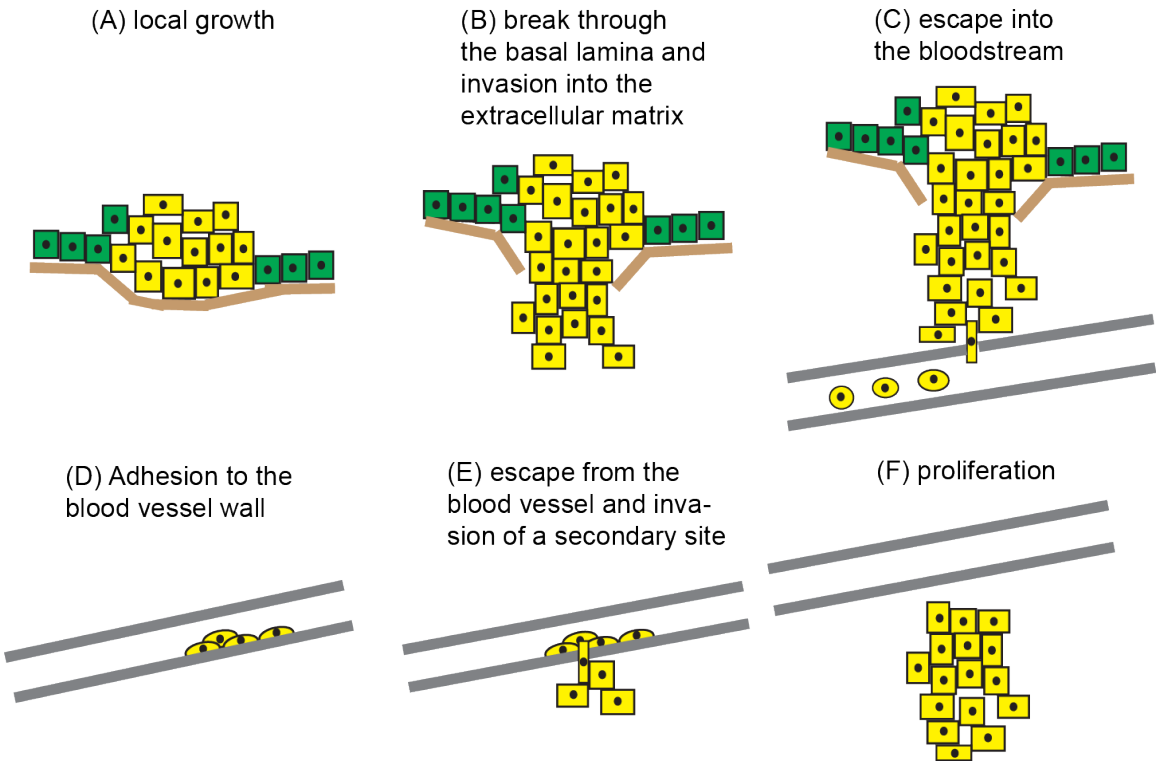



**Figure 1.2. Cancer metastasis (Epithelial): (A)** Cancer cells (yellow) grow amongst a healthy epithelium (green). **(B)** Cancer cells (yellow) break through the basal lamina (brown) and gain access to the extracellular matrix. **(C)** Cancer cells (yellow) traverse the blood vessel walls (grey) and enter into the bloodstream. **(D)** Cancer cells (yellow) adhere to the inner walls of a blood vessel (grey). **(E)** Cancer cells (yellow) traverse the blood vessel walls (grey) and enter into the extracellular matrix of a secondary site. **(F)** Cancer cells (yellow) proliferate into a metastasis. A similar diagram can be found in (Alberts, 2002).

CTCs essentially lose their support from contact with other cells, the ECM and essential growth factors. In addition, they become exposed to sheer force in the circulation. These factors can induce CTC death by anoikis, apoptosis induced by a loss of cell-matrix interaction (Weinberg, 2007). Two general mechanisms have been proposed for CTC extravasation: (a) integrin or lectin dependent arrest, adhesion, rolling and transition between endothelial cells lining the blood or lymphatic vessel, via a process similar to the diapedesis of leukocytes during their recruitment to sites of inflammation; or (b) CTC arrest in the narrow microvasculature and formation of a micro-thrombosis that leads to tumour cell proliferation and blood vessel rupture that allows tumour cells to colonise the secondary site (Weinberg, 2007).

Several hypotheses have been used to explain the progression of benign lesions towards invasive cancer. Fashionable theories have evolved by translating concepts established in developmental biology. The "cancer stem cell theory" suggests subpopulations of tumour cells fulfil a role in tumour progression that is similar to that of the stem cells that confer the development and maintenance of tissues and organs. The "EMT theory" suggests that epithelial cells lose their basal-apical polarity, transiently transform into migratory cells with front-rear polarity, follow chemotactic gradients and revert back to an epithelial phenotype by mesechymal-to-epithelial transition (MET) (see **Section 1.3**). These two notions now form part of one overarching theory (Chaffer and Weinberg, 2011; Hanahan and Weinberg, 2011; Thiery et al., 2009).

## 1.3 Epithelial-to-mesenchymal transition - EMT

### 1.3.1 Overview

The epithelium separates mesenchyme-derived connective tissue from body cavities. Single epithelial cell layers are the simplest type of epithelium. Multi-layering of epithelia helps to increase their physical strength and elasticity. Epithelial cells maintain the basal lamina at the interface with connective tissue. Mesenchymal cells (e.g. fibroblasts) localised in the connective tissue can secret a loosely organised reticular lamina adjacent to the epithelial basal lamina. The basal and reticular lamina combine to form the basement membrane. In addition to their different locations epithelial and mesenchymal cells also differ in their cytoskeletal structure and organisation of cell-cell contacts. Epithelial cells have strong basal-apical polarity and form tight junctions with neighbouring cells. Whereas on the other side of the basement membrane the mesenchymal cells display front-back polarity and establish loose gap junctions with proximal cells (Gilbert, 2000).

EMT can be described as a process where epithelial cells lose their basal-apical polarity and gain front-back polarity. The process involves the transition of the cell's expression profile from cell-cell junction proteins and cytokeratin intermediate filaments towards fibronectin and vimentin intermediate filaments. This leads to a functional change, where stationary cells have acquired the capability to migrate and invade the ECM of the connective tissue compartment (Boyer and Thiery, 1993; Hay, 1995; Thiery, 1984; Thiery et al., 2009; Thiery and Sleeman, 2006). EMT is observed in various species, including mammals, during the tissue remodelling events required for developmental processes like the formation of the mesoderm and neural crest (Duband et al., 1995; Kimelman, 2006; Thiery et al., 2009; Thiery and Sleeman, 2006; Viebahn, 1995) (see **Section 1.3.2**).

The potential role of EMT-like events in cancer progression is an intensive field of investigation (Chaffer and Weinberg, 2011; Hanahan and Weinberg, 2011; Huber et al., 2005; Lee et al., 2006; Thiery, 2002; Thiery et al., 2009; Yang and Weinberg, 2008)(see **Section 1.3.4**).

The terminology for the concepts of epithelial-to-mesenchymal transition, EMT, and the reverse process of mesenchymal-to-epithelial transition, MET, appear to originate from the field of cancer research in the early/mid 1990s (Bae et al., 1993). In the 1980s, the process was referred to as epithelial-to-mesenchymal transformation or epithelium-mesenchyme interconversion in developmental biology. For example, Jean Pierre Thiery, a dominant figure in this field, wrote a review early in his career where he referred to the process as epithelium-mesenchyme-interconversion (Thiery, 1984). Since the late 1990s, the "transition" terminology is used in cancer/fibrosis research as well as developmental biology.

### 1.3.2 EMT in development

The signalling networks that control EMT in development are covered in two comprehensive reviews (Thiery et al., 2009; Thiery and Sleeman, 2006). EMT and the reverse process, MET, are essential for several steps in development. This process is conserved in both vertebrates and invertebrates. Organogenesis requires cell populations to undergo multiple cycles of EMT and MET, which has led to the distinction between primary, secondary and tertiary EMT (Thiery et al., 2009). Primary EMT and MET events occur during early embryonic development leading to the formation of transient epithelial structures (e.g. notochord and somites). Secondary EMT occurs in organogenesis where EMT programmes lead to differentiation via MET into specialised cells (e.g. pancreatic Langerhans cells)(Johansson and Grapin-Botton, 2002). Tertiary EMT includes the formation of the endocardial cushion of the heart (Nakajima et al., 2000; Thiery et al., 2009).

The signalling network that controls EMT is well defined for gastrulation in the sea urchin. This involves Wnt8 signalling, which controls E-cadherin expression and endocytosis via the Twist and Snail signalling axis. More complex networks orchestrate neural crest formation in embryonic drosophila where Toll controls Snail and Twist initiating small GTPase signalling, marker expression and cell cycle control in addition to the loss of E-cadherin and disruption of cell-cell junctions. The signalling networks that control EMT during embryogenesis of amniotes, including

vertebrates, are only partially characterised. Several signalling pathways control cell fate and EMT; the main drivers being the TGF-β superfamily, Nodal, VG1, EGF, FGF and Wnt (Thiery et al., 2009; Thiery and Sleeman, 2006).

### 1.3.3 EMT in prostate development

While a large body of literature addresses disease development, comparatively few articles focus on developmental biology. The majority of those involve rodent models. A recent review addresses the significant physiological difference between the rodent and human prostate but postulates that their developmental processes are similar (Meeks and Schaeffer, 2011; Prins and Putz, 2008). The central zone of the prostate is believed to arise from the Wolffian ducts during development while in contrast, both, the transition and peripheral zone are believed to originate from the urogenital sinus (Standring and Gray, 2008). In humans the prostate is fully differentiated at birth, while in rodents it continues to grow for up to 15 days after birth. In humans the prostate grows to approximately 2 grams in a newborn infant and up to 20 grams during puberty (Meeks and Schaeffer, 2011; Prins and Putz, 2008). The prostate weighs approximately 8g in young males (Standring and Gray, 2008). At age 45-55 there is further growth to 30-150 grams (Meeks and Schaeffer, 2011; Prins and Putz, 2008; Standring and Gray, 2008).

**Table 1.3** lists the transcription factors and signalling pathways implicated in EMT and cited work where this has been linked to prostate cancer. However, the role of EMT in prostate development has not been clarified. A recent article (published in Chinese) reports that EMT plays a crucial role during prostate development in humans. The abstract (available in English) states that the expression of E-cadherin in prostate epithelial cells is increased during human gestation, whereas vimentin, N-cadherin and Twist1 are decreased (Zhou et al., 2011). In contrast to kidney or heart development (Thiery et al., 2009) it is unknown which cell populations in the prostate undergo EMT-MET, where they migrate and how this process is controlled.

| Transcription factor/ signalling pathway | Involvement in prostate development |
|---|---|
| DHT/AR | (Prins and Putz, 2008) |
| Hoxa-13 and Hoxd-13 | (Oefelein et al., 1996; Podlasek et al., 1999b; Podlasek et al., 1997; Warot et al., 1997) |
| Hoxb-13 | (Economides and Capecchi, 2003; Edwards et al., 2005; Huang et al., 2007; Sreenath et al., 1999) |
| Hoxa-9, Hoxa-10, Hoxa-11 | (Takahashi et al., 2004) |
| Nkx3.1 | (Bhatia-Gaur et al., 1999; Bieberich et al., 1996; Kim et al., 2002; Prins et al., 2006; Schneider et al., 2000; Sciavolino et al., 1997; Tanaka et al., 2000) |
| Fox A1 (formerly Hnf3), A2 | (Gao et al., 2005; Kopachik et al., 1998; Mirosevich et al., 2005) |
| Notch1 | (Shou et al., 2001; Wang et al., 2006; Wang et al., 2004) |
| Sonic hedgehog (Shh) | (Barnett et al., 2002; Berman et al., 2004; Lamm et al., 2002; Podlasek et al., 1999a; Pu et al., 2004; Zhu et al., 2007) |
| FGF10 | (Donjacour et al., 2003; Kuslak and Marker, 2007) |
| Noggin, BMP4, BMP7 | (Grishina et al., 2005) |
| TGFβ$_1$ TGFβRI, TGFβRII | (Chang et al., 1999; Itoh et al., 1998; Tanji et al., 1994; Timme et al., 1994; Tomlinson et al., 2004)<br>NB. testosterone affects TGFβ$_1$ expression the canine prostate (Shidaifat et al., 2007) and TGFβ family members regulate prostate development in the human foetus (Raghow et al., 1999). |
| Activin β, activin βB | (Cancilla et al., 2001) |
| Wnt2, Wnt2b, Wnt7b, Wnt4, Wnt5a, Wnt11, Fzd2, Fzd4, Dsh1 | (Bierie et al., 2003; Huang et al., 2009; Pu et al., 2007) |
| SFrp1, sFrp2 | (Joesting et al., 2005; Zhang et al., 2006) |

**Table 1.3. Growth factors important in prostate development**. This table is largely based on two reviews (Meeks and Schaeffer, 2011; Prins and Putz, 2008).

### 1.3.4 Potential role for EMT-like processes in carcinoma progression

Loss of E-cadherin is a hallmark in EMT and is strongly correlated with carcinoma progression and poor prognosis (Vincent-Salomon and Thiery, 2003; Yang and Weinberg, 2008). EMT-associated transcription factors can drive this loss of E-cadherin expression; direct mutations in *CDH1* or post-transcriptional control can also play a part (Yang and Weinberg, 2008). The upregulation of EMT-inducing transcription factors is observed in many tumours (Yang and Weinberg, 2008).

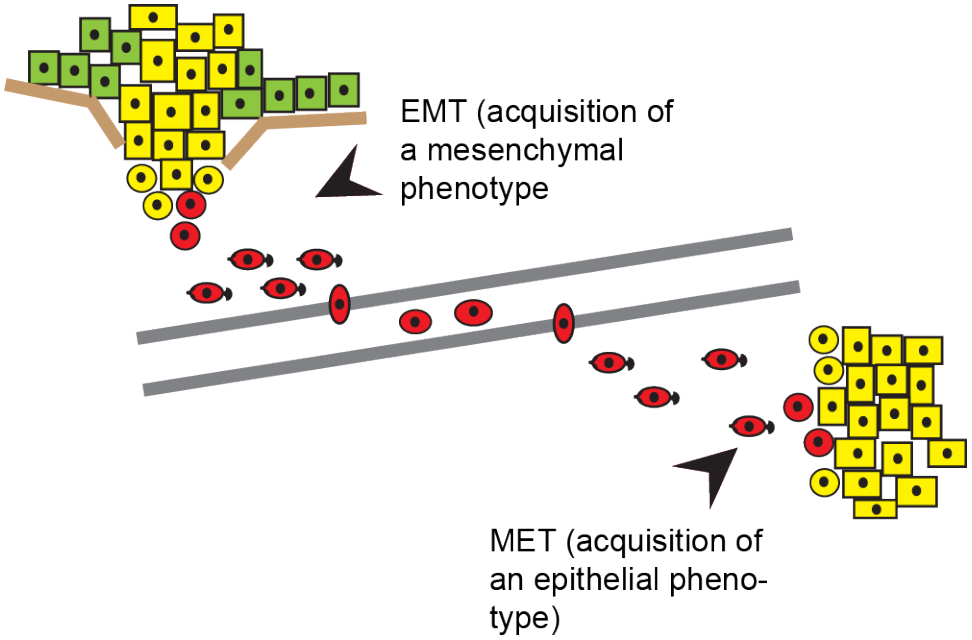



**Figure 1.3.4. EMT and MET in cancer metastasis**. Cancer cells (yellow) undergo epithelial to mesenchymal transition, EMT, and acquire an invasive and migratory phenoptype (red). After passing through the bloodstream and nesting in a secondary site (metastasis), the cancer cells undergo the reverse process, mesenchymal to epithelial transition, MET, and acquire an epithelial phenotype. A similar diagram can be found in (Chaffer and Weinberg, 2011; Kalluri and Weinberg, 2009).

The idea that carcinoma cells might undergo EMT in order to gain the capability to migrate through the ECM and undergo MET at a distant site to form a metastasis is intriguing. Growth factors in the tissue of origin may induce EMT in carcinoma cells, whereas the absence of these growth factors will induce MET once the cell has escaped from the primary site. The first proposition that EMT might be involved in

cancer metastasis is often attributed to Elizabeth Hay (Hay, 1995). The theory is strongly advocated and supported by Jean-Pierre Thiery and Robert Weinkauf (Chaffer and Weinberg, 2011; Hanahan and Weinberg, 2011; Thiery et al., 2009; Thiery and Sleeman, 2006). Reviews written by both authors depict EMT as the best model to explain cancer metastasis. As mentioned in **Section 1.3** the current concept involves cancer stem cell EMT. The theory of EMT in cancer progression is not universally accepted. The process of EMT and subsequent MET during development is a rapid process. In carcinomas there is a gradual shift towards the upregulation of mesenchymal and downregulation of epithelial markers over several months or years (Tarin et al., 2005). The transient nature of "real" (developmental-type) EMT makes it very difficult to study in cancer biology. In development the process can be studied in real-time, for example by using optical sheet microscopy. Observing a cancer cell undergoing EMT, following it through the circulation and observing it to undergo MET in foreign tissue is far more challenging.

### 1.3.5 EMT in prostate cancer progression

Nauseef and Henry recently reviewed the state of investigation into EMT in prostate cancer (Nauseef and Henry, 2011). The authors make the distinction between "real EMT" and "apparent EMT". The first is a fast process induced by growth factors while the latter is a slow transformation over many generations from a clear epithelial phenotype to mixed or pure mesenchymal phenotype. Apparent EMT in prostate cancer tissue was shown in several studies that measured the expression of individual markers for EMT in prostate cancer specimens, namely E-cadherin, vimentin, ZEB1, Twist and N-cadherin. The overall trend is an increase of mesenchymal markers with Gleason grade and metastasis with a decrease of epithelial markers. However, not all studies surveyed in the article support this trend (Nauseef and Henry, 2011).

The study of fast or "real" EMT in prostate cancer was limited to cell line and animal work. One of the major set backs for progress in this area is the limited availability

of appropriate cell lines to study EMT-like processes in prostate cancer. As highlighted at the outset of this introduction (**Section 1.1.5**) the prostate cancer field is dominated by the use of three cell lines that were derived from metastatic lesions (LNCaP, DU145 and PC3). This origin negates their clinical relevance in models that attempt to recapitulate EMT *in vitro*. Interestingly, a recent study has reported that TGF-$\beta_1$can induce EMT-like events in the benign prostate hyperplasia cell line, BPH-1 (Slabakova et al., 2011). In this thesis a panel of cell lines derived from normal, benign, primary tumour and metastatic prostate tissue have been used in experiments characterising their response to EMT-inducing factors, their pro-migratory and invasive properties, their expression of EMT markers as well as the expression of the Endo180-uPA-uPAR and Endo180-Rho-ROCK-MLC2 chemotactic and migratory signalling axes (**Section 5**).

## 1.4 Endo180 and its interaction partners

### 1.4.1 Synonyms

CD280; collagen-binding factor Endo180; C-type mannose receptor 2; endocytic receptor 180; **Endo180 (used throughout the thesis)**; macrophage mannose receptor 2; mannose receptor, C-type 2; *MRC*2; urokinase-type plasminogen activator receptor associated protein (uPARAP).

### 1.4.2 Historical background

Endo180 was originally identified and characterised as a constitutively recycling type I transmembrane receptor (Isacke et al., 1990; Sheikh et al., 2000). Endo180 was next confirmed to be part of the mannose receptor family (Wu et al., 1996), which includes three other members: DEC-205 (CD205), mannose receptor (CD206) and M-type phospholipase A2 receptor. Later Endo180 was identified to be urokinase plasminogen activator receptor associated protein (uPARAP), a name adopted through its ability to form a tri-molecular complex with pro-urokinase plasminogen activator (pro-uPA) and urokinase plasminogen activator receptor (uPAR) (Behrendt et al., 2000).

The majority of research studies on Endo180 reported to date have been carried out by Professor Clare Isacke (Institute of Cancer Research, London) and Dr Neils Behrendt (Copenhagen), who are respective authors on 20 and 11 of the 46 research articles that have been published to date. Research by other groups was limited due to the lack of a commercial antibody. However, Santa Cruz (anti-human) and R&D (anti-human and anti-mouse) now stock anti-Endo180 antibodies, which have been successfully used to generate data reported in a number of recent publications (Bianchetti et al., 2011; Ye et al., 2011).

Endo180 has been the focus of several comprehensive reviews (Behrendt, 2004; East and Isacke, 2002; Engelholm et al., 2009; Llorca, 2008).

### 1.4.3 Endo180 gene locus, alternative splicing and regulation of expression

*MRC2*, which encodes Endo180, is located at chromosomal position 17q24.2, consists of 36 exons and is 67.4 kb long (East and Isacke, 2002). One splice variant has been detected in human foetal liver (Wu et al., 1996).

A homozygous mutation in the ORF of *MRC2* in Belgian Blue cattle results in rapid degradation of Endo180 mRNA and loss of Endo180 protein. Absence of Endo180 in affected animals leads to crooked tail syndrome (Fasquelle et al., 2009). A similar observation was made in some litters of partial Endo180 knockout mice but these results were not reproducible (J. Sturge, personal communication).

MCF7 human breast cancer cells were investigated for the identification of factors that induce the expression of Endo180, with a specific focus on transforming growth factor-beta-1 (TGF-$\beta_1$), hepatocyte growth factor (HGF), insulin-like growth factor-II (IGF-II), basic fibroblastic growth factor (bFGF), which can promote EMT-like responses in cancer (Thiery, 2002). TGF-$\beta_1$ was the only factor to induce Endo180 upregulation in MCF-7-cell monolayers (Wienke et al., 2007). Endo180-overexpression was able to induce EMT-like events in MCF7 cells (cell scattering, elongated morphology, loss of E-cadherin) (J. Sturge, unpublished). Similarly, EGF, PDGF and TGF-$\beta_1$ were tested in for their ability to upregulate Endo180 in U87MG glioma cells. Again TGF-$\beta_1$ was the only factor to upregulate Endo180. Suppression of Smad3 signalling reduced Endo180 expression to below baseline levels indicating that its expression is maintained via a TGF-$\beta_1$-dependent autocrine loop in this human glioma cell line (Huijbers et al., 2010).

Western blot and RT-PCR analysis revealed that Endo180 expression is induced by TGF-$\beta_1$, EGF and PDGF in human gingival fibroblasts and with TGF-$\beta_1$, EGF, HB-EGF or KGF in HaCaT keratinocytes (Honardoust et al., 2006). Interferon-gamma (IFN-$\gamma$) induces co-expression of Endo180 and MT1-MMP in murine macrophages on type I collagen and this response was inhibited by interleukin-10 (IL-10) (Ye et al., 2010). Endo180 expression in hepatic stellate cells (HSC) of human, mouse and rat origin (Mousavi et al., 2009) confers their ability for collagen uptake (Mousavi et al., 2005).

Endo180-dependent collagen uptake is increased in HSC following their differentiation into myofibroblast-like cells, an event that normally follows response-to-injury in the liver and can be activated by the culture of primary HSC's.

Endo180 expression has been quantified in various human and rat tissue types using Western blot and Northern blot analysis (Isacke et al., 1990; Wu et al., 1996). This analysis has been extended to include a wide panel of human tissue types in this thesis (see **Section 4**). The Endo180 status of certain cell lines has been confirmed (**Table 1.4.3**). Endo180 expression in a panel of normal, benign and malignant prostate cell lines has been confirmed in this thesis (see **Section 5**).

| Cell line/type | Classification | Species | Status | First publication |
|---|---|---|---|---|
| F1084 | embryonic, fibroblast | human | + | Isacke et al., (1990) |
| U937 | haematopoietic, monocyte | human | + | Behrendt et al., (2000) |
| AG1523 | mesenchymal, fibroblast | human | + | Sheikh et al., (2000) |
| Flow 2000 | mesenchymal, fibroblast | human | + | |
| HMEC-1 | mesenchymal, fibroblast | human | + | |
| MRC-5 | mesenchymal, fibroblast | human | + | |
| DMEC | vascular, endothelial | human | + | |
| HUVEC | vascular, endothelial | human | + | |
| HepG2 | hepatic, normal | human | - | |
| Hofbauer | mesenchymal, placental | human | + | |
| Primary cells | haematopoietic, macrophage | human | + | |
| RPM-MC | dermis, melanoma | human | + | |
| NIH-3T3 | mesenchymal, fibroblast | mouse | + | Howard, Isacke (2002) |
| MG63 | bone, osteosarcoma | human | + | |
| MCF7 | epithelial, breast carcinioma | human | - | Wienke et al., (2003) |
| Primary cells | dermis, fibroblast | mouse | + | Engelholm et al., (2003) |
| MEF | embryonic, fibroblast | mouse | + | East et al., (2003) |
| MDA-MB-231 | myoepithelial, breast carcinoma | human | + | Sturge et al., (2003) |
| MC615 | cartilage, chondrocyte | mouse | + | Howard et al., (2004) |
| HT1080 | connective, fibrosarcoma | human | + | |
| HEK293 | embryonic, kidney | human | - | Fernandez et al., (2005) |
| Gingival cells | gingival, fibroblast | human | + | Honardoust et al., (2006) |
| HaCat | dermal, keratinocyte | human | + | |

| | | | | |
|---|---|---|---|---|
| BE | epithelial, colorectal carcinoma | human | + | Sturge et al., (2006) |
| Primary cells | Haematopoietic, dentritic | human | + | Butler et al., (2007) |
| BMM<br>BMSC | haematopoietic<br>fibroblast | mouse<br>mouse | -<br>+ | Sturge et al., (2007) |
| HSC<br>LX-2<br>M1-4<br>BSC<br>MFBY2 | hepatic, stellate | rat<br>human<br>mouse<br>rat<br>rat | +<br>+<br>+<br>+<br>+ | Mousavi et al., (2009) |
| U87MG<br>SF188 | brain glial, glioma | human<br>human | -<br>+ | Huijbers et al., (2010) |
| Primary cells | myofibroblast | mouse | + | Shi et al., (2010) |
| KNS42<br>KNS81 | brain glial, glioma | human<br>human | +<br>+ | Takahashi et al., (2011) |
| Primary cells | haematopoietic, macrophage | mouse | + | Ye et al., (2010) |
| Fibrocytes | mesenchymal | human | + | Bianchetti et al., (2011) |
| LNCaP<br>CaCo-2<br>HeLa<br>LLC<br>B16F10<br>HGF-1<br>RDNCTC 2472<br>F1084 | epithelial, prostate carcinoma<br>epithelial, colorectal carcinoma<br>epithelial, cervical carcinoma<br>epithelial, lung carcinoma<br>dermal, melanom AG1523<br>gingival, fibroblast<br>connective tissue, sarcoma<br>embryonic, fibroblast | human<br>human<br>human<br>mouse<br>mouse<br>human<br>mouse<br>human | -<br>-<br>+<br>-<br>+<br>+<br>+<br>+ | Madsen et al., (2011) |

**Table 1.4.3** Endo180 expression. The first recorded reference is cited. HSC: hepatic stellate cell; HUVEC: human umbilical vein endothelial cells; MEF: murine embryonic fibroblasts; DMEC: dermal microvascular endothelial cells; BMM: bone marrow derived macrophages; BMSC; bone marrow derived stromal cells.

### 1.4.4 Endo180 partial knockout mice and Endo180 in development

The role of Endo180 in developmental biological processes has only been analysed in mice to date. Endo180 is expressed during murine bone development in all tissues undergoing ossification. The presence of Endo180 mRNA has also been shown in immature as well as mature osteoblasts (Engelholm et al., 2001b). Endo180 expression is high in young but low in old CBA and STR/ort mice (Howard et al., 2004). Therefore, a role for Endo180 in bone and cartilage development could be confirmed but a role in homeostasis, as well as osteoarthritis, was not apparent (Howard et al., 2004).

Two partial knockout mice (Endo180ΔEx2–6) lacking exons 2-6, the first three N-terminal domains of the Endo180 protein (CRD, FNII and CTLD1) were created independently (East et al., 2003; Engelholm et al., 2003) (see **Figure 1.4.5** and **Section 1.4.5** for details of Endo180 structure). Engelholm et al., and East et al., used similar strategies to target a complete deletion in *MRC2* and both groups generated a genotype with partial receptor expression, a genotype that was possibly due to strong sequence homology within the *MRC2* gene locus. Both partial knockout mice were viable, fertile and appeared phenotypically normal, with the exception of litters that displayed a stunted tail defect (J. Sturge, personal communication).

#### 1.4.4.1 Engelholm mouse

Dermal fibroblasts isolated from the Engelholm partial knockout mouse displayed a complete defect in the internalisation of type I, IV and V collagen; and their adhesion to type I and IV collagens was decreased by 25% and to type V collagen by 50%. The migratory rate of dermal fibroblasts on a type I collagen matrix was decreased by 25% compared to wild-type control cells (Engelholm et al., 2003). Inhibition of lysosomal proteases leads to an accumulation of intracellular collagen types IV and V following Endo180-dependent internalisation. This suggests a pathway in which

these matrix proteins undergo trafficking to the lysosomal compartment (Kjoller et al., 2004).

The role of Endo180 in development of the murine lung has been studied in detail. Endo180 is strongly expressed in the mesenchyme of the developing lung where its expression directly correlated with type IV but not type I collagen IV. Histological differences were not detected between partial Endo180 knockout mice and wild-type controls (Smith et al., 2008). It was suggested that the interaction of Endo180 with collagen type IV has relevance in the pathological setting.

Crossing of the Engelholm mouse with mouse mammary tumour virus (MMTV) mice led to the development of tumour-associated fibrosis and smaller tumour size (Curino et al., 2005). The observed phenotype was attributed to a loss in the collagen degradation function of Endo180 within the tumour-associated stroma (Curino et al., 2005).

Although MT1-MMP knockout and partial Endo180 knockout mice are viable and healthy, their double knockout counterpart displayed impaired bone formation and postnatal death (Wagenaar-Miller et al., 2007). This phenotype indicates that defects in extracellular collagen degradation by MT1-MMP can be compensated by intracellular degradation via the Endo180 route and vice-versa. Although the precise mechanism underlying their skeletal defect has not been determined further clues may become apparent following the investigation of Endo180 function in cartilage and bone-forming cells, which in the double knockout mouse were seen to have survival defects within their native collagen-rich microenvironment (Wagenaar-Miller et al., 2007).

#### 1.4.4.2 Isacke/East mouse

Mouse embryonic fibroblasts (MEFs) derived from the partial knockout mouse generated by the Isacke lab display a decrease (30-50%) in collagen IV and gelatin internalisation. However, binding of Endo180 to N-acetylglucosamine was unaffected due to the retention of an intact functional C-type lectin domain (see

**Section 1.4.5**). Although their overall migratory speed was decreased, MEFs from partial knockout mice were able to chemotax in response to uPA (East et al., 2003).

In a subsequent study the Isacke mouse was crossed with the macrophage mannose receptor (MMR) knockout mouse. Endo180/MMR knockout animals were free of any obvious phenotypic abnormalities. Bone marrow-derived macrophages (BMM) from the MMR knockout mice displayed increased random motility in comparison to wild-type mice. This defect in migratory behaviour was retained in the Endo180/MMR double knockout BMM. In contrast to the decreased motility of MEFs derived from the partial Endo180 knockout mouse (East et al., 2003) their BMM counterparts retained a normal migratory phenotype, which was attributed to a lack of Endo180 expression in this subset of macrophages (Sturge et al., 2007).

### 1.4.5 Endo180 structure

Endo180 has a similar domain structure to other members of the mannose receptor family and can be subdivided into twelve structural elements (East and Isacke, 2002; Wu et al., 1996). The 150 kDa ectodomain of Endo180 is comprised of a cysteine-rich domain (CRD), a fibronectin type II-like domain (FNII) and eight repeated C-type lectin domains (CTLD-1–8) and is glycosylated at several sites (East et al., 2002; Isacke et al., 1990) (**figure 1.4.5**). Following its single transmembrane domain Endo180 has a cytoplasmic tail comprised of 42 amino acid residues that include several predicted phosphorylation sites (Isacke et al., 1990; Sheikh et al., 2000) (**figure 1.4.7**).

The 3-D structural arrangement of the amino terminal domains of Endo180 has been modelled at a resolution of 17 ångströms following its analysis by single-particle electron microscopy. Amino-terminal CRD can bind to CTLD-2 resulting in the formation of a loop structure that spans over the FNII domain and CTLD-1 (Rivera-Calzada et al., 2003). Predictions suggest that conformational changes in this hairpin structure can be induced by ligand binding or environmental changes, such as the low pH of endocytic vesicles (Boskovic et al., 2006; Llorca, 2008).

Several antibodies have been raised against the full-length human Endo180 protein. Mouse anti-human mAb E1/183 binds to the CRD domain, mouse anti-human mAb A5/158 binds to CTLD2, mouse anti-human mAb 39:10 binds to CTLD4. Two rabbit pAb sera have been raised against the cytoplasmic tail, Cat1 and Cat2. E1/183 and A5/158 only interact with Endo180 as long as di-sulphide bonds within the protein structure have not been reduced, the other three antibodies interact with Endo180 regardless (Huijbers et al., 2010; Kogianni et al., 2009; Palmieri et al., 2013; Sturge et al., 2003; Wienke et al., 2007).

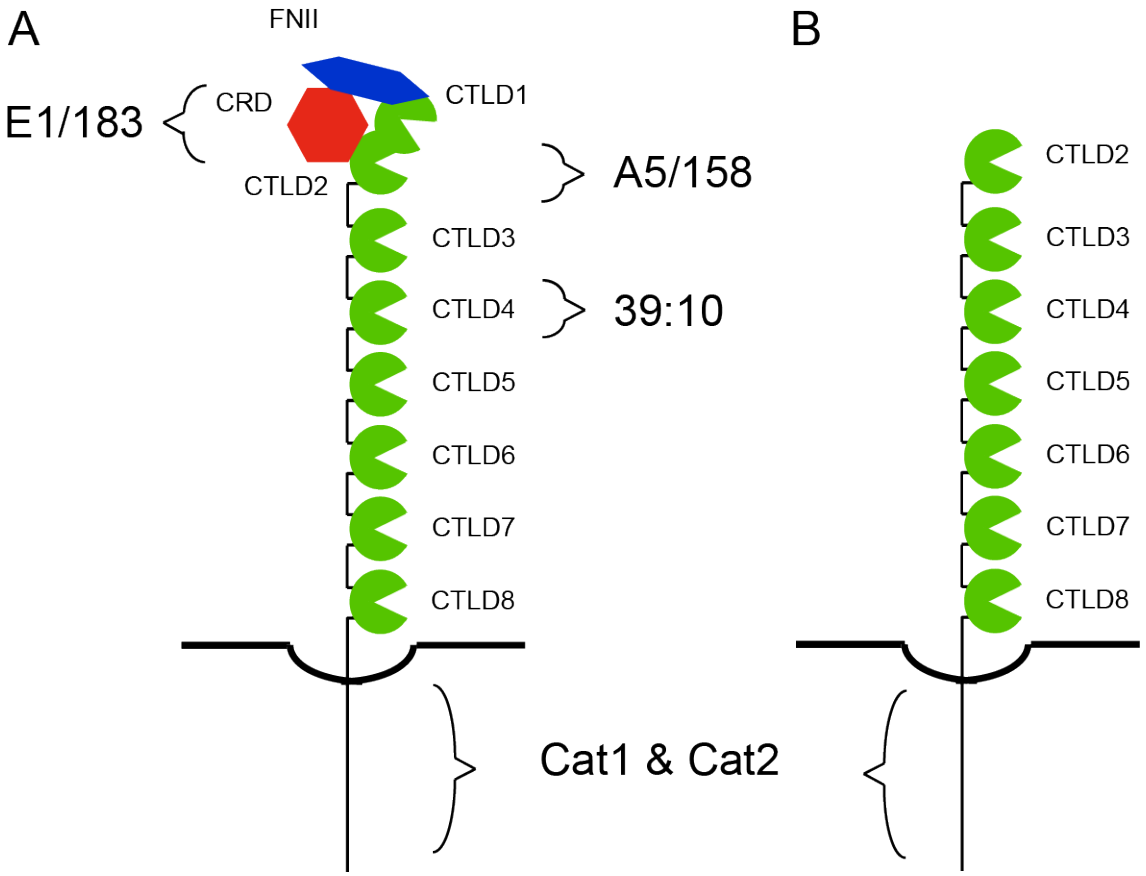



**Figure 1.4.5. Endo180: structure, interaction partners and antibodies. (A)** The Endo180 protein is formed by several domains: An N-terminal cysteine-rich domain (CRD), a Fibronectin type II domain (FNII), eight C-type lectin domains (CTLD-1-8) a single transmembrane domain followed by a 44aa intracellular C-terminus. CRD, FNII and CTLD1-2 form a loop structure on top of the receptor. Monoclonal mouse anti-human Abs bind to CRD (E1/183), CTLD2 (A5/158) and CTLD4 (39:10). Two polyclonal rabbit sera (Cat1 and Cat2) have been raised against the cytoplasmic tail. The polyclonal rabbit sera bind murine Endo180 as well as human Endo180. All three monoclonal Abs only bind human but not murine Endo180. **(B)** The Endo180ΔEx2–6 Protein as expressed by both, the East and Engelholm, partial knockout mice. Modified from: Gronau, Iascke & Sturge. MRC2. Encyclopedia of Signalling Molecules. Springer Press; 2012).

### 1.4.6 Post-translational modification and phosphorylation of Endo180

The ectodomain of Endo180 is modified by approximately 25 kDa of N-linked sugars (7-10 complex N-linked oligosaccharides) and 5 kDa of sialic acid residues (East et al., 2002; Isacke et al., 1990). The sum of a predicted mass of 167 kDa and glycosylation of 30 kDa exceeds the mass of 180 kDa determined using SDS-PAGE.

The glycosylation status of Endo180 has not been investigated following its identification by Isacke *et al.,* in 1990, which makes it is difficult to explain this observation. Glycosylation levels of 30 kDa can significantly affect band diffusion. Interestingly, band diffusion is not apparent in published immunoblot images.

$^{32}P_i$-labelling has revealed that Endo180 contains at least three residues, which are constitutively phosphorylated in F1084 fibroblasts and Flow 2000 embryonic lung diploid fibroblasts under normal growth conditions. This conclusion was drawn from thin-layer chromatography prepared from peptide digests of immuno-precipitated Endo180 protein (Isacke et al., 1990; Sheikh et al., 2000). Treatment of Flow 2000 cells with phorbol 12-myristate 13-acetate (PMA) increased the phosphorylation of one of these sites and revealed two additional phosphorylation sites. In the original publication, it was discussed that all three PMA responsive phosphorylation sites have been identified as serine residues. However, the data was not shown. PKC purified from rat brain showed a strong preference to only one these three phosphorylation sites *in vitro*. Endo180 has been tested *in vitro* for a kinase activity against itself and a number of common substrates with negative results (Isacke et al., 1990; Sheikh et al., 2000). Subsequent to the 2000 study by Sheikh et al., further attempts to investigate the phosphorylation of Endo180 in the Isacke lab using non-radioactive methods produced inconclusive results (J. Sturge personal communication). This potential regulatory modification of the Endo180 cytoplasmic tail is revisited in this thesis (see **Section 3**).

### 1.4.7 Endo180 subcellular localisation and receptor recycling

Endo180 displays a subcellular localisation similar to the transferrin receptor, low-density lipoprotein (LDL) receptor and clathrin. However, although clathrin and Endo180 have a similar subcellular localisation, the overlap is not perfect. Endo180 and clathrin can be detected in different subcellular compartments as well. Approximately 7-10 x $10^5$ molecules of Endo180 are expressed by a single F1084 fibroblast, with 20-30% of the receptor located on the cell surface and 70-80% localised on intracellular membranes. Endo180 distribution on the cell surface is not homogenous but appears punctuated (Isacke et al., 1990; Sheikh et al., 2000), which suggests that receptor clustering may occur. Following the internalisation of Endo180, it can be transported to early endosomes and recycled back to the plasma membrane. The recycling process is rapid with more than 50% of the receptor being internalised within 2 minutes. Endo180 also has a relatively long half-life of 24 hours (Isacke et al., 1990).

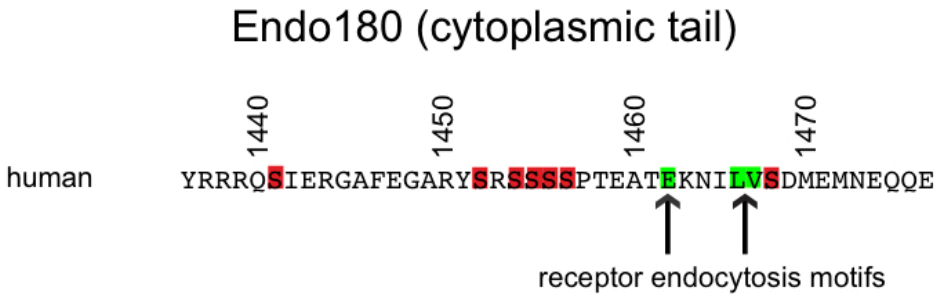



**Figure 1.4.7: Endo180 (cytoplasmic tail only) and potential phosphorylation sites.** All potential targets for PKC have been marked in red. Mutation E1464A slightly alters surface distribution of Endo180. Co-Mutation of L1468A and V1469A leads to an accumulation of Endo180 on the cell surface while intracellular Endo180 is almost absent. From: Gronau, Iascke & Sturge. MRC2. Encyclopedia of Signalling Molecules. Springer Press; 2012).

Two putative endocytosis motifs can be detected in the cytoplasmic tail of Endo180: an LDL receptor endocytosis motif (FxNxxY) and a dihydrophobic motif (ExxxLV) similar to that found in the cytoplasmic tail of transferrin receptor. In contrast to other members of the mannose receptor family, mutation of the LDL receptor-type

endocytosis motif did not alter the subcellular localisation of Endo180. Mutation of the dihydrophobic motif resulted in translocation of Endo180 to the cell surface after complete loss of Endo180 uptake into clathrin coated vesicles (Sheikh et al., 2000). In contrast to MMR, both endocytosis motifs in the cytoplasmic tail of Endo180 are located upstream of serine residues (**Figure 1.4.7**). As mentioned above (**Section 1.4.5**), three unidentified serine residues can be phosphorylated following PMA dependent activation of PKC (Sheikh et al., 2000). A functional link between phosphorylation and receptor shuttling or functionality has not been demonstrated. As mentioned above (**Section 1.4.6**), this post-translational modification has been considered in this thesis (see **Section 3**).

### 1.4.8 Endo180 ligands

#### 1.4.8.1 MMP-13 and MMP-14/MT1-MMP

Endo180 is co-expressed with MMP-13 during osteogenesis (Engelholm et al., 2001b), however, initial suggestions that Endo180 might internalise MMP-13 (Engelholm et al., 2001a) were later disproved (Bailey et al., 2002). It was mentioned earlier (**Section 1.4.4**) that the Endo180/MT1-MMP knockout was lethal (Wagenaar-Miller et al., 2007). Following the discovery of this phenotype co-dependent and distinct roles for Endo180 and MT1-MMP during collagen degradation were established (Madsen et al., 2007). In HT1080 fibrosarcoma cells Endo180 has been shown to control MT1-MMP activity and surface localisation in a collagen-dependent manner (Messaritou et al., 2009). Interestingly, Endo180 is co-expressed with MT1-MMP in murine macrophages during degradation of non-denatured, but not denatured, collagen disks implanted into mice (Ye et al., 2011).

#### 1.4.8.2 uPA and uPAR

In the year 2000, Endo180 was discovered for the third time as a member of a tri-molecular complex with uPA and uPAR (Behrendt et al., 2000). The complex was isolated from the U937 monocytic cell line after chemical cross-linking and was

subsequently identified by mass spectometry. Collagen V was found to interfere with complex formation while collagens I, III and IV had no effect. BSA-galactosamide- and BSA-glucosamide-conjugates also suppressed complex formation, while BSA-conjugated with other sugars displayed no interfering function (Behrendt et al., 2000). Interestingly, uPA has recently been shown to interfere with collagen uptake by Endo180 (Bianchetti et al., 2011). Antibodies that target Endo180-uPA-uPAR complex formation have also been developed (Engelholm et al., 2001a). Later attempts to detect Endo180-uPA-uPAR tri-molecular complex formation in BIAcore experiments failed (Engelholm et al., 2009). This may be explained by the fact that a steric orientation within the 2-D space of the cell membrane is important for complex formation.

The CTLD-4 domain of Endo180 contains an *in silico* predicted uPA interaction site (Liang et al., 2003). This uPA-binding motif interacts with uPA at a site distinct from the interaction site of uPA with uPAR. Therefore, it is feasible that the tri-molecular complex of Endo180-uPA-uPAR forms by the standard interaction between uPA and uPAR at the same time as uPA interaction with the CTLD-4 domain of Endo180. The potential uPA-binding motif in the CTLD-4 domain of Endo180 has so far only been predicted at the sequence level. In this thesis bio-informatic information was used to establish whether the residues of the putative uPA-binding motif are accessible at the surface of the domain or buried within an inaccessible fold within the domain (see **Section 3.1**).

Endo180 was shown to be essential in chemotaxis towards uPA gradients (see **Section 1.4.9**). However, requirement of uPAR co-expression has never been investigated (East et al., 2003; Sturge et al., 2003), which leaves open the possibility that Endo180 can act as chemotactic receptor for uPA independent of uPAR. Endo180 coordinates the activation of Rho GTPases (Cdc42, Rac and Rho), cytoskeletal remodelling events (the regulation of filopodia, lamellipodia and stress fibres), cell-matrix adhesion turnover and cell-cell adhesion disassembly during tumour cell migration and/or uPA-dependent chemotaxis (Sturge et al., 2003; Sturge et al., 2006; Takahashi et al., 2011). Two monoclonal antibodies that bind

CTLD-2 (A5/158) or CRD (E1/183) in the N-terminus of Endo180 can interfere with uPA-uPAR mediated chemotaxis (Sturge et al., 2003). Endo180-dependent signalling during these specific cellular functions is discussed later in this introduction (see **Section 1.4.9**). In addition to the bio-informatic evaluation and structural modelling of the Endo180-uPA-uPAR tri-molecular complex that involves CTLD-4 this thesis has investigated the co-expression of uPAR, uPA and Endo180 in a panel of normal, benign and malignant prostate cell lines, which were also characterised for markers of EMT (see **Section 3.4**).

#### 1.4.8.3 Carbohydrates

In studies of Endo180-uPA-uPAR tri-molecular complex formation several BSA-sugar conjugates were tested for their interfering capabilities. BSA-galactosamide and BSA-glucosamide conjugates successfully suppressed complex formation probably through binding to the Endo180 protein (Behrendt et al., 2000). In the presence of calcium, the Endo180 protein (purified from Flow 2000 fibroblasts, AG 1523 fibroblasts and HUVEC cells) is retained in N-acetylglucosamine columns but not in mannose columns (Sheikh et al., 2000). In a later study sugar binding was mapped to the CTLD-2 domain of Endo180 (East et al., 2002). CTLD-2 binds N-acetylglucosamine, mannose and fucose but not galactose. MMR displayed similar sugar binding capabilities via its CTLD-4 domain. However, in contrast to MMR the CRD of Endo180 was unable to bind sulfated sugars (East et al., 2002). These findings were confirmed when Endo180 lacking CRD, FNII and CTLD1 was purified from partial knockout mice and retained the capability to bind to N-acetylglucosamine (East et al., 2003).

The capability of Endo180-CTLD-2 to bind mannose with a similar affinity to MMR-CTLD-4 has been questioned. According to Fernandez and co-workers CTLD-2 binds to N-acetylglucosamine but its interaction with mannose is predicted to be an artefact of high calcium concentrations (10 mM) being used and unlikely to occur under physiological conditions (Fernandez et al., 2005).

It has been shown that MMR can internalise collagen in a carbohydrate-independent manner. Furthermore, receptor loop formation via the interaction of CRD with CTLD-4 is not necessary for its interaction with collagen (Martinez-Pomares et al., 2006). In contrast to the MMR, in Endo180 the glycosylation state of collagen has a dramatic effect on this interaction. Experiments with truncated Endo180 showed that, especially for the internalisation of collagen IV the presence of CTLD-2 is necessary. Surface plasmon resonance showed that GlcNAc and EDTA (chelating calcium) compete with collagen IV binding. Similar results were obtained in ELISA assays. Mannose and GlcNAc also competed with collagen uptake in cell culture. Consequently, the de-glycosylation of collagen greatly reduced its affinity for binding to Endo180 (Jurgensen et al., 2011).

#### 1.4.8.4 Extracellular matrix - collagen

It was mentioned earlier in **Sections 1.4.8.1 and 1.4.8.2** that: (a) type V collagen can block Endo180-uPA-uPAR complex formation (Behrendt et al., 2000); (b) the uptake of type I, IV and V collagen is abrogated in dermal fibroblasts (Engelholm et al., 2003); and gelatin and collagen IV uptake is reduced in MEFs (East et al., 2003) derived from Endo180 partial-knockout mice; (c) fibroblasts from Endo180 partial-knockout mice degrade collagen via Endo180-dependent trafficking to lysosomes (Kjoller et al., 2004); and that (d) the adhesion and migration of fibroblasts on type I collagen from Endo180 partial-knockout mice was reduced by 25-50% (Engelholm et al., 2003).

Studies with truncated Endo180 receptor revealed that CTLD-2 is required for its interaction with collagen IV but not collagens I, II and V (Wienke et al., 2003). Interestingly, CTLD-2 also has to be present for correct loop formation in the N-terminus of the receptor (see **Section 1.4.5**).

The binding of the FNII domain of Endo180 to the C-terminal region of type I collagen has been mapped (Thomas et al., 2005). At a functional level the invasion of SF188 cells into thick type I collagen gels was reduced following Endo180 silencing (Huijbers et al., 2010). Interestingly, uPA can interfere with collagen I and IV uptake

by fibrocytes (Bianchetti et al., 2011). As mentioned in **Section 1.4.8.1** the co-expression of Endo180 and MT1-MMP was detected during degradation of gelatin disks containing non-denatured, but not denatured, collagen following their implantation into mice (Ye et al., 2011). It has also been established that the uptake of collagen IV requires its glycosylation and interaction with CTLD-2 (Jurgensen et al., 2011) (see **Section 1.4.8.3**). In a broad study the majority of stromal cells, but not epithelial cells, required Endo180 for collagen uptake (Madsen et al., 2011).

The enhanced phosphorylation of myosin (regulatory) light chain-2 (MLC2) downstream of Endo180-Rho-Rho kinase (ROCK) signalling that drives migration of MG63 cells was found to be independent of cell adherence to collagen (Sturge et al., 2006). The intracellular signalling events that follow the engagement of Endo180 with either soluble or fibrillar collagen are unknown (see **Section 1.4.9**).

#### 1.4.8.5 Fibronectin

Myofibroblasts isolated from partial Endo180 knockout mice were reported to have a defective in the uptake of polymerised, but not souble, fibronectin (Shi et al., 2010).

### 1.4.9 Endo180 signalling

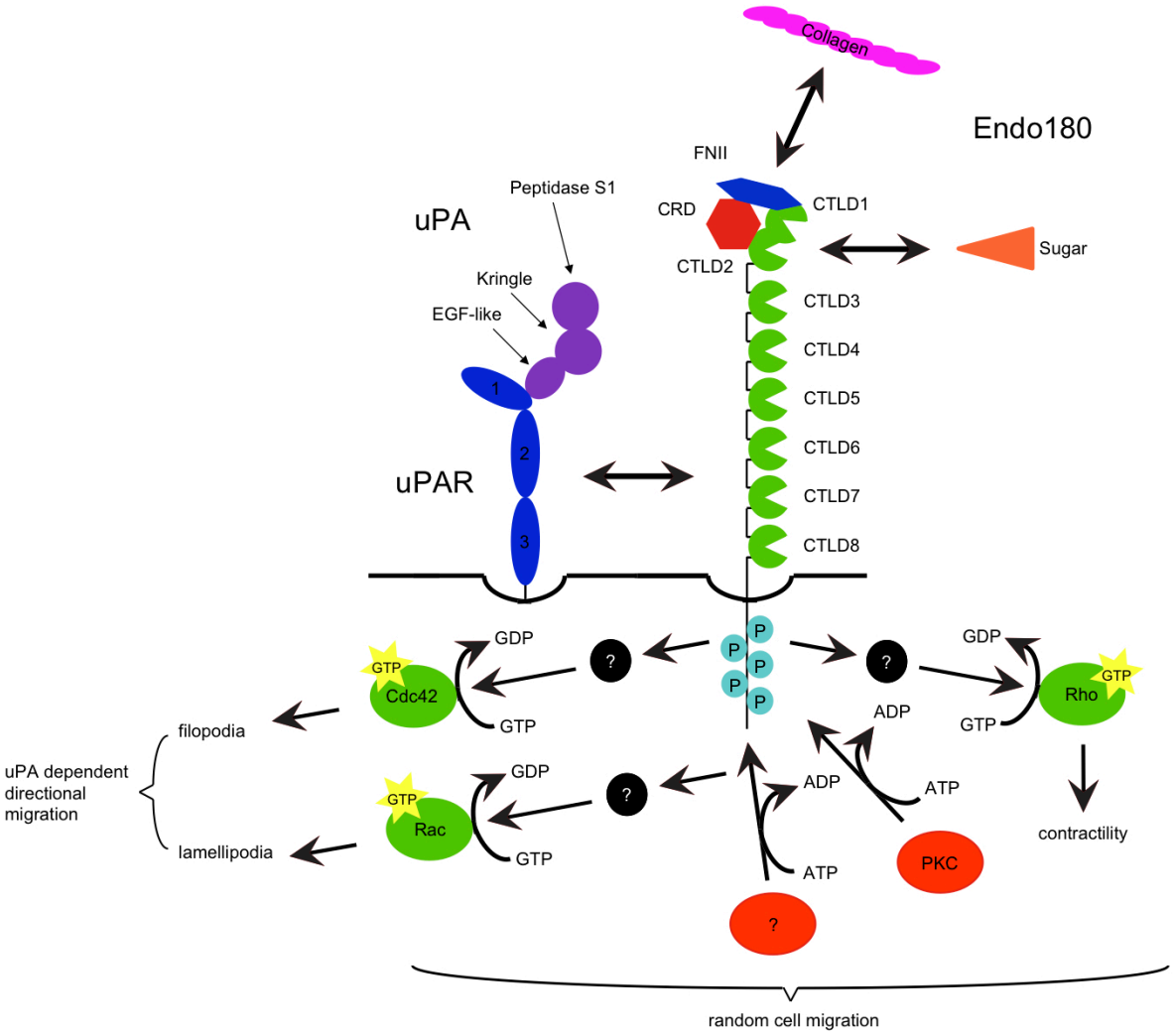



**Figure 1.4.9. Endo180: structure, interaction partners and signalling.** The Endo180 protein is formed by several domains: An N-terminal cysteine-rich domain (CRD), a Fibronectin type II domain (FNII), eight C-type lectin domains (CTLD-1-8) a single transmembrane domain followed by a 44aa intracellular C-terminus. CRD, FNII and CTLD1-2 form a loop structure on top of the receptor. Two domains have been attributed to a function: FNII as collagen binding domain and CTLD-2 as sugar binding domain. Endo180 has been characterised as co-receptor of the urokinase (uPA)-urokinase-receptor (uPAR)-complex. It has been shown *in vivo* and *in vitro* that the Endo180 protein has at least 5 phosphorylation sites. At least one of these sites has been characterised to be a substrate of protein kinase C (PKC). Functional studies showed that the Endo180 protein regulates the overall and tempero-spatial activation of the small GTPases Rho, Rac and Cdc42. From: Gronau, Iascke & Sturge. MRC2. Encyclopedia of Signalling Molecules. Springer Press; 2012).

### 1.4.9.1 Small GTPases and the regulation of the Actin cytoskeleton

The Rho family is part of the Ras superfamily of small GTPases (Hall, 1998). Rho and members of the Rho subfamily, Cdc42 and Rac have been studied for their role in the regulation of the actin cytoskeleton (Hall, 1998). Activation of Rho leads to the formation of contractile stress fibres (Hall, 1998; Ridley and Hall, 1992). Upon activation of Cdc42, protrusions, filipodia, are forming on the surface (Hall, 1998; Kozma et al., 1995). Lastly, activation of Rac results in the formation of lamellipodia, an actin meshwork at the cell periphery (Hall, 1998; Ridley et al., 1992). These lamellipodia are found at the leading edge of the cell and lift off the substrate, which can be observed as membrane ruffles (Van Aelst and D'Souza-Schorey, 1997). Those characteristics have initially been described in fibroblasts but can be observed in a variety of different cell types, including macrophages, neurons and epithelial cells (Hall, 1998). Interestingly, at least in murine bone marrow derived macrophages, Rac signalling is not required for cell motility. Bone marrow derived macrophages silenced for Rac1 expression display reduced but not a total loss of membrane ruffling. While cell shape is altered, overall cell motility is not impaired. Murine bone marrow derived macrophages express no Rac3 and low levels of Rac2 (Wells et al., 2004). Rho, Rac and Cdc42 also regulate the focal adhesion complexes associated with stress fibres, protrusions and membrane ruffles (Hall, 1998; Nobes and Hall, 1995).

The Rho family plays an important role in the migration of macrophages towards the chemoattractant CSF-1. Stimulation of macrophages with CSF-1 leads to Cdc42 dependent formation of filopodia/protrusions and Rac dependent formation of lamellipodia (Allen et al., 1997; Hall, 1998; Jones et al., 1998). Interestingly, Rho and Rac can enhance cell motility in response to CSF-1 independently of Cdc42. However, Cdc42 is essential for chemotaxis towards CSF-1 (Jones et al., 1998).

The small Rho GTPases are cycling between an inactive GDP-bound and an active GTP-bound state (Van Aelst and D'Souza-Schorey, 1997). They are transitioned into their active state by guanine nucleotide exchange factors, GEFs, which drive the

exchange of GDP for GTP (Hall, 1998; Van Aelst and D'Souza-Schorey, 1997). Guanine nucleotide dissociation inhibitors, GDIs, can prevent both, the dissociation of GDP and GTP from the Rho GTPase (Hall, 1998; Van Aelst and D'Souza-Schorey, 1997). GTPase activating proteins, GAPs, deactivate signalling by leading to the conversion of Rho GTPase bound GTP to GDP (Hall, 1998; Van Aelst and D'Souza-Schorey, 1997).

Rho GTPases regulate several downstream effector proteins (Jaffe and Hall, 2005). The signalling pathways are not purely responsible for the regulation of the actin cytoskeleton and cell motility (Allen et al., 1997; Hall, 1998). Some additional functions are cell growth control, transcription activation and membrane trafficking (Allen et al., 1997; Hall, 1998).

Only in their GTP bound state, Rho GTPases bind and activate downstream effector proteins (Jaffe and Hall, 2005). For example, stress fibre and focal adhesion formation are attributed to activation of the Rho Kinases, ROCKs, by GTP-bound, activated RhoA (Allen et al., 1997; Hall, 1998). Formation of membrane ruffles appears to be driven by activation of POR1 by activated Rac1 (Allen et al., 1997; Hall, 1998). The GDP/GTP switch can be exploited to measure the Rho GTPase activation level. Usually, the Rho GTPase binding domains of rhotekin, PAK and WASP are expressed as GST fusion proteins and used as 'bait' to co-precipitate activated, GTP-bound, RhoA, Rac1 and Cdc42 respectively (Allen et al., 1997; Hall, 1998; Wells et al., 2004).

There is considerable cross talk and cross activation displayed by small GTPases as well as of some of their substrates. For example, group I PAK proteins (PAK 1-3) can be activated by Rac1 and Cdc42 alike (Allen et al., 1997; Arias-Romero and Chernoff, 2008; Hall, 1998). Group I PAK proteins are well-studied downstream effectors of Rho GTPases and play a role in the dynamics/motility of the cytoskeleton, death/survival signalling and transcriptional regulation (Arias-Romero and Chernoff, 2008). Although it is understood that group II PAKs (PAK 4-6) interact at least with Cdc42, RhoD and RhoH, the exact mode of interaction and regulation between Rho GTPases and group II PAKs has not yet been fully characterised (Wells

et al., 2002; Wells and Jones, 2010). Group II PAK proteins regulate a spectrum of cellular functions similar to group I PAKs: hormone signalling, motility, survival and mitogen signalling, but perform those regulations mostly through different direct downstream interaction partners (Arias-Romero and Chernoff, 2008; Wells and Jones, 2010).

Another class of Rho GTPase downstream effectors, ezrin, radixin and moesin, ERM, have attracted increasing attention (Hall, 1998; Ivetic and Ridley, 2004). ERM proteins don't interact directly with Rho GTPases but their interaction with actin is essential to enable Rho and Rac induced formation of stress fibres and lamellipodia (Hall, 1998; Ivetic and Ridley, 2004; Jones et al., 1998).

#### 1.4.9.2 Endo180 and small GTPase signalling

A role for Endo180 in downstream signalling to the small Rho GTPases, Cdc42, Rac and Rho and the promotion of directed or random cell migration has been established in a number of tumour cell lines (MCF-7, MDA-MB-231, BE, HT1080, MG63). This cellular effect can be either uPA-dependent or -independent (Sturge et al., 2003; Sturge et al., 2006). However, the requirement for uPAR for this response has not been established. As mentioned in **Section 1.4.8.2** the requirement of uPAR co-expression is not known and leaves open the possibility that Endo180 *per se* is a chemotactic receptor for uPA. It is unknown how Endo180 interacts, directly or indirectly, with Rho GTPases on a molecular level.

#### 1.4.9.3 Endo180-dependent activation of Cdc42

The requirement for Endo180 in MDA-MB-231 metastatic breast cancer cells to sense chemotactic gradients of pro-uPA was demonstated by the use of Dunn chemotaxis chamber assays following genetic silencing of Endo180 by siRNA (Sturge et al., 2003). The role of Endo180 in this chemotactic response was supported by a gain in chemotactic migration towards a concentration gradient of pro-uPA following its overexpression in the non-metastatic MCF7 breast cancer cell line (Sturge et al., 2003). These changes in chemotactic behaviour were directly

linked to the altered dynamics of uPA-dependent Cdc42 activation, an event that was suppressed by Endo180 silencing in MDA-MB-231 cells and enhanced in MCF7 cells overexpressing Endo180. The activation of Cdc42 and chemosensing of a uPA gradient in MCF-7 cells expressing an Endo180 mutant that cannot undergo internalisation indicated that the chemosensory function of Endo180 is independent of receptor endocytosis (Sturge et al., 2003).

#### 1.4.9.4 Endo180-dependent activation of Rac

The rapid activation of Rac by uPA in MCF7 cells that overexpress Endo180 and the requirement for the internalization of Endo180 to activate Rac and promote an increase in migratory speed suggests that Endo180 can modulate Rac activity to promote increased random cell migration via a mechanism that is distinct from the Endo180-dependent activation of Cdc42 (Sturge et al., 2003). The localisation of Endo180 to lamellipodia and the requirement of Endo180 for the extension of lamellipodial protrusions (Takahashi et al., 2011) indicates its critical role in Rac-dependent signalling during cytoskeletal remodelling and cell migration.

#### 1.4.9.5 Endo180-dependent activation of Rho-ROCK-MLC2

Endo180 is required for the phosphorylation of MLC2 at serine19/threonine18 in MG-63, MDA-MB-231, BE and HT-1080 cells (Sturge et al., 2006). In MG-63 cells this effect was demonstrated to be independent of the expression of uPAR and several ECM substrata (fibronectin, type I collagen and Matrigel). Following Endo180 silencing by siRNA in MG63 cells a tail retraction phenotype that recapitulated the phenotype associated with Rho Kinase (ROCK) inhibition is observed (Sturge et al., 2006). Endo180 siRNA and ROCK-inhibition with H-1152 led to similar decreases in Myosin light chain 2 (MLC2), myosin phosphatase target subunit 1 (MYPT1) and LIM domain kinase 1 and 2 (LIMK1/2) phosphorylation, which are downstream targets of ROCK. MG-63 cells displayed a strong loss in Rho A activation upon treatment with Endo180 siRNA, which indicates Endo180 can modulate a signalling mechanism upstream of this small Rho GTPase. While Endo180 containing vesicles

are dispersed throughout the cell under normal growth conditions, treatment with ROCK inhibitor H-1152 resulted in clustering of Endo180-containing vesicles around unretracted tails and a mechanism has been proposed through which Endo180-containing vesicles are able to generate tail retraction force by Rho/ROCK dependent activation of myosin contraction (Sturge et al., 2006).

### 1.4.10 Potential role of Endo180 in disease

#### 1.4.10.1 Osteoarthritis

As mentioned in **Section 1.4.4** Endo180 is expressed during murine bone development (Engelholm et al., 2001b) but a role in bone and cartilage homeostasis and osteoarthritis was not detected in a murine model of the disease (Howard et al., 2004).

#### 1.4.10.2 Fibrosis

Endo180 is expressed in the stroma of murine kidneys during fibrogenesis caused by unilateral ureteral obstruction. Galectin 3 knockout mice displayed a more severe phenotype of renal fibrosis in this model. The more severe phenotype was found to be associated with a loss of Endo180 expression, while components of extracellular matrix degradation pathways, MMP-9/12/13, are not affected. This suggests that intracellular matrix degradation via Endo180 may have a protective role in fibrosis (Okamura et al., 2011). These results are in accordance with the findings in mouse breast cancer models where Endo180 was associated with a fibrotic response in the tumour-associated stroma (Curino et al., 2005; Wienke et al., 2007) (see **Sections 1.4.4 & 1.4.10.5**).

#### 1.4.10.3 Crooked tail syndrome

A mentioned earlier (**Section 1.4.3**) it has been shown that loss of Endo180 leads to crooked tail syndrome as well as muscle abnormalities in Belgian Blue cattle (Fasquelle et al., 2009). The mechanism that explains the relationship between Endo180 and crooked tail syndrome has not been established but is associated with loss of stable protein.

#### 1.4.10.4 Wound healing

Endo180 is dramatically upregulated during wound healing in subpopulations of myofibroblasts, pericytes, macrophages and endothelial cells (Honardoust et al., 2006) (see **Section 1.4.3**). The functional role of Endo180 in the different cell types that contribute to this complex response has not been determined.

#### 1.4.10.5 Cancer

Endo180 is not expressed in normal breast tissue but is expressed by tumour-associated mesenchymal cells in benign ductal carcinoma *in situ* and by fibroblast-like cells, myoepithelial cells, myofibroblasts and macrophages in malignant breast lesions. Endo180 was not detected on tumour cells in this study (Schnack Nielsen et al., 2002), a finding that may be due to its relatively low expression compared to the stroma. It has been suggested that the antibody used has lower affinity than an antibody used in a later study (Wienke et al., 2007). Another explanation for lack of detection could be epitope masking of the molecular domain detected by the antibody. Staining of a large breast cancer tissue micro array (TMA) confirmed that Endo180 is upregulated in a rare subset of metaplastic basal-like breast cancers (approximately 1.5 % of all breast cancers) and that this correlates with shorter disease-free survival in these patients (Wienke et al., 2007). Some of these tumours were found to have gains in Endo180 gene copies. In the same study Endo180-negative MCF-7 breast cancer cells were shown to regulate Endo180 following their

treatment with TGF-$\beta_1$ (Wienke et al., 2007). MCF-7 cells stably transfected with Endo180 also displayed enhanced growth in a tumour xenograft model. These tumours had a lower collagen content than wild-type controls. A similar effect was not achieved with an internalisation defect mutant of Endo180 (Wienke et al., 2007). As mentioned in **Section 1.4.4.1** the cross of breast tumour prone MMTV mice with partial Endo180 knockout mice also led to tumour fibrosis and smaller tumours (Curino et al., 2005).

In a TMA study with more than 100 samples of head and neck cancer patients, Endo180 expression by the tumour associated stroma correlated with tumour grade (Sulek et al., 2007). A prostate cancer TMA study carried out in the Sturge laboratory revealed that Endo180 was upregulated on tumour cells as well as the tumour-associated stroma. Moreover, the upregulation was correlated with tumour grade and coexpression of Endo180 co-factors: MT1-MMP, uPA and uPAR (Kogianni et al., 2009), suggesting that Endo180 is involved in the metastatic spread of the disease.

A database search using "Oncomine" revealed that Endo180 transcripts are upregulated in grade IV glioblastomas. These findings have been confirmed on protein level in a glioblastoma TMA (Huijbers et al., 2010). Similar to upregulation of Endo180 in MCF-7 breast cancer cells, Endo180 expression was upregulated by TGF-$\beta_1$ stimulation in U87MG glioblastoma cells. shRNA knockdown of Endo180 in SF188 glioblastoma cells reduced their invasive potential (Huijbers et al., 2010). Further analysis revealed that Endo180 is not expressed in healthy brain tissue, but is highly expressed by the KNS42 and KNS81 glioma cell lines. siRNA knockdown of Endo180 reduced the random cell migration and invasion of both cell lines into collagen gels. These findings were in alignment with the Endo180-dependent rearrangement of the actin cytoskeleton, lamellipodia and stress fibre formation and front-back polarity observed in these cell lines (Takahashi et al., 2011).

Expression of Endo180 by cells of an epithelial origin has been observed in a wide range of colorectal and breast cancer cell lines, where it was found to positively correlate with a more migratory and invasive phenotype (Sturge et al., 2003;

Wienke et al., 2007; Wienke et al., 2003), indicating that it may contribute role to metastasis when Endo180 expression is increased in tumour cells. As proposed above, this appears to have particular significance in the progression of prostate cancer (Kogianni et al., 2009).

### 1.4.11 Summary

Endo180 is an endocytic recycling receptor with binding capacity for uPA, several collagen isoforms and carbohydrate moieties. Within a uPA gradient, Endo180 transmits chemotactic signals through the small GTPases Rac and Cdc42 upon binding of uPA. At the cell's rear Endo180 containing vesicles can promote contractile signals via activation of the Rho-ROCK-MLC2 pathway. Endo180 is also an essential component of the cell's intracellular collagen degradation pathway, a function that is mainly attributed to stromal cells. The upregulation or loss of Endo180 expression is correlated with several disease-associated processes, including cancer progression.

## 1.5 Project aims and overview

### 1.5.1 Major aim

- Evaluate the role of Endo180 in prostate cancer pathology with a particular focus on its link to increased tumour cell migration and metastasis

### 1.5.2 Specific objectives

- Ascertain the co-evolution of Endo180, its interaction partners and domain function *in silico*
- Design a non-radioactive assay to enable the study of Endo180 phosphorylation *in vitro*
- Establish a multi-cell line model as a clinically relevant experimental tool to investigate the relevance of Endo180 expression with prostate cancer progression
- Conduct the first full clinicopathological evaluation of Endo180 in prostate cancer patients

### 1.5.3 Experimental approaches proposed at the outset of this project

- Apply bioinformatics strategies to study the evolutionary heritage and conservation of Endo180 and its functional domains
- Attempt to predict the location of Endo180's three PKC substrate residues by use of the GPS system
- Examine phosphorylation status of Endo180 by the use of generic phospho-serine/threonine antibodies
- Apply phosphorylation shift assays to study the phosphorylation status of Endo180
- Attempt to identify interaction partners of Endo180 by immunoprecipitation and mass spectroscopy
- Apply Western Blot analysis, immunofluorescent staining, confocal and screening microscopy to define a new multi cell line model to study prostate cancer progression
- Establishment of organotypic invasion assays for prostate cancer cell lines
- Perform tissue micro array studies to study Endo180 expression in clinical samples

- The proposed experiments will provide new insight into the under characterised molecular function of Endo180, an important component of extracellular matrix remodelling and cell migration, and may lead to a new approach for cancer therapy. It is hoped that inhibitors of Endo180 function may help to prevent localised invasion and metastasis during prostate cancer disease progression.

# 2 Materials and Methods

## 2.1 Materials

### 2.1.1 SDS-PAGE - 1-D

- β-mercapto-ethanol (Sigma)
- 1x Tris-HEPES-running-buffer (Sigma; 100 mM Tris, 100 mM HEPES, pH8)
- 4-20 % gradient gel (NuBlu Tris Glycine Gels, NuSep)
- 4-20 % gradient gel (Precise Protein Gels, Pierce, Thermo Scientific)
- 6X SDS-PAGE sample buffer (Current Protocols: 7 ml 4· Tris·Cl/SDS (0.5 M Tris·Cl containing 0.4 % w/v SDS) pH 6.8,;3.0 ml glycerol (30 % v/v final), 1 g SDS (10 % w/v final), 1.2 mg bromophenol blue (0.012 % w/v final), add $H_2O$ to 10 ml)
- 6X SDS loading buffer non-reducing (Boston Bioproducts)
- BCA-assay (Pierce, Thermo Scientific)
- Centrifuge 5810R, Rotor FL011 (Eppendorf)
- DC-assay (Bio-Rad)
- DTT (1 M stock in MilliQ-water) (company)
- Lucy-565 (Sigma)
- Mini Protean III cells (Bio-Rad)
- Phos-tag Agarose (Wako)
- Powerpack (Biorad)
- RIPA-buffer (Santa Cruz RIPA lysis buffer sc-24948: 1X TBS, 1 % v/v Nonidet P-40, 0.5 % w/v SDS, 0.004 % w/v sodiumazide, 1:100 PMSF, 1:100 protease inhibitor cocktail, 1:100 sodiumorthovanadate), RIPA-buffer was supplemented with protease-inhibitor-cocktails B and C (Santa Cruz: sc-45045 and sc-45065).
- Soniprep 150 (Sanya, MSE)

### 2.1.2 SDS-PAGE - 1-D - Phos-Tag

- 30 % w/v acrylamide solution (Sigma)
- di-ammonium peroxydisulfate (Sigma)
- 10 % w/v di-ammonium peroxydisulfate solution
- β-mercaptoethanol (Sigma)
- bromophenol blue (Sigma)
- glycerol (Sigma)
- $MnCl_2$ (Sigma)
- 10 mmol/L $MnCl_2$ solution
- Phos-Tag acrylamide (Wako)
- 5.0 mmol/L Phos-tag acryl-amide Solution containing 3% (v/v) MeOH
- 20 % w/v SDS in water (Fluka)
- TEMED (tetramethylethylenediamine) (Sigma)
- Tris (VWR)
- 0.50 mol/L Tris-HCl buffered solution (0.4 % w/v SDS, 100 mL) pH 6.8
- 1.5 mol/L Tris-HCl buffered solution (0.4 % w/v SDS, 100 mL) pH 8.8

| 3X SDS-PAGE Sample buffer for Phos-Tag gels | |
|---|---|
| bromophenol blue | 1.5 mg |
| SDS | 0.60 g |
| glycerol | 3.0 mL |
| 0.50 mol/L Tris-HCl buffered solution (0.4 % w/v SDS), pH 6.8 | 3.9 mL |
| 2-mercaptoethanol | 1.5 mL |
| 10 mL aliquoted and stored at –20˚C; diluted to 1X with distilled water prior to use; can be added to RIPA lysis buffer with phosphatase inhibitor cocktails | |

### 2.1.3 Gel electrophoresis -2-D

- bromophenol blue (Sigma)
- DryStrip cover fluid (GE Healthcare)
- DTT (dithiothreitol) (Sigma)
- Electrophoresis power supply EPS 3500 XL (GE Healthcare)
- IEF electrode strips (GE Healthcare)
- Immobiline DryStrip pH 3-10 L, 11 cm (GE Healthcare)
- Immobiline DryStrip kit (GE Healthcare)
- Multiphor II electrophoresis unit (GE Healthcare)
- Pharmalyte 3-10 (GE Healthcare)
- PMSF (phenylmethansulfonyl fluoride) (Santa Cruz) (part of RIPA buffer kit)
- 20 % w/v SDS in water (Fluka)
- glycerol (Sigma)
- Tris (VWR)
- Triton X-100 (Bio-Rad)
- urea (Sigma)

| Lysis solution | |
|---|---|
| urea | 13.5 g |
| Triton X-100 | 0.5 ml |
| DTT | 500 mg |
| Pharmalyte 3-10 | 0.5 ml |
| PMSF | 35 mg |
| make up to 25 ml with distilled water | |

| 2X SDS-PAGE sample solution | |
|---|---|
| urea | 13.5 g |
| DTT | 250 mg |
| Pharmalyte 3-10 | 0.5 ml |
| Triton X-100 | 0.13 ml |
| a few grains of Bromophenol Blue | |
| make up to 25 ml with distilled water | |

| Rehydration solution | |
|---|---|
| urea (8 M) | 12.0 g |
| Triton X-100 (0.5%) | 0.13 ml |
| Pharmalyte 3-10 | 0.13 ml |
| DTT | 50 mg |
| make up to 25 ml with distilled water | |

| Equilibration solution | |
|---|---|
| Tris-HCl stock solution | 20 ml |
| urea | 72 g |
| glycerol | 60 ml |
| SDS | 2 g |
| + 67 ml distilled water = final volume of 200 ml; add 25-100 mg DTT per 10 ml for the first equilibration step and 0.45 g iodoacetamide plus a few grains of BPB per 10 ml solution for second step | |

### 2.1.4 Western Blot

- 1x TG-buffer (BioRad, Current Protocols; 10X stock: 0.25 M Tris, 1.92 M glycine, pH 8.6)
- anti-mouse HRP (Jackson)
- anti-rabbit HRP (Santa Cruz)
- BSA (Sigma)
- 5 % w/v BSA in PBS + 0.02% NaN3
- ECL (GE Healthcare)
- ECL Plus (GE Healthcare)
- Immobilon Western HRP Substrate (Millipore)
- ImageQuant software (GE Healthcare)
- $NaN_3$
- PBS (137 mM NaCl, 2.7 mM KCl, 4.3 mM $Na_2HPO_4 \cdot 7H_2O$, 1.4 mM $KH_2PO_4$, pH~7.3)
- PVDF-FL membranes (Millipore)
- skimmed-dry-milk (Tesco)
- TBS-T (Sigma, Current Protocols; 10X stock: 500 mM Tris, 1500 mM NaCl, adjusted with HCl to pH 7.6, diluted to 1x and supplemented with 0.1 % v/v Tween-20)
- Transblot Mini Cells (Bio-Rad)
- Typhoon scanner (GE Healthcare)
- Odyssey infrared imaging system (LI-COR)
- Odyssey secondary antibodies (LI-COR)
- Odyssey blocking solution (LI-COR)
- ImageQuant LAS 4000 (GE Healthcare)

### 2.1.5 Immunprecipitation

- Protein-G magnetic beads (Invitrogen)
- Co-IP kit (Epoxy-beads) (Invitrogen)
- Magnet for 1.5-2.0 ml Eppendorf cups (Invitrogen)

### 2.1.6 Immunocytometry

- 96-well V-bottom plates (Fisher)
- propidium-iodide (PI) (Invitrogen)
- ethidium-monoazide-bromide (EMA) (Invitrogen)
- goat anti-mouse-IgG Alexa Fluor-405/-488/-546/-633 (H+L) (Invitrogen)
- goat anti-rabbit-IgG Alexa Fluor-488/-546/-633 (H+L) (Invitrogen)
- IFF (PBS + 1% w/v BSA+ 2 % FCS v/v)
- phalloidin Alexa Fluor-488/-546/-633 (Invitrogen)

- saponin (Sigma)
- FacsCanto (BD)
- FlowJo (Tree Star)

### 2.1.7 Immunofluorescence

- goat anti-mouse-IgG Alexa Fluor-488 (H+L) (Invitrogen)
- goat anti-rabbit-IgG Alexa-Fluor 488 (H+L) (Invitrogen)
- IFF (PBS + 1 % w/v BSA + 2 % FCS v/v)
- saponin (Sigma)
- Triton X-100 (Sigma)
- ImageXpress$^{MICRO}$ (IXM) (Molecular Devices)
- LSM510 (Zeiss)

### 2.1.8 Tissue staining

- DAB kit (Invitrogen)
- DPX (Sigma)
- Eosin Y
- Mayer's haematoxylin

### 2.1.9 Invasion sssay

- 24 and 6 well plates
- collagen type I (BD 354236)
- fetal calf serum (FCS)
- 10X DMEM (bought as powder from Sigma and added sodium bicarbonate)
- 25 % glutaraldehyde (Sigma, G-5882)
- Matrigel (BD 354234)
- microtome (Bright M3500)
- nylon mesh (Tetko, 3-100/5-sefar ltd) (cut to size of grids (20 mm x 20 mm) and autoclave)
- oven
- paraformaldehyde (PFA) (Riedel-de-Haen)
- steel grids (manufactured by workshop of chemical engineering department Imperial College London) fine and thin steel meshwork, 32.5 mm x 21.5 mm, bent on both sides to 90-degree angle -> elevation 5.5 mm, elevated area 21.5 x 21.5 mm
- waterbath (Raymand A Comb, digital sectioning mounting bath)

### 2.1.10 Dunn chamber

- beeswax, bleached white (Acros Organics, 222395000)

- brush (soft for watercolours, Selfridges)
- Dunn Chamber (Hawksley Scientific)
- paraffin wax (Fisher, P/0600/90)
- paraffin soft white (Fisher P/0480/53)
- paraffin soft yellow (Fisher P/0440/53)
- wax (mix equal weight of paraffin wax, paraffin soft (white or yellow) and beeswax)

### 2.1.11 Growth factors

- uPA (protease-null mutant) (Joceleyne Hamelyn, INSERM, Paris)
- uPA (full length) (America Diagnostica)
- bFGF (R&D Systems)
- HGF (R&D Systems)
- IGF-II (R&D Systems)
- PDGF-BB (R&D Systems)
- TGF-$\beta_1$ (R&D Systems)

### 2.1.12 Molecular Cloning

- QuikChange XL Site-Directed Mutagenesis Kit (Stratagene)
- Takara Ligation Kit V2.1 (Lonza)
- QIAEX Gel extraction kit (Qiagen)
- High fidelity polymerase kit (Roche)
- NotI enzyme and buffers (NEB)
- HindIII enzyme and buffers (NEB)
- Custom primers (Invitrogen)
- DH5 alpha super competent cells (Invitrogen)
- Agarose electrophoresis chamber (BioRad)
- Agarose (Fisher)
- Nanodrop (Thermo Fisher)

## 2.2 Methods

### 2.2.1 Cell culture

Primary cell lines RC170N, RC165N, RC92a and RC58T were provided by Prof Johng Rhim (NIH, Bethesda, USA). Professor Clare Isacke (Institute of Cancer Research) provided MG-63 and MCF-7 cells. Dr Claire Wells (King's College London) provided PC-3 and DU145 cells. Dr Robert Kypta (Imperial College London) provided LNCaP and RWPE-1 cells. MDA-MB-231 cells were obtained from CRUK. Primary humanosteoblasts were provided by Dr Giolanta Kogianni and Dr Matthew Caley who derived them as previously described (Mann, Huber et al. 2006) using femoral heads obtained post-operatively from Professor Justin Cobb (Imperial College London). hTert immortalised human dermal fibroblasts (HCA-2) were provided by Prof David Kipling (Cardiff University).

PC-3, LNCaP and DU145 cells were grown in RPMI1640 with 10 % v/v FCS. MG63, MCF-7, HCA2 and MB-MDA-231 cells were grown in DMEM with 10 % v/v FCS. In the case of MCF-7-cells the medium was additionally supplemented with insulin. RWPE-1, RC170N, RC165N, RC92a and RC58T were grown in Keratinocyte SFM-medium (Invitrogen). Cell lines were split by trypsination. For all non-Johng Rhim lines trypsination was quenched by the addition of medium containing FCS. For Johng Rhim lines trypsination was stopped by dilution 1:5 with growth medium, subsequent centrifugation (at 1,400 rpm for 5 minutes; Eppendorf 5810, A-4-62 rotor with buckers for 50 ml tubes), careful decantation and re-suspension of the cell pellet in trypsin-free growth medium.

### 2.2.2 Preparation of cell lysates for SDS-PAGE

#### 2.2.2.1 RIPA buffer

Cells were grown on petri dishes under assay specific conditions. The medium was decanted and the dishes placed on ice. The residual medium was aspirated and the cells washed with ice-cold PBS. The remaining PBS was aspirated and

an appropriate volume of RIPA-buffer was pipetted onto the dish. For 75 mm dishes 150 µl of lysis buffer was added; 350 µl for 100 mm dishes and 1 ml for 150 mm dishes. The surface of the dish was scraped with a spatula and the lysis buffer transferred into a 1.5 ml tube. After 10 minutes incubation on ice the tubes underwent centrifugation at 14,000 rpm (20,800 x g) for 15 minutes (5810R Centrifuge, Rotor FL011, Eppendorf, Germany). The supernatant was transferred into fresh tubes and the pellets containing cell debris discarded. The protein concentration of the cell lysate was quantified using a BCA-assay kit (Pierce, Thermo Scientific) and the samples supplemented with an appropriate volume of 6X SDS-PAGE sample buffer (Current Protocols) to give a final 1X concentration. In most cases the solution was split and one half was supplemented with DTT. Samples were heat-inactivated at 95°C for 5 minutes, shock frozen in a dry-ice methanol bath and stored at -20°C until required.

#### 2.2.2.2 Direct lysis in SDS-PAGE loading buffer

Cells were grown on petri dishes under assay specific conditions. The medium was decanted and the dishes placed on ice. The residual medium was aspirated and the cells washed with ice-cold PBS. The remaining PBS was aspirated and an appropriate volume of 2X SDS-PAGE loading buffer was pipetted onto the dish. For 75 mm dishes 150 µl of lysis buffer was added; 350 µl for 100 mm dishes and 1 ml for 150 mm dishes. A pipette tip was placed onto a 1.5 ml Gilson pipette and cut with scissors at a 30-degree angle to enlarge the opening. The enlarged opening was placed on the petri dish and slowly moved over the surface while carrying out a fast rotating movement. The resulting protein/DNA gel was carefully pipetted into 1.5 ml tubes. Samples were heat-inactivated at 95°C for 5 minutes and placed back on ice. Subsequently, the samples were sonicated three times at 10 Hz for 5 seconds (MSE, Soniprep 150, Sanyo, Japan) to sheer the DNA and reduce the viscosity. Samples were frozen in a dry-ice methanol bath and stored at -80$^{0}$C until further use. Samples were heated to 95 $^{0}$C, cooled to room temperature and the protein

concentration was quantified using a DC-assay kit (Bio-Rad). In most cases, the solution was subsequently split and one half was supplemented with DTT.

### 2.2.3 Preparation of cell lysates - 2D SDS-PAGE – urea based

Cells were grown on 150 mm petri dishes under assay specific conditions. The medium was decanted and the dishes placed on ice. The residual medium was aspirated and the cells washed with ice-cold PBS. The remaining PBS was aspirated and 1 ml of urea-DTT-based-buffer was pipetted onto the dish. The surface of the dish was scraped with a spatula and the lysis buffer transferred into a 1.5 ml tube. After 10 minutes incubation on ice the tubes underwent centrifugation at 14,000 rpm (20,800 x g) for 15 minutes (5810R Centrifuge, Rotor FL011, Eppendorf, Germany). The supernatant was transferred into fresh tubes and the pellets containing cell debris discarded. The protein concentration of the cell lysate was quantified using the Bio-Rad assay.

### 2.2.4 Immunoprecipitation

Cells were grown on 150 mm petri dishes under assay specific conditions. In the cold room, medium was decanted and petri dishes placed on ice. Residual medium was aspirated and cells washed with ice-cold PBS. Residual PBS was aspirated and 1 ml of lysis buffer added to the centre of the petri dish. Petri dishes were scraped with a spatula and lysates transferred into 1.5 ml tubes. After 10 minutes lysis on ice, the tubes underwent centrifugation at 14,000 rpm (20,800 x g) for 5 minutes (5810R Centrifuge, Rotor FL011, Eppendorf, Germany). Supernatant was transferred into fresh 1.5 ml tubes containing magnetic beads.

#### 2.2.4.1 Protein-G coupled magnetic beads

Antibody was loaded onto magnetic beads following kit manufacturers instructions (Invitrogen). Standard RIPA buffer supplemented with phosphatase inhibitor cocktail was used as lysis buffer. Lysate was incubated with magnetic beads following instructions by Invitrogen, washed and eluted accordingly.

### 2.2.4.2 Cross-linking of Protein-G coupled magnetic beads with $BS^3$

Antibody was loaded onto magnetic beads following kit manufacturers instructions (Invitrogen). Antibody-loaded beads were incubated with $BS^3$ solution following the standard protocol (Invitrogen). The chemically cross-linked beads have been used as described previously (see **Section 2.2.4.1**).

### 2.2.4.3 Epoxy activated magnetic beads

Epoxy beads were loaded with 5 ug A5:158 per 1.5 mg beads for 16 hours at $37^oC$ according to manufacturer's instructions (Invitrogen). The lysis buffer provided with the co-IP kit was supplemented with $NaCl_2$. Wash buffers were provided in the kit and used accordingly. We followed the described procedures for either Western Blotting or mass spectroscopy. Ammonia eluted pellets for mass spectroscopy were lyophilised in a vacuum centrifuge and subsequently analysed by shotgun proteomics in the mass spectroscopy support facility of the department of Biochemistry, Imperial College, South Kensington Campus.

### 2.2.5 2-D Gel Electrophoresis

| Programme for iso-electric focusing of pH 3-10 L, 110 mm Immobilon Dry-Strip | | | | | |
|---|---|---|---|---|---|
| Phase | Voltage | mA | W | Time (hr) | Vh |
| 1 | 300 | 1 | 5 | 0.01 | 1 |
| 2 | 300 | 1 | 5 | 4.5 | 1350 |
| 3 | 2000 | 1 | 5 | 5 | 5750 |
| 4 | 2000 | 1 | 5 | 6.5 | 13000 |
| Total | | | | 16 | 20100 |
| power supply programmed in "gradient" mode with voltage ramped up to programmed value starting from zero (300 V in first phase; 4.5 hours) and to maximum value (2000 V in last phase; 5 hours) and then maintained at 2000 V (6.5 hours) | | | | | |

110 mm Immobilon pH 3-10 L Dry-Strips were rehydrated over night in rehydration buffer. Samples were loaded according to the Dry-Strip kit manual and electrophoresis performed. Strips were subsequently equilibrated in solutions 1 and 2 for 10 minutes each. Standard SDS-PAGE gels were cast (7% v/v acrylamide, see **Section 2.2.7** without Phos-Tag and manganese). With the exception of one well for the molecular weight marker, a plastic spacer was modified with Scotch tape to create a large opening for the Dry-Strip in the stacking gel. Overhanging plastic was removed with scissors and the Dry-Strip placed with the pI 3 end facing towards the molecular weight marker into the cavity in the stacking gel. Dry-Strips were overlaid with agarose and normal SDS-PAGE performed at 100V. Gels were subsequently used for Western Blotting.

### 2.2.6 SDS-PAGE -1-D

Normally 12.5 µg protein of each sample was loaded onto a 4-20 % w/v acrylamide gradient gel (NuBlu Tris Glycine Gels, NuSep, UK) for the analysis of E-cadherin, vimentin, α-catenin and CD44. 20 µg protein of each sample was loaded onto the same gels for the analysis of Endo180, uPA, uPAR, phospho-MLC2 and MLC. Each sample was supplemented with 1 µl β-mercapto-ethanol prior to loading with the exception of samples used for the analysis of CD44, Endo180 or uPAR. Electrophoresis was performed in 1X TG-buffer (BioRad, Current Protocols) supplemented with 0.1 % w/v SDS using the BioRad Mini Protean III cell system and a BioRad power pack set at 150 V. Electrophoresis was stopped when the bromphenol blue dye front had migrated from of the bottom of the gel.

Normally 12.5 µg of protein was loaded onto a 4-20% w/v acrylamide gradient gel (Precise Protein Gels, Pierce, Thermo Scientific). Electrophoresis was performed in 1X Tris-HEPES-buffer (Sigma, UK) supplemented with 0.1 % w/v SDS using the BioRad Mini Protean III cell system and a BioRad power pack set at 150 V. All other procedures were as described above.

### 2.2.7 Phos-Tag

Cells were grown under assay and cell line specific conditions. In a cold room, medium was decanted from petri dishes and petri dishes placed on ice. Residual medium was aspirated and cell layer washed with ice-cold PBS. Remaining PBS was aspirated and 1X SDS-PAGE loading buffer added to the centre of the dish. A 1 ml Gilson pipette tip was cut at a 30-degree angle with scissors and moved describing small fast circles slowly over the whole surface of the petri dish. The DNA/protein gel was carefully pipetted into 1.5 ml tubes and heat inactivated at 95$^{o}$C for 5 minutes. Subsequently, the samples were sonicated three times at 10 Hz for 5 seconds (MSE, Soniprep 150, Sanyo, Japan) to sheer the DNA and reduce the viscosity. Samples were stored at -80$^{o}$C until usage in Phos-Tag gel shift assay.

#### 2.2.7.1 Standard assay - 100 µM Phos-Tag

| Example of a Phos-Tag resolving gel | |
|---|---|
| 30 % w/v acrylamide solution | 2.33 mL |
| 1.5 mol/L Tris-HCl buffered solution pH 8.8 (incl. SDS) | 1.75 mL |
| 5.0 mmol/L Phos-tag | 0.14 mL |
| 10 mmol/L MnCl2 solution (the same volume of Phos-tag) | 0.14 mL |
| distilled water | 2.52 mL |
| TEMED (tetramethylethylenediamine) | 20 uL |
| 10% w/v APS in distilled water | 0.10 mL |
| resolving gel solution (7 mL: 100 µmol/L Phos-Tag & 10 % w/v acrylamide); acrylamide and distilled water adjusted for final acrylamide concentration; Phos-Tag and $MnCl_2$ adjusted for final Phos-Tag concentration; $MnCl_2$ molarity = 2X Phos-Tag molarity | |

Phos-Tag containing and Phos-Tag and $MnCl_2$ free control gels were cast**.** 7% acrylamide gels were used unless otherwise indicated. The stacking gel was cast using standard conditions (Current Protocols). 10 µl of sample was loaded into each

lane and standard gel electrophoresis performed at 100 V. Gels were used for standard Western Blot assay including EDTA wash to remove manganese ions (see **Section 2.2.8**). This protocol is based on instructions by Wako Ver. 8 (2010/8).

### 2.2.7.2 Agarose-acrylamide-hybrid gels - 20 µM Phos-Tag

| Example of an agarose-stabilised Phos-Tag resolving gel | |
|---|---|
| 30 % w/v acrylamide/bis solution | 0.70 ml |
| 1.5 mol/L Tris-HCl buffered solution pH 8.8 (+SDS) | 1.75 ml |
| 5.0 mmol/L Phos-Tag | 28 µl |
| 10 mmol/L $MnCl_2$ solution (the same volume as Phos-Tag) | 28 µl |
| TEMED | 7 µl |
| distilled water | 2.05 ml |
| NB. warm mixture to 60°C | |
| 1.5 % w/v agarose solution (agarose with high gel strength) | 2.33 ml |
| NB. warm to 95°C | |
| 10 % w/v APS in distilled water | 100 µl |
| resolving gel solution (7 ml) = 20 umol/L Phos-Tag, 3 % w/v acrylamide, 0.5 % w/v agarose; acrylamide and distilled water adjusted for the final acrylamide concentration (2.7-3.5 % w/v); components mixed and warmed to 60°C; gel casting apparatus and pipettes warmed to 60°C in oven; boiling agarose added; APS added and rapidly mixed before quickly casting gel | |

| Example of an agarose-stabilised stacking gel | |
|---|---|
| 30 % w/v acrylamide/bis solution | 0.20 ml |
| 0.5 mol/L Tris-HCl buffered solution pH 6.8 (+ SDS) | 0.50 ml |
| TEMED | 2 µl |
| distilled water | 0.58 ml |
| NB. warm mixture to 60°C | |
| 1.5 % w/v agarose solution (agarose with high gel strength) | |
| NB. warm to 95°C | 0.67 ml |
| 10 % w/v APS in distilled water | 50 µl |
| stacking gel solution = 3 % w/v acrylamide + 0.5 % w/v agarose; mix components and warm to 60°C; gel casting apparatus and pipettes to 60°C oven; boiling agarose added; APS added and rapidly mixed before quickly casting gel | |

Gel casting apparatus with clean glass plates and pipettes have to be pre-warmed in an oven to 60°C. The gel mix was prepared in a 50 ml falcon tube and placed in a 60°C water bath. Subsequently, agarose solution was prepared in a microwave and added to gel mix while still piping hot. After addition of freshly prepared APS, the gel mix was pipetted into the pre-warmed casting apparatus. Stacking gel was allowed to polymerise for 20 minutes. After 20 minutes a small layer of agarose the separated from the gel was removed using a syringe needle. After removal of a 1-2 mm agarose layer, the stacking gel was prepared and cast in the same manner. However, the already cast resolving gels were not placed in the oven. Gels were allowed to polymerise for 20 minutes and subsequently loaded with 10 µl sample per well and resolved at 15 mA/gel using standard 1X TG running buffer. Similar to agarose-free acrylamide gels, hybrid gels were incubated for 10 minutes in transfer buffer with 1 mM EDTA for the removal of manganese ions and another 10 minutes

in EDTA free transfer buffer. Transfer sandwich was assembled as usual, however, the transfer was run at 3.5 V/cm for 16 hours. This protocolwas based on findings by Kinoshita and co-workers (Kinoshita et al., 2009).

#### 2.2.7.3 Low current assay - 3.5 µM Phos-Tag

Phos-Tag-containing and Phos-Tag/$MnCl_2$-free control gels were cast**.** The acrylamide concentration was lowered to 5 % v/v and the Phos-Tag concentration was adjusted to 3.5 µM. The stacking gel was cast using standard conditions (Current Protocols). 10 µl of sample was loaded into each lane and standard gel electrophoresis at 5 mA/gel performed. Gels were used for standard Western Blot assay including EDTA wash to remove manganese ions (see **Section 2.2.8**). The protocol was adapted from Nature Protocols Exchange (Tomida et al., 2008).

### 2.2.8 Western Blot

Gels were incubated in transfer-buffer (1X TG with 10 % v/v methanol) for 20 minutes. In the case of Phos-Tag containing gels the manganese ions were removed by incubation for 10 minutes in transfer-buffer with 1 mM EDTA, EDTA was removed by subsequent incubation for 10 minutes in pure transfer-buffer. Separated proteins were transferred onto PVDF-FL membranes using the BioRad Transblot Mini Cell system and a BioRad power pack set at 100 V for 2 hours. In the case of proteins smaller than 50 kDa the transfer was limited to 1h. PVDF-FL membranes were activated in methanol prior to equilibration in transfer buffer. After the transfer, PVDF-FL membranes were directly placed in methanol for a few seconds and dried on filter paper for 15 minutes to enhance protein binding to the membrane. Membranes were subsequently activated in methanol and blocked with 5% w/v skimmed dry milk (Tesco) diluted in PBS-T for 1 hour at room temperature. After 3X 5 minutes washes in 50 ml PBS-T, membranes were incubated with the appropriate primary antibody (**Table 2.1**) diluted in PBS-T + 5 % w/v BSA + 0.02 % w/v $NaN_3$ over night at 4°C. Next morning, membranes were washed 3X in PBS-T and incubated for 1 hour with the appropriate secondary antibody (anti-mouse and

anti-rabbit IgG HRP conjugates (Jackson or Santa Cruz, USA) diluted 1:10,000 in PBS-T + 5 % w/v skimmed dry milk. Milk was filtered through a funnel made out of standard kitchen paper prior to antibody addition. After 3 washes in PBS-T the PVDF-FL membranes were incubated with ECL/ECL plus or Western Blot reagent (GE Healthcare or Millipore) and exposed to ECL Hyperfilm (GE Healthcare, UK) or an ImageQuant LAS 4000 system (GE Healthcare).

In some cases fluorescent secondary antibodies (LI-COR) were used instead of HRP-conjugates. The fluorescent signal was recorded on a Odyssey Scanner (LI-COR). Under these circumstances a commercial blocking solution was used for initial blocking as well as primary and secondary antibody incubations. Band intensities were quantified using the ImageQuant or ImageJ software (GE Healthcare, NIH).

| Table 2.1. Antibodies used for immunoblot analysis | | | | | | |
|---|---|---|---|---|---|---|
| Antigen (species) | Clone (species) | Cat No. | Supplier | Stock conc. [mg/ml] | Dilution | Final conc. [µg/ml] |
| pan-cytokeratin (cow) | pAb (rabbit) | Z0622 | Dako | 10.7 | 1:10000 | 1.07 |
| E-cadherin (human) | HECD-1 mAb (mouse) | ab1416-500 | Abcam | 0.05 | 1:1000 | 0.05 |
| vimentin (human) | V9 mAb (mouse) | V6630 | Sigma | ascites | 1:200 | ~0.5 |
| α-catenin (human) | pAb (rabbit) | NB120-6299 | Novus Biologicals | NA | 1:4000 | NA |
| uPAR (human) | pAb (rabbit) | 399R | America Diagnostica | 0.5 | 1:500 | 1 |
| uPA (human) | pAb (rabbit) | ab24121 | Abcam | 0.5 | 1:500 | 1 |
| AR (human) | pAb (rabbit) | N-20 | Santa Cruz | 0.2 | 1:1000 | 0.2 |
| CD44 (human) | E1/2.8 mAb (mouse) | NA | Clare Isacke | hybridoma supernatant | 1:5 | 2 |
| p-MLC2 (Ser19) (human) | pAb (rabbit) | #3671 | Cell Signalling | NA | 1:1000 | NA |
| MLC (chicken) | MY21 mAb (mouse) | M4401 | Sigma | ascites | 1:1000 | ~0.1 |

| | | | | | | |
|---|---|---|---|---|---|---|
| Endo180 (human) | A5:158 mAb (mouse) | NA | Clare Isacke | hybridoma supernatant | 1:5 | 2 |
| Endo180 (human) | E1:183 mAb (mouse) | NA | Clare Isacke | hybridoma supernatant | 1:5 | 2 |
| Endo180 (human) | 39.10 mAb (mouse) | NA | Clare Isacke | 10 | 1:4000 | 2.5 |
| Endo180 (human) | pAb (rabbit) | CAT1 | Clare Isacke | 0.3 | 1:300 | 1 |
| Endo180 (human) | pAb (rabbit) | CAT2 | Clare Isacke | 0.3 | 1:300 | 1 |

### 2.2.9 Immunofluorescent staining and analysis using ImageXpress$^{MICRO}$

5 x $10^3$ cells/well were seeded in each well of a 96-well plate (Optilux clear bottom black plates). At assay specific time, medium was aspirated and replaced with pre-warmed 4 % w/v PFA diluted in PBS. Cells were incubated at 37°C for 10 minutes and the reaction quenched with 100 mM glycine in PBS and 0.02 % w/v $NaN_3$. Cells were stored at 4°C until staining. Cells were blocked and permeabilised for 30 minutes in IFF + 0.2 % w/v saponin or 0.3 % v/v Triton-X-100. When saponin was used, 0.2 % w/v saponin was added throughout all antibody incubations and in all washing buffers. Staining for structural elements (α-tubulin, F-actin was performed in Triton-X-100-buffer; staining for other markers (especially in vesicular compartments, such as Endo180) was carried out in saponin-buffer. Cells were incubated in 50 µl primary antibody overnight at 4°C and washed twice in permeabilisation/blocking-buffer. Incubation with 1:500 goat anti-mouse or rabbit Alexa Fluor-405/-488/-546/-633 (Invitrogen) was performed for 2 hours. To counter stain for the actin cytoskeleton 1:500 phalloidin Alexa Fluor-488/-546/-633 (Invitrogen) was diluted together with the secondary antibody. Cells were washed twice in permeabilisation/blocking buffer. To stabilise the antigen-antibody interactions cells were fixed after the staining procedure for 15 minutes with 4% w/v PFA diluted in PBS and washed twice in PBS. Nuclei were counterstained with 1:1000 DAPI or TO-PRO-3 (Invitrogen) for 5 minutes. Cells were washed twice in PBS. Images were acquired with IXM and analysed using MetaXpress and AcuityXpress software packages. Positive and negative cells were differentiated using the "Multiple-wave-length scoring" module of the MetaXpress 2.0 software package. Nuclei were detected in the DAPI/TO-PRO-3 channel and surrounding staining in the FITC/TRITC channel was counted towards the closest Nucleus. A maximum distance was defined to exclude extracellular staining.

### 2.2.10 Immunofluorescence and confocal microscopy

Cells were seeded on glass coverslips, grown to appropriate densities and fixed with pre-warmed 4 % w/v PFA in PBS for 10 minutes at 37°C. Cells were washed twice with PBS and then stained the same way as described (**Section 2.2.9.2**). Glass coverslips were mounted on glass slides with a glycerol based mounting medium (Vetcashield) and sealed using clear nail varnish (Boots). Images were acquired using a Zeiss LSM510 confocal microscope and processed using LSM (Zeiss, Germany) and ImageJ (NIH, USA) software.

| Table 2.2. Antibodies used for immunofluorescent staining and flow cytometry | | | | | | |
|---|---|---|---|---|---|---|
| Antigen (species) | Clone (species) | Product-code | Supplier | Stock-conc. [mg/ml] | Dilution | Final-conc. [µg/ml] |
| pan-cytokeratin (cow) | pAb (rabbit) | Z0622 | Dako | 10.7 | 1:500 | 21.4 |
| vimentin (human) | V9 mAb (mouse) | V6630 | Sigma | ascites | 1:40 | ~2.5 |
| E-cadherin (human) | HECD-1 mAb (mouse) | ab1416-500 | Abcam | 0.05 | 1:50 | 1 |
| CD44 (human) | E1/2.8 mAb (mouse) | NA | Clare Isacke | hybridoma supernatant | 1:5 | ~2 |
| α-catenin (human) | pAb (rabbit) | NB120-6299 | Novus Biologicals | NA | 1:2000 | NA |
| α-tubulin (human) | DM1A mAb (mouse) | T6199 | Sigma | 1 | 1:1000 | 1 |
| isotype-control | NA (mouse) | MCA928 | SeroTec | 0.1 | 1:50 | 2 |
| isotype-control | NA (rabbit) | 61-0100 | Invitrogen | 0.5 | 1:250 | 2 |

### 2.2.11 Cell motility

Cells were grown on a 96-well plate at low density (2 x $10^3$ cells/well) 24 hours prior to image acquisition. 9 fields of view and 3 wells were acquired per cell line. Images were taken every 10 minutes for 12 hours with the IXM microscope. Cells were kept at 37°C in 5 % $CO_2$ throughout the procedure. Cells were tracked with the object tracker platform of the Metamorph software package and subsequently analysed in Mathematica for the generation of Box plots.

### 2.2.12 Dunn chamber chemotaxis

Cells were grown on 6-well plates (50 x $10^3$ cells/well) supplemented with sterile glass cover slips 24 hours prior to image acquisition. Clean Dunn chambers were removed from 70 % v/v ethanol storage solution and air-dried on filter paper under sterile conditions. The cell chemotaxis area was washed 3X with 200 ul medium and subsequently filled with 200 ul medium. Coverslips were placed with cells facing down onto the medium filled chemotaxis area. Excess medium was removed with filter paper and the coverslip placed in a position that a tiny opening (5 mm) to the outer media ring was left open. The other three sides were sealed with wax. We have used a simple soft brush normally used for painting watercolours (Selfridges). The medium from the outer ring was removed via a filter paper (capillary forces). Finally, we filled the outer ring with growth factor containing medium and sealed the remaining edge with wax. Dunn chambers were placed in the IXM and images acquired every 10 minutes for 12 hours. Cells tracks were digitalised using the object tracker platform of the MetaXpress software suite and tracks were subsequently analysed for directional migration using Mathematica. The Mathematica notebook was provided by Professor Graham Dunn (King's College London) and modified by Julian Gronau. Dunn chambers (Hawksley Scientific) were cleaned by 30 minutes sonication in acetone, 3X washes in MilliQ water, treated for 5 minutes with 10 % v/v hydrogen peroxide, 3X washes in MilliQ water and stored in 70 % v/v ethanol until the next usage.

### 2.2.13 Organotypic invasion assay

The technique was modified from the protocol established by Dr John Marshall (Nystrom et al., 2005).

#### 2.2.13.1 Preparation of organotypic gels - day 1

A cell suspension containing fibroblasts at the desired concentration ($10^7$ cells/ml) was prepared in DMEM + 10 % v/v FCS. After trypsination the fibroblasts were pelleted by centrifugation to remove residual trypsin from the cell suspension.

| Organotypic gels | |
|---|---|
| collagen : Matrigel (1:1) | 7 Volumes (3.5 : 3.5) |
| 10X DMEM | 1 Volume |
| FCS | 1 Volume |
| cells (fibroblasts) | 1 Volume |
| Example: | |
| collagen | 1.75ml |
| Matrigel | 1.75ml |
| 10X DMEM | 0.5ml |
| FCS | 0.5ml |
| cell suspension | 0.5ml |
| mix the components by careful pipetting up and down with a 5 ml tissue culture pipette; pipette collagen and Matrigel using a 5 ml tissue culture pipette due to high viscosity | |

- 1 ml of the mixture was placed into each well of a 24 well plate and the gels allowed to solidify at 37°C for 1 hour in a tissue culture incubator. Subsequently 1ml of DMEM + 10% v/v FCS was added to the top of each gel and left in the incubator overnight.

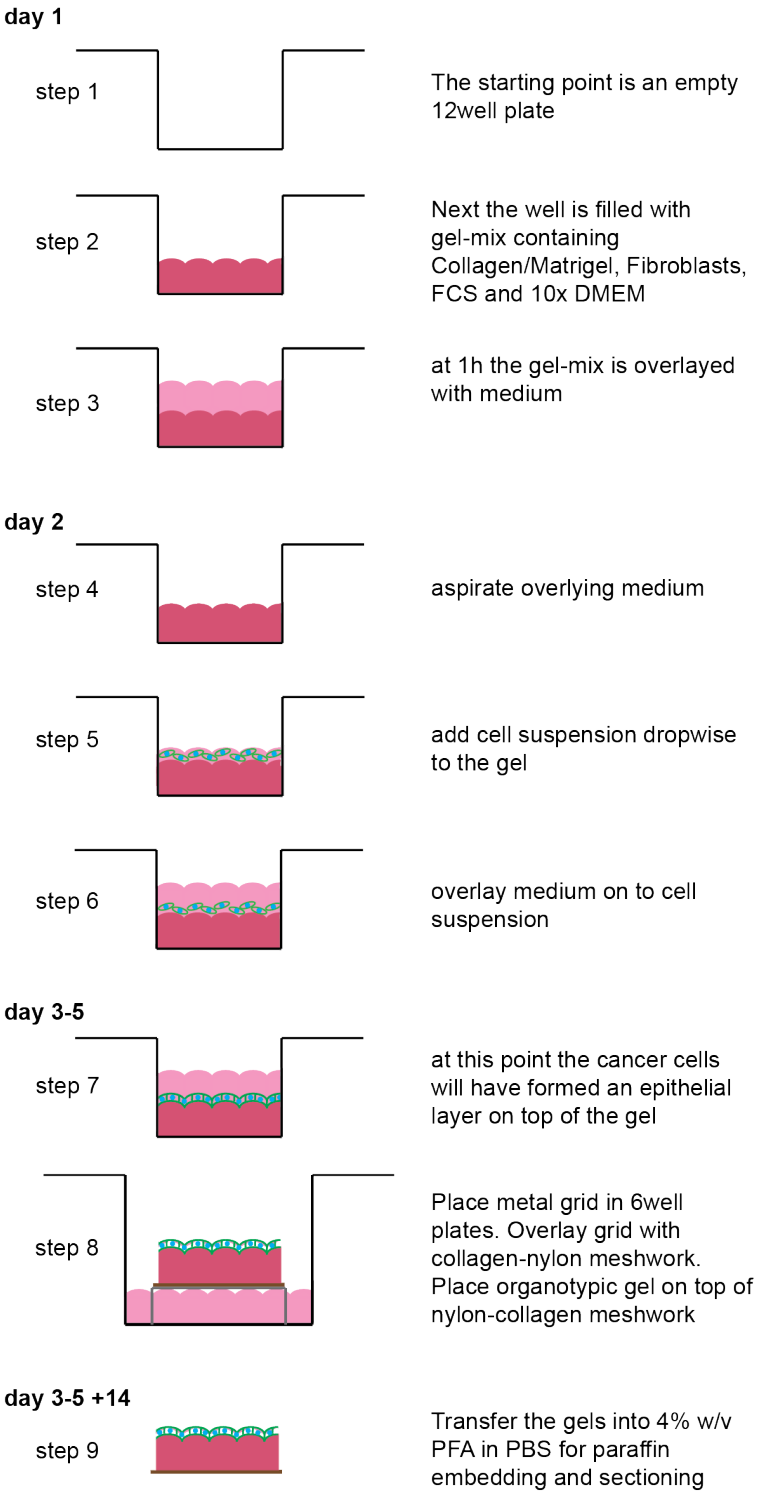



**Figure 2.2.13 Organotypic invasion assay:** On **day 1**, fibroblasts are embedded into a mixture of Collagen and Matrigel. On **day 2**, this organotypic gel is overlaid with the cancer cell suspension. On **day 3-5** (1-3 days after addition of the cancer cell suspension), the gels are raised onto metal grids with collagen embedded nylon meshwork as under layer for support. **During the 14 day long** incubation period the medium in the 6well plate is changed every 2-3 days. **After 14 days**, the gels are fixed in 4% w/v PFA in PBS

### 2.2.13.2 Addition of cancer cells - day 2

- Prostate cells were trypsinised and residual trypsin removed by centrifugation and resuspension in DMEM + 10 % v/v FCS or keratinocyte growth medium. The concentration of the cell suspension was adjusted to 5 x $10^6$ cells/ml. After careful aspiration of the overlay media (1 ml Gilson pipette) from the gels prepared on the day before, 100µl of cancer cell suspension (5 x $10^5$ cells) was added drop-wise to the centre. Gels were subsequently overlaid with 1 ml of DMEM 10 % v/v FCS or keratinocyte growth medium. The gels were incubated for 2-3 days.

### 2.2.13.3 Preparation of nylon sheets - day 2

| Gel mixture for nylon sheets used to support organotypic gels | |
|---|---|
| collagen | 7 Volumes |
| 10X DMEM | 1 Volume |
| FCS | 1 Volume |
| 1X DMEM + 10% FCS | 1 Volume |
| Example: | |
| collagen | 3.5 ml |
| 10X DMEM | 0.5 ml |
| FCS | 0.5 ml |
| 1X DMEM + 10% FCS | 0.5 ml |
| mix components by carefully pipetting up and down with a 5 ml tissue culture pipette; only pipette collagen with a 5 ml tissue culture pipette due to high viscosity | |

- For each gel one nylon sheet was required. The nylon sheets were autoclaved and transferred with sterile tweezers into petri dishes. The necessary amount of NaOH needed to neutralise the acid via the method indicated on the datasheet that comes with the collagen I solution was calculated. After mixing and neutralising the gel solution a 1 ml Gilson pipette was used to add 250 µl of the mixture drop wise to the centre of each nylon-sheet. The solution distributed itself over the entire meshwork. The gels were allowed to solidify at 37°C for 15-30 minutes. To enhance stability the gels were cross-linked with glutaraldehyde for 1 hour at 4°C. 10 ml of 1 % v/v

glutaraldehyde in PBS was used for each 10 ml petri dish. Subsequently, the petri dishes were carefully washed 3X with 25 ml of PBS and 1x with 25 ml DMEM-10% v/v FCS and stored in 25 ml DMEM-10% v/v FCS at 4°C overnight.

### 2.2.13.4 Raising gels to grids - day 3-5

- Sterile tweezers were used to place one autoclaved steel grid into each well of a 6-well plate. Each grid was overlaid with a gel-coated nylon sheet. The fibroblast gels overlaid with tumour cells were removed from the 24-well plate using one or two spatulas and carefully placed onto the gel-coated nylon sheets. The wells were subsequently filled with 4.9 ml DMEM + 10 % v/v FCS or keratinocyte growth medium. The medium was added to reach the lower surface of the grid but not to submerge the gel. In order to maintain growth factor levels and control the pH media was replaced every 2 days.

### 2.2.13.5 Harvesting gels - day 3-5 + 14 (17-19)

- 14 days after raising the gels onto the grids the gels were transferred into tubes containing standard tissue fixative (4 % w/v PFA in PBS) and after 2 days the gels were transferred into cassettes for paraffin embedding and submerged in 70 % v/v alcohol in MilliQ water. Cassettes were handed over to the histopathology service at Hammersmith hospital and embedded into paraffin blocks. Blocks were cut into 10 μm sections and stained with haematoxylin and eosin Y or used for fluorescent immunohistochemistry for cell and marker visualisation.

### 2.2.14 Paraffin embedded tissue staining

#### 2.2.14.1 De-paraffinisation

Slides were submerged in xylene for 5 minutes in three different baths. Subsequently, slides passed through two baths of 100 % ethanol and 2 baths of 95 % v/v ethanol for 1 minute each. Slides were incubated in 80% v/v and 70% v/v ethanol for 1 minute until they were rinsed under running tap water for 5 minutes.

#### 2.2.14.2 Antigen retrieval

##### 2.2.14.2.1 Antigen retrieval - proteinase K

| TE-$CaCl_2$ buffer<br>50 mM Tris Base, 1 mM EDTA, 5 mM $CaCl_2$, 0.5 % v/v Triton X-100, pH 8.0 | |
|---|---|
| Tris Base<br>EDTA<br>$CaCl_2$<br>Triton X-100<br>distilled water | 6.10 g<br>0.37 g<br>0.56 g<br>5 ml<br>1000 ml |
| mix to dissolve, adjust to pH 8.0 using 10 N HCl, store at room temperature | |

| 20X Proteinase K stock solution<br>400 ug/ml (12 units/ml) | |
|---|---|
| proteinase K (30 units/mg)<br>TE-CaCl2 Buffer, pH8.0<br>glycerol | 0.008 g (8 mg)<br>10 ml<br>10 ml |
| proteinase K added to TE-$CaCl_2$ buffer until dissolved, glycerol added, mix well; aliquots store at –20°C for 2-3 years | |

| 1X working solution<br>20 ug/ml or 0.6 units/ml | |
|---|---|
| Proteinase K Stock Solution (20X)<br>TE-$CaCl_2$ Buffer, pH8.0 | 1 ml<br>19 ml |
| mix well; solution stable for 6 month at 4°C | |

Slides were covered with Proteinase K working solution, incubated for 20 minutes at 37°C in an humidified chamber, cooled to room temperature for 10 minutes and washed 3X in PBS. This protocol is from the IHC world database.

### 2.2.14.2.2 Antigen retrieval - citrate buffer

| Citrate Buffer<br>10 mM citric acid, 0.05% Tween 20, pH 6.0 | |
|---|---|
| citric acid (anhydrous)<br>distilled water<br>Tween-20 | 1.92 g<br>1000 ml<br>0.5 ml |
| mix to dissolve, adjust pH to 6.0 with 1N NaOH, add Tween-20, store at room temperature for 3 months or 4°C for longer storage | |

A staining jar containing citrate buffer was placed into a 95°C water bath and the citrate buffer was allowed to reach 95°C. Slides were placed into the jar and incubated for 20 minutes. The jar was removed from the water bath, the jar was allowed to cool at room temperature for 20 minutes. Slides were washed 3X in PBS. Protocol was from the IHC world database and adapted by Dr Matthew Caley and Julian Gronau.

### 2.2.14.3 DAB staining

DAB staining was performed using a commercial kit (Invitrogen) with one modification: primary antibody incubation over night at 4°C in an humidified chamber. After DAB-staining, 1 ml of Mayer's haematoxylin was pipetted onto the slide and incubated for 5 minutes. Slides were washed for 5 minutes under running tap water, blued with ammonia water and subsequently de-hydrated (see **Section 2.2.14.1** - but in the reverse order). A drop of DPX mounting medium was pipetted onto sections and overlaid with a cover slip. Images were acquired using a slide-scanning microscope.

#### 2.2.14.4 DAB staining controls

Staining of human tissue sections for Endo180 using the A5/158 and 39:10 antibodies was established in the Isacke lab and the Sturge lab. Those antibodies were used by both labs for staining of human tissue sections in several prior studies (Caley et al., 2012; Honardoust et al., 2006; Huijbers et al., 2010; Kogianni et al., 2009; Wienke et al., 2007).

A5/158, 39:10 and Collagen antibodies were tested by co-workers in conjunction with the applied DAB staining kit (Invitrogen), the citrate buffer antigen retrieval method as well as the proteinase K antigen retrieval method (Caley et al., 2012; Kogianni et al., 2009) (Rodriguez-Teja et al in preparation). The exact tissue (PR208 and FDA TMAs) stained for this work was not separately stained with an isotype control antibody.

The Newcastle tissue micro array was stained by Prof Robson's group in Newcastle (see **declaration of originality**). The 39:10 and A5/158 antibodies underwent their standard tests before being applied to the patient arrays slides. TMA generation and antigen retrieval (citrate buffer method) are described in (Sahadevan et al., 2007).

### 2.2.14.5 Eosin Y and haematoxylin staining

| Eosin Y working solution | |
|---|---|
| eosin Y stock solution<br>95 % v/v ethanol<br>glacial acetic acid | 100 ml<br>780 ml<br>4 ml |
| mix well | |

| Acid alcohol solution (1 %) | |
|---|---|
| hydrochloric acid<br>70 % v/v ethanol | 1 ml<br>50 ml |
| mix well | |

After de-paraffinisation 1 ml of Mayer's Haematoxylin was pipetted onto the sections, incubated for 5 minutes and washed under running tap water for 5 minutes. Staining was differentiated by dipping slides for 5 seconds in acid alcohol, washing under running tap water for 1 minute and blued by dipping in 0.2 v/v % ammonia solution for 30 seconds. After washing for 5 minutes under running tap water slides were dipped ten times in 95 % v/v ethanol then counterstained in eosin Y working solution for 1 minute and dehydrated (see **Section 2.2.14.1** - but in the reverse order, starting with 95% ethanol). Stained sections were mounted using DPX mounting medium.

### 2.2.15 Molecular Cloning

Site directed mutagenesis was carried out using a commercial Site-directed mutagenesis kit (Strategene). The kit contained XL10-Gold ultra competent cells, PfuTurbo DNA Polymerase and all necessary buffers, dNTP mix and controls. Primer sequences (**figure 3.6.3**) were designed according to the instructions provided by Strategene. The oligos were procured from Invitrogen. Clones were screened by restriction digest and sequencing of the mutated region.

In order to clone phmKO2NMLinker Endo180, PCR was carried out using high fidelity polymerase kit (Roche). The forward primer was designed to bind upstream of the Endo180 encoding sequence in order to ensure that the PCR product contained the NotI restriction site that is located several bases upstream of the Endo180 sequence in the pcDNA3 Endo180 template vector (**figure 4.9.2**). The reverse primer was designed with an overhang to add another NotI restriction to the PCR product and to exclude the stop codon. The PCR product was resolved on an Ethidium bromide supplemented agarose gels and excised from the gel using a scalpel under UV light. The product was extracted from the excised agarose using the QIAEX kit (Qiagen). NotI enzyme and buffer were procured from NEB. PCR products and empty vectors were digested under standard conditions as described in the NEB catalogue. Ligation of PCR products and vector was performed using the Takara Ligation Kit V 2.1 (Lonza). Super competent DH5 alpha cells (Invitrogen) were transformed with ligated vector according to the instructions provided by Invitrogen. Several individual clones were analysed by restriction digestion with HindIII (NEB) and resolution on Agarose gels. Correctly orientated Endo180 resulted in two bands at approximately 4350bp and 4350bp whereas incorrectly ligated insert produced one single band of 9100bp.

# 3. Structural analysis of Endo180

## 3.1 Introduction

Before investigating the role of Endo180 in prostate cancer progression, EMT and its potential as a new biomarker the biochemical and cell biological characterisation of this receptor was re-addressed. Some of this data was generated more than two decades ago, before *MRC2* (the gene which encodes Endo180) was cloned and sequenced (Isacke et al., 1990; Sheikh et al., 2000; Wu et al., 1996). As a first step, we set out to shed more light on Endo180's physiological function by re-evaluating its evolutionary history and some aspects of its biochemistry.

The investigation was started with an *in silico* analysis of the evolution of the Endo180 encoding gene *MRC2*. To date, Endo180 has been characterised, cloned and sequenced in mice and humans. All sequences inventoried in the NCBI database were analysed for homology to *MRC2*. Later the evolutionary conservation of the individual domains that define the Endo180 protein was analysed, namely the Ricin-B (CRD) fold, the FNII fold and the CTLD fold. Afterwards the evolutionary conservation of individual residues that had a function attributed in biochemical and cell biological studies in the past was addressed. Lastly, a potential putative uPA-binding domain in the CTLD-4 domain of Endo180 was analysed for its localisation in the three-dimensional fold of the domain and for evolutionary conservation. The evolutionary conservation of the uPA-uPAR-Endo180 tri-molecular complex was analysed before this background. Lastly, a null-mutant for the potential uPA-binding site was generated in an Endo180 expression vector.

## 3.2 Evolutionary conservation of Endo180

All sequences inventoried in the NCBI database were screened for homology to members of the mannose receptor gene family. The family consists of four members: the macrophage mannose receptor, Endo180, DEC-205 and phospholipase A2 receptor.

Genes homologous to members of the mannose receptor family were identified in several vertebrates, in addition to mice, humans and cattle where the presence of Endo180 has already been confirmed. The results were not limited to mammals. For example, the *Danio rerio* (zebrafish) genome was found to contain genes homologous to all four members of the family. Homologues for some family members, including Endo180, were found in *Xenopus tropicalis*. In species other than vertebrates for example *Drosophila melanogaster* the entire family was absent. A phylogenetic tree of all species containing a gene homologous to *MRC2* is shown in **Figure 3.3.1 and Figure 3.4.4.3**.

## 3.3 Evolutionary conservation of the cytoplasmic tail of Endo180

Based on a list of predicted Endo180 encoding genes stored in the NCBI database an alignment model was built using the COBALT suite of the NCBI toolkit. **Figure 3.3.1** shows the multiple alignment of the full length cytoplasmic tail of Endo180 of all species in which an encoding gene was identified. Isacke and co-workers mutated four residues (a dihydophic endocytosis motif and an LDL receptor type endocytosis motif) in the cytoplasmic tail of human Endo180 (marked in light blue in **Figure 3.3.1)** and studied the effect of these mutations on receptor recycling (see **Section 1.4.7**) (Howard and Isacke, 2002).

Although no function was attributed to the Arginine and Glutamate residues (LDL receptor type endocytosis motif), all four residues (both endocytosis motifs) were conserved with 100% homology across all species. Interestingly, a potential 14-3-3-protein binding site (RxxS/TxP, marked in yellow in **Figure 3.3.1**) was conserved in all species with the exception of *Tetraodon nigroviridis*. Both rodent genes contain

an additional amino acid residue between the Arginine and the Serine what might render the motif non-functional.

Overall, the region around the functional dihydrophobic internalisation motif, LV, is most conserved within the cytoplasmic tail. Four amino acids upstream and four amino acids downstream of the motif show 100% homology between all species. Another region of conservation is found around the essential Arginine for the supposedly non-functional LDL-type receptor endocytosis motif. One amino acid upstream and two amino acids downstream are 100 % conserved across all species.

The 14-3-3-protein binds and masks phosphorylated substrates (the Serine residue within the RxxS/TxP motif) of PKC. Furthermore, Isacke and co-workers showed phosphorylation of unidentified Serine residues within the Endo180 protein. In order to further investigate Serine phosphorylation in the cytoplasmic tail of Endo180 and the potential functionality of the predicted 14-3-3 motif, phosphorylation was predicted in the Endo180 cytoplasmic tail *in silico*. The group based prediction system (GPS) contains patterns for phosphorylation substrates for a wide range of kinases (Xue et al., 2008). The cytoplasmic tail of human, rat, mouse and frog Endo180 was analysed with the GPS tool. The raw scores were normalised and ranked. The five highest-ranking potential kinase substrates within the Endo180 cytoplasmic tail are marked in red in **Figure 3.3.1.** GPS predicted the Serine/Threonine residue of the potential 14-3-3-motif in frogs and humans to be a potential kinase substrate. Interestingly, the Serine residues in rodents at the same position generated lower scores and were not amongst the five sites with the highest probability to be kinase substrates. Furthermore, in all four tested species, the Serine residues in juxta-position to the dihydrophobic internalisation motif are identified as potential kinase substrates.

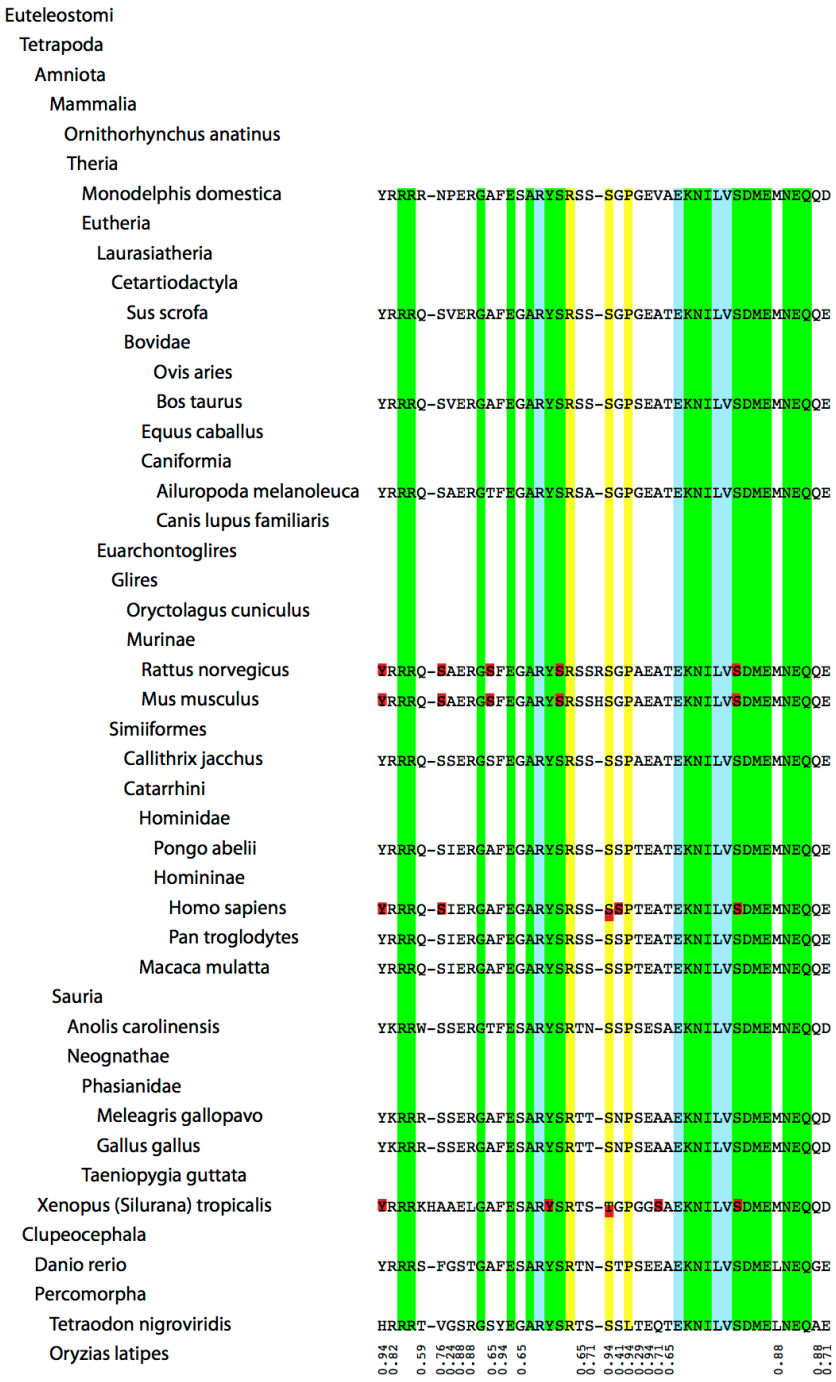



**Figure 3.3.1 Evolutionary conservation of the cytoplasmic tail of Endo180.** The full-length cytoplasmic tail of Endo180 is shown for all organisms with an Endo180 encoding gene stored on the NCBI database. Putative phosphorylation sites were predicted using the group based prediction system (GPS) in *Homo sapiens*, *Xenopus tropicalis*, *Mus musculus* and *Rattus norvegicus*. The five highest scoring residues in each species are marked in red. A potential 14-3-3 protein-binding motif is marked in yellow. Residues previously tested for a function in receptor internalisation are marked in light blue. The percentage of sequence identity is indicated below each residue wherever this has been calculated as less than 1.0 (100%). All organisms were ordered in genetic trees using the tax-id system of NCBI.

## 3.4 Evolutionary conservation of ectodomains in the mannose receptor family

One Ricin-B folded domain (CRD), one FNII domain and eight CTLDs (see **Figure 1.4.5**) constitute the extracellular part of Endo180. Other members of the mannose receptor family have a similar domain structure. The conserved domain database was used to investigate the evolutionary heritage of the three folds that can be found in the extracellular parts of members of the mannose receptor family. Phylogenetic trees were generated for each of the three folds via the NCBI conserved domain database. Next to each phylum it is indicated how many domains were detected in all sequences inventoried in the NCBI database. Furthermore, the database provides information about attributed functions of these domains.

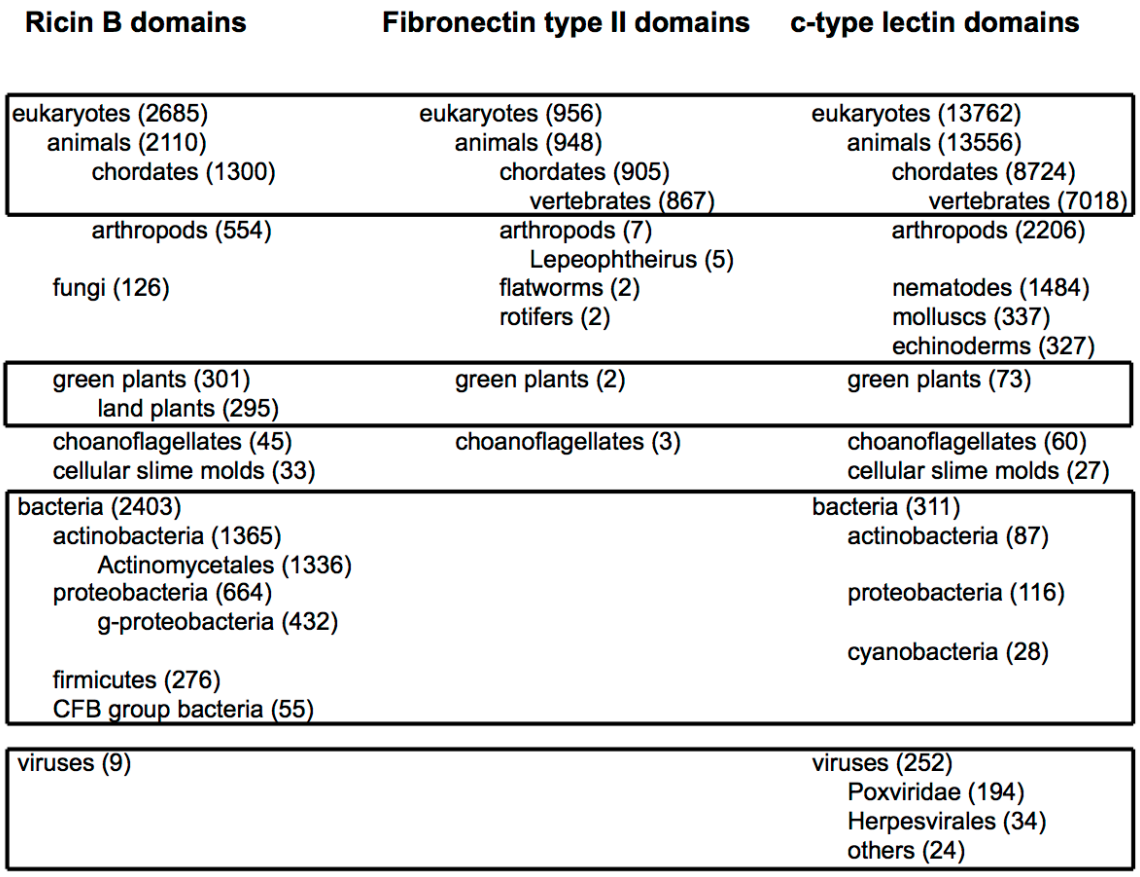



**Figure 3.4.1 Evolutionary conservation of Endo180 ectodomains.** Taxonomy trees were generated using the conserved domain database of NCBI. The number of open reading frames stored in the NCBI database, which contain one or more receptor domains is indicated in brackets after each class. Classes were broke out for more details if domains were significantly enriched in one particular subclass. Results have been simplified for better presentation. Original data can be found in the appendix (**figure 8.1**). The analysis includes evaluation of the ricin B domain (or cysteine-rich domain; CRD), fibronectin type II (FNII) domain and c-type lectin-like domains (CTLDs) of Endo180.

### 3.4.1 Ricin B – cysteine rich domain - CRD

According to the NCBI database, the function attributed to Ricin B domains is mainly sugar binding. 2685 Ricin B domain folds were detected in all eukaryotic genes inventoried and 2403 in bacterial genes. In comparison to the other two domains, approximately half of all sequenced domains are found in bacteria. Within eukaryotes, more than two thirds of all domains are found in animals. In the bacterial kingdom, large chunks are found in Actinomycetales and Proteobacteria (**Figure 3.4.1**).

### 3.4.2 Fibronectin type II domain - FNII

FNII domain folds mainly function as collagen binding domains. As shown in **Figure 3.4.1** FNII domains are almost exclusively present in vertebrates. Approximately, 90% of all domains are detected in sequenced vertebrates genomes.

### 3.4.3 C-type lectin-like domains - CTLDs

The CTLD fold is mostly associated with innate immune response according to the NCBI conserved domains database. The most attributed function is binding of bacterial cell walls. Less than 1 % of all detected domains with a CTLD fold are found in bacterial or viral genomes. The fold is limited to Pox and Herpes viruses, known for their advanced capabilities to modify the immune system of their hosts. While the FNII domain fold was mostly limited to vertebrates, the CTLD fold is common within a broad spectrum of animals. This aligns with its importance for the innate immune response. Only background levels can be detected in other eukaryotes such as plants.

## 3.5 interaction of Endo180 with uPA

As mentioned in **Section 1.4.8.2** a putative uPA interaction motif (KxxSSxR) was identified in Endo180 by Priessner and co-workers (Liang et al., 2003). However, it has never been investigated whether this potential interaction site is accessible for ligand binding on the surface of the Endo180 protein or buried inside the structure.

Sequence analysis revealed that the KxxSSxR motif is located in the fourth c-type lectin domain (CTLD-4) of Endo180. The crystal structure of Endo180 is not available. However, a high-resolution electron microscopy structure has been generated. This structure shows that the tip of the Endo180 protein forms a loop structure (see **Section 1.4.5**) and that the CTLD-4 domain appears to be accessible (Boskovic et al., 2006; Llorca, 2008; Rivera-Calzada et al., 2003). However, it remains to be clarified whether the KxxSSxR-motif is buried within the fold of the CTLD-4 domain or accessible on the surface of the CTLD-4 domain. The known structure of the CTLD-4 domain of the macrophage mannose receptor was selected as a template to build a three-dimensional structure of the CTLD-4 domain of Endo180 using the Swiss-model platform (**Figure 3.5.1**). In automatic mode, the Swiss model system selected a protein with high sequence homology but completely different fold as a template, this was probably caused by the variable loop sequences of the CTLD fold. Similar structural predictions were performed by using the Ricin B domain of MMR and the FNII domains of fibronectin as templates. The alignment between the CTLD-4 of MMR (template) and the CTLD-4 of Endo180 (target) is shown in **Figure 3.5.1**. Several gaps needed to be introduced in the middle of the sequence, residues 55-62 and 74-80. However, in **Figure 3.5.1** where the degree of sequence homology is colour-coded it can be seen that the several gaps and regions of low sequence homology are mainly located within the loop regions, whereas the structural helices and beta-sheets display almost perfect sequence homology.

```
TARGET    3                    RYCYKVF SSERLQDKKS WVQAQGACQE LGAQLLSLAS
1eggA     628   cpedwgassr t--slcfkly akg-khekkt wfesrdfcra lggdlasinn

TARGET                           sssss            hhhhhhhhhh    sss
1eggA                 sss      sssssss            hhhhhhhhhh    sss


TARGET    40    YEEEHFVANM LNKIFGESEP EIHEQHWFWI GLNRRDPRGG QSWRWSDGVG
1eggA     675   keeqqtiwrl itasg----- --syhklfwl glty------ ggftwsdgsp

TARGET          hhhhhhhhhh hhhh             sssss  sss
1eggA           hhhhhhhhhh hhhh             sssss  sss


TARGET    90    FSYHNFDRSR HDD-DDIRGC AVLDLA-SLQ WVAMQCDTQL DWICK --
1eggA     716   vsyenwayge pnnyqnveyc gelkgdptms wndincehln nwicqiqk

TARGET                             sss sssss    s ssssss      ssss
1eggA                              sss ssssss sss ssssss      sssssss
```



**Figure 3.5.1 Swiss model alignment of the CTLD-4 domain of Endo180.** The target (CTLD-4 domain of Endo180) was aligned against the template (CTLD-4 domain of the macrophage mannose receptor, 1EGG, chain A). (**upper half**) The sequence of the CTLD-4 domain of Endo180 starts at position 1 while the residues in 1EGG have been numbered by their position in the entire macrophage mannose receptor. The CTLD-4 domain starts at residue 628 in the macrophage mannose receptor. (**bottom half**) The sequence homology of the template with the CTLD-4 of Endo180 is rainbow colour-coded from high (blue) to low (red) in the predicted structural model of the CTLD-4 domain of Endo180.

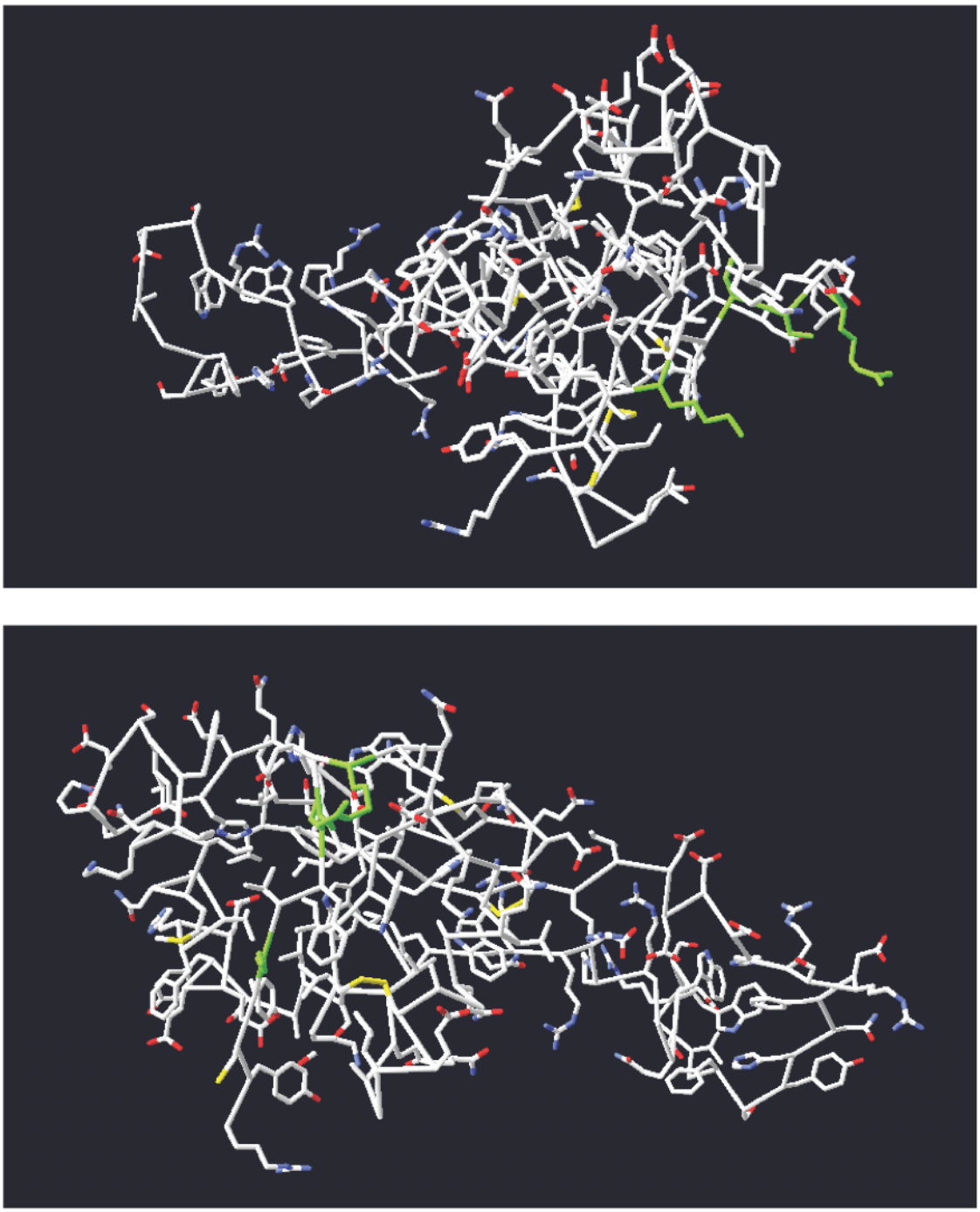


**Figure 3.5.2 3-D-projection of Swiss model for CTLD-4 of Endo180.** Structural model generated using Swiss model with the CTLD-4 of Endo180 selected as a target. Automatic template selection was deactivated and a template of the CTLD-4 domain of the macrophage mannose receptor was manually inserted. Residues KxxSSxR are highlighted in green. Two projections from different angles are shown.

A three-dimensional projection of the predicted CTLD4-domain of Endo180 revealed that the potential uPA interaction site is located in an accessible location at the protein surface (**Figure 3.5.2**).

These structural findings support the hypothesis that the predicted uPA-interaction motif is indeed functional and responsible for the formation of the uPA-uPAR-Endo180 trimolecular complex.

The earlier analysis of the cytoplasmic tail of Endo180 (**Section 3.3**) revealed that key functional residues are evolutionary conserved over all species containing a gene potentially encoding the Endo180 protein. To further test the hypothesis that the KxxSSxR motif is indeed functional, the evolutionary conservation of the motif was investigated. The potential uPA-binding motif is located within the first ten amino acids of the CTLD-4 domain of Endo180 (**Figure 3.5.3)**. The motif is 100 % conserved across all mammals. However, the motif is not found in any other animal. Overall conservation of CTLD-4 appears to be high.

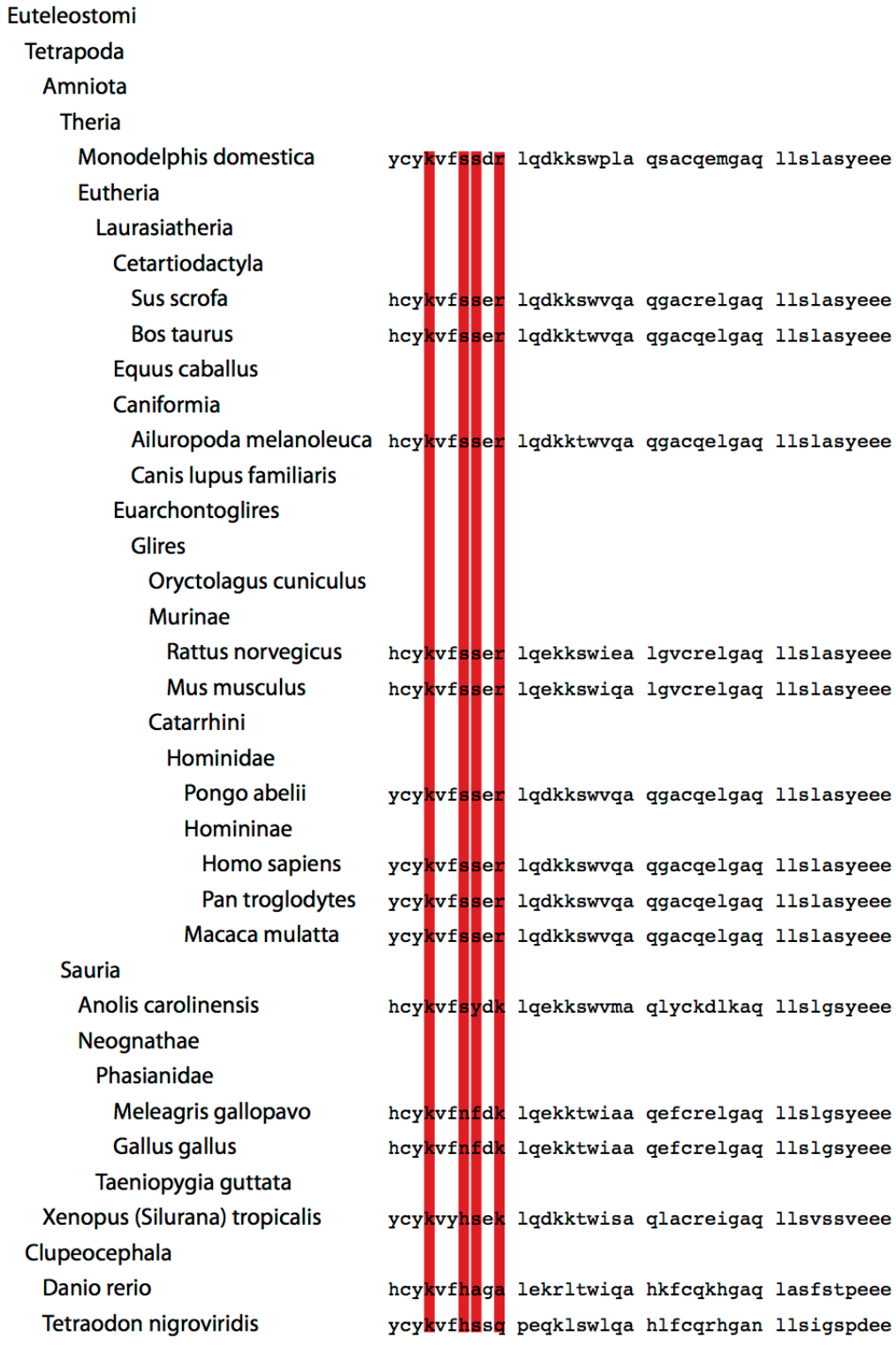



**Figure 3.5.3 Evolutionary conservation of potential uPA interaction site.** The first 40 amino acid residues of the CTLD-4 domain of Endo180 in all organisms with an Endo180 encoding gene stored in the NCBI database are shown. The putative uPA interaction motif KxxSSxR is marked in red. All organisms were ordered into genetic trees using the tax-id system of NCBI. (**red**) Only Theria display identical amino acid residues.

It is possible that uPA and uPAR are not present or may function differently in non-mammals. To test the latter hypothesis NCBI blast was used to identify all organisms that posses a gene encoding a protein homologous to uPA or uPAR in *Homo sapiens*.

uPA and uPAR were both present in mammals and other animals. However, the presence of a homologous gene does not guarantee that all functional residues/domains are conserved. To test the potential for uPA and uPAR to interact in a similar manner across all species the uPAR-binding domain of uPA, the ATF, was compared across all species. The ATF of uPA differs heavily in its first 30 amino acid residues (**Figure 3.5.4**). The COBALT introduced up to 15 gaps over this short stretch to compute the best possible alignment. ATF sequence homology was highly conserved where it binds to uPAR, no gap introduction was necessary to build the alignment (**Figure 3.5.4**). The only exception being *Danio rerio*, which lacks a uPAR interaction site. These findings suggest that uPA and uPAR interact in a similar manner across different species.

The kringle domain of uPA was aligned for all species containing an open reading frame that encodes uPA (**Figure 3.5.5**). The kringle domain was highly conserved between all mammals. However, with the exception of *Anolis carolinensis*, between 10 and 20 residues were missing in all non-mammals. This required gap introduction for building the alignment model (**Figure 3.5.5**). As shown in **Figure 3.5.3**, the putative RxxSSxR motif that we have postulated to bind the kringle domain of uPA is conserved across all mammals and absent in non-mammals.

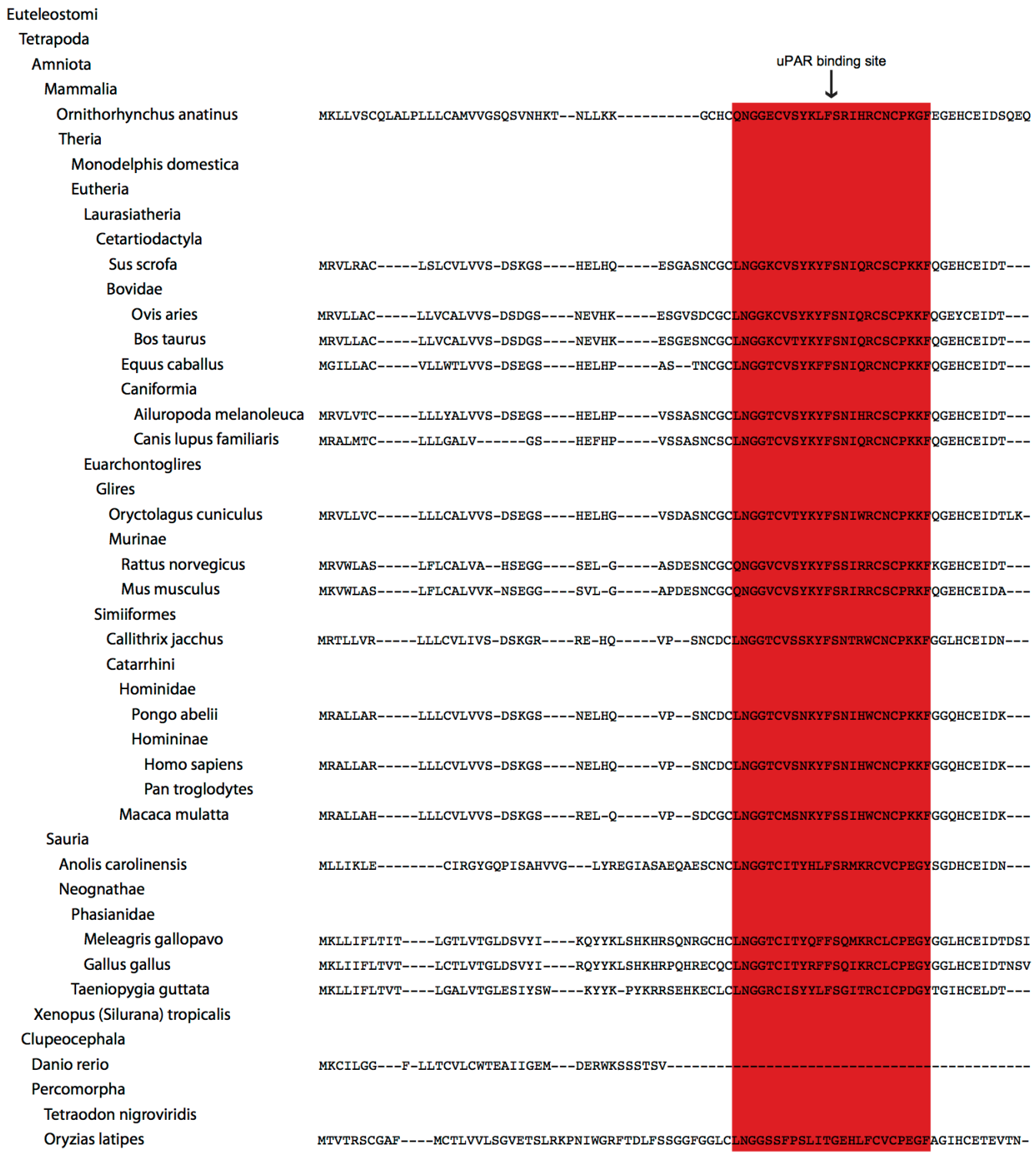



**Figure 3.5.4 Evolutionary conservation of the uPAR interaction site within uPA.** The full-length amino-terminal fragment of uPA is shown for all organisms with an uPA-encoding gene stored in the NCBI database. The uPAR interaction site is marked in red. All organisms have been ordered into genetic trees using the tax-id system of NCBI. (**red**) All animals display a uPAR interaction site with the exception of Danio Rerio. No gap introduction is necessary to build the alignment

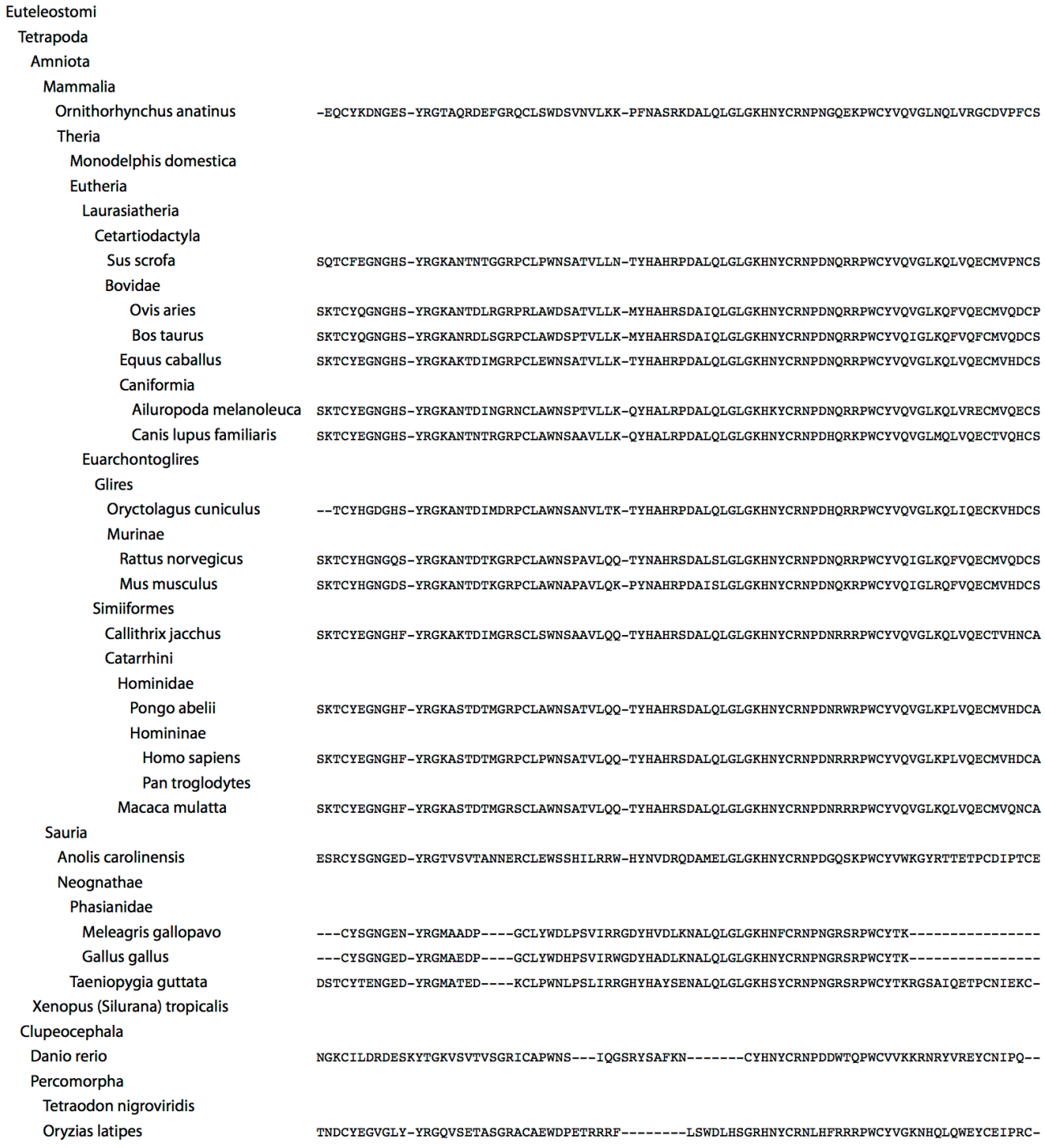



**Figure 3.5.5 Evolutionary conservation of the kringle domain of uPA.** The full-length kringle domain of uPA is shown for all organisms with an uPA-encoding gene stored in the NCBI database. The precise location where the RxxSSxR motif interacts with the kringle domain is unknown. All organisms have been ordered into genetic trees using the tax-id system of NCBI. Theria sequences align without the need of introducing gaps whereas other animals exclusing Anolis carolinensis require significant gap introduction

## 3.6 Mutation of KxxSSxR motif in human Endo180

It was decided to create a null-mutant of the potential uPA interaction motif for future studies. Primers were created as instructed by the Stratagene QuikChange XL Site-Directed Mutagenesis Kit (**figure 3.6.3**).

A full length Endo180 EST was identified in the lambda gt11 library. The Endo180 encoding sequenced was excised from the phagemid and ligated into the pcDNA3 expression vector (Sheikh et al., 2000) (**figure 3.6.1 and 3.6.2**). This expression vector was provided by Clare Isacke. PCR of Endo180 was reported as very challenging and cloning was limited to restriction excision and ligation (Sturge/Rodriguez-Teja personal communication).

The basis of the site-directed mutagenesis kit is the PCR of the full-length template vector. Surprisingly, following the standard instructions as provided by the commercial site-directed mutagenesis kit, it was possible to identify clones for two out of three attempted mutations that showed no difference to the wild type vector in restriction digest and were sequenced positive for the mutated region. The finding that PCR of the Endo180 encoding sequence is indeed possible will be revisited in **section 4**. The mutated vector will be a useful tool in future chemotaxis and invasion studies.

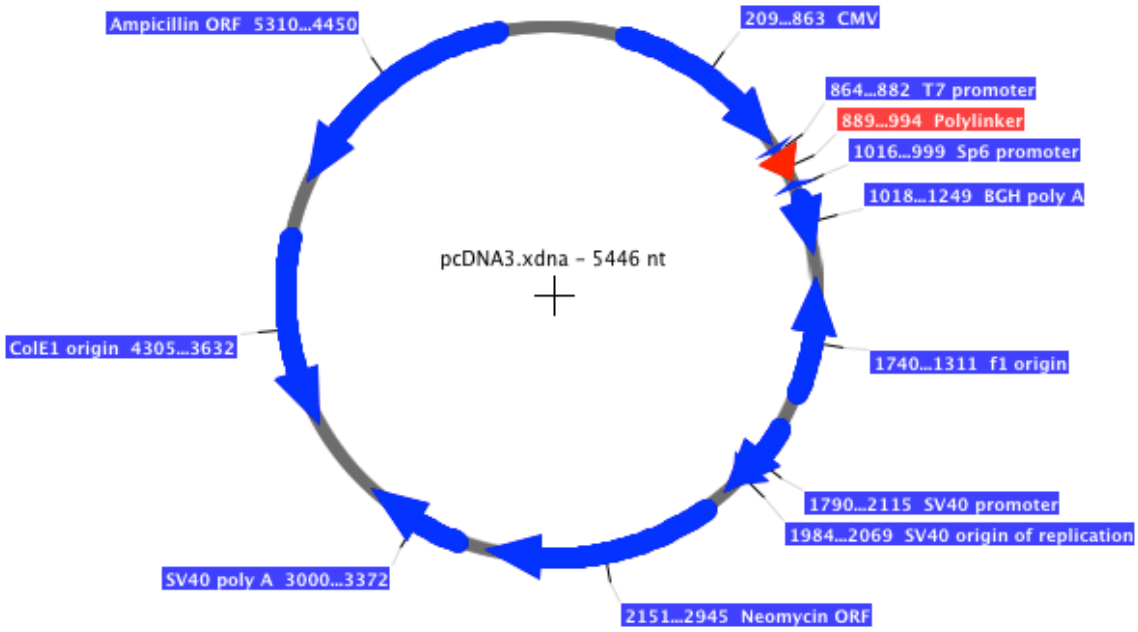



**Figure 3.6.1 pcDNA3 empty vector**

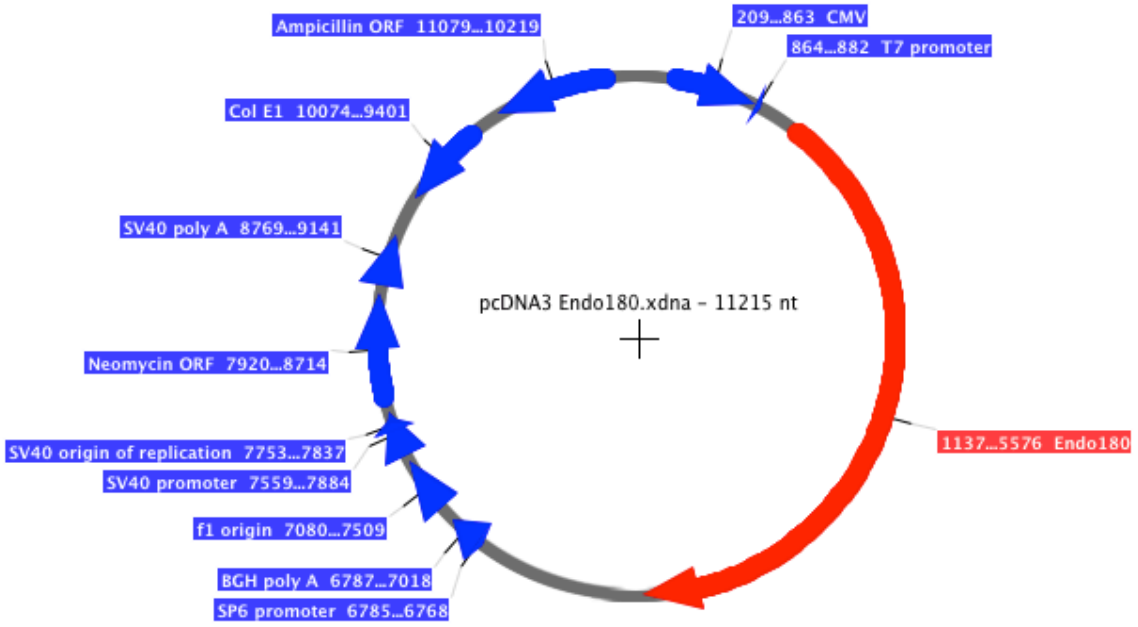



**Figure 3.6.2 pcDNA3 Endo180 expression vector**

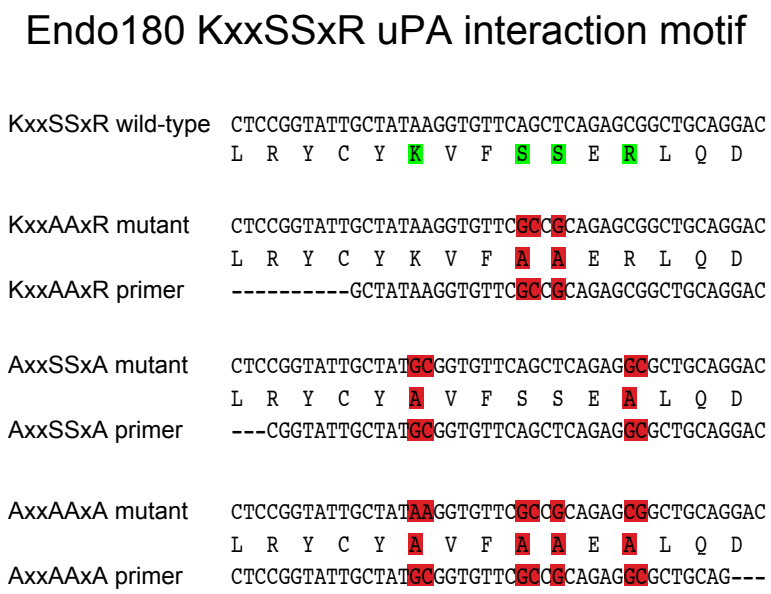



**Figure 3.6.3 Primers and sequences to generate null-mutants of the KxxSSxR interaction motif** Reverse primers are reverse complement to the forward primers displayed in this figure. PCR generates full length copies of the template vector

## 3.7 Discussion

Before this study, the Endo180 protein has only been characterised in humans, mice and cattle (Belgian Blue). Here, a search for homologous proteins revealed that a gene potentially encoding Endo180 is present throughout the vertebrate kingdom. Similar findings were made for other members of the mannose receptor family. It was found that both the dihydrophobic and the potentially non-functional LDL-receptor endocytosis motif are evolutionary conserved in all vertebrates. Interestingly, the mutation introduced by Isacke and co-workers almost a decade ago was found to actually alter receptor distribution, however, not to the same degree as the dihydrophobic motif (Justin Sturge, personal communication). The strong conservation implies that the LDL-receptor endocytosis motif might be functional. This function might be important in a biological context that has not been identified. Furthermore, a Serine residue juxta-positioned to the dihydrophobic internalisation motif, LV, is a potential kinase substrate. Phosphorylation of this Serine residue might stop receptor internalisation in a physiological context. This finding is of particular interest with cell-cell-junction localised Endo180 discovered in DU145 cells (see **Section 4**). Another potential Kinase substrate predicted via the GPS system is part of a 14-3-3 binding motif. Phosphorylation by PKC detected by Isacke and co-workers might be subject to complex regulation via 14-3-3 epitope masking.

Overall, the evolutionary heritage of the individual domains of the mannose receptor family aligns with the function attributed to the macrophage mannose receptor as well as Endo180. The presence of CTLDs and their importance in the innate immune response goes along with the phagocytosis function displayed by the macrophage mannose receptor. However, no role in the innate immune response has been attributed to the Endo180 protein in the past.

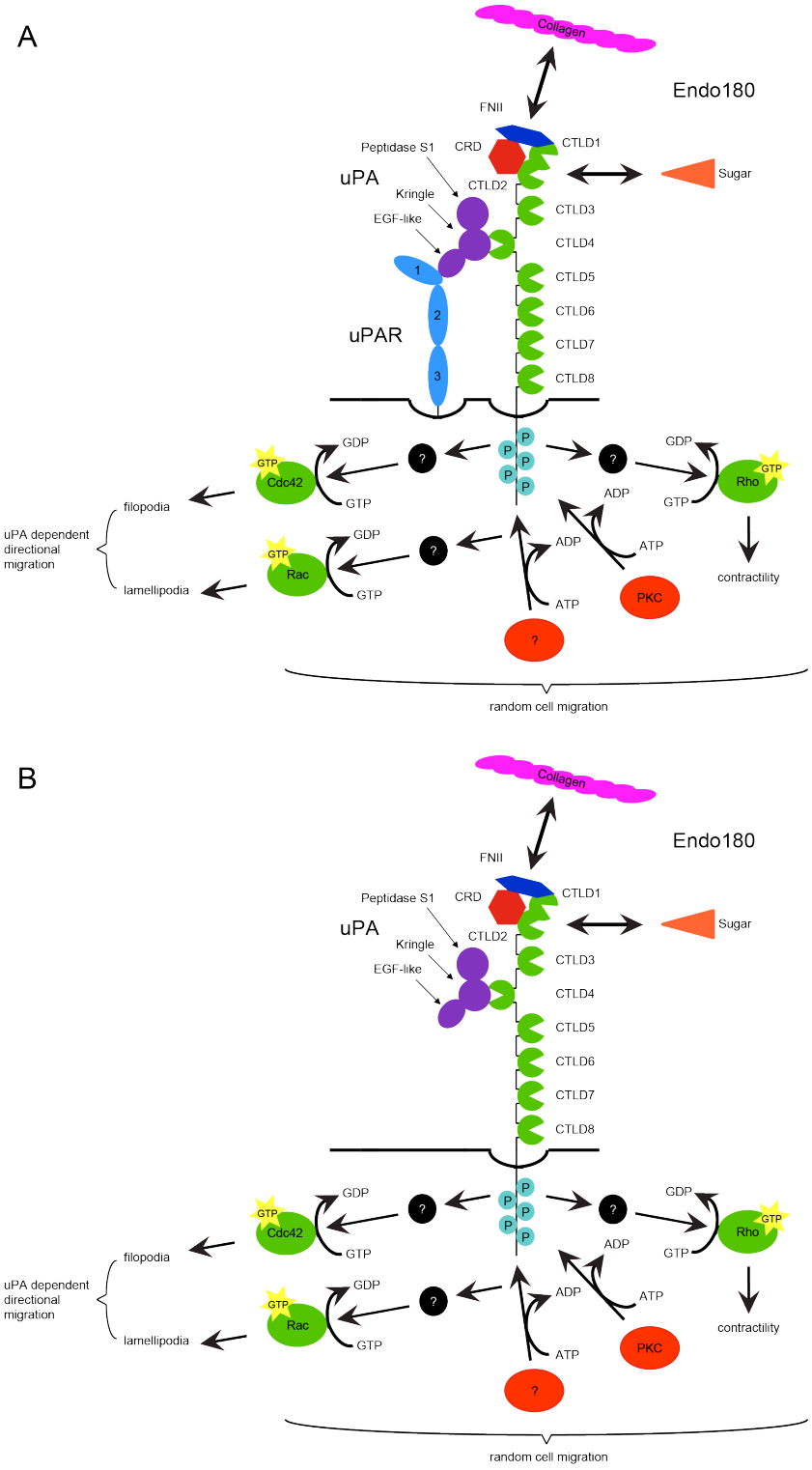



**Figure 3.7.1 Endo180: Two models for uPA interaction. (A)** The CTLD4 domain of Endo180 interacts with the kringle domain of uPA when uPA is bound to uPAR **(B)** The CTLD4 domain of Endo180 interacts with the kringle domain of uPA without a uPAR interaction. (Additional elements are described in **figure 1.4.9**) (Adapted from: Gronau, Iascke & Sturge. MRC2. Encyclopedia of Signalling Molecules. Springer Press; 2012).

The potential uPA interacting motif RxxSSxR was discovered in a phage display (random mutation) study by Priessner and colleagues (Liang et al., 2003) and defined as a novel class of uPA binding peptides. The common uPA-binding motif identified was used as a search tool to identify putative interaction partners for uPA. NCBI Blast was used to generate a list of genes that encode cell surface receptors that contain the novel uPA-binding motif. Endo180 was one of the highest scoring proteins in this screen. This finding fell in line with the discovery that Endo180 is essential for directional breast cancer cell (MCF-7, MDA-MB-231) migration (chemotaxis) up a gradient of uPA (Sturge et al., 2003) and can be isolated in complex with uPA-uPAR from a monocytic cell line (U937) following chemical crosslinking (Behrendt et al., 2000).

The novel uPA-binding motif was shown to interact with the kringle domain of uPA; whereas GPI-anchored uPAR binds to the amino-terminal fragment (ATF) of uPA (Liang et al., 2003). In effect, proteins containing this uPA-binding-motif could form a tri-molecular complex with uPA and uPAR (**figure 3.7.1**). The interaction between uPA and uPAR has been widely implicated in signal transduction; however, since uPAR is GPI-anchored and lacks a cytosolic domain it cannot initiate intracellular signaling *per* se (Smith and Marshall, 2010). As a consequence the uPA-uPAR complex requires clustering with other cell surface receptors to initiate signalling cascades inside the cytosol. In this respect we have hypothesised that Endo180 forms its tri-molecular cell surface cluster with uPA-uPAR via direct interaction with this novel uPA-binding motif to confer a signalling platform that can direct cell migration towards chemotactic cues within the stromal microenvironment of metastatic solid tumours.

Since the amino acid residues that form part of motifs with known function in the cytoplasmic tail of Endo180 display evolutionary conservation across species with an Endo180 encoding gene it was reasoned that the novel uPA-binding motif identified *in silico* may also be evolutionary conserved in Endo180, therefore validating its evolutional functionality *in vivo.* It was found that the novel uPA-binding motif is indeed evolutionary conserved but the conversation was limited to

mammals. However, conservation of the kringle domain of uPA, which interacts with the novel uPA-binding motif, was only highly conserved between mammals. In conclusion, the kringle domain of uPA and the RxxSSxR motif in the CTLD4 domain of Endo180 are co-conserved, lending evolutionary support to their molecular interaction and biological and pathological relevance. As supporting evidence, structural calculations predicted the motif to be located accessible on the surface of the Endo180 receptor.

# 4. Functional studies of Endo180

## 4.1 Introduction

In 1990 Clare Isacke and co-workers characterised several new Ser/Thr-phospho-peptides. Flow 2000 cells were stimulated with PMA, the entire Endo180 protein was immunoprecipitated using anti-human Endo180 mouse E1:183 mAb and phosphorylation demonstrated by $^{32}$P-labeling using PKC extract from rat brain (Isacke et al., 1990). At this time *MRC2* (the gene encoding Endo180) had not been cloned and the receptor domain structure and peptide sequences were not known. As described earlier (**Sections 1.4.5, 1.4.6 and 1.4.7; Figures 1.4.5 & 1.4.7**) Endo180 has a short cytoplasmic tail of approximately 42 amino acids, which is the only region of Endo180 accessible to cytosolic PKC under physiological conditions. In **Section 3** several phosphorylation sites within the cytoplasmic tail of Endo180 were predicted *in silico*. In this section the goal was to design an assay that could be used to measure Endo180's phosphorylation status *in vivo*.

The hTert immortalised human dermal fibroblast cell line HCA2 and the osteosarcoma cell line MG63 express relatively high levels of Endo180 compared to prostate cell lines (**Section 5**). HCA2 and MG63 cells are also easy to expand and grow in normal DMEM medium supplemented with 10% FCS. To enhance Endo180's phosphorylation status we stimulated HCA2/MG63 cells with 100 nM PMA for 10 minutes similar to the Isacke study in 1990. As backup strategy we procured the cytoplasmic tail of Endo180 as a synthesised peptide and planned *in vitro* phosphorylation studies using PKC from rat brain.

Surprisingly, robust Endo180 expression levels in E-Cadherin positive DU145 prostate cancer cells was detected (**section 5**). Here, DU145 cells were stained using two antibodies targeting different domains of Endo180.

Furthermore, as it was discovered that PCR of Endo180 is possible (**section 3**), at least using a commercial site-directed mutagenesis kit, this finding was to be revisited. The aim was to clone a fluorescent Endo180 fusion protein where the fluorescent protein is joined to the n-terminal end of the Endo180 protein ideally

with a flexible linker region to minimise adverse affects of the fusion to physiological Endo180 receptor function.

## 4.2 2-D gel electrophoresis

The initial strategy to measure the phosphorylation status of Endo180 was to use mouse anti-phospho-serine/threonine mAb in Western Blot. To separate the Endo180 signal from other proteins in a whole cell lysate lysates of HCA2 cells were resolved on 2-D gels. The theoretical pI of Endo180 was predicted *in silico*. To perform isoelectric focussing of proteins contained within the lysates they were denatured in urea and reduced with DTT. Only two anti-Endo180 mAbs are able to bind to Endo180 protein under reducing conditions: anti-human mouse 39:10 mAb and anti-mouse rabbit CAT2 pAb (which cross reacts with human Endo180). To optimise the absorption of Endo180 protein HCA2 whole cell lysates were incubated on a pI gradient strip over night at 4$^{o}$C. This protocol is recommended to help overcome the potential inefficiency of loading large proteins (>130 kDa) onto pI gradient strips. Iso-electric focussing was conducted following the supplier's instructions and molecular weight separation was subsequently carried out using SDS-PAGE. Proteins were transferred to PVDF membranes by Western Blot and membranes incubated with the appropriate antibody dilutions.

**Figure 4.2.1** shows an immunoblot of MG63 whole cell lysates resolved on a 2-D gel. Each spot represents one or several proteins detected by 39:10 or 4A4 (anti-phospho Ser/Thr) mAb. Proteins were clearly resolved in spots with no band stretching. The two antibodies failed to detect proteins in the molecular weight range for Endo180 (180 kDa). Using standard SDS-PAGE 39:10 mAb binds exclusively to Endo180 protein. The results shown in **Figure 4.2.1** confirm that the 39:10 mAb detects proteins with molecular weights different from Endo180. This presented two major problems: (a) the potential for inefficient loading of Endo180 onto pI gradient strips; and (b) the detection of non-specific signals by the two antibodies compatible with reducing conditions. The 39:10 antibody has been used in many previous studies in immunostaining and Western Blot analysis without producing unspecific background staining. Therefore, this latter finding may be the

result of whole cell lysate denaturation in urea, which results in the exposure of antigens not normally accessible to 39:10 mAb. Alternatively Endo180 denaturation with urea may irreversibly destroy the antigen-binding sites for 39:10 mAb. To investigate whether urea-based lysis buffer is compatible with the detection of Endo180 by Western Blot standard 1-D SDS-PAGE without prior isoelectric focusing was performed. The results shown in **Figure 4.2.1 B** show that Endo180 protein can be detected by 39:10 mAb under these conditions, which confirms urea-based lysis is capable of solubilising Endo180 and that the epitopes recognised by 39:10 mAb remain intact. Furthermore, no unspecific binding is apparent over the full length of the lanes (**Figure 4.2.1 B)**. It was therefore concluded that the absorption of Endo180 protein onto the pI gradient strip was too inefficient to allow for the use of this technique.

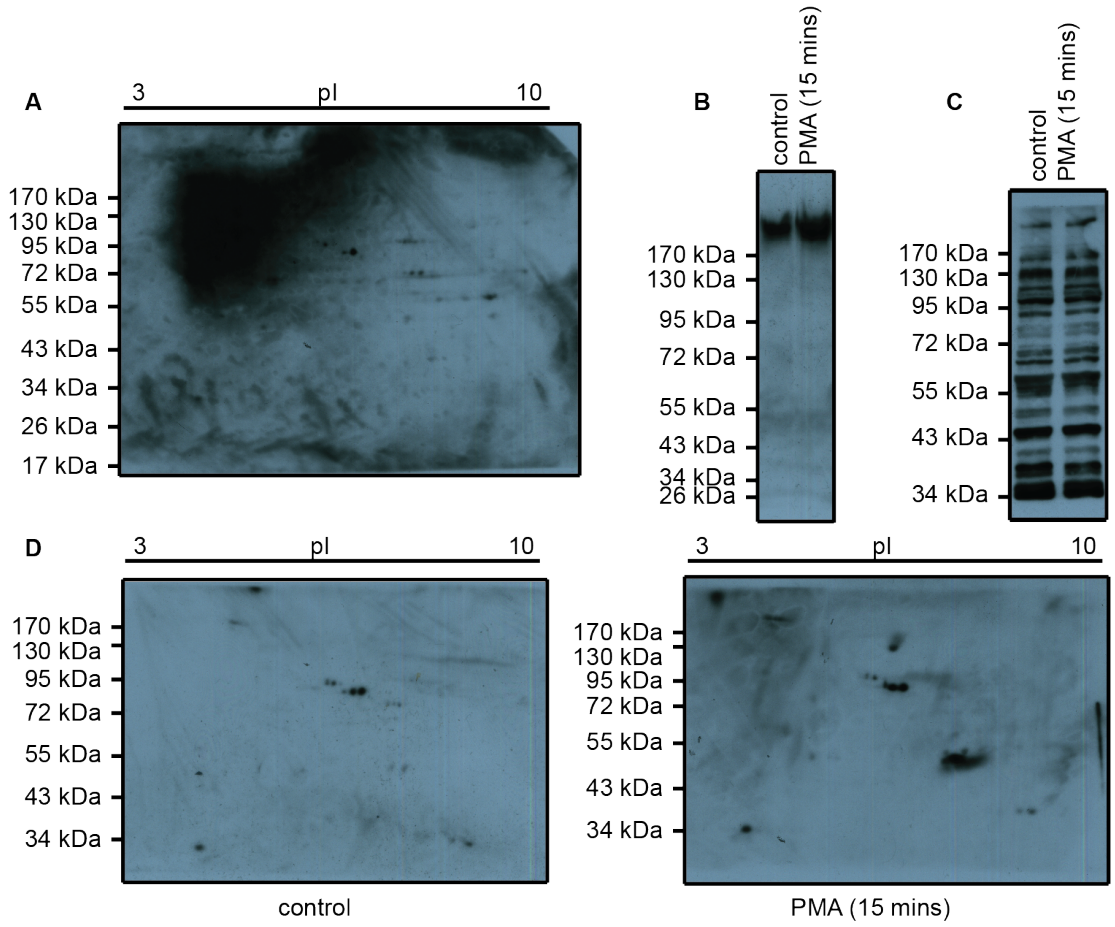



**Figure 4.2.1 Endo180 phosphorylation by 2D gel electrophoresis.** MG63 cells were seeded on 150 mm tissue culture plates and grown to confluency under normal growth conditions. The medium was supplemented for 10 minutes with 100 nM PMA or solvent (DMSO). Subsequently, whole cell lysates were prepared in 2D lysis buffer supplemented with phosphatase inhibitor cocktail. Lysate was pre-cleared by centrifugation and (A and D) supernatant subjected to over-night loading onto Immobilon DryStrips. 2D isoelectric focusing was performed for 16 hours and strips were resolved via SDS-PAGE after equilibration. (B and C) Proteins were resolved by standard SDS-PAGE. The panels show immunoblots obtained using the primary antibody concentrations listed in Table 2.1 followed by the appropriate HRP-conjugated secondary antibody: (A and B) anti-Endo180 39:10 (MW = 180 kDa) and (C, D and E) anti-p-Ser/Thr 4A4. For all blots visualisation of immunoreactive bands/spots was carried out using chemiluminesence. Molecular weight (MW) markers (kDa) and proteins of interest are indicated for each blot. (n=2)

## 4.3 Immunoprecipitation - Protein-G magnetic beads

Immunoprecipitation was carried out as alternative technique to 2-D SDS-PAGE. Conventional Protein-G coupled magnetic beads were loaded with mouse anti-human Endo180 mAbs (A5:158 or 39:10) or control IgG1. HCA2 were treated for 10 minutes with 100 nM PMA to enhance the phosphorylation status of Endo180 and whole cell lysates were prepared in RIPA buffer supplemented with phosphatase inhibitor cocktail. After pre-clearing by centrifugation the lysates were incubated with Protein-G magnetic beads for 30 minutes. Immunoprecipitated proteins were eluted from beads by heat denaturation in 2x SDS-PAGE loading buffer. 1% of input as well as 10/90% of the elute from the beads were subjected to SDS-PAGE using 4-20% gradient gels, followed by Western Blot analysis. **Figure 4.3.1 (A)** shows the detection of Endo180 using CAT2 pAb in the input and A5:158 immunoprecipitate. A diffuse 150 kDa band is present in all three lanes loaded with immunoprecipitates eluted from IgG loaded magnetic beads.

The gel in **Figure 4.3.1 (B)** was loaded with 1% of input and 90% of elute from the magnetic beads for control (DMSO) and PMA-treated samples. The first panel shows the high molecular weight range (> 110 kDa) probed with mouse anti-phospho-serine/threonine mAb (4A4). Several proteins migrating at different molecular weights were detected in both input lanes while no visible bands appear in lanes loaded with elutes from non-conjugated magnetic beads. A strong signal is present in all lanes loaded with elutes from magnetic beads that have been conjugated with any of the antibodies. This is due to the fact that all antibodies used for immunoprecipitation and the antibody used to stain the membrane were all raised in mouse.

The second and fourth panel show the potential Endo180 interaction partners Ezrin/Radixin/Moesin (investigated as part of a potential collaboration with Dr Aleksandar Ivetic, King's College London) and uPAR (both detected using rabbit anti-human pAbs). Ezrin/Radixin/Moesin migrate at approximately 75 kDa in both input lanes. After high exposure a diffuse signal is apparent in all lanes loaded with elutes from beads conjugated to all antibodies but bands were not observed in the

75 kDa molecular weight range. Signals did not appear in the input fractions and diffuse signals were observed in all lanes loaded with antibody-conjugated beads following immunodetection with rabbit anti-human uPAR pAb (399R) and a long exposure time. 399R is reported to weakly interact with uPAR under reducing conditions. Since the third panel, which shows mouse IgG1 heavy chain detected by goat anti-rabbit pAb the conclusion was drawn that the HRP-conjugated secondary goat anti-rabbit pAb cross reacts with mouse $IgG_1$ leading to a sensitivity limiting background signal in the Western Blot analysis. This is best demonstrated in the third panel where mouse $IgG_1$ heavy chain can be clearly detected by goat anti-rabbit $IgG_1$. Although all samples were reduced using 100 mM DTT the mouse anti-human Endo180 mAbs did not appear as distinct bands but as strong background covering the whole lane, which may be due to the high amount of antibody (5 μg) loaded in each sample.

Unfortunately the CAT2 pAb could not be used as a substitute for immunoprecipitation due to the epitope for this antibody being the exact region where the predicted phosphorylation events would occur. This could lead to steric hindrance and problems with epitope masking. CAT2 also binds α-tubulin, which could lead to the co-precipitation of several γ-tubulin interaction partners. **Figure 4.3.1** clearly demonstrates, the presence of 5 μg of antibody in each sample leads to cross-reaction with secondary antibodies even if antibodies from different species are used for immunoprecipitation and subsequent Western Blot analysis. Due to these technicalities it was decided not to change the antibody configuration but to prevent the antibody from being co-eluted from the beads alongside the antigen.

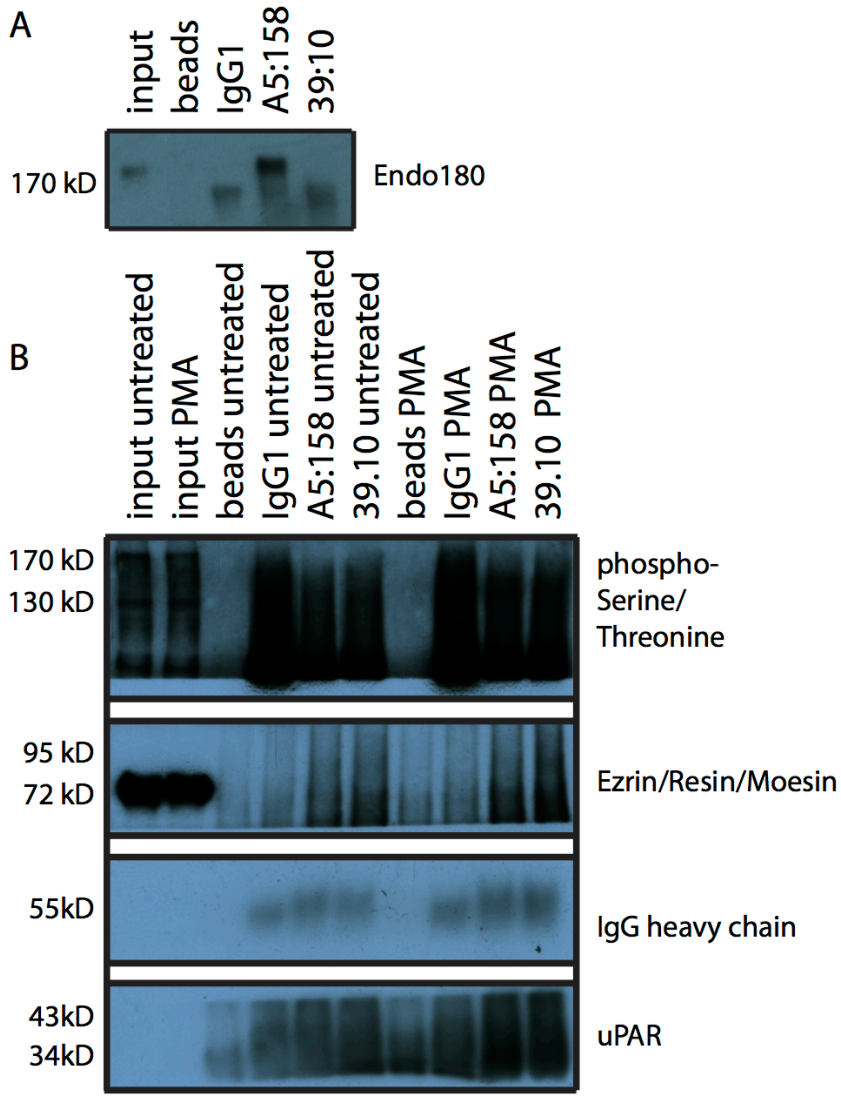



**Figure 4.3.1 Immunoprecipitation of Endo180.** HCA2 cells were seeded on 150 mm tissue culture plates and grown under normal growth conditions until they reached confluency. The growth medium was supplemented with 100 nM PMA or solvent control (DMSO) for 10 minutes. Whole cell lysates were prepared in complete RIPA buffer supplemented with phosphatase inhibitor cocktail. The lysate was incubated for 30 minutes with anti-Endo180-antibody coupled Protein-G magnetic beads (A5:158 and 39:10 mouse anti-human mAb). Immunoprecipitates were eluted from beads by boiling in 2x SDS-PAGE loading buffer and subjected to SDS-PAGE using 4-20% acrylamide gradient gels under reducing conditions (A: 90% of elute; B: 10% of elute). (A) Endo180 protein migrating as 180 kDa band detected by rabbit anti-human-Endo180 pAb (CAT2) followed by anti-rabbit HRP-conjugated IgG. (B) The four panels show immunoblots obtained using the primary antibody concentrations listed in **Table 2.1** followed by the appropriate HRP-conjugated secondary antibody. Phospho-serine/threonine (MW 110-200 kDa); ezrin/radixin/moesin (MW = 75 kDa); IgG heavy chain (MW = 50 kDa); uPAR (MW = 35-55 kDa) For all blots visualisation of immunoreactive bands was carried out using chemiluminesence. For all blots visualisation of immunoreactive bands was carried out using chemiluminesence. Molecular weight markers (kDa) and proteins of interest are indicated for each blot (n=1).

## 4.4 Covalent binding of antibody to Protein-G magnetic beads

To avoid mouse $IgG_1$ interference with Western Blot analysis we attempted to chemically couple mouse $IgG_1$ to Protein-G magnetic beads. The recommended procedure is to treat Protein-G magnetic beads after antibody loading with $BS^3$ (a commercially available cross-linking agent). The protocol provided by the supplier mentions that this method is compatible with most antibodies but might irreversibly damage the antigen binding capacity of some antibodies.

HCA2 cells were treated with 100 nM PMA and solvent control (DMSO) for 10 minutes before lysis in complete RIPA buffer supplemented with phosphatase inhibitors. Pre-cleared lysates were incubated with normal and cross-linked antibody bound to Protein-G magnetic beads for 30 minutes and eluted by heat denaturing in 2x SDS-PAGE loading buffer. 1% of input, the unbound fraction and 10% of immunoprecipitate were resolved using SDS-PAGE and analysed by Western Blot. **Figure 4.4.1** shows Endo180 protein migrating as a 180 kDa band in the input and unbound fractions, as well as in the lane loaded with elutes from normal A5:158 coupled Protein-G magnetic beads. Two much weaker bands appear in the two lanes loaded with elutes from $BS^3$ crosslinked A5:158 coupled magnetic beads. The membrane needed an overnight exposure to detect these weak signals, as indicated by the strong overexposure of all other bands on the gel. Lanes loaded with elutes from IgG control antibody and 39:10 coupled beads show no band at all. The expected α-tubulin band (55 kDa) was detected in all lanes loaded with input and unbound fraction. Similar to the results presented in **Figure 4.4.1** cross reactivity of goat anti-rabbit pAb with mouse $IgG_1$ is seen in both lanes loaded with elutes from non-crosslinked antibody coupled Protein-G beads. However, no visible background can be detected in lanes loaded with elutes from cross-linked magnetic beads. While cross-linking successfully prevented mouse $IgG_1$ from co-eluting with the antigens from the magnetic beads the antigen binding capacity was also greatly reduced. It was assumed that the antibody is incompatible with $BS^3$ cross-linking. Additionally, the mouse anti-human Endo180 39:10 mAb was excluded from further experiments because of its repeated failure to immunoprecipitate Endo180.

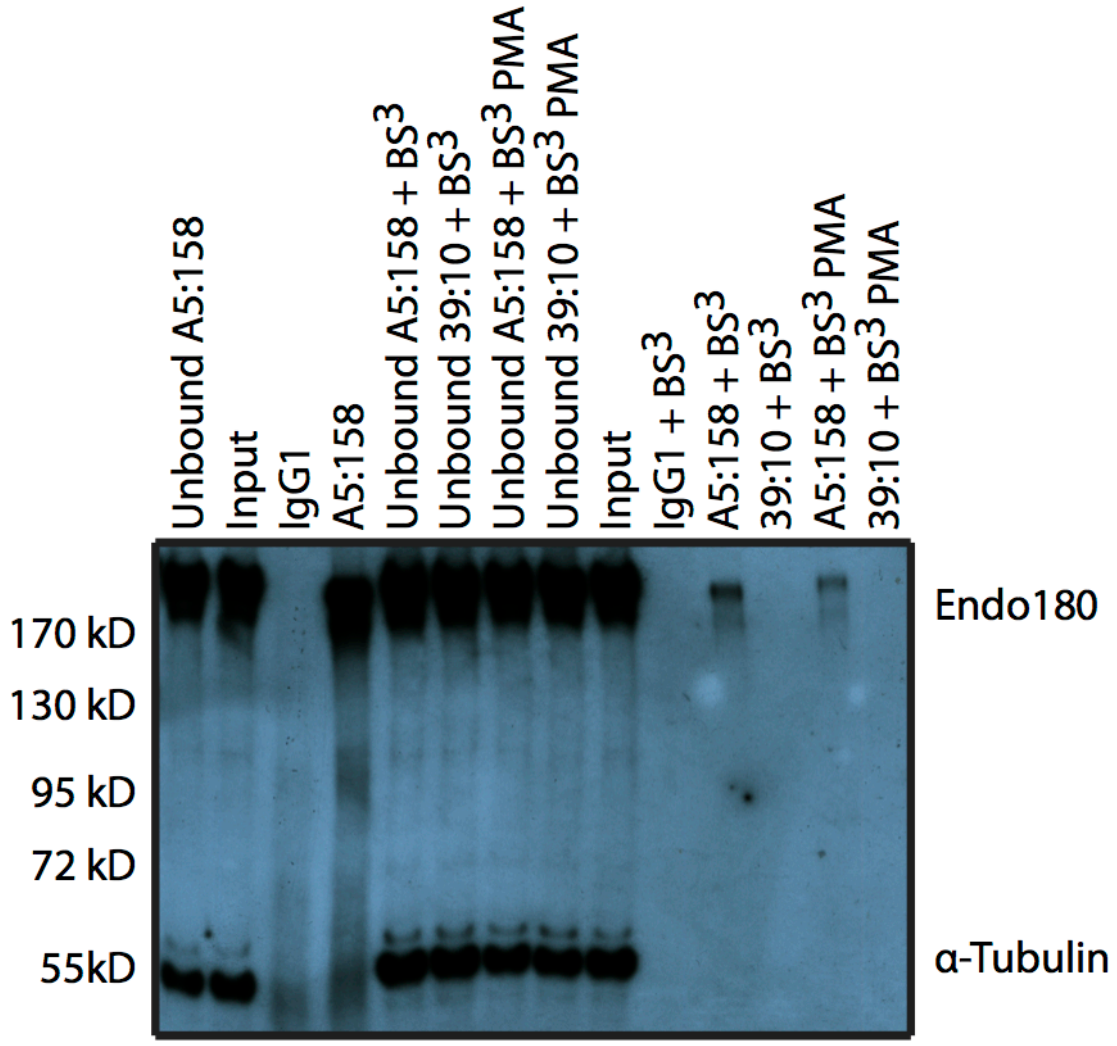



**Figure 4.4.1 Immunoprecipitation of Endo180 – BS³ crosslinking.** HCA2 cells were seeded on 150 mm tissue culture plates and grown to confluency under normal growth conditions. The medium was supplemented for 10 minutes with 100 nM PMA or solvent (DMSO). Subsequently, whole cell lysates were prepared in complete RIPA buffer supplemented with phosphatase inhibitor cocktail. Lysate was incubated for 30 minutes with antibody coupled magnetic beads. Protein-G magnetic beads were prepared with mouse anti-human-Endo180 mAbs (A5:158 and 39:10) as well as a mouse $IgG_1$ control and subsequently incubated with the cross-linking agent $BS^3$. After three washes, immunoprecipitates were eluted from magnetic beads by boiling in 2x SDS-PAGE loading buffer and subsequently subjected to SDS-PAGE using a 4-20% acrylamide gradient gel under reducing conditions. The Figure shows 2% of input and unbound fraction as well as 10% of immunoprecipitate. Endo180 and α-tubulin protein migrate as 180 kDa and 55 kDa bands respectively. Both are detected by CAT2 rabbit anti-human pAb followed by anti-rabbit HRP-conjugated IgG. For all blots visualisation of immunoreactive bands was carried out using chemiluminesence. Molecular weight markers (kDa) and proteins of interest are indicated for each blot (n=2).

## 4.5 Covalent coupling of antibodies to Epoxy activated magnetic beads

The finding that A5:158 mAb binding to Endo180 is impaired by the cross-linking reagent $BS^3$ an alternate method was used to covalently bind the antibody to magnetic beads. Epoxy-beads, supplied by Invitrogen, are magnetic beads with a chemically active group on their surface that can covalently bind any protein/peptide under stringent buffer conditions. The reaction can be irreversibly quenched after the procedure to prevent protein lysate binding the beads following immunoprecipitation. The manufacturer states that the antibody cannot be eluted from the beads. In the approach taken for these experiments Epoxy-beads were linked to A5:158 mAb and non-specific control $IgG_1$.

HCA2 human dermal fibroblasts seeded on 150 mm diameter cell culture plates were grown to confluency under normal growth conditions. The cells were treated with control solvent (DMSO) or 100 nM PMA for 10 minutes. Whole cell lysates were prepared using an assay specific lysis buffer. The lysates were pre-cleared by centrifugation and 50% of the lysate was incubated with the antibody coupled to Epoxy-beads and the remaining 50% was incubated with antibody loaded to conventional Protein-G magnetic beads for 30 minutes. The antigen was eluted using citrate buffer, mixed with loading buffer, pH adjusted, heat denatured and subjected to SDS-PAGE on 4-20% acrylamide gradient gels. **Figure 4.5.1** shows Western Blot analysis for 1% of input and 10% (Endo180 and α-tubulin)/90% (phospho-serine/threonine) of eluted antigen probed for Endo180 and α-tubulin using CAT2 pAb.

The first and second panels of **Figure 4.5.1** show that Endo180 was present at an equal level in all input and unbound fractions, lower in antigen elutes obtained from Protein-G magnetic beads and higher in elutes from Epoxy-beads. In the third panel the 55 kDa α-tubulin band was absent only from antigen elutes. In the fourth panel anti-phospho-serine/threonine mAb detects a strong non-specific signal in elutes from A5:158 mAb co-eluted from conventional Protein-G magnetic beads but no signal for elutes eluted from Epoxy-beads. Band patterns did not differ between input and unbound fractions. The low signal for Endo180 protein detected in elutes

from the Protein-G beads is counterintuitive since it was previously demonstrated (**Figures 4.3.1 & 4.4.1**) that they efficiently precipitate Endo180 when loaded with A5:158 antibody. It is suspected that the assay-specific lysis buffer supplied with Epoxy-beads interferes with the capacity of A5:158-loaded Protein-G magnetic beads to interact with Endo180 or that elution from Protein-G beads with citrate buffer is inefficient. On the other hand Epoxy-beads loaded with A5:158 efficiently immunoprecipitated Endo180 (**Figure 4.5.1**). The fourth panel of the same figure indicates that the amount of antibody co-eluted with its antigen from the Epoxy-beads is lower than the detection limit of this Western Blot analysis. However, no signal can be seen in Epoxy-beads elutes following immunodetection with mouse anti-phospho-serine/threonine mAb (**Figure 4.5.1**).

Explanations for the lack of immunoreactivity could be that the percentage of phosphorylated Endo180 compared to native protein is below the detection limit of the assay. Alternatively, the phosphorylated state of the protein may be unstable and susceptible to hydrolysis during sample processing - however, samples were handled at 4$^{o}$C and phosphatase inhibitors were added to all buffers, which makes this a less likely explanation. It is more likely that the anti-phospho-serine/threonine mAb does not bind to phosphorylated Endo180 with a high enough affinity for detection by Western blot - in support of this notion it has been determined that unlike anti-phospho-tyrosine mAbs (e.g. 4G10), which bind with high affinity and specificity to phospho-tyrosine residues, the commercial anti-phospho-serine/threonine mAbs that are available have a relatively low affinity and specificity for their target.

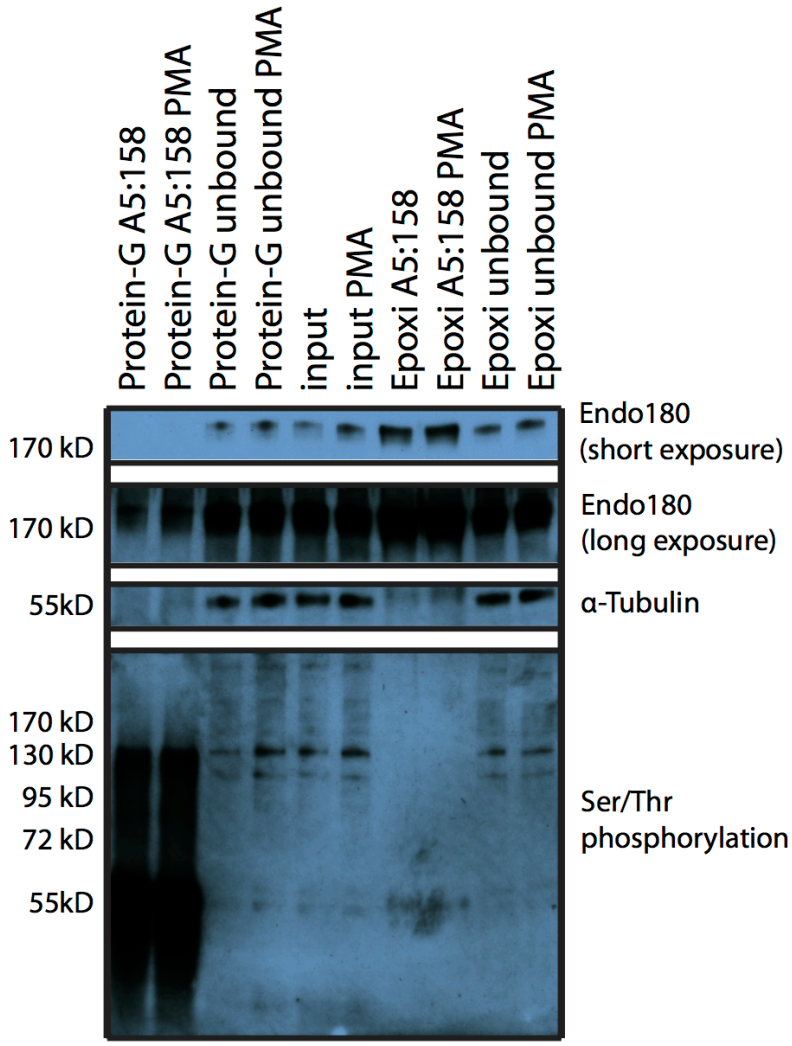



**Figure 4.5.1 Immunoprecipitation of Endo180 - comparing Protein-G and Epoxy magnetic beads.** HCA2 cells were seeded onto 150 mm tissue culture plates and grown to confluency under normal growth conditions. The medium was supplemented for 10 minutes with 100 nM PMA or solvent (DMSO). Subsequently, whole cell lysates were prepared in assay specific lysis buffer supplemented with phosphatase inhibitor cocktail. Lysates were incubated for 30 minutes with antibody coupled magnetic beads. Protein-G and Epoxy magnetic beads were prepared with mouse anti-human-Endo180 mAb (A5:158) and mouse $IgG_1$ control. After three washes, immunoprecipitates were eluted from magnetic beads in citric acid, mixed with SDS PAGE-loading buffer and after pH adjustment and heat denaturion were subjected to SDS-PAGE using a 4-20% acrylamide gradient gel under reducing conditions. The upper three panels show 2% of input and unbound fraction as well as 10 % of immunoprecipitate. Endo180 and α-tubulin protein migrate at 180 kDa and 55 kDa respectively. Both were detected using the bi-specific CAT2 rabbit anti-human pAb followed by anti-rabbit HRP-conjugated IgG. The lower panel shows 2 % of input and unbound fraction as well as 90% of immunoprecipitate. Phosphorylated Ser/Thr residues are detected using a mouse mAb followed by anti-mouse HRP-conjugated IgG. For all blots visualisation of immunoreactive bands was carried out using chemiluminesence. Molecular weight markers (kDa) and proteins of interest are indicated for each blot (n=1).

## 4.6 Phosphorylation shift assay - Phos-Tag system

Endo180 can be immunoprecipitated from whole cell lysates using different methods but phosphorylated protein cannot be detected using any of the techniques used so far (see **Sections 4.2, 4.3, 4.4 & 4.5**). To rule out the suggestion that phospho-serine/threonine residues in Endo180 cannot interact with phospho-serine/threonine mAb (4A4) a recently available antibody-independent methodology was applied. This technique involves the use of a chelating agent, Phos-Tag that interacts with phosphorylated protein residues. Phos-Tag has the capability of enriching phosphorylated proteins for chromatographic detection or can delay phosphorylated protein resolution in SDS-PAGE gels, which enables higher molecular weight phosphorylated forms to be detected using non-phosphorylation specific antibodies that recognise a protein of interest.

**Figure 4.6.1** shows the results obtained from HCA2 cells stimulated for 1-10 minutes with 100 nM PMA. The highest recommended concentration (100 μM) An acrylamide-coupled version of Phos-Tag was used in the SDS-PAGE gel to achieve the highest possible band-shift. Endo180 did not migrate into this 7% acrylamide + 100 μM Phos-Tag gel. On the contrary, Erk1/2 proteins migrated into the gel and their phosphorylated isoforms displayed reduced (≤ 30%) resolution.

Two strategies developed to analyse high molecular weight (>100 kDa) proteins were attempted: (a) lysate resolution on a 5% acrylamide + 7 μM Phos-Tag gel at low current for 12 hours; and (b) reduction of acrylamide to 3.5 % and inclusion of agarose to strengthen the gel. The results presented in the second and third panels of **Figure 4.6.1** indicate that Endo180 migrates into both types of gel. Even at high film exposure times high molecular weight bands could not be detected. The transfer of proteins from 3.5% acrylamide/agarose gels at low voltage to prevent agarose melting also resulted in highly inefficient transfer. Several attempts using these methods led to inconsistent results.

To overcome the potential problem that low concentrations of Phos-Tag were not sufficient to retain phosphorylated Endo180 protein a 5% acrylamide + 20 μM Phos-Tag gel was used (**Figure 4.6.2**). Again after several attempts the result remained

inconclusive. In gels without Phos-Tag 39:10 mAb can detect Endo180 migrating at 180 kDa and a low intensity band at 160 kDa. Band separation between these 180 kDa and 160 kDa bands did not occur on Phos-Tag supplemented gels, which may be caused by less band separation or the presence of a low intensity third band. A band between the 160 kDa and 180 kDa bands could indicate the presence of phosphorylated and native Endo180 isoforms. Since Phos-Tag gels prevent the resolution of phosphorylated isoforms interpretation suggested that the majority of Endo180 protein could be in its phosphorylated state in HCA2 cells grown under normal culture conditions. To investigate this Endo180 lysates from serum-starved and non-starved cells were compared; and a PMA (100 nM) stimulation time course was carried out in serum-starved cells. Lysates from serum-starved cells were also treated with alkaline phosphatase (CIP).

The results presented in **Figure 4.6.3** indicate that total Endo180 levels were dramatically reduced following serum starvation. Endo180 protein was observed to migrate at the same molecular weight across all samples with the exception of the CIP treated lysate. No clear band separation was observed. The expected result following dephosphorylation by CIP treatment is an increase in migration of non-phosphorylated protein. Paradoxically Endo180 migration into the gel following CIP treatment was decreased.

There are several explanations for the negative findings presented in this Section. The first possibility is that the assay systems used were limited by their lack of sensitivity in the detection of phosphorylated Endo180, which may only be present if a small fraction of Endo180 is phosphorylated in response to PMA treatment. The second possibility is the choice of cell line. Although the HCA2 dermal fibroblasts used here have fully functional Endo180 the recptor may not be regulated in the same way in the Flow 2000 cells used in the Isacke et al., (1990) study. It is also possible that any phosphorylation of the protein is unstable and hydrolysed during sample processing. In addition to the sodium-orthovanadate used by Isacke et al., (1990) the RIPA buffer used in this study included phosphatase inhibitors that target PKC substrates, such as Calyculin A.

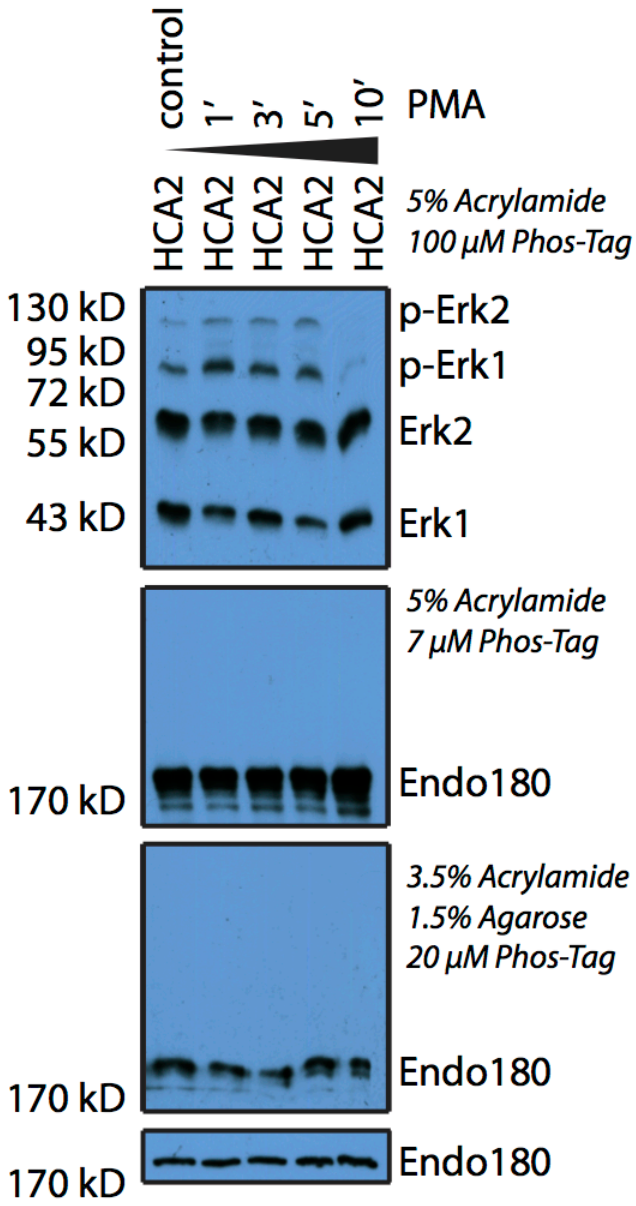



**Figure 4.6.1 Phosphorylation shift assay using different concentrations of Phos-Tag.** HCA2 human dermal fibroblasts were seeded on 100 mm tissue culture plates and grown to confluency under normal growth conditions. The medium was supplemented for 10 minutes with 100 nM PMA or solvent (DMSO). Subsequently, whole cell lysates were prepared in complete 2x SDS-PAGE loading buffer, heat denatured and sonicated. Lysates were subjected to SDS-PAGE using 7%/5%/3.5% acrylamide gel under reducing conditions. Acrylamide gels were supplemented with 100/20/7 µM Phos-tag. Gels were run at either 100 V constant (100/20 µM Phos-tag) or at 10 mA (7 µM Phos-tag). The upper panel shows Erk protein migrating at 43 kDa and its phosphorylated isoforms migrating at higher molecular weight. All are detected by rabbit anti-Erk1/2 pAb. The lower three panels show Endo180 protein migrating at 180 kDa in Phos-Tag and non-Phos-Tag supplemented gels. For all blots visualisation of immunoreactive bands was carried out using chemoluminesence. Molecular weight markers (kDa) and proteins of interest are indicated for each blot (n=1).

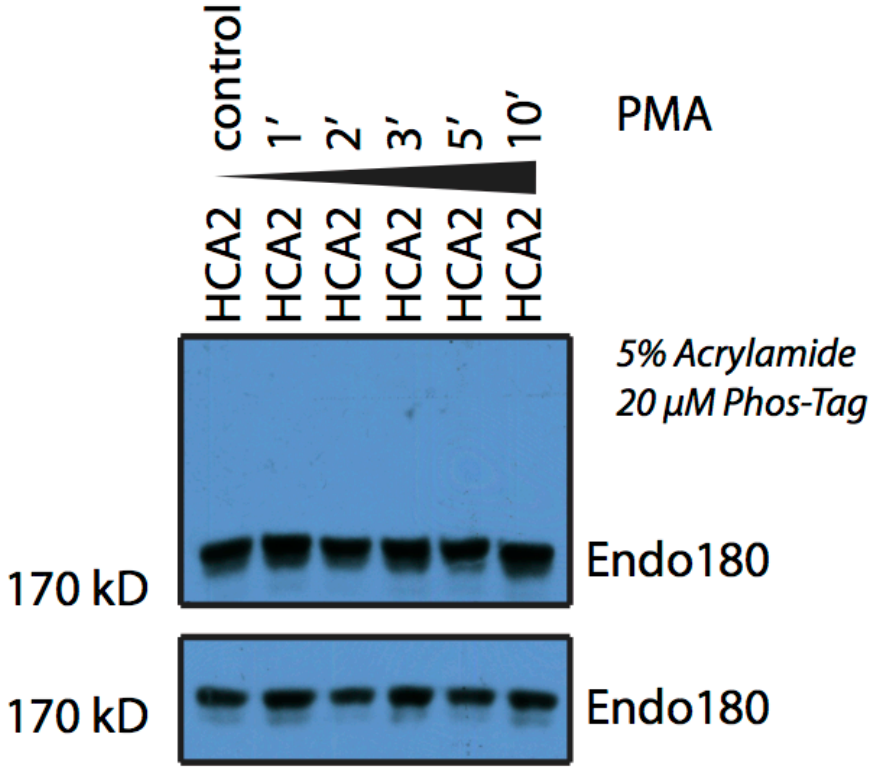



**Figure 4.6.2 Phosphorylation shift assay using optimised concentration of Phos-Tag:** HCA2 human dermal fibroblasts were seeded on 100 mm tissue culture plates and grown to confluency under normal growth conditions. The medium was supplemented for 10 minutes with 100 nM PMA or solvent (DMSO). Subsequently, whole cell lysates were prepared in complete 2x SD-PAGE loading buffer, heat denatured and sonicated. Lysates were subjected to SDS-PAGE using a 5 % acrylamide gel under reducing conditions. Acrylamide gels were supplemented with 0/20⌈M Phos-tag. Gels were run at at 10 mA for approximately 12 hours. Both panels show Endo180 protein migrating at 180 kDa in Phos-Tag and non-Phos-Tag supplemented gels. For all blots visualisation of immunoreactive bands was carried out using chemoluminesence. Molecular weight markers (kDa) and proteins of interest are indicated for each blot (n=3).

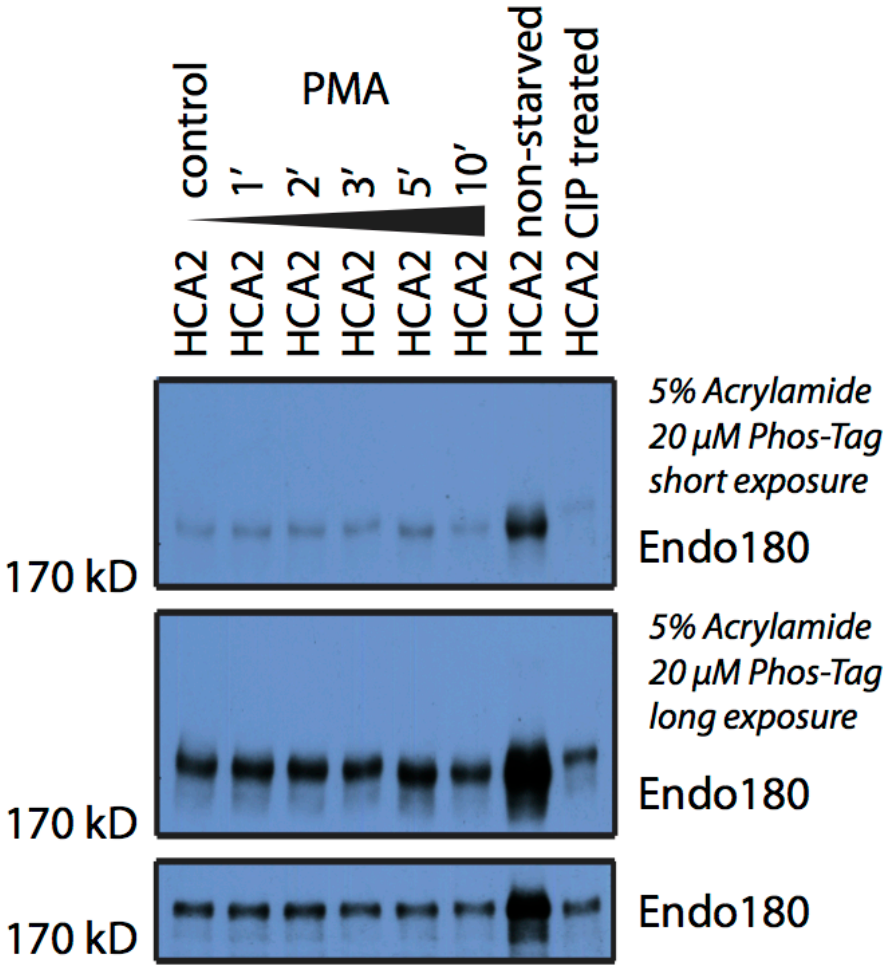



**Figure 4.6.3 Phosphorylation shift assay using optimised concentration of Phos-Tag:** HCA2 human dermal fibroblasts were seeded on 100 mm tissue culture plates and grown to confluency under normal growth conditions. The medium was supplemented for 10 minutes with 100 nM PMA or solvent (DMSO). Subsequently, whole cell lysates were prepared in RIPA buffer supplemented with phosphatase inhibitor cocktail and pre-cleared by centrifugation. One sample was incubated for 30 minutes at 37°C with alkaline phosphatase (CIP). Subsequently samples have been supplemented with loading buffer and heat denatured. Lysates were subjected to SDS-PAGE using a 5% acrylamide gel under reducing conditions. Where indicated acrylamide gels were supplemented with 20 µM Phos-Tag. Gels were run at 10 mA for approximately 12 hours. Both panels show Endo180 protein migrating at 180 kDa in Phos-Tag and non-Phos-Tag supplemented gels. For all blots visualisation of immunoreactive bands was carried out using chemiluminesence. Molecular weight markers (kDa) and proteins of interest are indicated for each blot (n=3).

## 4.7 Usage of Epoxy-beads to identify proteins interacting with Endo180

Usually, protein complexes isolated from cell lysates via immunoprecipitation contain large quantities of antibodies. The antibody is co-eluted from the magnetic beads with the protein complex. Unfortunately, the quantity of antibody in the elution is by several magnitudes greater than proteins interacting with the antigen. The dynamic range of mass spectroscopy is too small to identify any other protein than the antibody.

However, the epoxy-beads assay, established in **section 4.5** allows for an antibody free elution of the protein complex from the antibody-loaded beads. A modification of the protocol suggested by Invitrogen allows for a detergent and salt free elution of the protein complex from the magnetic beads. After several optimisation rounds in the mass spectroscopy suppert unit at Imperial College and the help of Dr Paul Hitchen, it was possible to perform shotgun proteomics on the Endo180 protein complex after immunoprecipitation from HCA2 cell lysates. **Table 4.7.1** shows a list of proteins that have been identified as being potential Endo180. The peptides were matched against all peptide sequences inventoried in SwissProt (**Table 4.7.1A**) or against peptides sequences calculated from human proteins only (**Table 4.7.1B**). Interestingly, apart from several structural proteins (Tubulin, Vimentin, …) two RhoGEFs (SwissProt-ID: ARHG1_HUMAN and ARHGH_HUMAN) were identified. These proteins might be the missing link between Endo180 and Rho GTPase activation.

However, this first experiment lacked any controls. In a subsequent experiment, epoxy-beads coupled with A5:158 mAb were compared to IgG1-control-coupled beads. A5:158 and IgG-control beads both precipitated RO52_HUMAN, identifying it as a false positive (**Table 4.7.2**). Unfortunately, none of the two RhoGEFs was identified in this experiment. However, problems with the cold room that day led to insufficient cooling and delays during the procedure. The results are encouraging and worth future investigation.

Furthermore, Endo180 protein expressing was knocked down using two different siRNA oligos as described in (Caley et al., 2012; Sturge et al., 2006). Again, it was no

possible to detect any of the two RhoGEFs in either the wild type or any of the knockdown control samples (**Table 4.7.3**). Ignoring nuclear proteins and Keratins as contaminations, only Vimentin is present in all four samples, untreated, scramble control and 2x siRNA knockdown. Interestingly, the Vimentin ion score is reduced from 418&501 in untreated and scramble to 83&66 in the knockdown samples. This is the same 5x reduction that was detected for the Endo180 ion score, which decreased from 465&411 to 46&163.

**A**

| Rank | Protein Name | Accession No. | Protein MW | Total Ion Score |
|---|---|---|---|---|
| 1 | C-type mannose receptor 2 OS=Homo sapiens GN=MRC2 PE=1 SV=1 | MRC2_HUMAN | 166548.9 | 884 |
| 2 | Nucleoprotein OS=Simian virus 5 (strain W3) GN=NP PE=1 SV=1 | NCAP_SV5 | 56499.2 | 644 |
| 3 | E3 ubiquitin-protein ligase TRIM21 OS=Homo sapiens GN=TRIM21 PE=1 SV=1 | RO52_HUMAN | 54135.1 | 578 |
| 4 | Vimentin OS=Homo sapiens GN=VIM PE=1 SV=4 | VIME_HUMAN | 53619.1 | 487 |
| 5 | Keratin, type II cytoskeletal 1 OS=Homo sapiens GN=KRT1 PE=1 SV=6 | K2C1_HUMAN | 65999.0 | 406 |
| 6 | Trypsin OS=Sus scrofa PE=1 SV=1 | TRYP_PIG | 24393.8 | 252 |
| 9 | Vimentin-1/2 OS=Xenopus laevis GN=vim1 PE=2 SV=1 | VIM1_XENLA | 52812.3 | 152 |
| 10 | Vimentin-4 OS=Xenopus laevis GN=vim4 PE=2 SV=1 | VIM4_XENLA | 53463.7 | 136 |
| 19 | Histone H4 OS=Acrolepiopsis assectella GN=His4 PE=3 SV=2 | H4_ACRAS | 11374.4 | 83 |
| 22 | Glial fibrillary acidic protein OS=Danio rerio GN=gfap PE=1 SV=2 | GFAP_DANRE | 51218.0 | 77 |
| 24 | Anionic trypsin-1 OS=Rattus norvegicus GN=Prss1 PE=1 SV=1 | TRY1_RAT | 25942.7 | 73 |
| 25 | Ig gamma-1 chain C region secreted form OS=Mus musculus GN=Ighg1 PE=1 SV=1 | IGHG1_MOUSE | 35681.8 | 72 |

**B**

| Rank | Protein Name | Accession No. | Protein MW | Total Ion Score |
|---|---|---|---|---|
| 1 | C-type mannose receptor 2 OS=Homo sapiens GN=MRC2 PE=1 SV=1 | MRC2_HUMAN | 166548.9 | 902 |
| 2 | E3 ubiquitin-protein ligase TRIM21 OS=Homo sapiens GN=TRIM21 PE=1 SV=1 | RO52_HUMAN | 54135.1 | 598 |
| 3 | Vimentin OS=Homo sapiens GN=VIM PE=1 SV=4 | VIME_HUMAN | 53619.1 | 505 |
| 4 | Keratin, type II cytoskeletal 1 OS=Homo sapiens GN=KRT1 PE=1 SV=6 | K2C1_HUMAN | 65999.0 | 406 |
| 9 | Histone H4 OS=Homo sapiens GN=HIST1H4A PE=1 SV=2 | H4_HUMAN | 11360.4 | 101 |
| 10 | Titin OS=Homo sapiens GN=TTN PE=1 SV=2 | TITIN_HUMAN | 3812906.2 | 77 |
| 13 | Tubulin alpha-1C chain OS=Homo sapiens GN=TUBA1C PE=1 SV=1 | TBA1C_HUMAN | 49863.5 | 65 |
| 14 | Nesprin-1 OS=Homo sapiens GN=SYNE1 PE=1 SV=3 | SYNE1_HUMAN | 1010397.5 | 60 |
| 16 | Rho guanine nucleotide exchange factor 1 OS=Homo sapiens GN=ARHGEF1 PE=1 SV=2 | ARHG1_HUMAN | 102371.4 | 55 |
| 18 | Serine/threonine-protein kinase mTOR OS=Homo sapiens GN=MTOR PE=1 SV=1 | MTOR_HUMAN | 288706.6 | 52 |
| 20 | Bromodomain-containing protein 1 OS=Homo sapiens GN=BRD1 PE=1 SV=1 | BRD1_HUMAN | 119443.8 | 50 |
| 21 | Mucin-16 OS=Homo sapiens GN=MUC16 PE=1 SV=2 | MUC16_HUMAN | 2351813.5 | 50 |
| 22 | MAM domain-containing glycosylphosphatidylinositol anchor protein 2 OS=Homo sapiens GN=MDGA2 PE=2 S | MDGA2_HUMAN | 107368.4 | 49 |
| 23 | Alpha-actinin-3 OS=Homo sapiens GN=ACTN3 PE=1 SV=2 | ACTN3_HUMAN | 103176.0 | 46 |
| 24 | ERO1-like protein alpha OS=Homo sapiens GN=ERO1L PE=1 SV=2 | ERO1A_HUMAN | 54358.1 | 46 |
| 25 | Rho guanine nucleotide exchange factor 17 OS=Homo sapiens GN=ARHGEF17 PE=1 SV=1 | ARHGH_HUMAN | 221534.8 | 44 |

**Table 4.7.1 Identification of Endo180 interaction partners** HCA2 human dermal fibroblasts were seeded on 150 mm tissue culture plates and grown to confluency under normal growth conditions. Whole cell lysates were prepared in CoIP-IP buffer and pre-cleared by centrifugation. Lysates underwent CoIP with A5:158 conjugated magnetic beads for 10 minutes. Beads were subsequently washed, proteins eluted in Ammonia buffer, lyophilised, trypsinised and subsequently analysed by chromatography coupled mass spectroscopy. Hits were generated using the Masscot software. (n=1).

**A**

| Rank | Protein Name | Accession No. | Protein MW | Total Ion Score |
|---|---|---|---|---|
| 1 | C-type mannose receptor 2 OS=Homo sapiens GN=MRC2 PE=1 SV=1 | MRC2_HUMAN | 166548.9 | 1666 |
| 2 | E3 ubiquitin-protein ligase TRIM21 OS=Homo sapiens GN=TRIM21 PE=1 SV=1 | RO52_HUMAN | 54135.1 | 718 |
| 3 | Trypsin OS=Sus scrofa PE=1 SV=1 | TRYP_PIG | 24393.8 | 247 |
| 4 | Serum albumin OS=Bos taurus GN=ALB PE=1 SV=4 | ALBU_BOVIN | 69248.4 | 211 |
| 5 | Tubulin alpha-1B chain OS=Cricetulus griseus GN=TUBA1B PE=2 SV=1 | TBA1B_CRIGR | 50119.6 | 157 |
| 6 | Tubulin beta-2C chain OS=Homo sapiens GN=TUBB2C PE=1 SV=1 | TBB2C_HUMAN | 49799.0 | 111 |
| 7 | Tubulin alpha-8 chain OS=Homo sapiens GN=TUBA8 PE=1 SV=1 | TBA8_HUMAN | 50061.6 | 103 |
| 8 | Serum albumin OS=Felis catus GN=ALB PE=1 SV=1 | ALBU_FELCA | 68614.9 | 99 |
| 9 | Tubulin alpha-3/alpha-5 chain OS=Arabidopsis thaliana GN=TUBA3 PE=2 SV=1 | TBA3_ARATH | 49622.5 | 89 |
| 10 | Keratin, type II cytoskeletal 1 OS=Pan troglodytes GN=KRT1 PE=2 SV=1 | K2C1_PANTR | 65449.7 | 83 |

**B**

| Rank | Protein Name | Accession No. | Protein MW | Total Ion Score |
|---|---|---|---|---|
| 1 | E3 ubiquitin-protein ligase TRIM21 OS=Homo sapiens GN=TRIM21 PE=1 SV=1 | RO52_HUMAN | 54135.1 | 724 |
| 2 | Keratin, type II cytoskeletal 8 OS=Homo sapiens GN=KRT8 PE=1 SV=7 | K2C8_HUMAN | 53671.1 | 294 |
| 3 | Tubulin alpha-1B chain OS=Cricetulus griseus GN=TUBA1B PE=2 SV=1 | TBA1B_CRIGR | 50119.6 | 246 |
| 4 | Trypsin OS=Sus scrofa PE=1 SV=1 | TRYP_PIG | 24393.8 | 230 |
| 5 | Tubulin beta-5 chain OS=Cricetulus griseus GN=TUBB5 PE=2 SV=1 | TBB5_CRIGR | 49639.0 | 221 |
| 6 | Tubulin beta-3 chain OS=Homo sapiens GN=TUBB3 PE=1 SV=2 | TBB3_HUMAN | 50400.2 | 171 |
| 7 | Tubulin alpha chain OS=Notophthalmus viridescens PE=2 SV=1 | TBA_NOTVI | 50061.4 | 167 |
| 8 | Tubulin beta-6 chain OS=Bos taurus GN=TUBB6 PE=2 SV=1 | TBB6_BOVIN | 49868.0 | 161 |
| 9 | Tubulin alpha chain OS=Enteroctopus dofleini PE=2 SV=1 | TBA_ENTDO | 50161.7 | 159 |
| 10 | Heterogeneous nuclear ribonucleoprotein U-like protein 1 OS=Homo sapiens GN=HNRNPUL1 PE=1 SV=2 | HNRL1_HUMAN | 95679.3 | 156 |

**Table 4.7.2 Identification of Endo180 interaction partners** HCA2 human dermal fibroblasts were seeded on 150 mm tissue culture plates and grown to confluency under normal growth conditions. Whole cell lysates were prepared in CoIP-IP buffer and pre-cleared by centrifugation. Lysates underwent CoIP with (A) A5:158 or (B) IgG1-control conjugated magnetic beads for 10 minutes. Beads were subsequently washed, proteins eluted in Ammonia buffer, lyophilised, trypsinised and subsequently analysed by chromatography coupled mass spectroscopy. Hits were generated using the Masscot software. (n=1).

| HCA2 untreated | Rank | Protein Name | Accession No. | Protein MW | Total Ion Score | Total Ion C. I. % |
|---|---|---|---|---|---|---|
| | 1 | C-type mannose receptor 2 OS=Homo sapiens GN=MRC2 F | MRC2_HUMAN | 166568.0 | 465 | 100.000 |
| | 2 | Vimentin OS=Homo sapiens GN=VIM PE=1 SV=4 | VIME_HUMAN | 53619.1 | 418 | 100.000 |
| | 3 | E3 ubiquitin-protein ligase TRIM21 OS=Homo sapiens GN=T | RO52_HUMAN | 54135.1 | 246 | 100.000 |
| | 4 | Keratin, type II cytoskeletal 1 OS=Homo sapiens GN=KRT1 | K2C1_HUMAN | 65999.0 | 216 | 100.000 |
| | 5 | Keratin, type I cytoskeletal 10 OS=Homo sapiens GN=KRT1 | K1C10_HUMAN | 58791.7 | 119 | 100.000 |
| | 6 | Cytoskeleton-associated protein 4 OS=Homo sapiens GN=C | CKAP4_HUMAN | 65982.7 | 85 | 100.000 |
| | 7 | Histone H4 OS=Homo sapiens GN=HIST1H4A PE=1 SV=2 | H4_HUMAN | 11360.4 | 67 | 99.999 |
| | 8 | 60S ribosomal protein L6 OS=Homo sapiens GN=RPL6 RL6 | RL6_HUMAN | 32707.6 | 64 | 99.998 |
| | 9 | Titin OS=Homo sapiens GN=TTN PE=1 SV=2 | TITIN_HUMAN | 3813809.5 | 54 | 99.981 |
| | 10 | Tubulin alpha-1B chain OS=Homo sapiens GN=TUBA1B PE | TBA1B_HUMAN | 50119.6 | 51 | 99.959 |
| | 11 | 60S ribosomal protein L14 OS=Homo sapiens GN=RPL14 P | RL14_HUMAN | 23417.0 | 49 | 99.930 |
| | 12 | Keratin, type II cytoskeletal 6B OS=Homo sapiens GN=KRT | K2C6B_HUMAN | 60030.3 | 41 | 99.606 |
| | 13 | Myotubularin-related protein 7 OS=Homo sapiens GN=MTM | MTMR7_HUMAN | 75784.4 | 38 | 99.196 |
| | 14 | LIM domain kinase 2 OS=Homo sapiens GN=LIMK2 PE=1 S | LIMK2_HUMAN | 72185.2 | 38 | 99.189 |
| | 15 | Cadherin EGF LAG seven-pass G-type receptor 3 CELR3_H | CELR3_HUMAN | 357959.8 | 38 | 99.112 |
| | 16 | 60S ribosomal protein L15 OS=Homo sapiens GN=RPL15 P | RL15_HUMAN | 24131.1 | 37 | 99.087 |
| | 17 | Biorientation of chromosomes in cell division protein 1-like O | BOD1L_HUMAN | 330263.8 | 37 | 98.908 |
| | 18 | Polyadenylate-binding protein 1 OS=Homo sapiens GN=PAE | PABP1_HUMAN | 70625.9 | 37 | 98.893 |
| | 19 | Replicase polyprotein 1ab OS=Human SARS coronavirus GI | R1AB_CVHSA | 789736.3 | 36 | 98.838 |
| | 20 | A/G-specific adenine DNA glycosylase OS=Homo sapiens G | MUTYH_HUMAN | 60031.5 | 36 | 98.645 |

| HCA2 scramble | Rank | Protein Name | Accession No. | Protein MW | Total Ion Score | Total Ion C. I. % |
|---|---|---|---|---|---|---|
| | 1 | Vimentin OS=Homo sapiens GN=VIM PE=1 SV=4 | VIME_HUMAN | 53619.1 | 501 | 100.000 |
| | 2 | C-type mannose receptor 2 OS=Homo sapiens GN=MRC2 F | MRC2_HUMAN | 166568.0 | 411 | 100.000 |
| | 3 | Keratin, type II cytoskeletal 1 OS=Homo sapiens GN=KRT1 | K2C1_HUMAN | 65999.0 | 257 | 100.000 |
| | 4 | Keratin, type I cytoskeletal 10 OS=Homo sapiens GN=KRT1 | K1C10_HUMAN | 58791.7 | 151 | 100.000 |
| | 5 | E3 ubiquitin-protein ligase TRIM21 OS=Homo sapiens GN=T | RO52_HUMAN | 54135.1 | 140 | 100.000 |
| | 6 | Keratin, type II cytoskeletal 6B OS=Homo sapiens GN=KRT | K2C6B_HUMAN | 60030.3 | 102 | 100.000 |
| | 7 | Keratin, type II cytoskeletal 2 epidermal OS=Homo sapiens ( | K22E_HUMAN | 65393.2 | 81 | 100.000 |
| | 8 | Desmin OS=Homo sapiens GN=DES PE=1 SV=3 | DESM_HUMAN | 53503.1 | 72 | 100.000 |
| | 9 | Keratin, type II cytoskeletal 4 OS=Homo sapiens GN=KRT4 | K2C4_HUMAN | 57249.8 | 65 | 99.998 |
| | 10 | Histone H4 OS=Homo sapiens GN=HIST1H4A PE=1 SV=2 | H4_HUMAN | 11360.4 | 60 | 99.995 |
| | 11 | 60S ribosomal protein L6 OS=Homo sapiens GN=RPL6 PE= | RL6_HUMAN | 32707.6 | 60 | 99.995 |
| | 12 | Histone H2A type 1-C OS=Homo sapiens GN=HIST1H2AC F | H2A1C_HUMAN | 14096.9 | 46 | 99.882 |
| | 13 | Centrosome-associated protein CEP250 OS=Homo sapiens | CP250_HUMAN | 280965.7 | 42 | 99.644 |
| | 14 | Leiomodin-2 OS=Homo sapiens GN=LMOD2 PE=2 SV=2 | LMOD2_HUMAN | 61637.6 | 38 | 99.237 |
| | 15 | Keratin, type II cytoskeletal 8 OS=Homo sapiens GN=KRT8 | K2C8_HUMAN | 53671.1 | 37 | 98.961 |
| | 16 | Probable E3 ubiquitin-protein ligase MYCBP2 OS=Homo sap | MYCB2_HUMAN | 509759.1 | 35 | 98.402 |
| | 17 | Coiled-coil domain-containing protein 87 OS=Homo CCD87_ | CCD87_HUMAN | 96341.7 | 35 | 98.376 |
| | 18 | ProSAP-interacting protein 1 OS=Homo sapiens GN=PROS/ | PRIP1_HUMAN | 71747.1 | 33 | 97.631 |
| | 19 | Glutamate [NMDA] receptor subunit 3A OS=Homo sapiens C | NMD3A_HUMAN | 125385.0 | 32 | 96.497 |
| | 20 | Highly divergent homeobox OS=Homo sapiens GN=HDX PE | HDX_HUMAN | 77157.8 | 31 | 96.211 |

**Table 4.7.3A Identification of Endo180 interaction partners** HCA2 human dermal fibroblasts were seeded on 150 mm tissue culture plates and transfected with siRNA oligos (2x targeting Endo180, 1x scramble of siRNA5) 12h later. After 72h, whole cell lysates were prepared in CoIP-IP buffer and pre-cleared by centrifugation. Lysates underwent CoIP with (A) A5:158 conjugated magnetic beads for 10 minutes. Beads were subsequently washed, proteins eluted in Ammonia buffer, lyophilised, trypsinised and subsequently analysed by chromatography coupled mass spectroscopy. Hits were generated using the Masscot software. (n=1).

| HCA2 siRNA 3 | Rank | Protein Name | Accession No. | Protein MW | Total Ion Score | Total Ion C. I. % |
|---|---|---|---|---|---|---|
| | 1 | E3 ubiquitin-protein ligase TRIM21 OS=Homo sapiens RO52 | RO52_HUMAN | 54135.1 | 232 | 100.000 |
| | 2 | Keratin, type II cytoskeletal 1 OS=Homo sapiens GN=KRT1 | K2C1_HUMAN | 65999.0 | 86 | 100.000 |
| | 3 | Vimentin OS=Homo sapiens GN=VIM PE=1 SV=4 | VIME_HUMAN | 53619.1 | 83 | 100.000 |
| | 4 | Keratin, type II cuticular Hb6 OS=Homo sapiens GN=KRT86 | KRT86_HUMAN | 53466.3 | 77 | 100.000 |
| | 5 | 60S ribosomal protein L6 OS=Homo sapiens GN=RPL6 RL6 | RL6_HUMAN | 32707.6 | 68 | 100.000 |
| | 6 | Titin OS=Homo sapiens GN=TTN PE=1 SV=2 | TITIN_HUMAN | 3812906.2 | 59 | 99.994 |
| | 7 | 60S ribosomal protein L26 OS=Homo sapiens GN=RPL26 P | RL26_HUMAN | 17247.5 | 57 | 99.989 |
| | 8 | Coiled-coil domain-containing protein 87 OS=Homo sapiens | CCD87_HUMAN | 96341.6 | 49 | 99.939 |
| | 9 | Cadherin EGF LAG seven-pass G-type receptor 3 OS=Hom | CELR3_HUMAN | 357959.8 | 47 | 99.900 |
| | 10 | C-type mannose receptor 2 OS=Homo sapiens GN=MRC2 F | MRC2_HUMAN | 166568.0 | 46 | 99.863 |
| | 11 | 40S ribosomal protein S18 OS=Homo sapiens GN=RPS18 F | RS18_HUMAN | 17707.9 | 44 | 99.818 |
| | 12 | Microtubule-actin cross-linking factor 1, isoforms 1/2/3/5 OS= | MACF1_HUMAN | 837801.3 | 41 | 99.625 |
| | 13 | Keratin, type II cytoskeletal 6B OS=Homo sapiens GN=KRT6 | K2C6B_HUMAN | 60030.3 | 39 | 99.427 |
| | 14 | Neuron navigator 3 OS=Homo sapiens GN=NAV3 PE=1 SV= | NAV3_HUMAN | 255488.7 | 39 | 99.403 |
| | 15 | Myotubularin-related protein 7 OS=Homo sapiens GN=MTM | MTMR7_HUMAN | 75784.4 | 39 | 99.346 |
| | 16 | LIM domain kinase 2 OS=Homo sapiens GN=LIMK2 LIMK2_ | LIMK2_HUMAN | 72185.2 | 38 | 99.283 |
| | 17 | Probable tRNA (uracil-O(2)-)-methyltransferase OS=Homo s | TRM44_HUMAN | 84575.6 | 36 | 98.835 |
| | 18 | Tubulin alpha-1B chain OS=Homo sapiens GN=TUBA1B PE | TBA1B_HUMAN | 50119.6 | 36 | 98.794 |
| | 19 | 40S ribosomal protein S8 OS=Homo sapiens GN=RPS8 PE= | RS8_HUMAN | 24190.2 | 36 | 98.587 |
| | 20 | Zinc finger CW-type PWWP domain protein 1 OS=Homo sap | ZCPW1_HUMAN | 71962.0 | 35 | 98.530 |

| HCA siRNA 5 | Rank | Protein Name | Accession No. | Protein MW | Total Ion Score | Total Ion C. I. % |
|---|---|---|---|---|---|---|
| | 1 | E3 ubiquitin-protein ligase TRIM21 OS=Homo sapiens RO52 | RO52_HUMAN | 54135.1 | 240 | 100.000 |
| | 2 | C-type mannose receptor 2 OS=Homo sapiens GN=MRC2 F | MRC2_HUMAN | 166568.0 | 163 | 100.000 |
| | 3 | Keratin, type II cytoskeletal 1 OS=Homo sapiens GN=KRT1 | K2C1_HUMAN | 65999.0 | 159 | 100.000 |
| | 4 | 60S ribosomal protein L18a OS=Homo sapiens GN=RPL18A | RL18A_HUMAN | 20748.9 | 83 | 100.000 |
| | 5 | Keratin, type II cytoskeletal 6B OS=Homo sapiens GN=KRT6 | K2C6B_HUMAN | 60030.3 | 79 | 100.000 |
| | 6 | 40S ribosomal protein S2 OS=Homo sapiens GN=RPS2 PE= | RS2_HUMAN | 31304.6 | 71 | 100.000 |
| | 7 | Titin OS=Homo sapiens GN=TTN PE=1 SV=2 | TITIN_HUMAN | 3813809.5 | 68 | 99.999 |
| | 8 | Vimentin OS=Homo sapiens GN=VIM PE=1 SV=4 | VIME_HUMAN | 53619.1 | 66 | 99.999 |
| | 9 | 60S ribosomal protein L6 OS=Homo sapiens GN=RPL6 RL6 | RL6_HUMAN | 32707.6 | 64 | 99.998 |
| | 10 | 60S ribosomal protein L27a OS=Homo sapiens GN=RPL27A | RL27A_HUMAN | 16551.0 | 54 | 99.979 |
| | 11 | Dolichyl-diphosphooligosaccharide--protein glycosyltransfera | RPN1_HUMAN | 68526.8 | 53 | 99.976 |
| | 12 | Keratin, type I cytoskeletal 10 OS=Homo sapiens GN=KRT1 | K1C10_HUMAN | 58791.7 | 49 | 99.937 |
| | 13 | 40S ribosomal protein S18 OS=Homo sapiens GN=RPS18 F | RS18_HUMAN | 17707.9 | 47 | 99.888 |
| | 14 | Striated muscle preferentially expressed protein kinase OS= | SPEG_HUMAN | 354070.6 | 46 | 99.880 |
| | 15 | 40S ribosomal protein S10 OS=Homo sapiens GN=RPS10 F | RS10_HUMAN | 18885.9 | 46 | 99.877 |
| | 16 | 40S ribosomal protein S24 OS=Homo sapiens GN=RPS24 F | RS24_HUMAN | 15413.4 | 45 | 99.812 |
| | 17 | 60S ribosomal protein L26 OS=Homo sapiens GN=RPL26 P | RL26_HUMAN | 17247.5 | 43 | 99.730 |
| | 18 | 40S ribosomal protein S8 OS=Homo sapiens GN=RPS8 PE= | RS8_HUMAN | 24190.2 | 43 | 99.704 |
| | 19 | Keratin, type II cytoskeletal 2 epidermal OS=Homo sapiens ( | K22E_HUMAN | 65393.2 | 41 | 99.544 |
| | 20 | LIM domain kinase 2 OS=Homo sapiens GN=LIMK2 LIMK2_ | LIMK2_HUMAN | 72185.2 | 41 | 99.535 |

**Table 4.7.3B Identification of Endo180 interaction partners** HCA2 human dermal fibroblasts were seeded on 150 mm tissue culture plates and transfected with siRNA oligos (2x targeting Endo180, 1x scramble of siRNA5) 12h later. After 72h, whole cell lysates were prepared in CoIP-IP buffer and pre-cleared by centrifugation. Lysates underwent CoIP with (A) A5:158 conjugated magnetic beads for 10 minutes. Beads were subsequently washed, proteins eluted in Ammonia buffer, lyophilised, trypsinised and subsequently analysed by chromatography coupled mass spectroscopy. Hits were generated using the Masscot software. (n=1).

## 4.8 Sub-cellular localisation of Endo180 in DU145 cells

Preliminary experiments were conducted to investigate whether there was evidence for functionally different forms of Endo180 to exist in the highly invasive epithelioid-mesenchymal prostate cancer cell line DU145. The A5/158 antibody was chosen since it binds to the functional sugar-binding domain CTLD2 that could be masked by conformational alterations in the N-terminal region of the receptor (Boskovic et al., 2006; Llorca, 2008; Rivera-Calzada et al., 2003). The 39.10 antibody was chosen as this binds to a region of the extracellular domain with no predicted conformational interactions with other regions of the receptor. Although it should be considered that an as yet uncharacterised consensus binding motif for uPA exists in the CTLD4 region of Endo180 (Liang et al., 2003), so it could be hypothesised that this epitope has the potential to be masked upon the formation of a trimolecular complex between Endo180, uPA and uPAR (Behrendt et al., 2000). Staining of endogenous Endo180 with the 39:10 antibody failed. Surprisingly, A5:158 appeared to stain a subcellular compartment localised in close proximity with the plasma membrane at cell-cell junctions (**Figure 4.8.1.5; controls 4.8.1.1 – 4.8.1.4**). Furthermore, it was observed that some DU145 cell clusters that stain positive for Endo180 expression using the A5:158 antibody stain comparatively low for E-Cadherin and vice versa. However, this preliminary observation requires proper quantification in a future study. A potential heterogeneity with one subpopulation expressing higher levels E-Cadherin while another expresses higher levels Endo180 is worth investigating.

From the localisation at cell-cell junctions it can be hypothesised that the conformation of Endo180 visualised by staining with A5/158 in DU145 cells is involved in the regulation of cell-cell junctions. This functionality was previously proposed in studies where Endo180 overexpression in MCF7 cell monolayers resulted in the disruption of E-cadherin positive cell-cell junctions via the generation of RhoA-ROCK-MLC2 based contractile signals (Sturge et al., 2006).

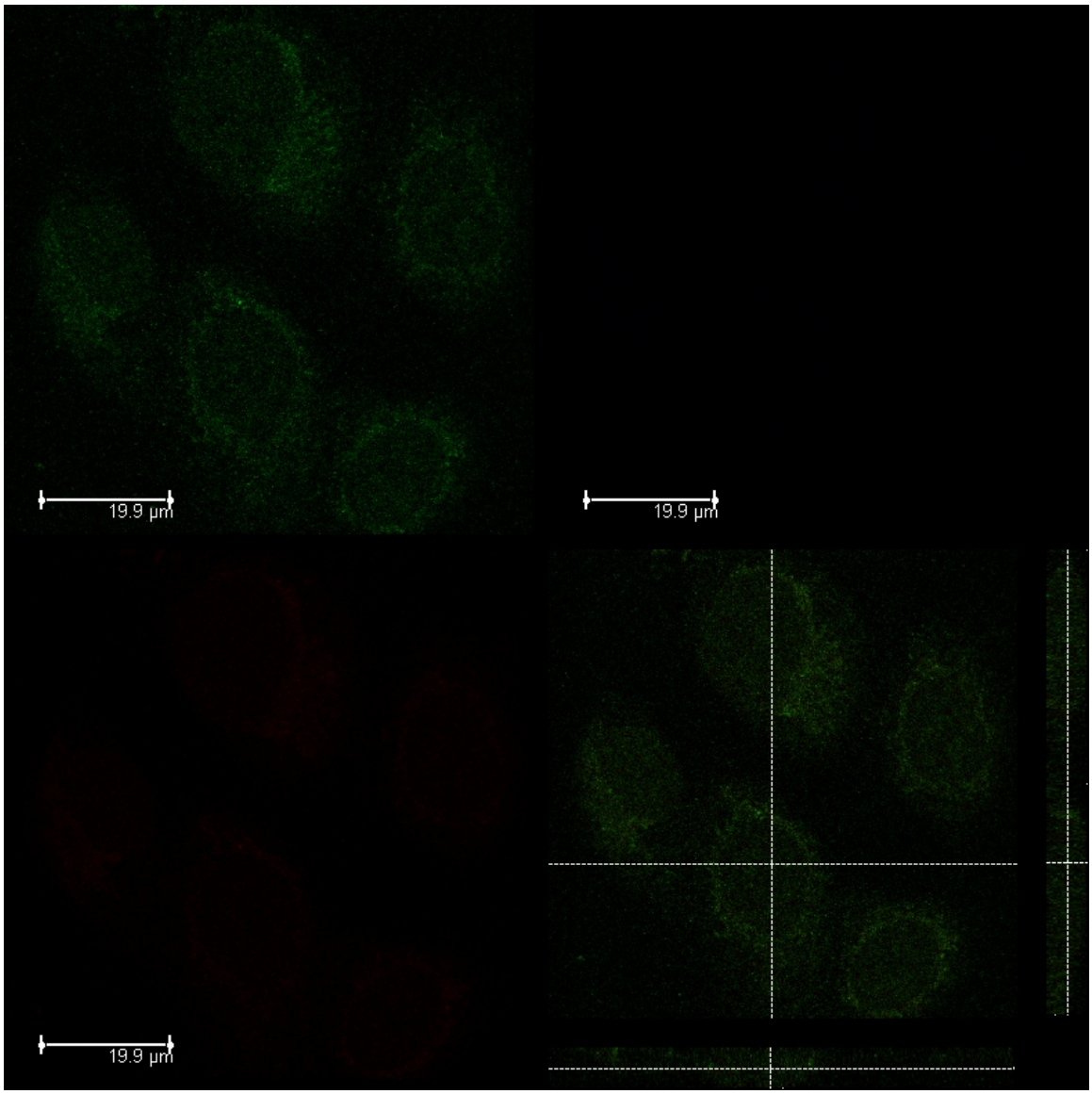



**Figure 4.8.1.1 Staining of endogenous Endo180 in DU145 cells (unstained control):** DU145 were seeded on Matrigel coated coverslips and grown under their normal growth conditions for four days. Fixed cells were subsequently permeabilised using 0.2 % w/v saponin and immunostained using either A5:158 or 39.10 mouse anti-human Endo180 mAbs followed by Alexa-555 Fluor conjugated IgG, as well as E-Cadherin 24E10 rabbit mAb Alexa 488 conjugate. Nuclei were counterstained with DAPI. 36 z-sections were acquired using a Leica SP5 confocal microscope and a 63x/1.4 oil immersion objective. (**upper left**) Endo180, (**upper right**) E-Cadherin, (**lower left**) Nuclei, (**lower right**) z-projection. (n=3)

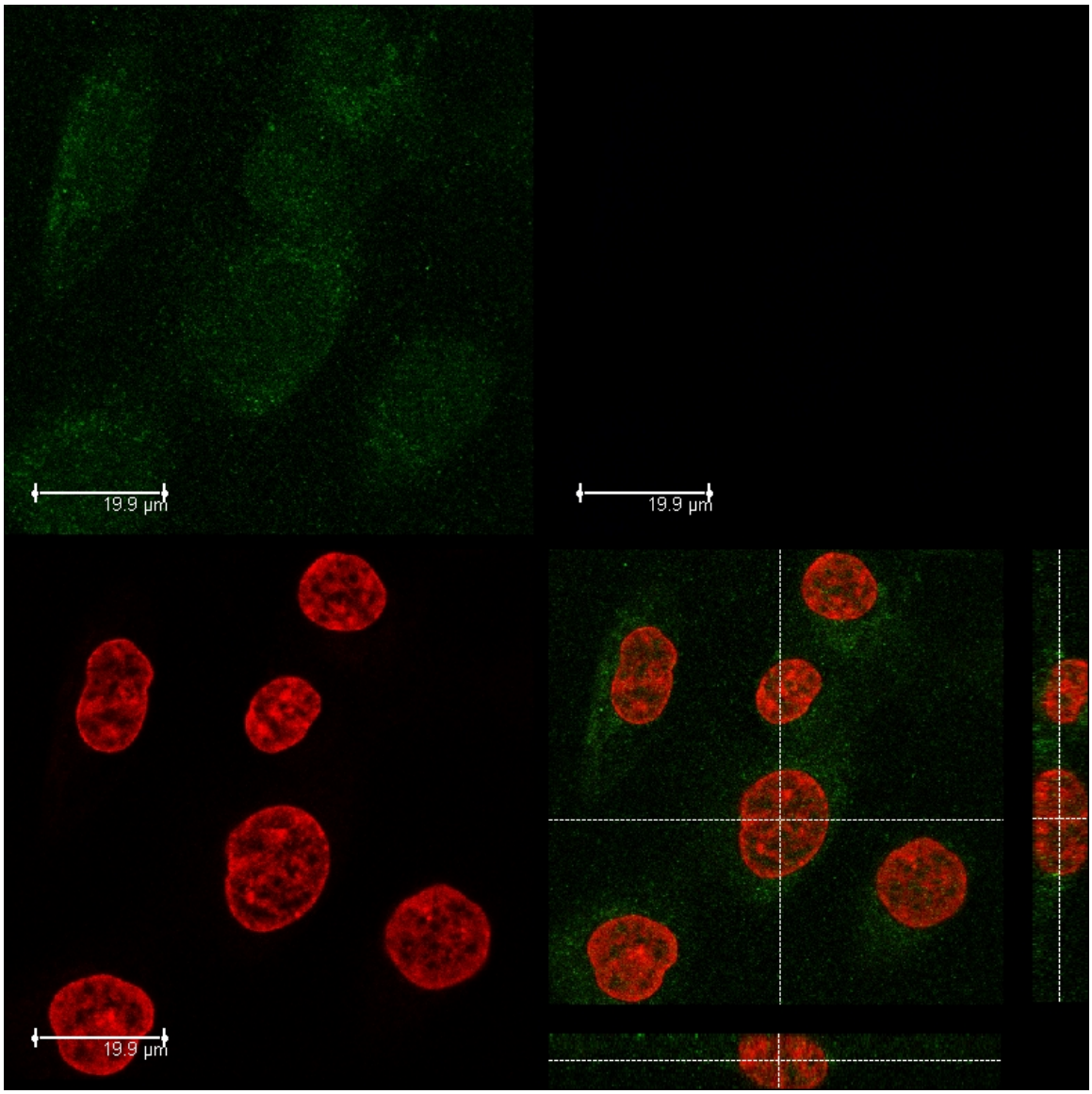



**Figure 4.8.1.2 Staining of endogenous Endo180 in DU145 cells (secondary antibody only control):** DU145 were seeded on Matrigel coated coverslips and grown under their normal growth conditions for four days. Fixed cells were subsequently permeabilised using 0.2 % w/v saponin and immunostained using either A5:158 or 39.10 mouse anti-human Endo180 mAbs followed by Alexa-555 Fluor conjugated IgG, as well as E-Cadherin 24E10 rabbit mAb Alexa 488 conjugate. Nuclei were counterstained with DAPI. 36 z-sections were acquired using a Leica SP5 confocal microscope and a 63x/1.4 oil immersion objective. (**upper left**) Endo180, (**upper right**) E-Cadherin, (**lower left**) Nuclei, (**lower right**) z-projection. (n=3)

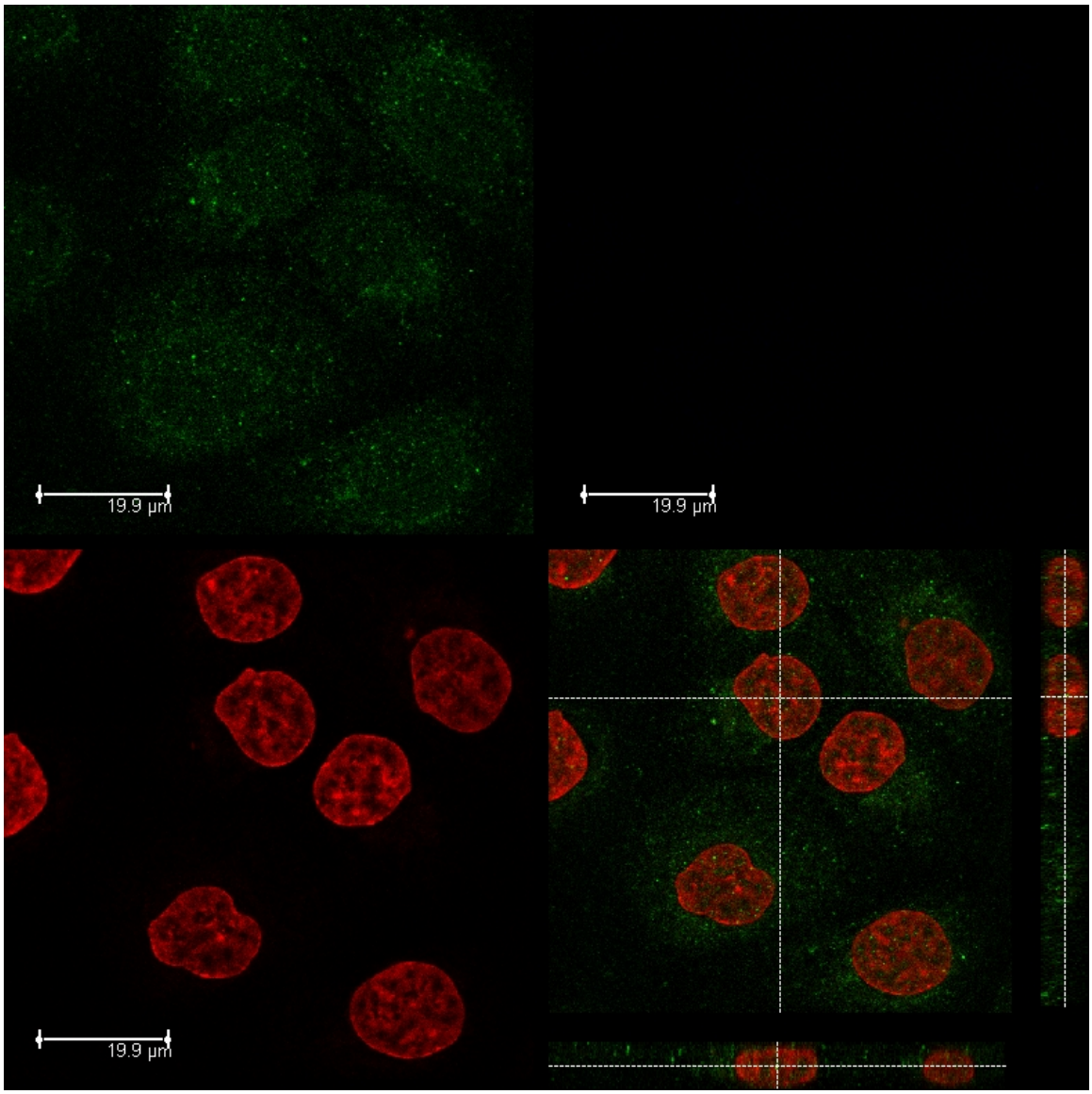



**Figure 4.8.1.3 Staining of endogenous Endo180 in DU145 cells (isotype control):** DU145 were seeded on Matrigel coated coverslips and grown under their normal growth conditions for four days. Fixed cells were subsequently permeabilised using 0.2 % w/v saponin and immunostained using either A5:158 or 39.10 mouse anti-human Endo180 mAbs followed by Alexa-555 Fluor conjugated IgG, as well as E-Cadherin 24E10 rabbit mAb Alexa 488 conjugate. Nuclei were counterstained with DAPI. 36 z-sections were acquired using a Leica SP5 confocal microscope and a 63x/1.4 oil immersion objective. (**upper left**) Endo180, (**upper right**) E-Cadherin, (**lower left**) Nuclei, (**lower right**) z-projection. (n=3)

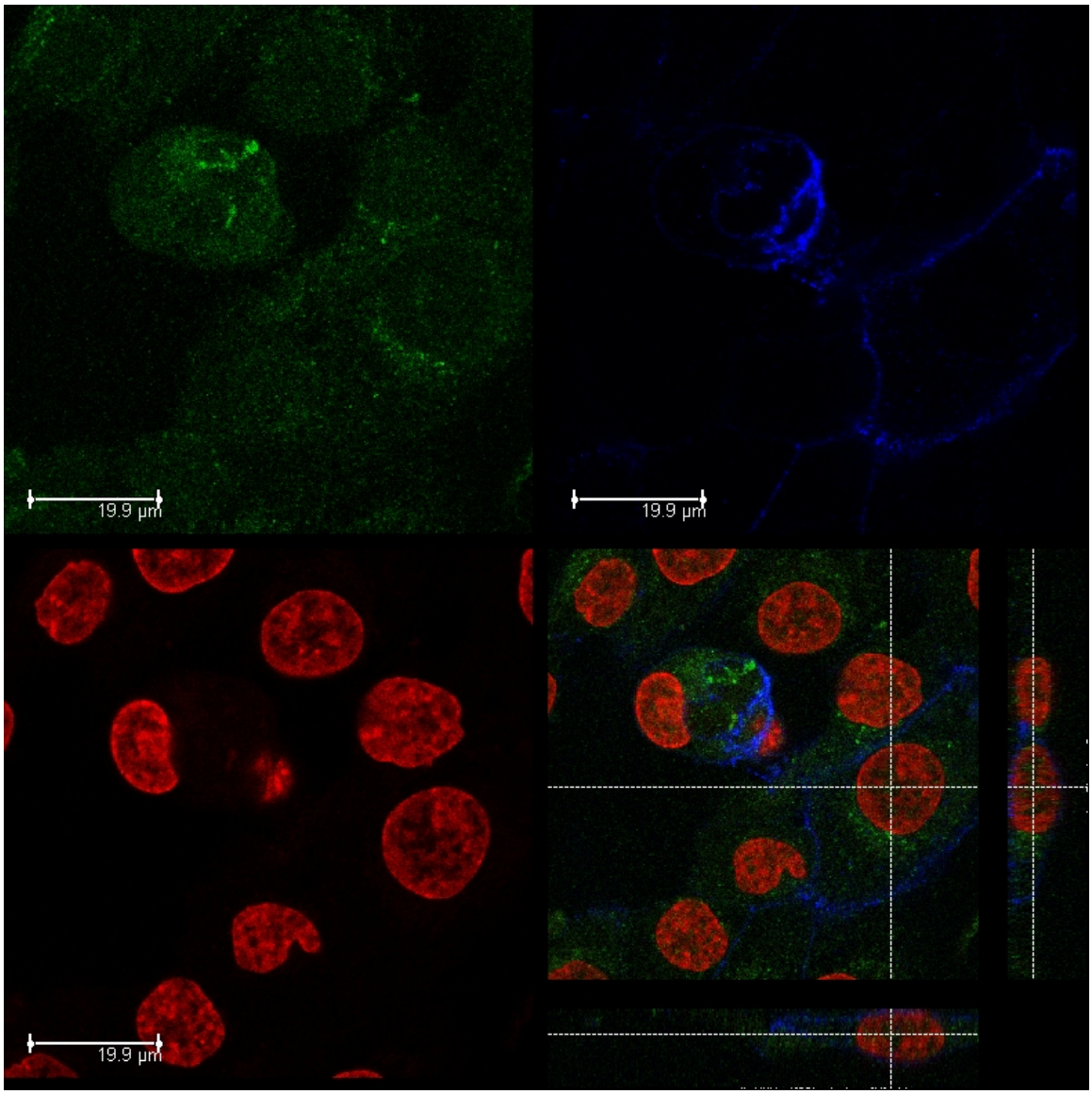



**Figure 4.8.1.4 Staining of endogenous Endo180 in DU145 cells (Endo180 39:10 and E-Cadherin 24E10):** DU145 were seeded on Matrigel coated coverslips and grown under their normal growth conditions for four days. Fixed cells were subsequently permeabilised using 0.2 % w/v saponin and immunostained using either A5:158 or 39.10 mouse anti-human Endo180 mAbs followed by Alexa-555 Fluor conjugated IgG, as well as E-Cadherin 24E10 rabbit mAb Alexa 488 conjugate. Nuclei were counterstained with DAPI. 36 z-sections were acquired using a Leica SP5 confocal microscope and a 63x/1.4 oil immersion objective. (**upper left**) Endo180, (**upper right**) E-Cadherin, (**lower left**) Nuclei, (**lower right**) z-projection. (n=3)

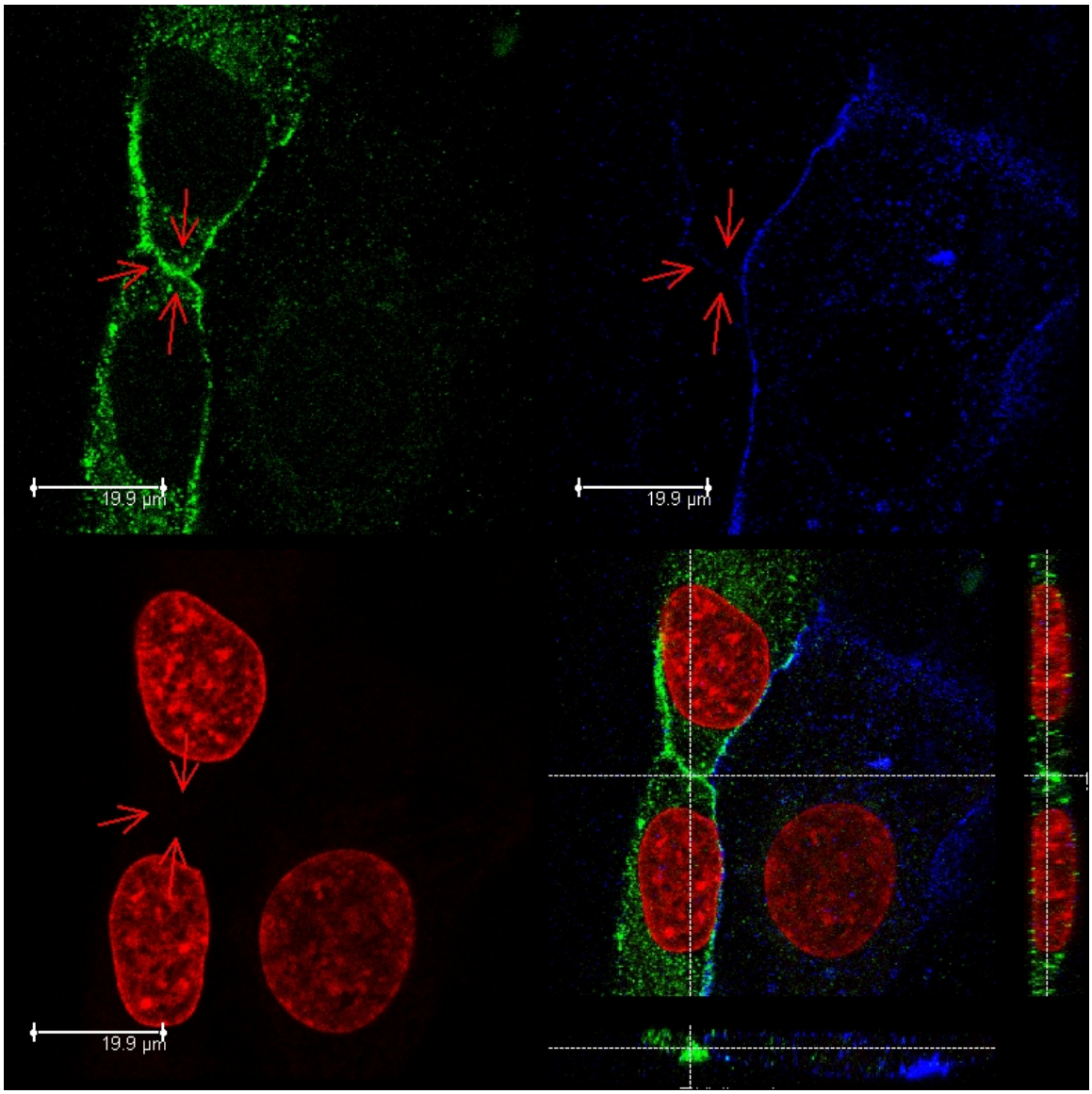



**Figure 4.8.1.5 Staining of endogenous Endo180 in DU145 cells (Endo180 A5:158 and E-Cadherin 24E10):** DU145 were seeded on Matrigel coated coverslips and grown under their normal growth conditions for four days. Fixed cells were subsequently permeabilised using 0.2 % w/v saponin and immunostained using either A5:158 or 39.10 mouse anti-human Endo180 mAbs followed by Alexa-555 Fluor conjugated IgG, as well as E-Cadherin 24E10 rabbit mAb Alexa 488 conjugate. Nuclei were counterstained with DAPI. 36 z-sections were acquired using a Leica SP5 confocal microscope and a 63x/1.4 oil immersion objective. (**upper left**) Endo180, (**upper right**) E-Cadherin, (**lower left**) Nuclei, (**lower right**) z-projection. (n=3)

## 4.9 Sub-cellular localisation in DU145 cells overexpressing Endo180-hmKO2 fluorescent fusion protein

Leveraging on the positive results achieved with the site-directed mutagenesis kit (**section 3.6**), PCR of the Endo180 encoding sequence captured in the pcDNA3 expression vector by the Isacke lab (**figures 3.6.1 and 3.6.2**) was revisited. Titration of different temperatures with and without DMSO supplementation revealed that the Endo180 encoding sequence is amplified cleanly by PCR as long as 5% v/v DMSO are added to the reaction mix. Surprisingly, a sequence encoding murine Endo180 that was procured from the mammalian gene collection, MGC, required no addition of DMSO to the reaction mix. In fact, the yield was higher without DMSO.

The human Endo180 encoding sequence excluding the stop codon was amplified by PCR using a NotI primer adaptor at the n-terminal end (**figure 4.9.2**). Another NotI restriction site was present upstream the c-terminal end in the pcDNA3 expression vector (**section 3.4.5**), the upstream primer was designed to allow for this NotI restriction site to be amplified as well (**figure 4.9.2**). The encoding sequenced was excised from the PCR product by NotI digest only and ligated into a NotI digested Kusabira orange expression vector (**figure 4.9.1 and 4.9.3**). Correct orientation was confirmed using HindIII restriction digest.

In this construct, the fluorescent monomeric Kusabira orange protein was connected to the cytoplasmic tail of Endo180 via a flexible linker peptide. Previous attempts to fluorescently label Endo180 failed (J. Sturge personal communication). In contrast, this construct was transiently expressed in DU145 cells (**figure 4.9.4.5; controls 4.9.4.1 – 4.9.4.4**).

An attempt to generate stable DU145 cell lines overexpressing Endo180-phmKO2 and phmKO2 failed. Therefore, DU145 cells were titrated against Lipofectamin LTX and Plus reagent to allow for transient transfection of the construct. Any combination of concentration of reagents and DNA that achieved transfection of DU145 cells displayed at least some cytotoxic effects. Pre-coating of glass coverslips

with 0.5% Matrigel for 1h improved cell survival but the transfection efficiency was low.

hmKO2 expressed on its own localises to the cytosol and nucleus (**figure 4.9.4.1 – 4.9.4.4**). The Endo180-hmKO2 fusion protein expression is not detectable in the nucleus (**figure 4.9.5.1 – 4.9.5.4**). Interestingly, cells expressing phmKO2 show nuclei not distinct from untransfected cells in their proximity (**figure 4.9.4.1 – 4.9.4.4**) whereas phmKO2-Endo180 transfected cells display deformed nuclei (**figure 4.9.5.1 – 4.9.5.4**).

However, the fluorescent pattern looked distinct from endogenous Endo180 staining (**section 4.8**). While in some cells the distribution almost looks vesicular, in other cells the distribution appears to be cytosolic or even filamentous (**figure 4.9.5.1 – 4.9.5.4**). In order to address these issues, it was decided to overexpress wild type Endo180 in DU145 cells (**section 4.10**).

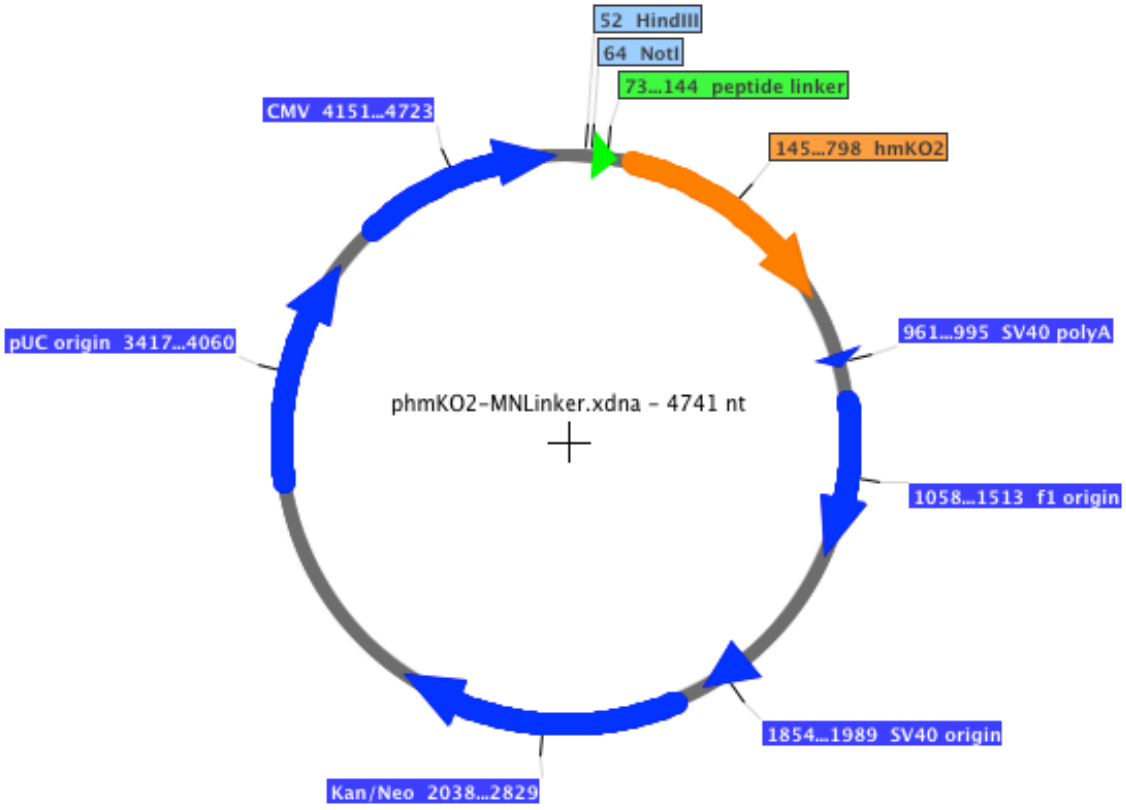



**Figure 4.9.1 phmKO2 MNLinker empty vector**

Cloning of phmKO2-MNLinker Endo180

forward primer CGAGCTCGGATCCACTAGTAACG

reverse primer atagtttagcggccgcTTCTTGTTGCTCATTCATTTCCATGTCTG

overhang
to add NotI
restriction site

**Figure 4.9.2 phmKO2 MNLinker primers**

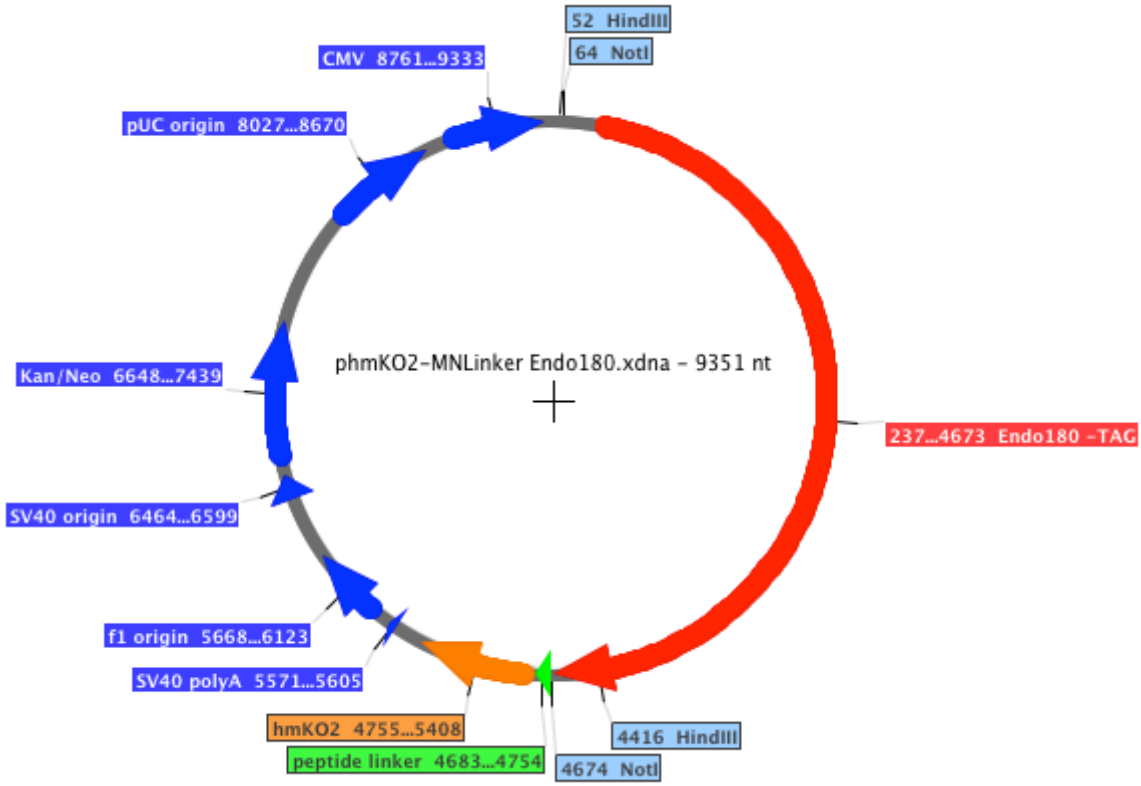



**Figure 4.9.3 phmKO2 MNLinker Endo180 vector**

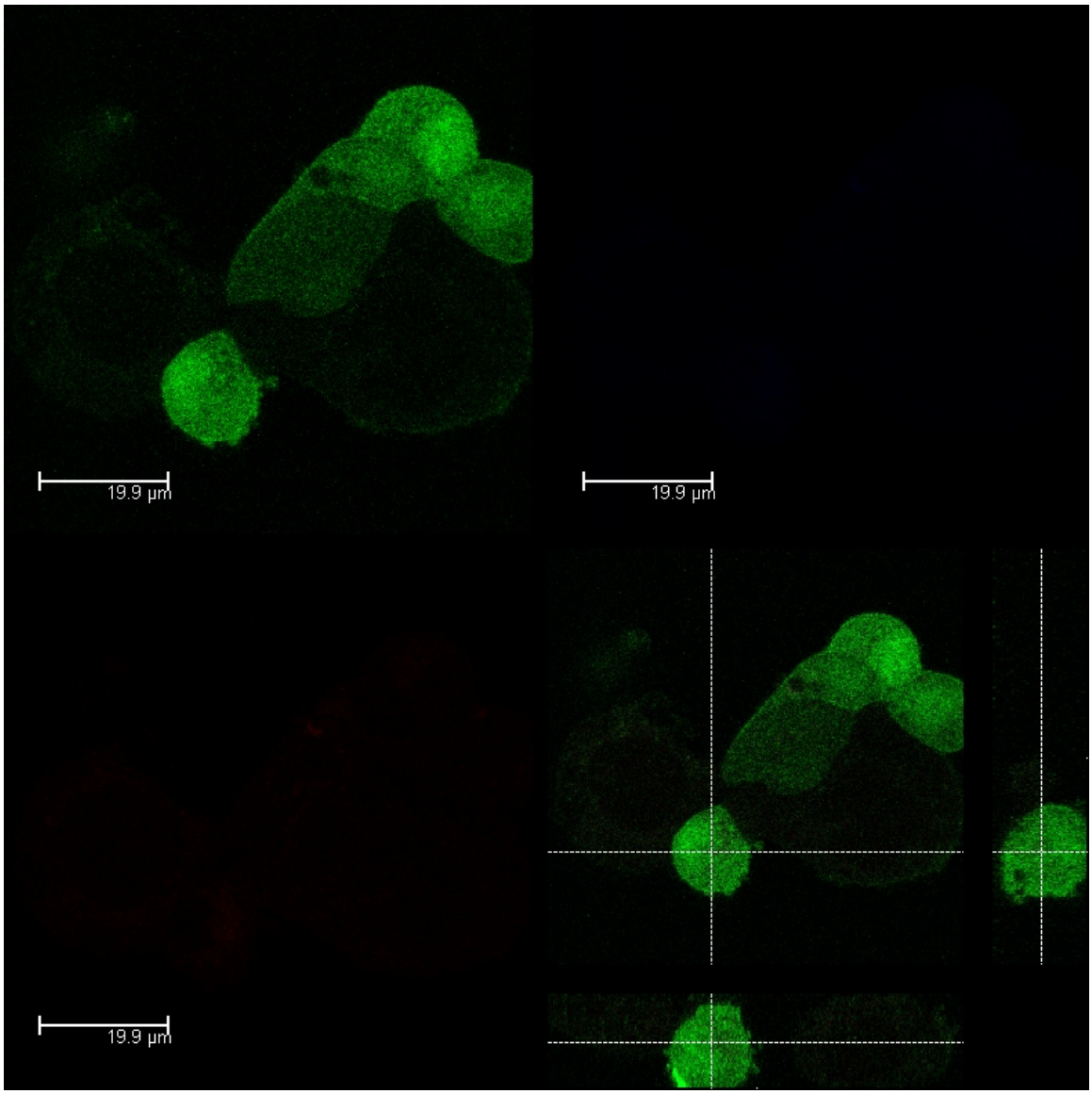



**Figure 4.9.4.1 Staining of E-Cadherin in DU145 cells transiently expressing phmKO2-MNLinker empty vector (unstained control):** DU145 were seeded on Matrigel coated coverslips and grown under their normal growth conditions. After 12hours cells were transfected using Lipofectamin LTX and Plus reagent. Cells were fixed after 72 hours. Fixed cells were subsequently permeabilised using 0.2 % w/v saponin and immunostained using E-Cadherin 24E10 rabbit mAb. Nuclei were counterstained with DAPI. 36 z-sections were acquired using a Leica SP5 confocal microscope and a 63x/1.4 oil immersion objective. (**upper left**) mKO2 fluorescence, (**upper right**) E-Cadherin, (**lower left**) Nuclei, (**lower right**) z-projection. (n=3)

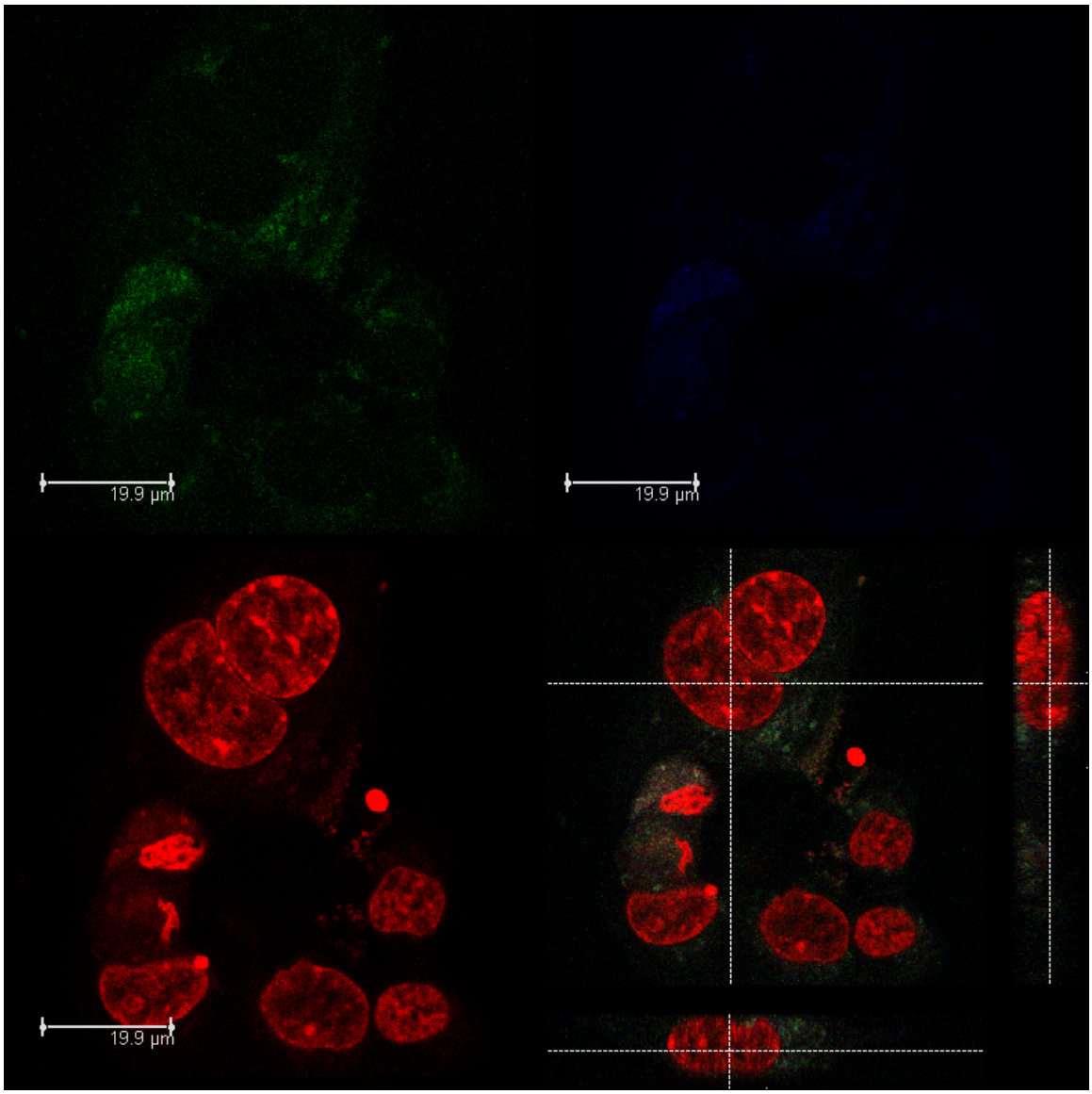



**Figure 4.9.4.2 Staining of E-Cadherin in DU145 cells transiently expressing phmKO2-MNLinker empty vector (secondary antibody only):** DU145 were seeded on Matrigel coated coverslips and grown under their normal growth conditions. After 12hours cells were transfected using Lipofectamin LTX and Plus reagent. Cells were fixed after 72 hours. Fixed cells were subsequently permeabilised using 0.2 % w/v saponin and immunostained using E-Cadherin 24E10 rabbit mAb. Nuclei were counterstained with DAPI. 36 z-sections were acquired using a Leica SP5 confocal microscope and a 63x/1.4 oil immersion objective. (**upper left**) mKO2 fluorescence, (**upper right**) E-Cadherin, (**lower left**) Nuclei, (**lower right**) z-projection. (n=3)

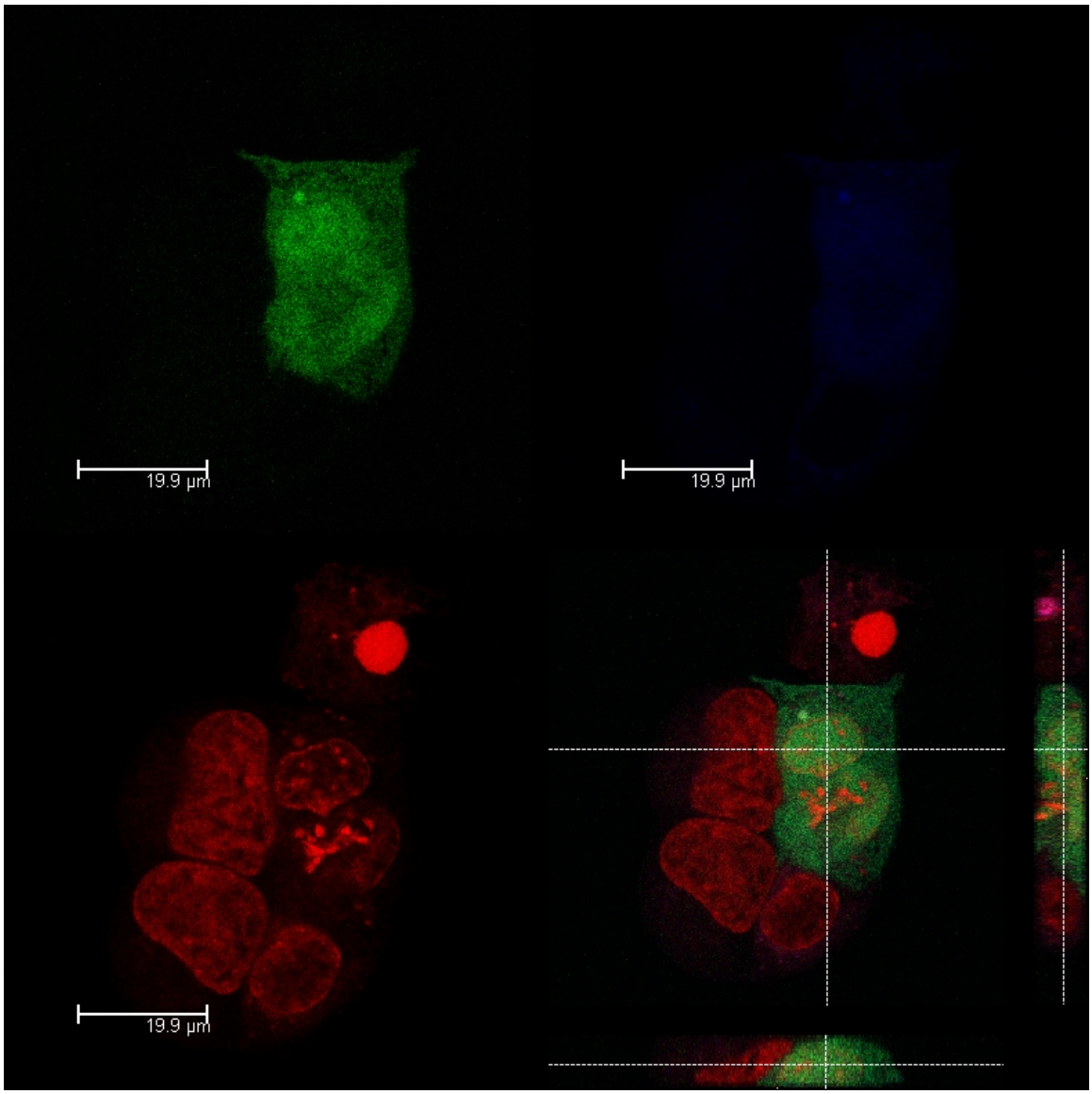



**Figure 4.9.4.3 Staining of E-Cadherin in DU145 cells transiently expressing phmKO2-MNLinker empty vector (isotype control):** DU145 were seeded on Matrigel coated coverslips and grown under their normal growth conditions. After 12hours cells were transfected using Lipofectamin LTX and Plus reagent. Cells were fixed after 72 hours. Fixed cells were subsequently permeabilised using 0.2 % w/v saponin and immunostained using E-Cadherin 24E10 rabbit mAb. Nuclei were counterstained with DAPI. 36 z-sections were acquired using a Leica SP5 confocal microscope and a 63x/1.4 oil immersion objective. (**upper left**) mKO2 fluorescence, (**upper right**) E-Cadherin, (**lower left**) Nuclei, (**lower right**) z-projection. (n=3)

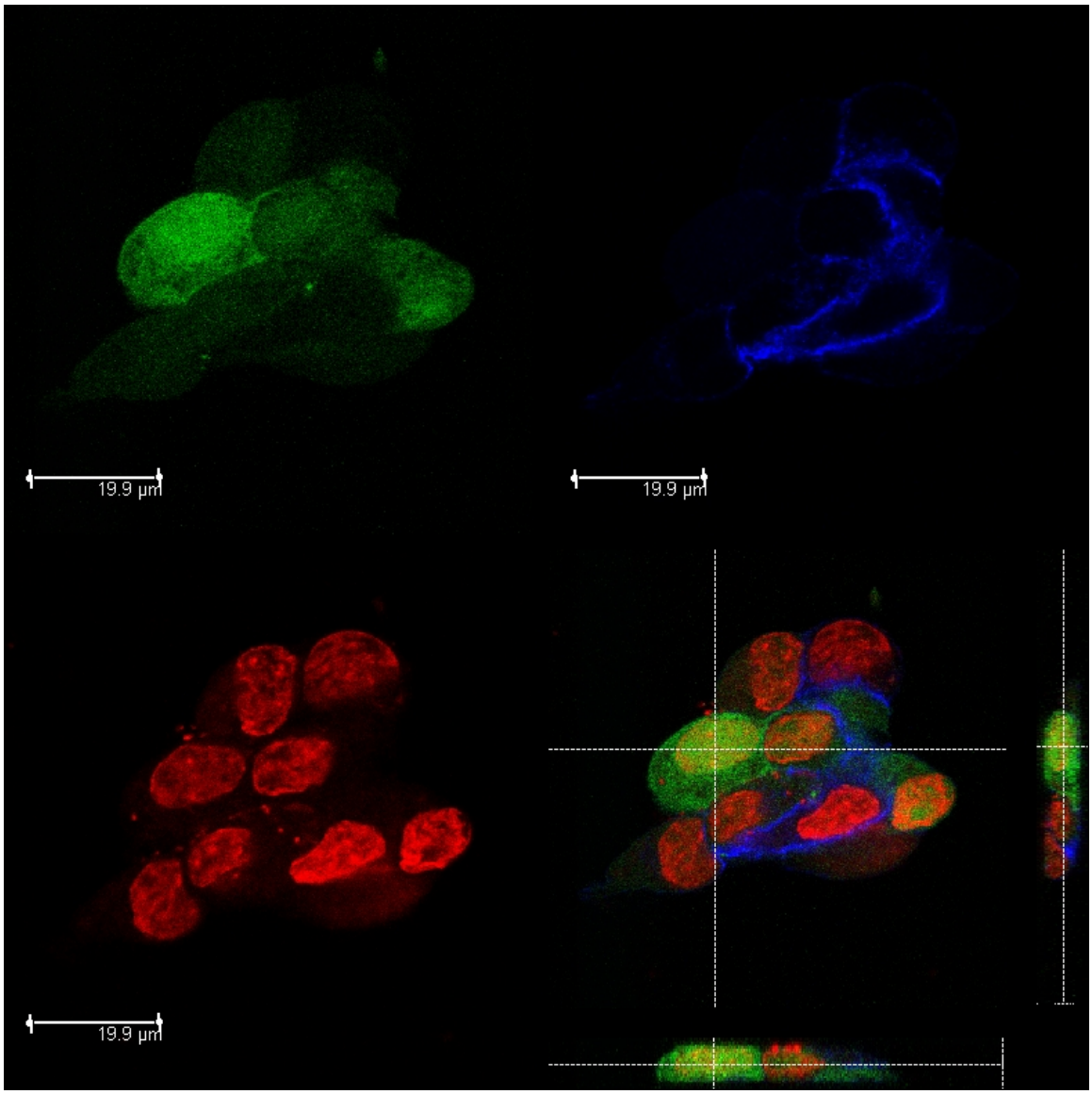



**Figure 4.9.4.4 Staining of E-Cadherin in DU145 cells transiently expressing phmKO2-MNLinker empty vector (E-Cadherin 24E10):** DU145 were seeded on Matrigel coated coverslips and grown under their normal growth conditions. After 12hours cells were transfected using Lipofectamin LTX and Plus reagent. Cells were fixed after 72 hours. Fixed cells were subsequently permeabilised using 0.2 % w/v saponin and immunostained using E-Cadherin 24E10 rabbit mAb . Nuclei were counterstained with DAPI. 36 z-sections were acquired using a Leica SP5 confocal microscope and a 63x/1.4 oil immersion objective. (**upper left**) mKO2 fluorescence, (**upper right**) E-Cadherin, (**lower left**) Nuclei, (**lower right**) z-projection. (n=3)

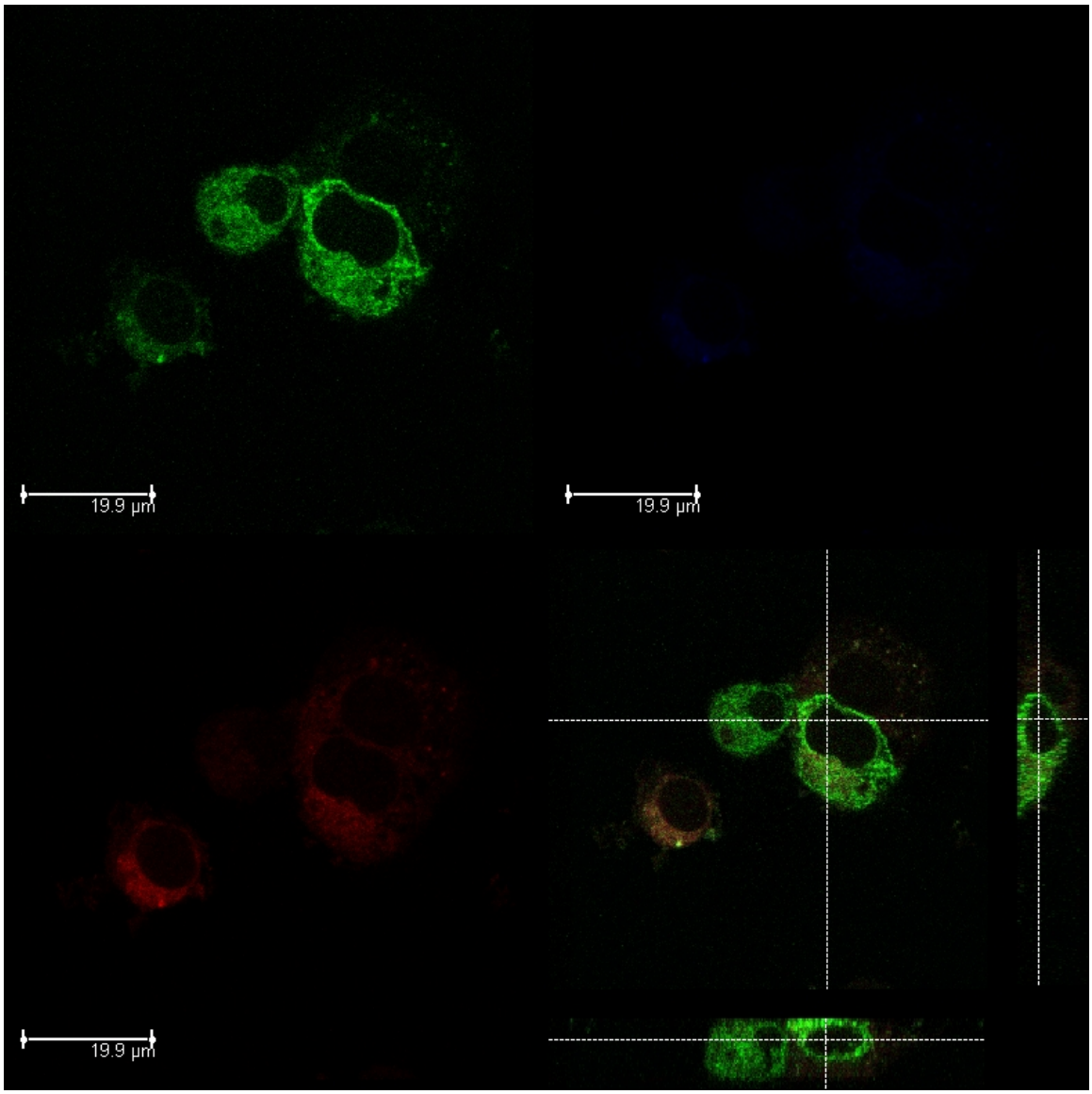



**Figure 4.9.5.1 Staining of E-Cadherin in DU145 cells transiently expressing phmKO2-MNLinker Endo180 vector (unstained control):** DU145 were seeded on Matrigel coated coverslips and grown under their normal growth conditions. After 12hours cells were transfected using Lipofectamin LTX and Plus reagent. Cells were fixed after 72 hours. Fixed cells were subsequently permeabilised using 0.2 % w/v saponin and immunostained using E-Cadherin 24E10 rabbit mAb. Nuclei were counterstained with DAPI. 36 z-sections were acquired using a Leica SP5 confocal microscope and a 63x/1.4 oil immersion objective. (**upper left**) mKO2 fluorescence, (**upper right**) E-Cadherin, (**lower left**) Nuclei, (**lower right**) z-projection. (n=3)

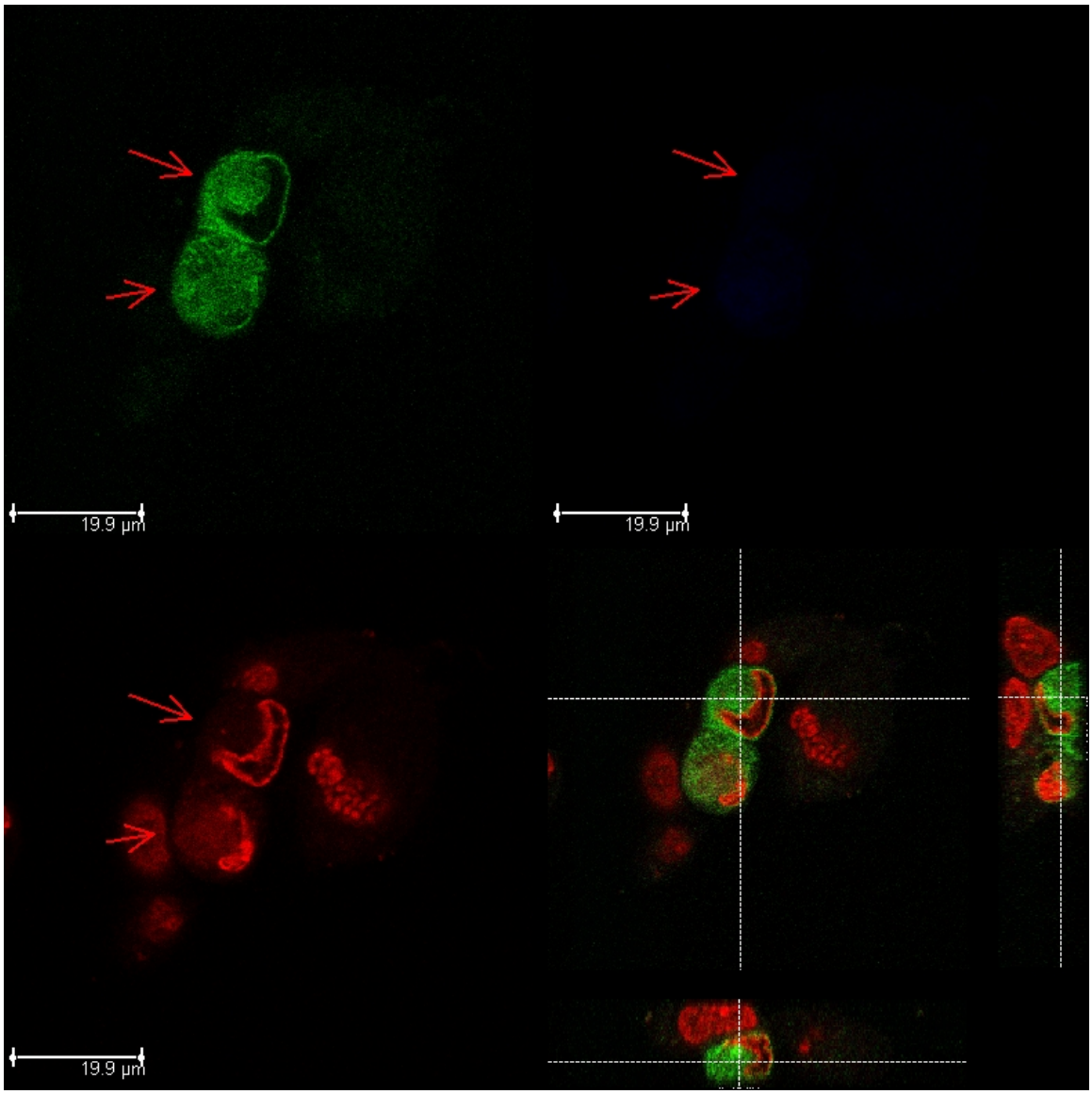



**Figure 4.9.5.2 Staining of E-Cadherin in DU145 cells transiently expressing phmKO2-MNLinker Endo180 vector (secondary antibody only):** DU145 were seeded on Matrigel coated coverslips and grown under their normal growth conditions. After 12hours cells were transfected using Lipofectamin LTX and Plus reagent. Cells were fixed after 72 hours. Fixed cells were subsequently permeabilised using 0.2 % w/v saponin and immunostained using E-Cadherin 24E10 rabbit mAb. Nuclei were counterstained with DAPI. 36 z-sections were acquired using a Leica SP5 confocal microscope and a 63x/1.4 oil immersion objective. (**upper left**) mKO2 fluorescence, (**upper right**) E-Cadherin, (**lower left**) Nuclei, (**lower right**) z-projection. (n=3)

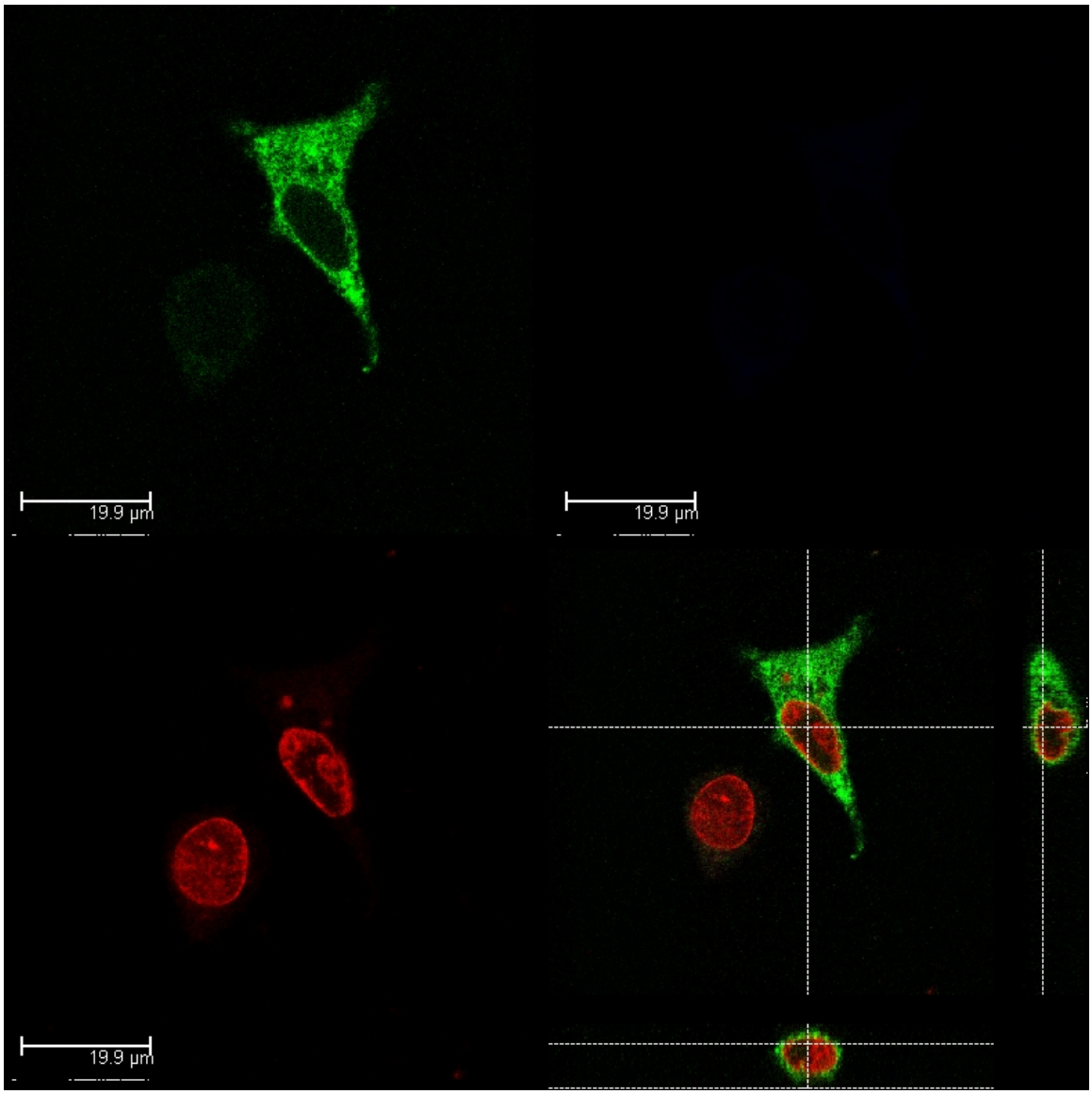



**Figure 4.9.5.3 Staining of E-Cadherin in DU145 cells transiently expressing phmKO2-MNLinker Endo180 vector (isotype control):** DU145 were seeded on Matrigel coated coverslips and grown under their normal growth conditions. After 12hours cells were transfected using Lipofectamin LTX and Plus reagent. Cells were fixed after 72 hours. Fixed cells were subsequently permeabilised using 0.2 % w/v saponin and immunostained using E-Cadherin 24E10 rabbit mAb. Nuclei were counterstained with DAPI. 36 z-sections were acquired using a Leica SP5 confocal microscope and a 63x/1.4 oil immersion objective. (**upper left**) mKO2 fluorescence, (**upper right**) E-Cadherin, (**lower left**) Nuclei, (**lower right**) z-projection. (n=3)

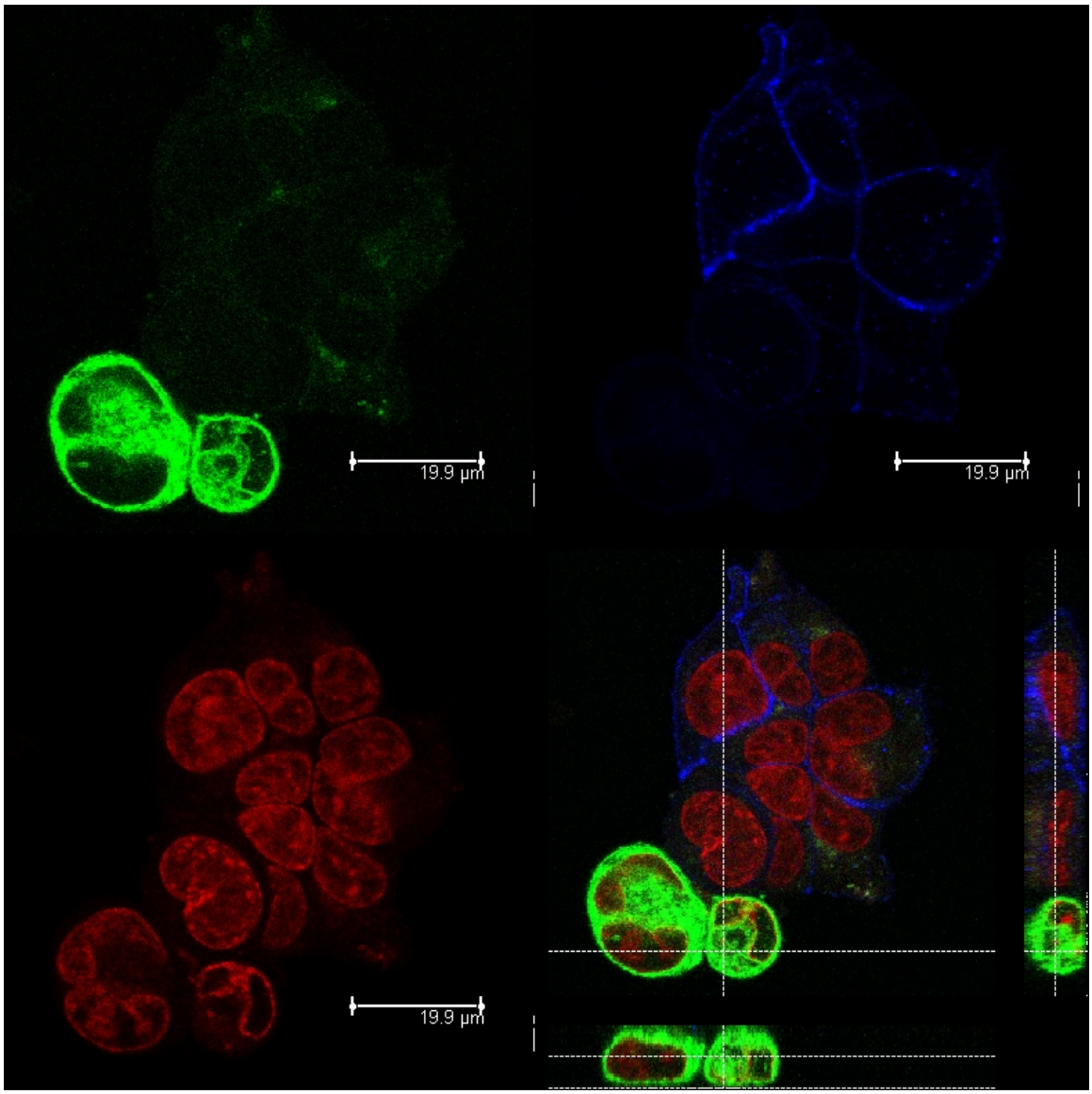



**Figure 4.9.5.4 Staining of E-Cadherin in DU145 cells transiently expressing phmKO2-MNLinker Endo180 vector (E-Cadherin 24E10):** DU145 were seeded on Matrigel coated coverslips and grown under their normal growth conditions. After 12hours cells were transfected using Lipofectamin LTX and Plus reagent. Cells were fixed after 72 hours. Fixed cells were subsequently permeabilised using 0.2 % w/v saponin and immunostained using E-Cadherin 24E10 rabbit mAb . Nuclei were counterstained with DAPI. 36 z-sections were acquired using a Leica SP5 confocal microscope and a 63x/1.4 oil immersion objective. (**upper left**) mKO2 fluorescence, (**upper right**) E-Cadherin, (**lower left**) Nuclei, (**lower right**) z-projection. (n=3)

## 4.10 Sub-cellular localisation in DU145 cells overexpressing Endo180

The results gathered by overexpressing Endo180 hmKO2 fusion protein were inconclusive as the fusion protein showed a different distribution pattern than endogenous Endo180 (**section 4.9**). Therefore it was decided to overexpress wild type Endo180 using the pcDNA3 Endo180 expression vector originally generated by the Isacke lab. DU145 cells were transfected under the same conditions as in the Endo180 mKO2 fusion protein experiment (**figure 4.10.1.5 empty vector control; figure 4.10.2.5 Endo180 expression vector; figure 4.10.1.1 – 4.10.1.4 and 4.10.2.1 – 4.10.2.4 staining controls**). The laser settings on the confocal microscope were readjusted to take the new dynamic range of overexpressed Endo180 into considerations. Therefore, DU145 cells transfected with pcDNA3 empty vector appear negative for Endo180 using both the A5:158 and the 39:10 antibody under these conditions.

However, strong Endo180 staining was detected in DU145 cells transfected with pcDNA3 Endo180 vector. Both, the A5:158 and 39:10 antibody gave positive staining results. However, no obvious difference in staining pattern can be detected between both antibodies. Furthermore, Endo180 is not consistently localised at cell-cell junctions. Therefore, the staining pattern produced by the A5:158 antibody looks different in DU145 cells expressing endogenous levels of the protein (**figure 4.8.1.5**) than in DU145 cells overexpressing Endo180 (**figure 4.10.2.4 and 4.10.2.5**). It appears that overexpressed Endo180 localises to a lesser degree into the proximity of or to cell-cell junctions.

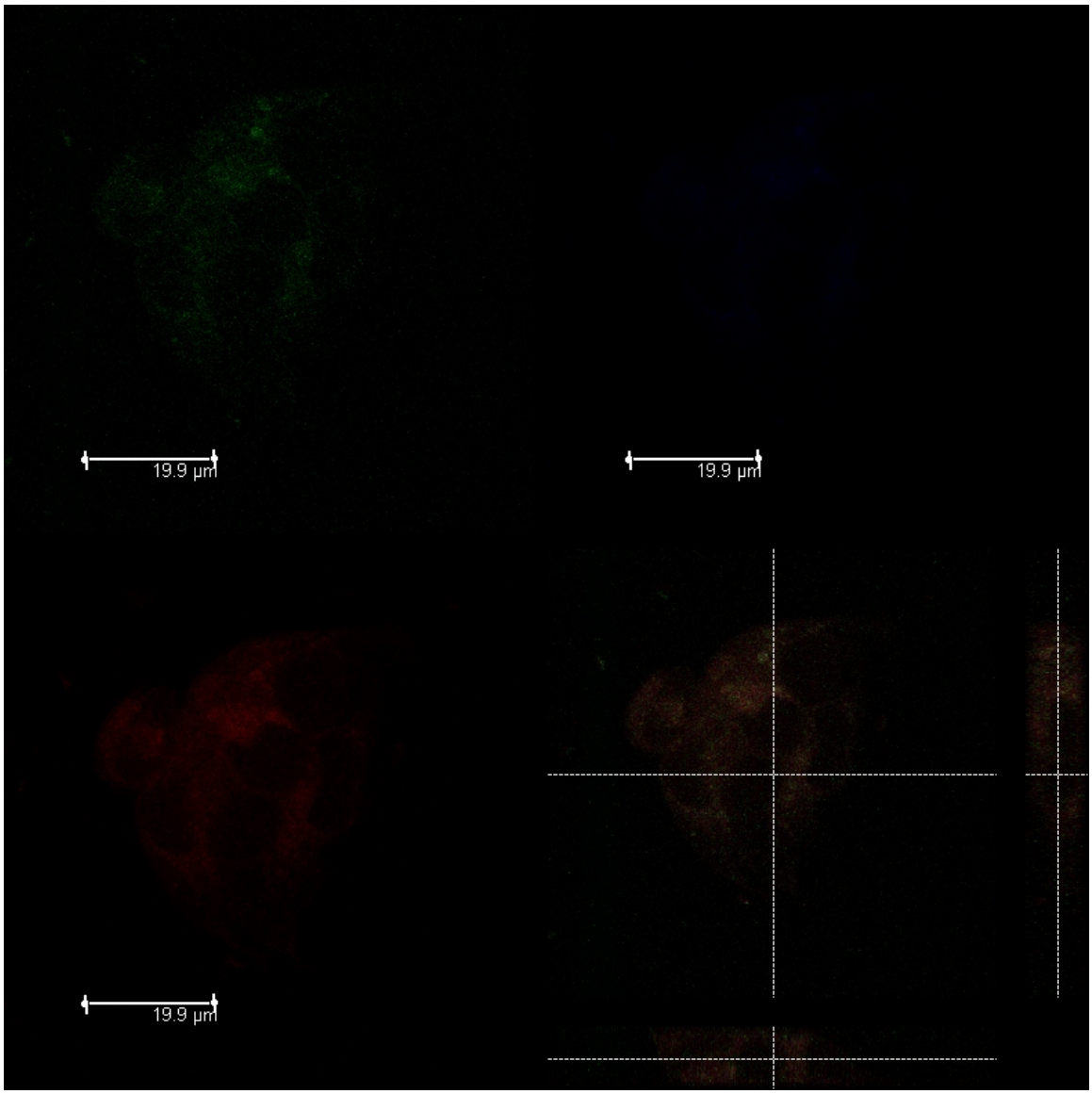



**Figure 4.10.1.1 Staining of E-Cadherin in DU145 cells transiently expressing pcDNA3 empty vector (unstained control):** DU145 were seeded on Matrigel coated coverslips and grown under their normal growth conditions. After 12hours cells were transfected using Lipofectamin LTX and Plus reagent. Cells were fixed after 72 hours. Fixed cells were subsequently permeabilised using 0.2 % w/v saponin and immunostained using E-Cadherin 24E10 rabbit mAb. Nuclei were counterstained with DAPI. 36 z-sections were acquired using a Leica SP5 confocal microscope and a 63x/1.4 oil immersion objective. (**upper left**) mKO2 fluorescence, (**upper right**) E-Cadherin, (**lower left**) Nuclei, (**lower right**) z-projection. (n=3)

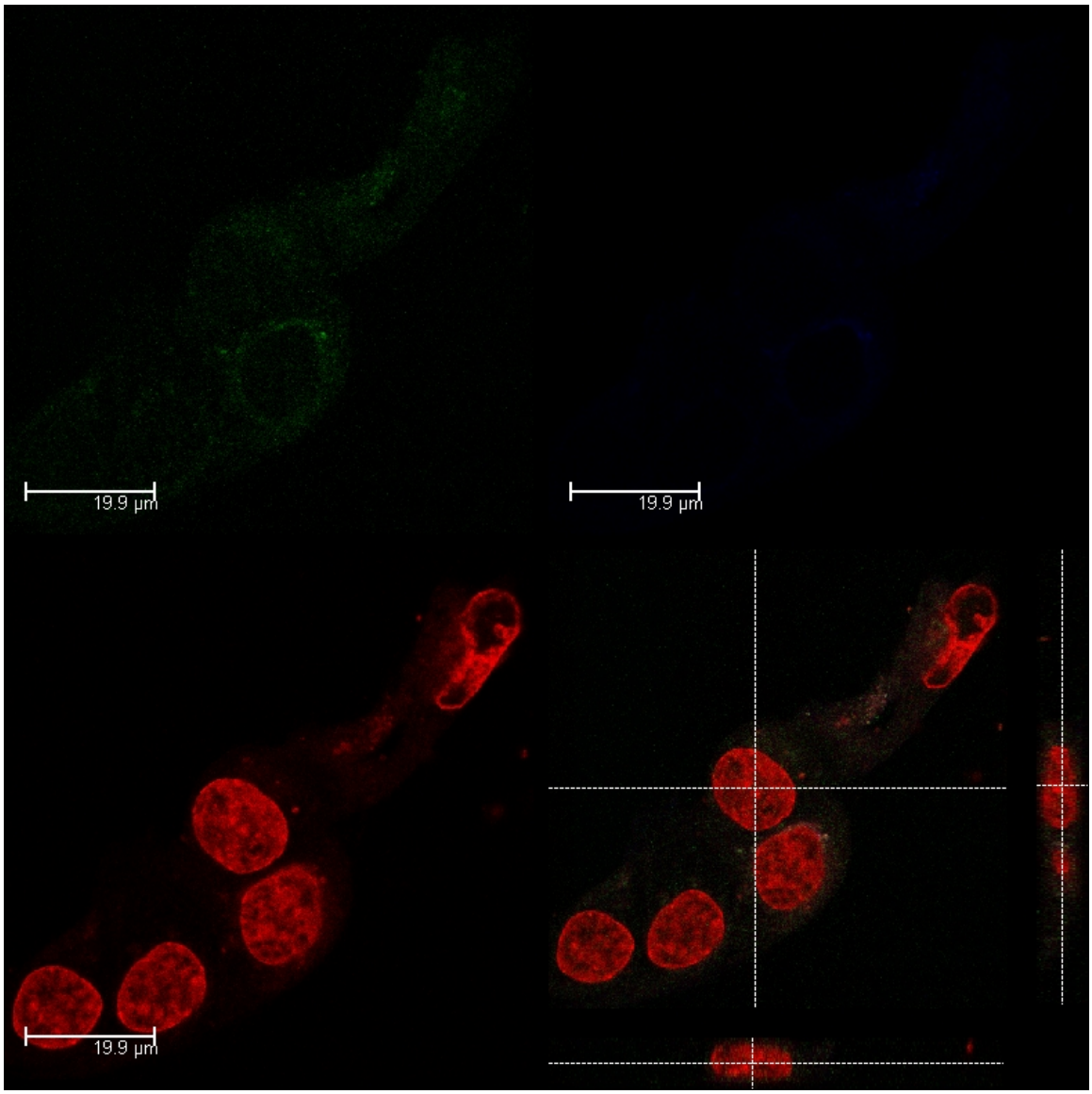



**Figure 4.10.1.2 Staining of E-Cadherin in DU145 cells transiently expressing pcDNA3 empty vector (secondary antibody only):** DU145 were seeded on Matrigel coated coverslips and grown under their normal growth conditions. After 12hours cells were transfected using Lipofectamin LTX and Plus reagent. Cells were fixed after 72 hours. Fixed cells were subsequently permeabilised using 0.2 % w/v saponin and immunostained using E-Cadherin 24E10 rabbit mAb. Nuclei were counterstained with DAPI. 36 z-sections were acquired using a Leica SP5 confocal microscope and a 63x/1.4 oil immersion objective. (**upper left**) mKO2 fluorescence, (**upper right**) E-Cadherin, (**lower left**) Nuclei, (**lower right**) z-projection. (n=3)

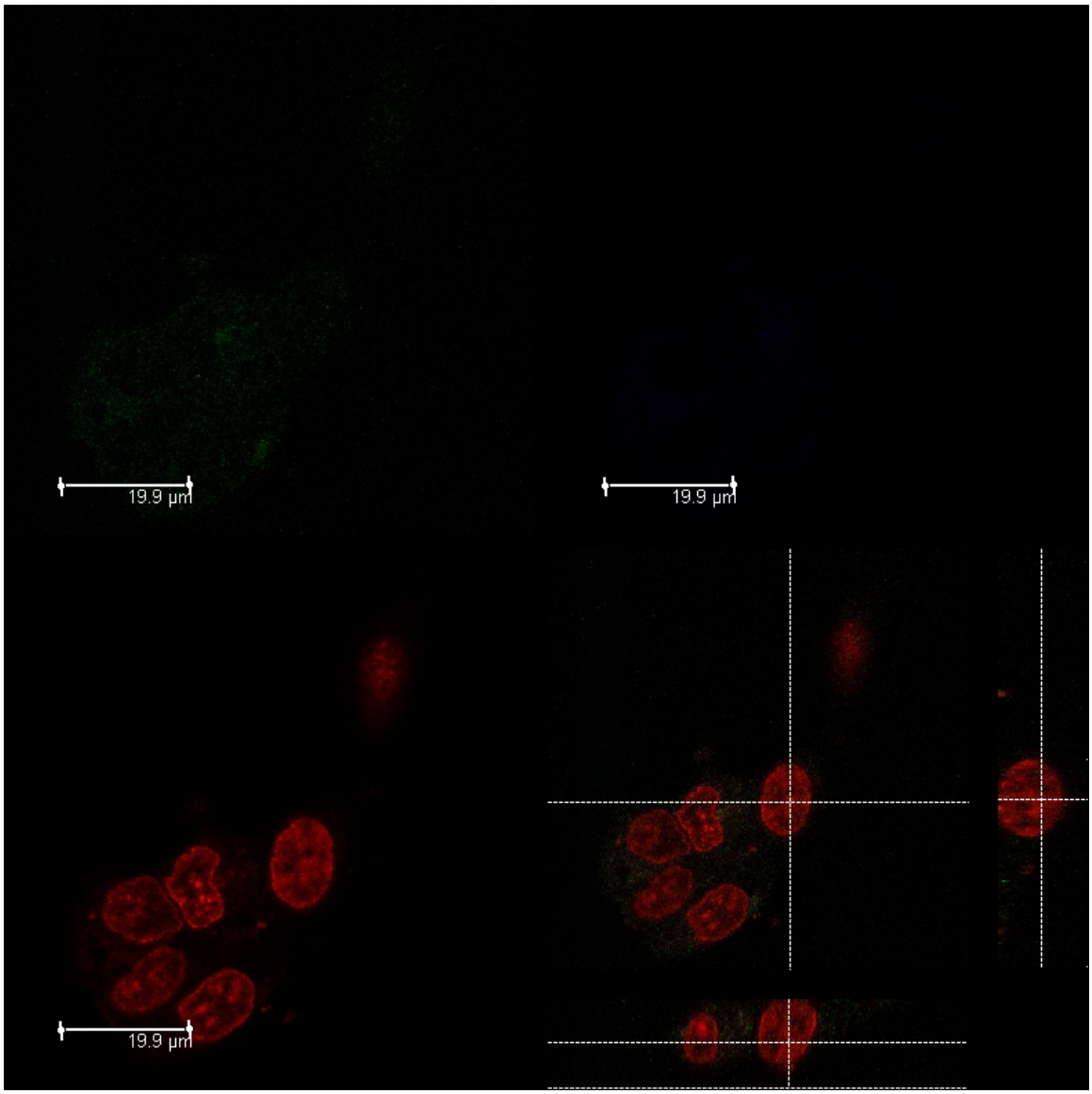



**Figure 4.10.1.3 Staining of E-Cadherin in DU145 cells transiently expressing pcDNA3 empty vector (isotype control):** DU145 were seeded on Matrigel coated coverslips and grown under their normal growth conditions. After 12hours cells were transfected using Lipofectamin LTX and Plus reagent. Cells were fixed after 72 hours. Fixed cells were subsequently permeabilised using 0.2 % w/v saponin and immunostained using E-Cadherin 24E10 rabbit mAb. Nuclei were counterstained with DAPI. 36 z-sections were acquired using a Leica SP5 confocal microscope and a 63x/1.4 oil immersion objective. (**upper left**) mKO2 fluorescence, (**upper right**) E-Cadherin, (**lower left**) Nuclei, (**lower right**) z-projection. (n=3)

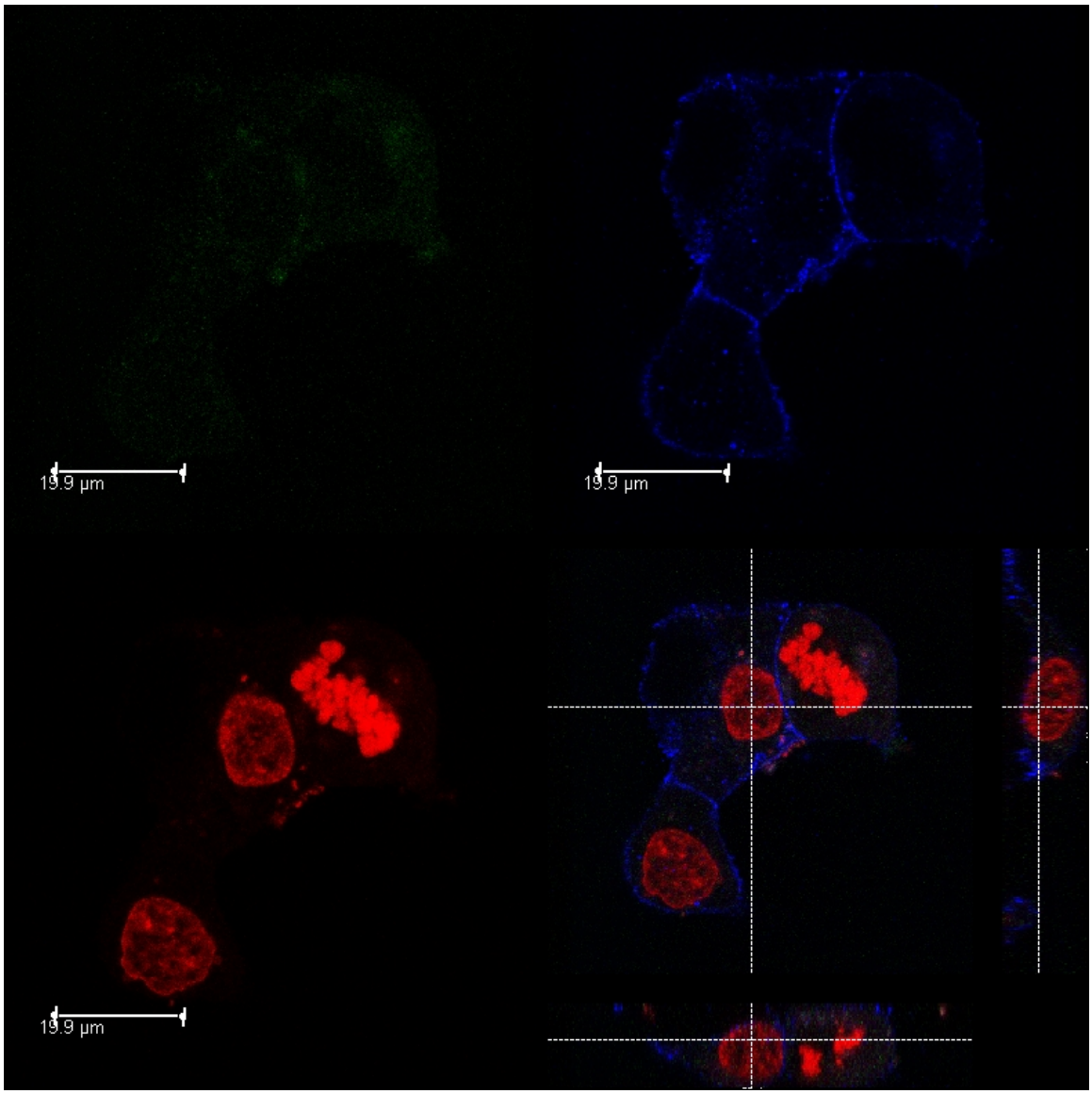



**Figure 4.10.1.4 Staining of E-Cadherin in DU145 cells transiently expressing pcDNA3 empty vector (Endo180 39:10 and E-Cadherin):** DU145 were seeded on Matrigel coated coverslips and grown under their normal growth conditions. After 12hours cells were transfected using Lipofectamin LTX and Plus reagent. Cells were fixed after 72 hours. Fixed cells were subsequently permeabilised using 0.2 % w/v saponin and immunostained using E-Cadherin 24E10 rabbit mAb . Nuclei were counterstained with DAPI. 36 z-sections were acquired using a Leica SP5 confocal microscope and a 63x/1.4 oil immersion objective. (**upper left**) mKO2 fluorescence, (**upper right**) E-Cadherin, (**lower left**) Nuclei, (**lower right**) z-projection. (n=3)

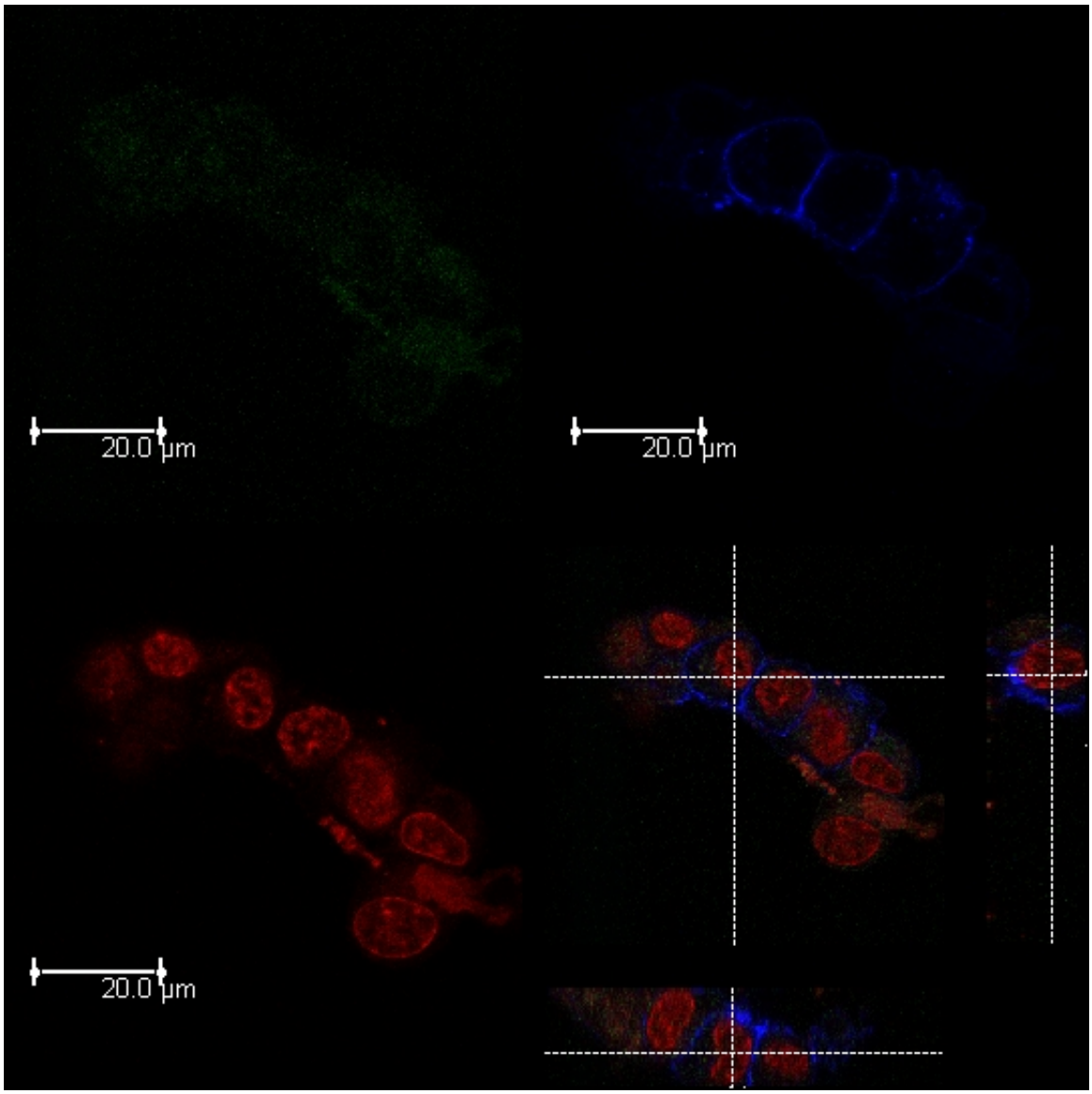



**Figure 4.10.1.5 Staining of E-Cadherin in DU145 cells transiently expressing pcDNA3 empty vector (Endo180 A5:158 and E-Cadherin):** DU145 were seeded on Matrigel coated coverslips and grown under their normal growth conditions. After 12hours cells were transfected using Lipofectamin LTX and Plus reagent. Cells were fixed after 72 hours. Fixed cells were subsequently permeabilised using 0.2 % w/v saponin and immunostained using E-Cadherin 24E10 rabbit mAb . Nuclei were counterstained with DAPI. 36 z-sections were acquired using a Leica SP5 confocal microscope and a 63x/1.4 oil immersion objective. (**upper left**) mKO2 fluorescence, (**upper right**) E-Cadherin, (**lower left**) Nuclei, (**lower right**) z-projection. (n=3)

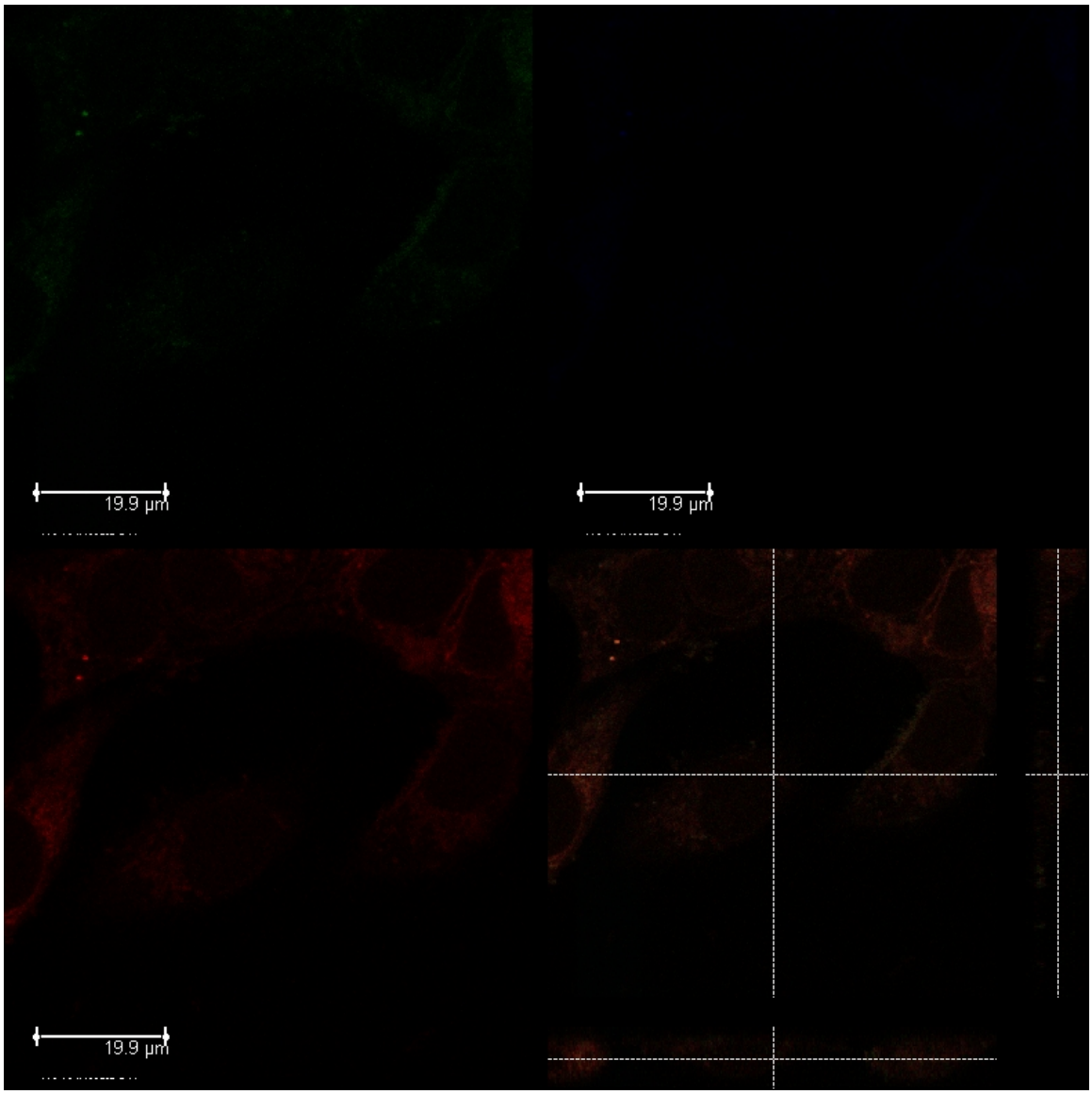



**Figure 4.10.2.1 Staining of E-Cadherin in DU145 cells transiently expressing pcDNA3 Endo180 vector (unstained control):** DU145 were seeded on Matrigel coated coverslips and grown under their normal growth conditions. After 12hours cells were transfected using Lipofectamin LTX and Plus reagent. Cells were fixed after 72 hours. Fixed cells were subsequently permeabilised using 0.2 % w/v saponin and immunostained using E-Cadherin 24E10 rabbit mAb. Nuclei were counterstained with DAPI. 36 z-sections were acquired using a Leica SP5 confocal microscope and a 63x/1.4 oil immersion objective. (**upper left**) mKO2 fluorescence, (**upper right**) E-Cadherin, (**lower left**) Nuclei, (**lower right**) z-projection. (n=3)

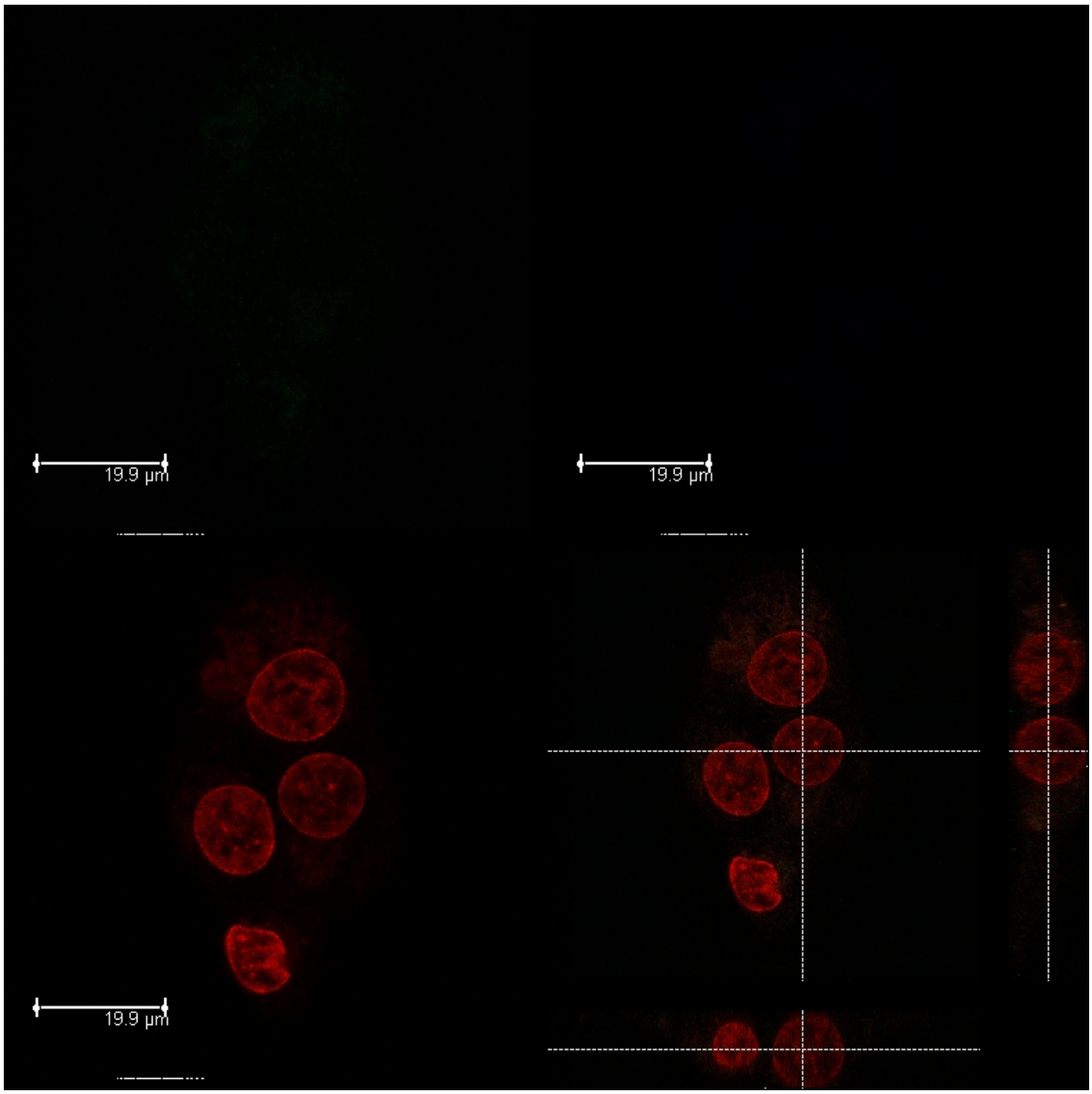



**Figure 4.10.2.2 Staining of E-Cadherin in DU145 cells transiently expressing pcDNA3 Endo180 vector (secondary antibody only):** DU145 were seeded on Matrigel coated coverslips and grown under their normal growth conditions. After 12hours cells were transfected using Lipofectamin LTX and Plus reagent. Cells were fixed after 72 hours. Fixed cells were subsequently permeabilised using 0.2 % w/v saponin and immunostained using E-Cadherin 24E10 rabbit mAb. Nuclei were counterstained with DAPI. 36 z-sections were acquired using a Leica SP5 confocal microscope and a 63x/1.4 oil immersion objective. (**upper left**) mKO2 fluorescence, (**upper right**) E-Cadherin, (**lower left**) Nuclei, (**lower right**) z-projection. (n=3)

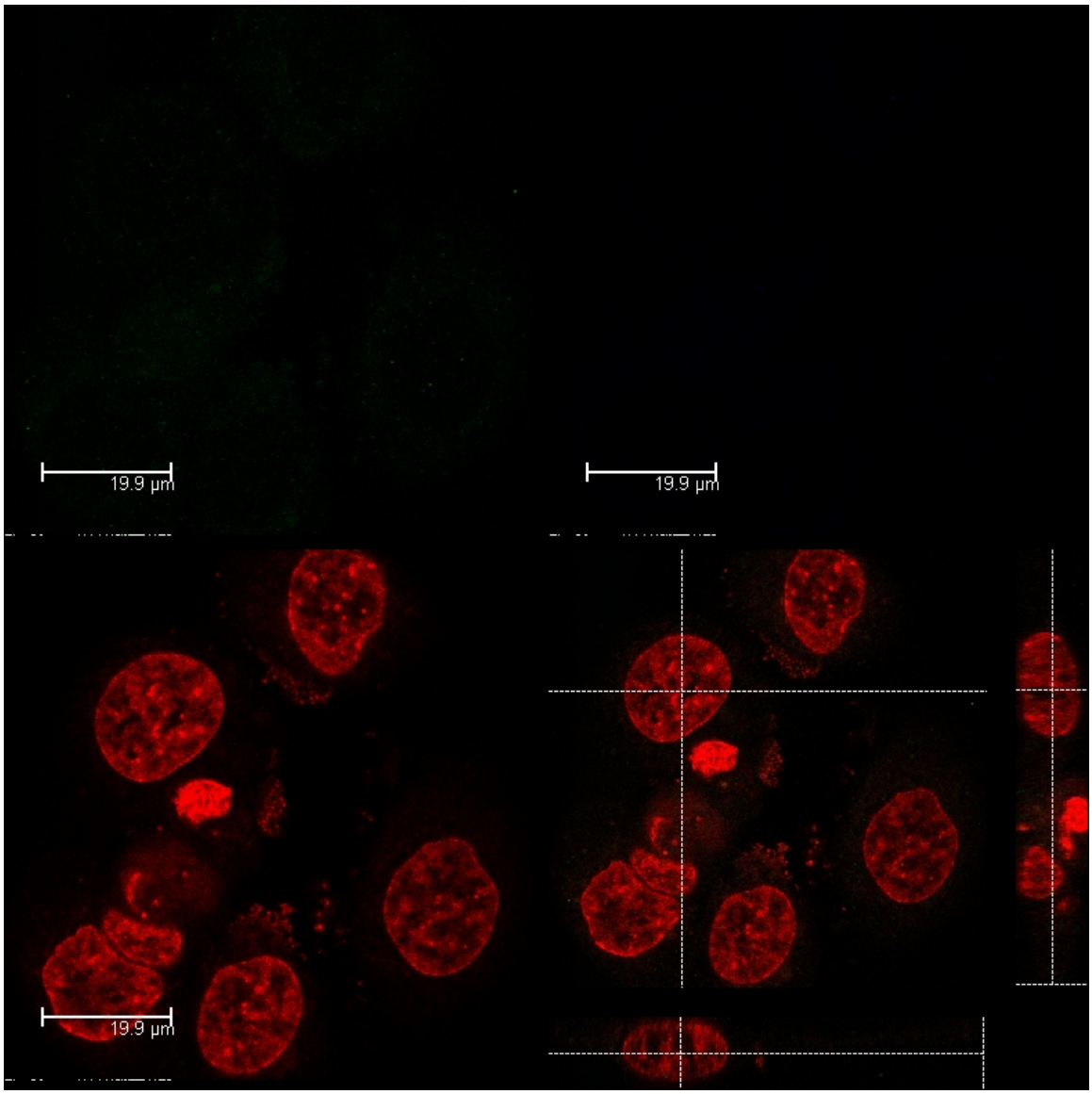



**Figure 4.10.2.3 Staining of E-Cadherin in DU145 cells transiently expressing pcDNA3 Endo180 vector (isotype control):** DU145 were seeded on Matrigel coated coverslips and grown under their normal growth conditions. After 12hours cells were transfected using Lipofectamin LTX and Plus reagent. Cells were fixed after 72 hours. Fixed cells were subsequently permeabilised using 0.2 % w/v saponin and immunostained using E-Cadherin 24E10 rabbit mAb. Nuclei were counterstained with DAPI. 36 z-sections were acquired using a Leica SP5 confocal microscope and a 63x/1.4 oil immersion objective. (**upper left**) mKO2 fluorescence, (**upper right**) E-Cadherin, (**lower left**) Nuclei, (**lower right**) z-projection. (n=3)

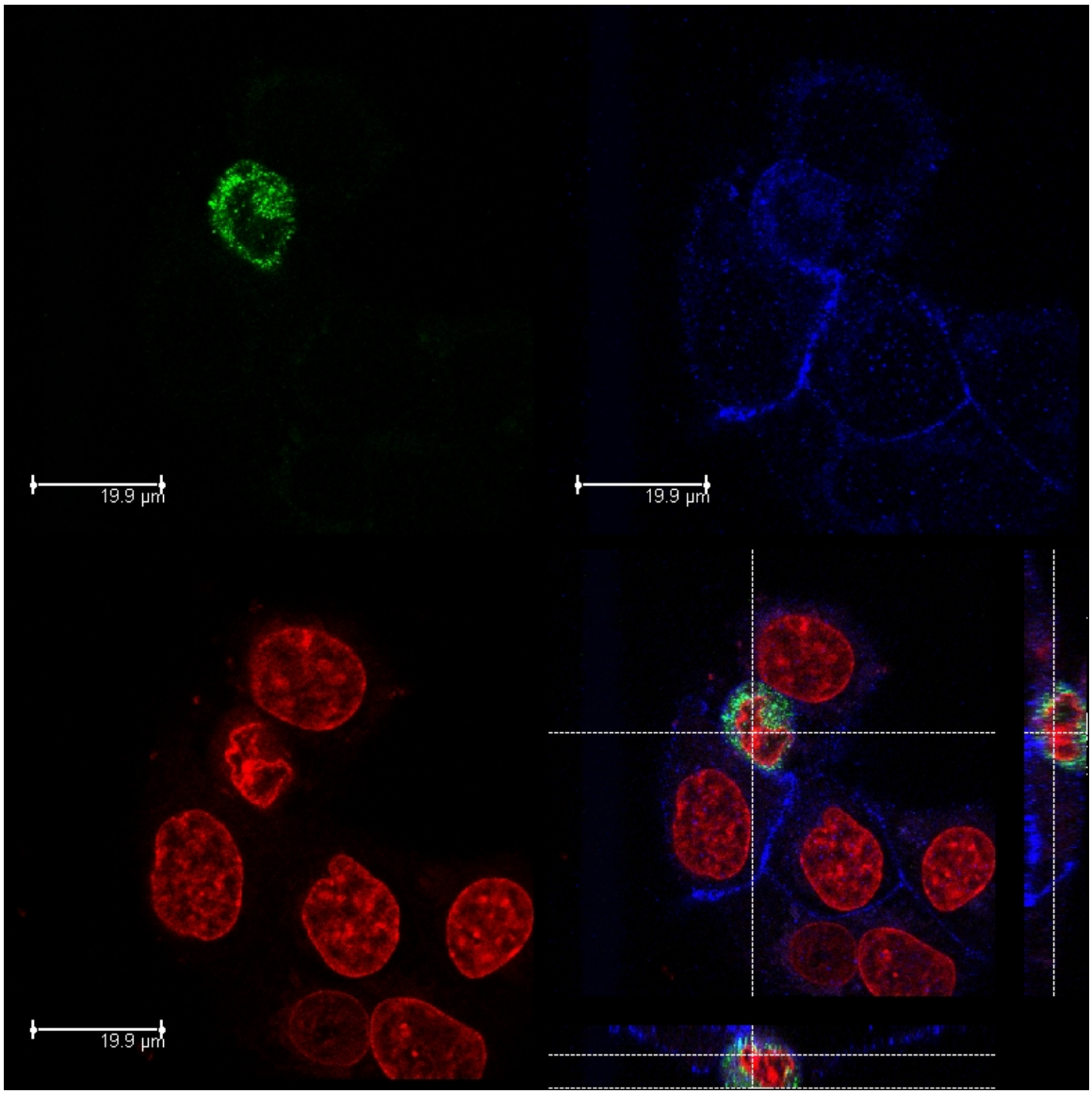



**Figure 4.10.2.4 Staining of E-Cadherin in DU145 cells transiently expressing pcDNA3 Endo180 vector (Endo180 39:10 and E-Cadherin 24E10):** DU145 were seeded on Matrigel coated coverslips and grown under their normal growth conditions. After 12hours cells were transfected using Lipofectamin LTX and Plus reagent. Cells were fixed after 72 hours. Fixed cells were subsequently permeabilised using 0.2 % w/v saponin and immunostained using E-Cadherin 24E10 rabbit mAb . Nuclei were counterstained with DAPI. 36 z-sections were acquired using a Leica SP5 confocal microscope and a 63x/1.4 oil immersion objective. (**upper left**) mKO2 fluorescence, (**upper right**) E-Cadherin, (**lower left**) Nuclei, (**lower right**) z-projection. (n=3)

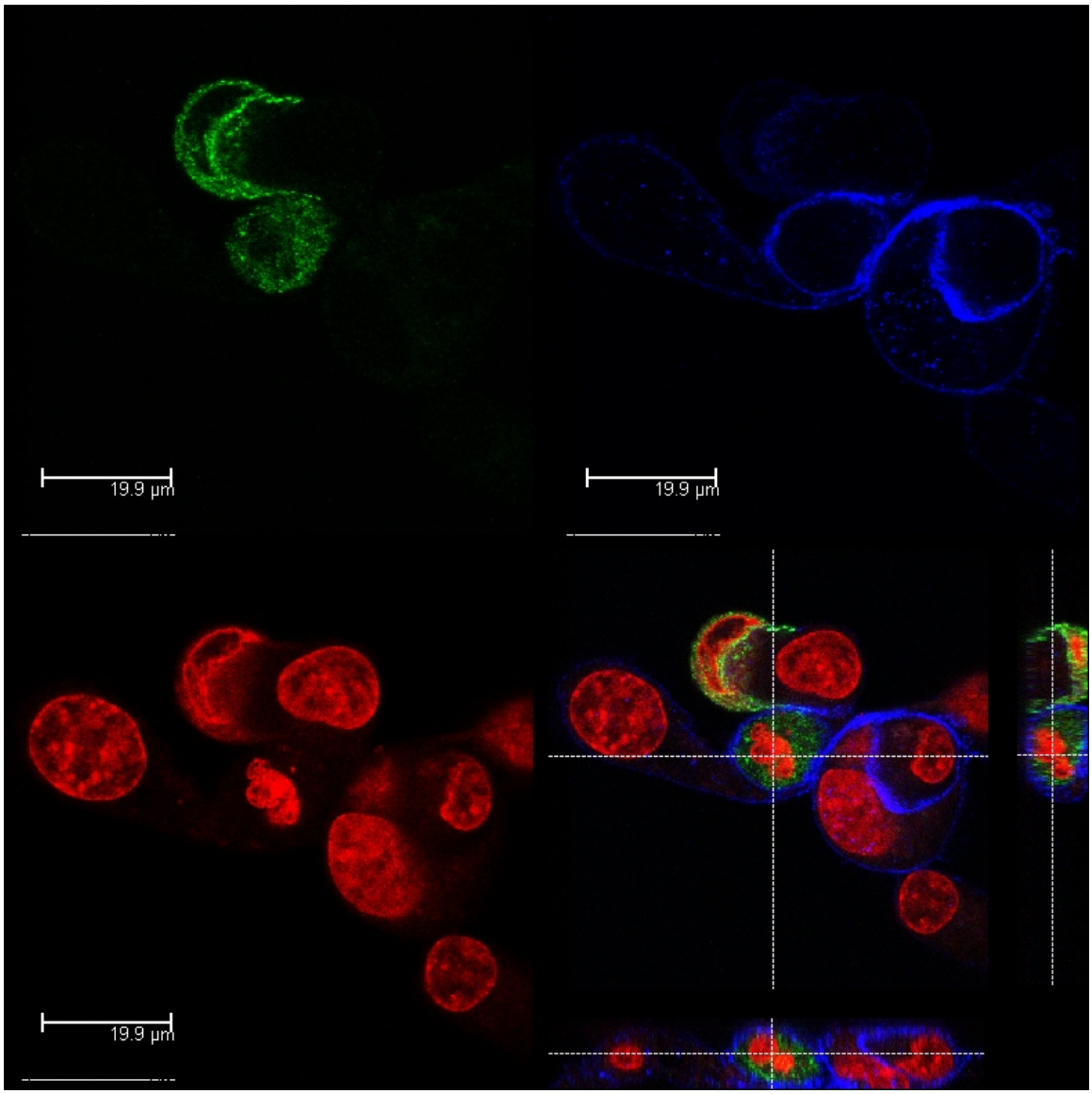



**Figure 4.10.2.5 Staining of E-Cadherin in DU145 cells transiently expressing pcDNA3 Endo180 vector (Endo180 A5:158 and E-Cadherin 24E10):** DU145 were seeded on Matrigel coated coverslips and grown under their normal growth conditions. After 12hours cells were transfected using Lipofectamin LTX and Plus reagent. Cells were fixed after 72 hours. Fixed cells were subsequently permeabilised using 0.2 % w/v saponin and immunostained using E-Cadherin 24E10 rabbit mAb . Nuclei were counterstained with DAPI. 36 z-sections were acquired using a Leica SP5 confocal microscope and a 63x/1.4 oil immersion objective. (**upper left**) mKO2 fluorescence, (**upper right**) E-Cadherin, (**lower left**) Nuclei, (**lower right**) z-projection. (n=3)

## 4.11 Overexpression of Endo180 in PC3 cells (PC3 Endo180)

### 4.11.1 Myosin light chain phosphorylation in PC3 Endo180 cells

The pcDNA3 Endo180 expression vector was stably transfected into PC3 cells. The PC3 Endo180 cell line was isolated by cultivation in G418 supplemented medium and FACS sorting. Western blot analysis revealed that overexpression of Endo180 enhanced myosin light chain phosphorylation. siRNA knockdown of overexpressed Endo180 restored Myosin light chain phosphorylation to initial levels (**figures 4.11.1 and 4.11.2**).

### 4.11.2 Chemotaxis of PC3 Endo180 cells towards uPA gradients

Endo180 overexpressing PC3 cells underwent Dunn chamber assays to assess their potential to chemotax towards growth factor gradients. PC3 Endo180 cells as well as wild type PC3 cells displayed no clear directional migration because overall displacement and average migration speed were very low (**figure 4.11.3** and compare to **section 5** for PC3 migration speed). uPA migration assays were initially carried out under serum starvation conditions for both MDA-MB-231 and MCF7 cells (Sturge personal communication). An assessment of the general capability of PC3 cells to display directional migration towards a strong chemoattractant, CSF-1, was assessed under both, normal growth conditions and serum starvation (**figure 4.11.4).** While PC3 are migratory and capable of chemotaxis under normal growth conditions, serum starvation abrogated their migratory and chemotactic behaviour. For future experiments, it will be crucial to titrate serum concentrations towards a point where PC3 cells and PC3 Endo180 cells display migratory behaviour and are susceptible to uPA as a chemoattractant.

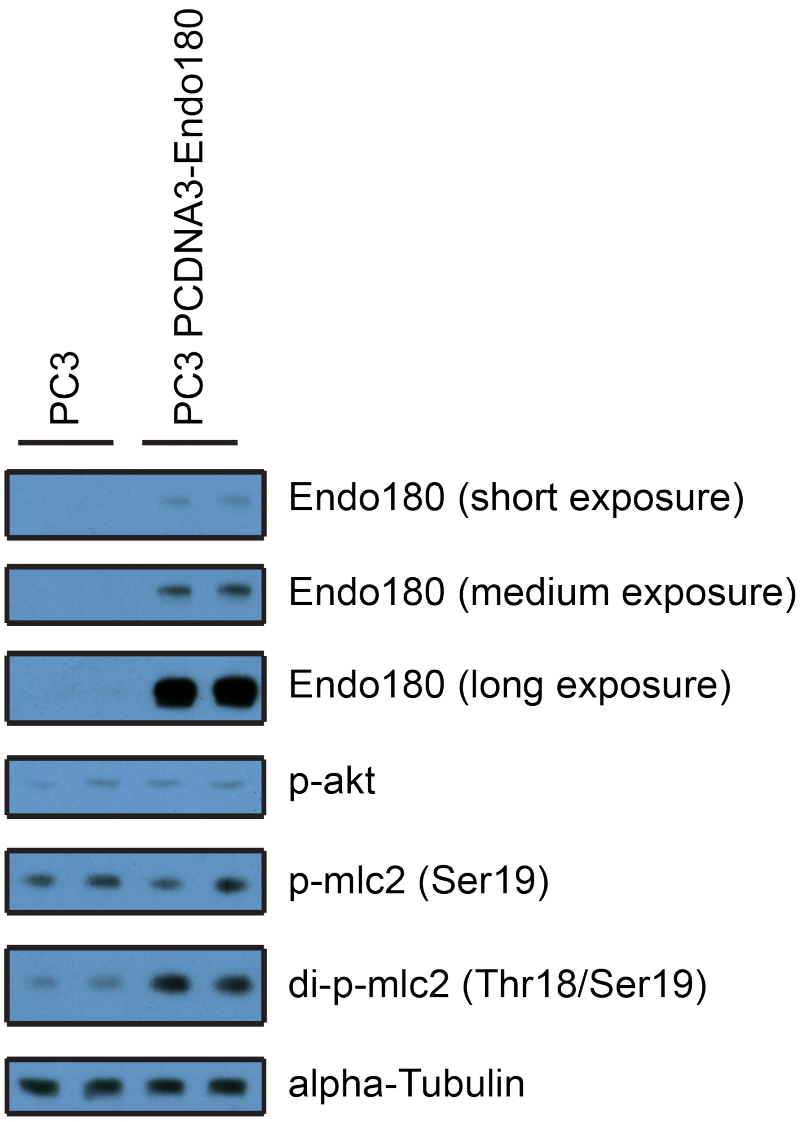



**Figure 4.11.1 siRNA knockdown of Endo180 in PC3 cells overexpressing Endo180.** PC3 cells were treated with a smartpool of siRNA targeting Endo180. Whole cell lysates were prepared and subjected to SDS-PAGE using a 4-20% acrylamide gradient gel. The panels show immunoblots obtained using the primary antibody concentrations listed in **Table 2.1** followed by the appropriate HRP-conjugated secondary antibody: Endo180 (MW = 180 kDA); phosphorylated AKT (MW = 62 kDa) and Myosin light chain (mlc2) phosphorylated at Ser19 or Thr18/Ser19 as well as total mlc2 (MW = 18 kDa). Molecular weight (MW) markers (kDa) and proteins of interest are indicated for each blot: (n=1).

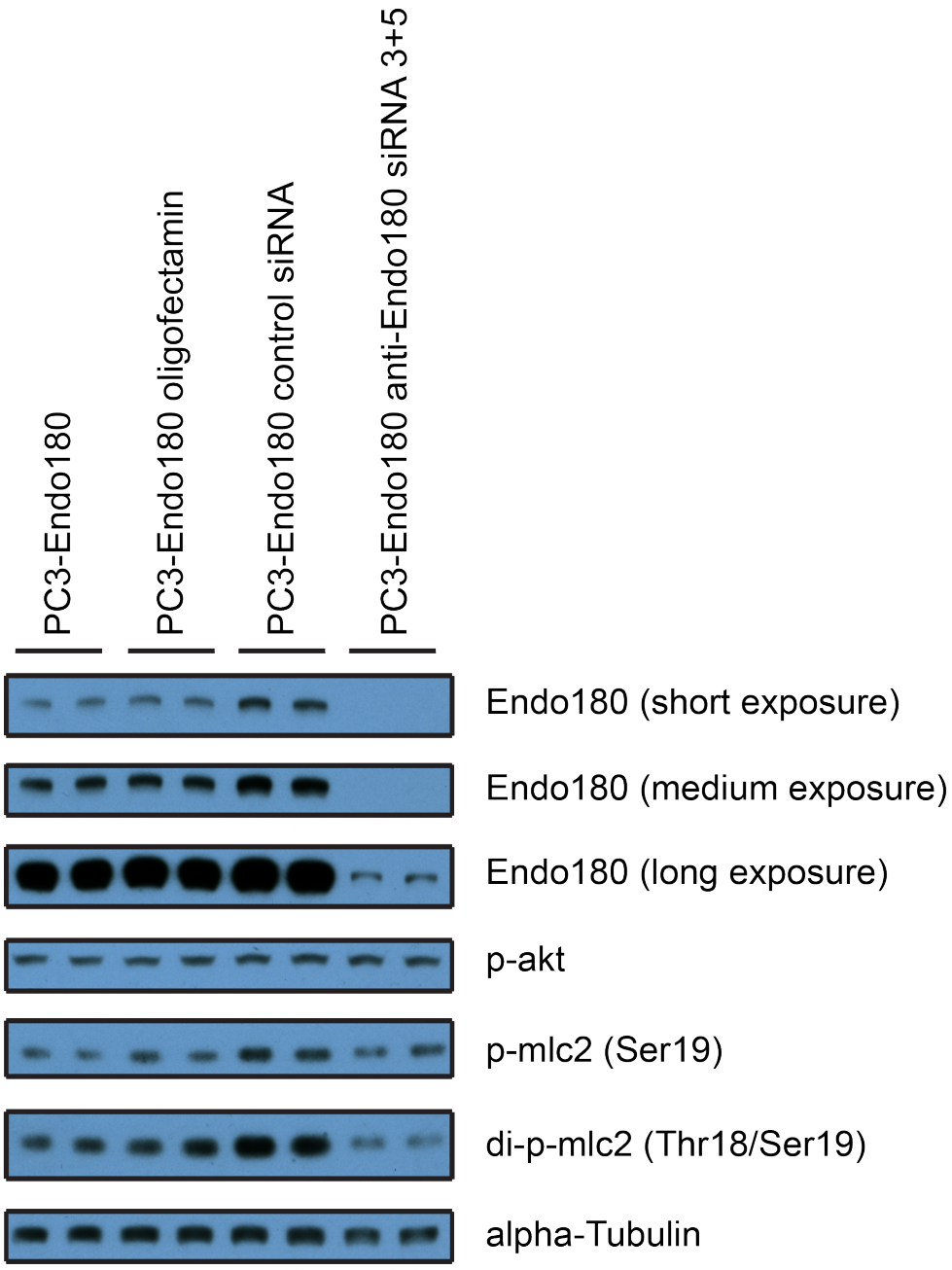



**Figure 4.11.2 siRNA knockdown of Endo180 in PC3 cells overexpressing Endo180.** PC3 cells were treated with a smartpool of siRNA targeting Endo180. Whole cell lysates were prepared and subjected to SDS-PAGE using a 4-20% acrylamide gradient gel. The panels show immunoblots obtained using the primary antibody concentrations listed in **Table 2.1** followed by the appropriate HRP-conjugated secondary antibody: Endo180 (MW = 180 kDA); phosphorylated AKT (MW = 62 kDa) and Myosin light chain (mlc2) phosphorylated at Ser19 or Thr18/Ser19 as well as total mlc2 (MW = 18 kDa). Molecular weight (MW) markers (kDa) and proteins of interest are indicated for each blot: (n=1).

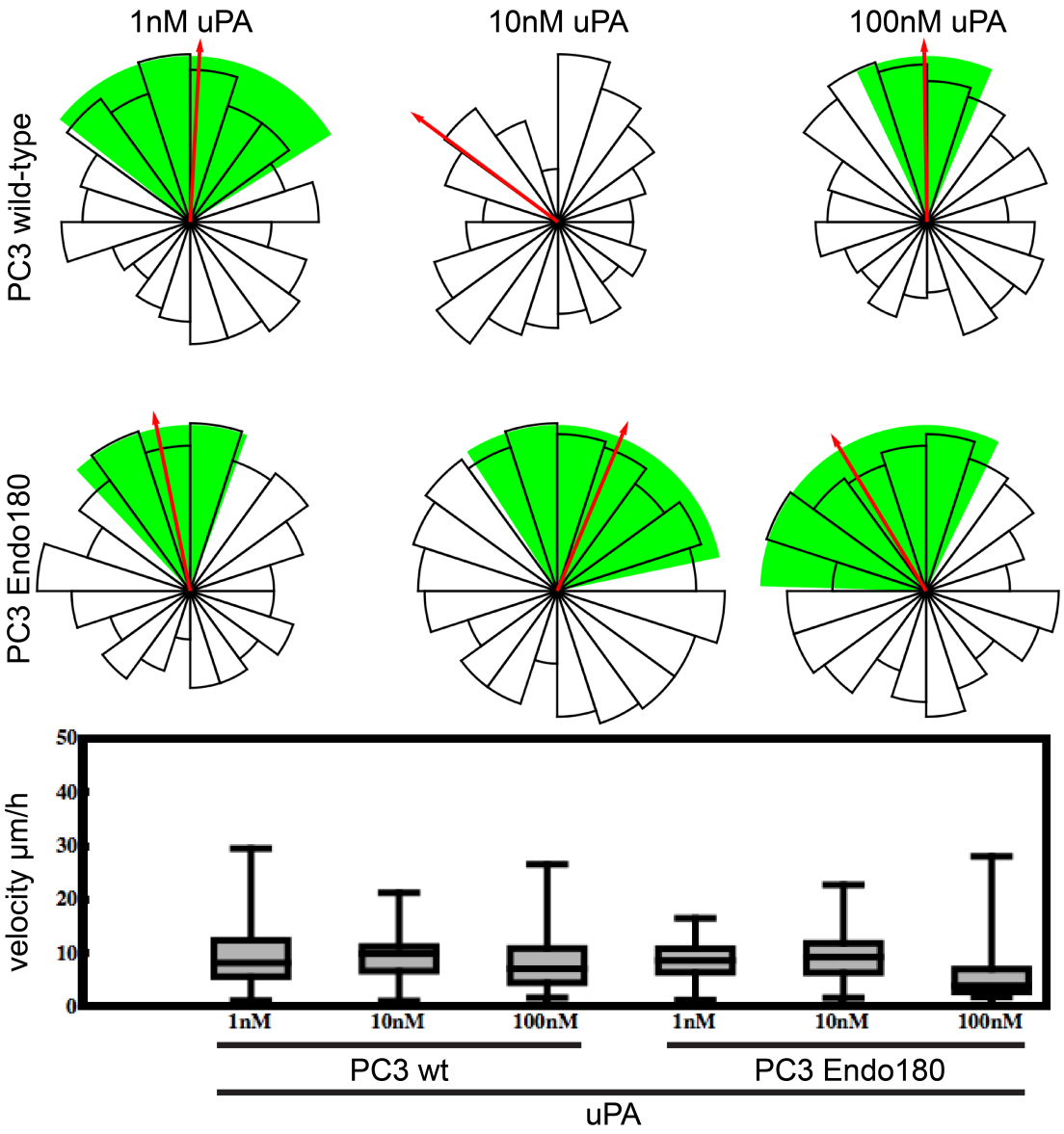



**Figure 4.11.3 Chemotactic potential of parental PC3 cells.** 50,000 PC3 cells were plated onto 18x18mm square glass cover slips in a 6-well plate. After 24h the cover slips were mounted on Dunn chemotaxis chambers. Cells were exposed to 1, 10 and 100nM uPA gradients and filmed with a 10x phase-contrast objective for 12 hours every 10 minutes. Cell tracks were generated using Metamorph/xpress 2.0 software and Rose plots were generated using Mathematica 6.0. The maximum displacement was determining for a direction in which a cell migrated. The gradient is on the top of each Rose plot. Every triangle covers an 18 degrees window and its area corresponds to the amount of cells migrating into the respective direction. A red arrow indicates the overall directionality. The green area represents the 99% confidence interval, which correlates to the uncertainty of the directionality. (n=1)

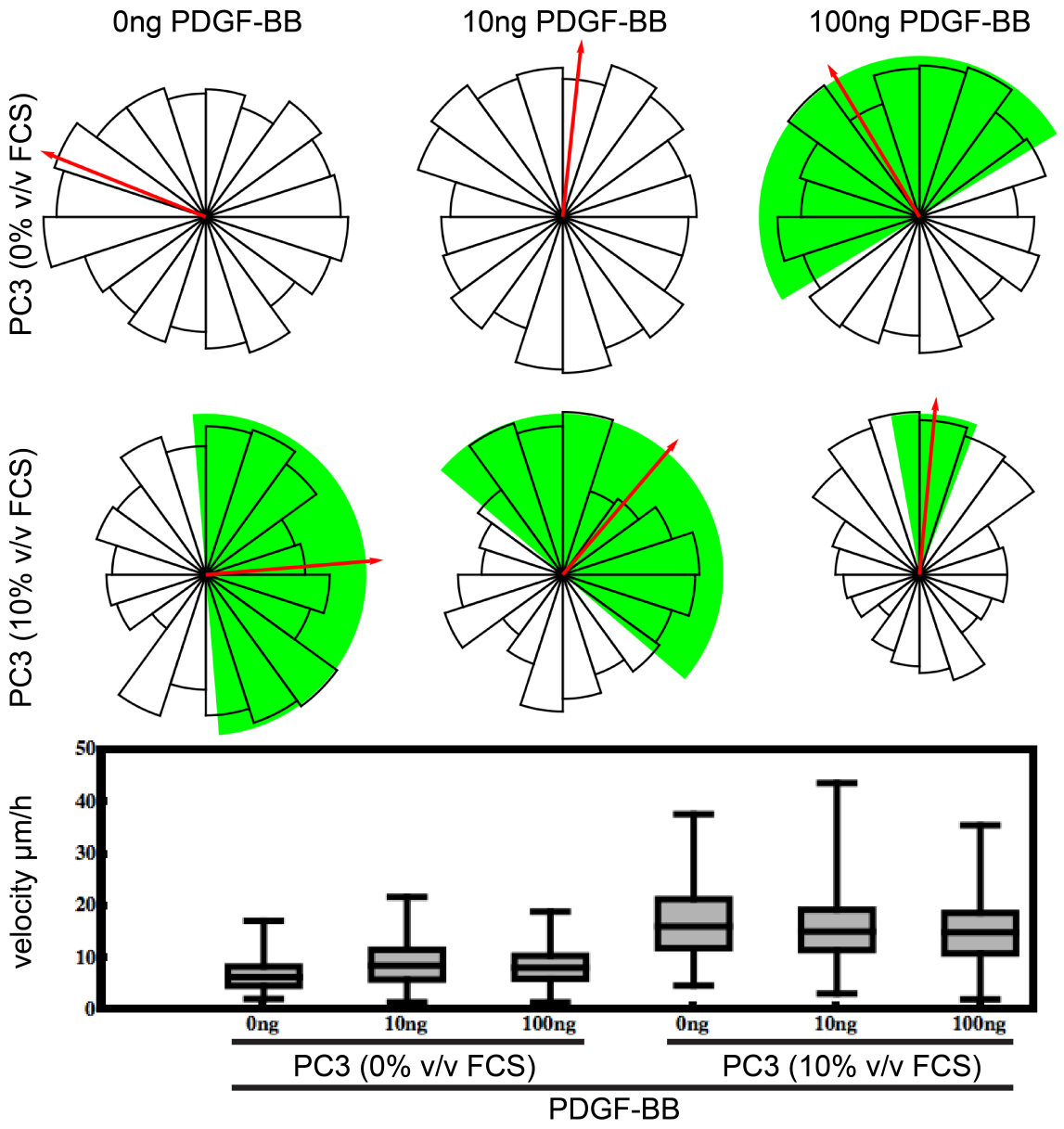



**Figure 4.11.4 Chemotactic potential of parental PC3 cells.** 50,000 PC3 cells were plated onto 18x18mm square glass cover slips in a 6-well plate. After 24h the cover slips were mounted on Dunn chemotaxis chambers. Cells were exposed to 0, 10 and 100ng PDGF-BB gradients and filmed with a 10x phase-contrast objective for 12 hours every 10 minutes. Cell tracks were generated using Metamorph/xpress 2.0 software and Rose plots were generated using Mathematica 6.0. The maximum displacement was determining for a direction in which a cell migrated. The gradient is on the top of each Rose plot. Every triangle covers an 18 degrees window and its area corresponds to the amount of cells migrating into the respective direction. A red arrow indicates the overall directionality. The green area represents the 99% confidence interval, which correlates to the uncertainty of the directionality. (n=1)

## 4.12 Discussion

Several non-radioactive techniques were applied to detect and study Endo180 phosphorylation in vitro. However, none of the strategies applied detected any phosphorylated Endo180 protein. Basis for this study were earlier reports where Endo180 phosphorylation was detected in Flow 2000 fibroblasts using radioactive labelling.

Failure to detect phosphorylated Endo180 can be caused by a number of different reasons. The earlier study was performed in Flow 2000 fibroblasts whereas these studies were performed using hTert immortalised HCA2 fibroblasts. Additionally, the earlier study used the currently unavailable E1/183 antibody whereas this study had to rely on the A5/158 and 39:10 antibodies of which the 39:10 antibody was unable to immunoprecipitate Endo180 protein. Interestingly, both, the A5:158 and the E1:183 antibody, were shown to interfere with Rho GTPase signalling upon chemotactic stimulation of MDA-MB-231 cells with uPA (Sturge et al., 2003).

Furthermore, it is possible that the phosphorylation only occurs at a relatively small percentage of Endo180 receptors. The strategies applied here might simply be not sensitive enough to detect such small amounts of phosphorylated Endo180. It is also possible that the phosphorylation was lost during sample handling although several phosphatase inhibitors were supplemented to the lysis buffer and washing solutions.

The phospho-peptides observed in the earlier study were not sequenced and the Endo180 amino acid sequence and gene sequence were not available at the time (Isacke et al., 1990). Remotely, there is the possibility that the E1/183 antibody co-precipitated an interaction partner of Endo180 that cannot be co-precipitated by the A5/158 antibody. It might have been this interaction partner and not Endo180 itself that originated the phospho-peptides that appeared on the thin-layer chromatography plate.

Surprisingly, it was possible to stain Endo180 in proximity to cell-cell junctions in DU145 prostate cancer cells. Furthermore, such cells that stained positive for

Endo180 appeared negative for E-Cadherin and vice-versa. This might indicate a new role for Endo180 in epithelial cells. This is especially interesting in front of the background that Endo180 preferentially binds to Collagen IV, which is usually restricted to the basal lamina. Therefore it is imaginable that Endo180 plays a role in the interaction between epithelial cells and the basal lamina. Attempts to overexpress wild type and fluorescently labelled Endo180 were unable to confirm these results. Fluorescently labelled Endo180 gave inconclusive results in regards to subcellular localisation. No localisation towards cell-cell junctions was detected for overexpressed wild type Endo180. It is imaginable that localisation of Endo180 towards the proximity of cell-cell junctions is dependent on other factors. Those factors might not be in sufficient supply to translocate overexpressed Endo180 into the proximity of cell-cell junctions. The observation that Endo180 and E-Cadherin appear to be differentially expressed amongst DU145 cell layers is worth exploring and aligns with earlier results that attribute an EMT inducing role to Endo180 in MCF7 cells.

## 5. The role of Endo180 in prostate cancer progression

To date only one study has been carried out to investigate expression levels of Endo180 in prostate cancer progression. Two commercially available TMAs (US Biomax) were stained for Endo180 and several potential interaction partners as well as epithelial and mesenchymal/stromal markers. The study revealed that the percentage of Endo180 positive cells (epithelial and stromal) correlates with Gleason grade. However, no follow up data was available for these TMAs and a potential role of Endo180 in predicting patient survival could not be investigated (Kogianni et al., 2009).

Although the antibodies have been used for Endo180 staining in several earlier studies, an official FDA approved multi-tissue array to demonstrate marker expression in a wide array of normal/healthy tissue was not yet performed. Therefore it was decided to test both the 39:10 and the A5:158 antibodies in this array to characterise Endo180 expression in healthy tissue.

Initially, a larger TMA was purchased from the US Biomax corporation to investigate Endo180 expression and to correlate it with abundance of Collagens I and IV in adjacent sections with the prospect of testing for other potential interaction partners such as AdamTS2.

Additionally, through collaboration with the research group of Professor Craig Robson at Newcastle University access was gained to their collection of TMAs, which include follow up data. Five of their TMAs were investigated for a potential correlation of Endo180 with disease progression, metastasis status, capsular invasion, Gleason grade and several other factors.

In their 2007 study of Endo180's role in breast cancer progression Professor Clare Isacke's research group used the 39:10 antibody to stain paraffin embedded tissue and chose to use the A5:158 antibody for immunofluorescence (Wienke et al., 2007). In their study of a large Glioma array, they used the 39:10 antibody again (Huijbers et al., 2010). However, the single study based on prostate tissue has been carried out

using the A5:158 antibody for staining of paraffin embedded tissue (Kogianni et al., 2009). Therefore, it was decided to test both the 39:10 and the A5:158 antibody.

## 5.1 Validation of antibodies on an FDA approved multi-tissue array

On the outset of this study it was decided to validate both antibodies (39:10 and A5:158) on an FDA approved multi-tissue array. This array consists of paraffin embedded biopsies taken from various human tissues (three cores per tissue from different individuals). For the 39:10 mAb two different antigen retrieval methods were tested: proteinase K digestion and boiling in citrate buffer. The A5:158 antibody has only previously been used in combination with antigen-retrieval by boiling in citrate buffer.

### 5.1.1 Antigen retrieval by proteinase K - 39:10 mAb staining

The multi-tissue TMA was treated with proteinase K (see methods for details). The conditions were modelled on the previous study carried out with the smaller prostate cancer TMAs (Kogianni et al., 2009). The TMA was subsequently DAB-stained using standard conditions using 39:10 mAb (10 μg/ml) (**data not shown**). Following histopathological inspection the sections appeared over-digested by the proteinase K and could not be analysed (Dr Francesco Mauri, Imperial College London).

### 5.1.2 Antigen retrieval by boiling in citrate buffer - 39:10/A5:158 mAb staining

Antigen retrieval by boiling the multi-tissue TMA in citrate buffer and subsequent DAB-staining for Endo180 expression using 39:10 mAb (10 μg/ml) resulted in clear but weak tissue staining (**Figure 5.1.2.1**). A5:158 mAb (50 μg/ml) but not lower concentrations also produced good results (**Figure 5.1.2.2**). The multi-tissue TMAs were analysed and positive cell populations of interest identified using an online histology database (**Tables 5.1.2.3 and 5.1.2.4**).

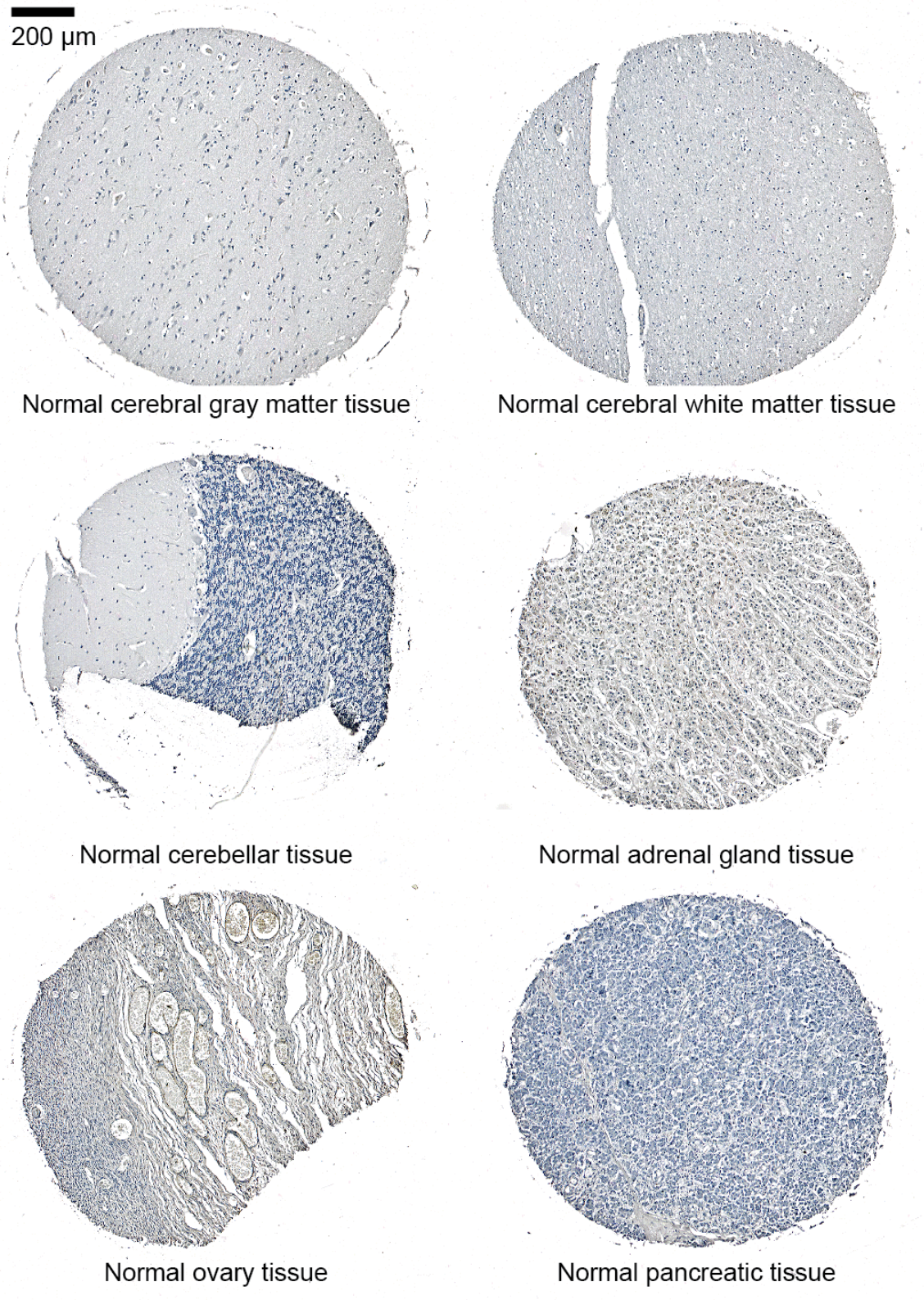



**Figure 5.1.2.1 (page 1 of 6)**

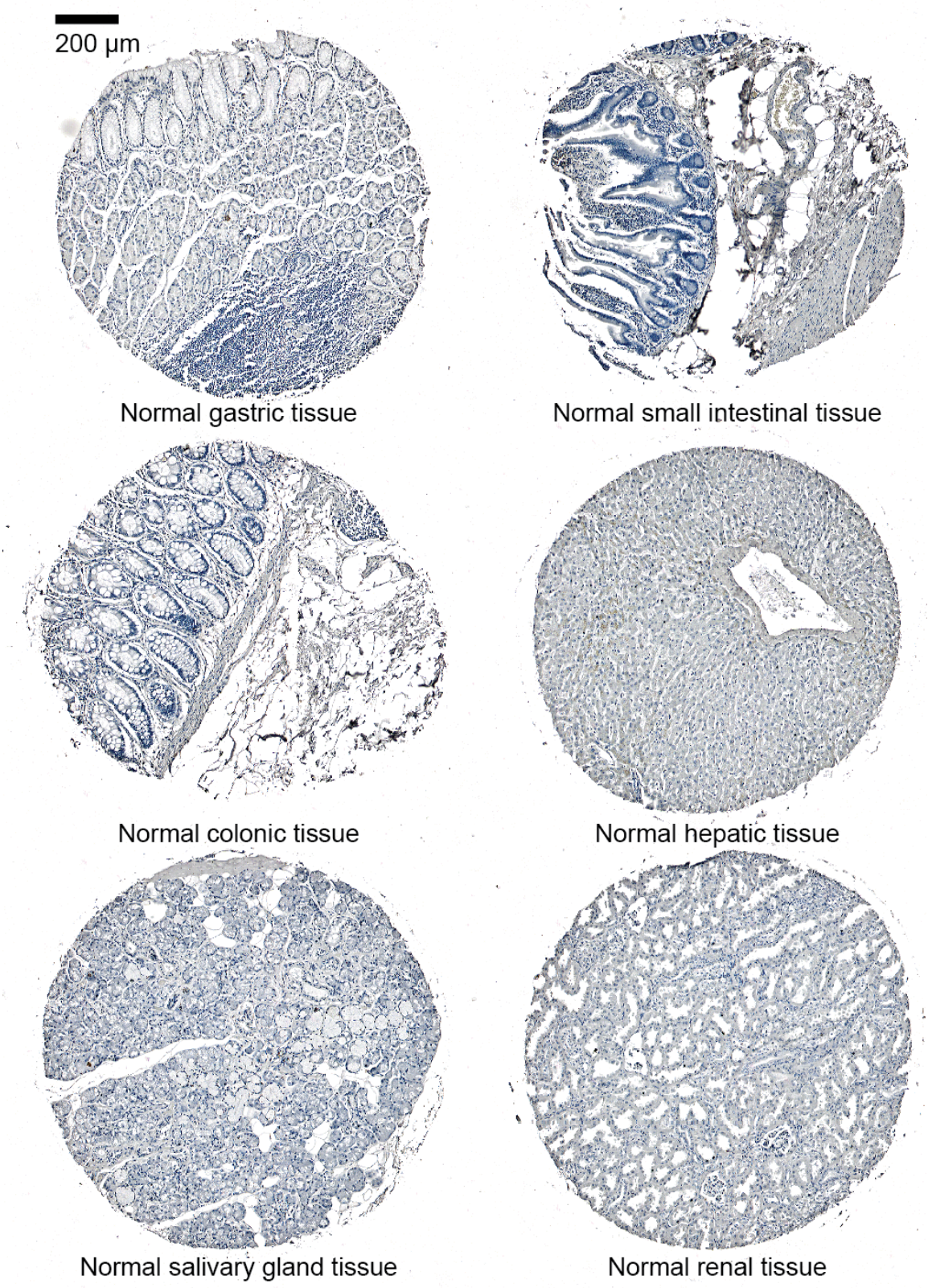



Figure **5.1.2.1** (page 2 of 6)

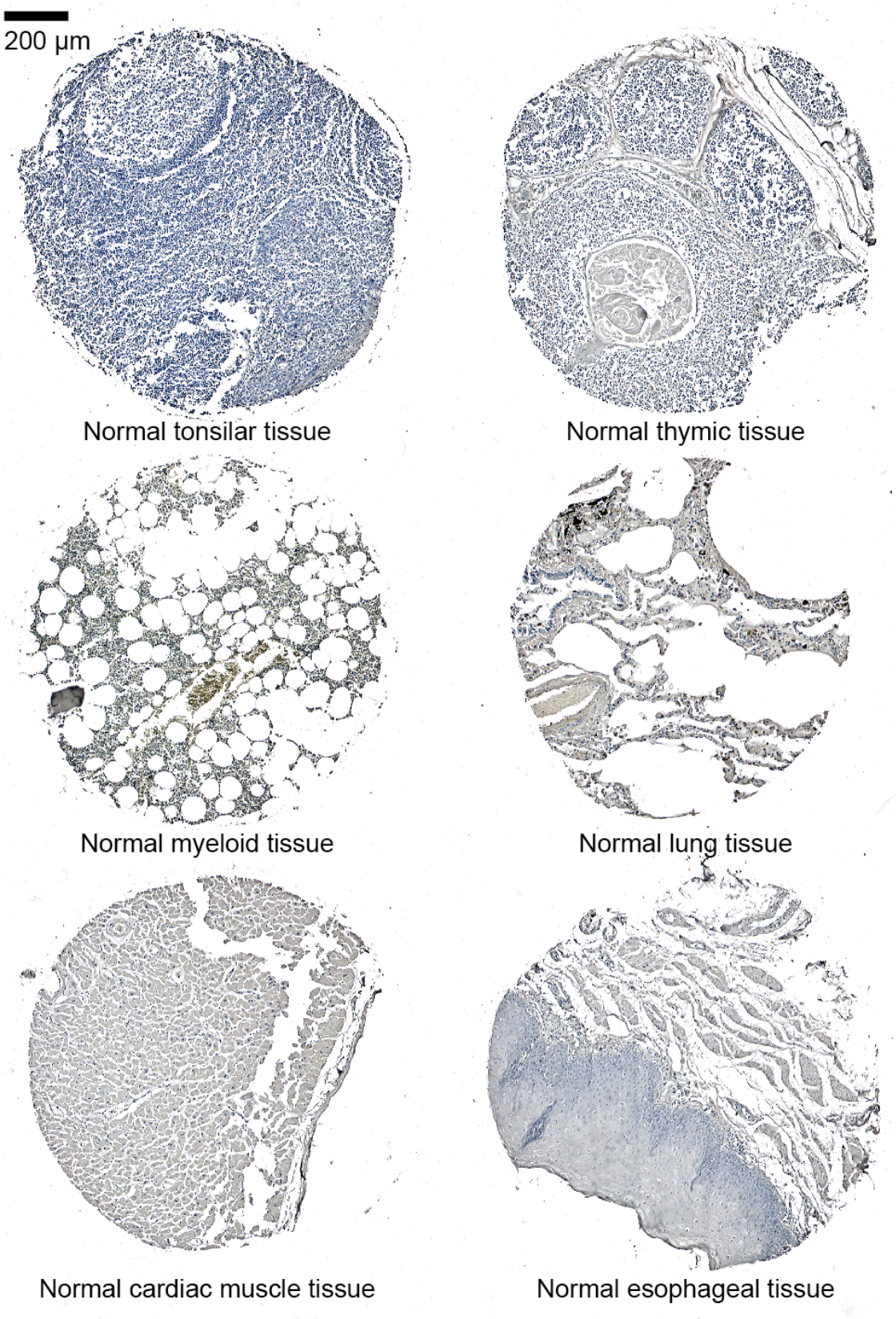



Figure **5.1.2.1** (page 3 of 6)

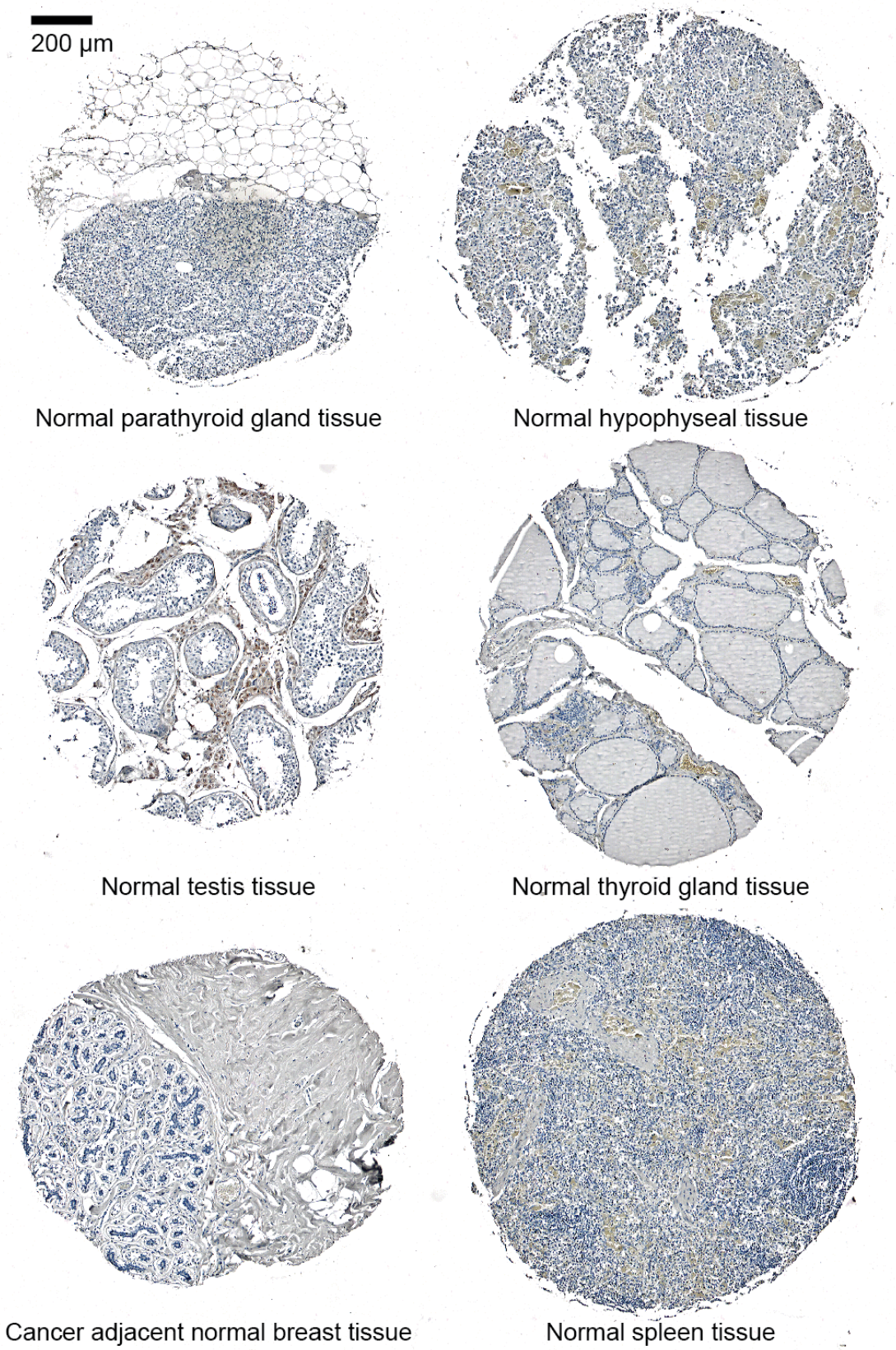



Figure **5.1.2.1** (page 4 of 6)

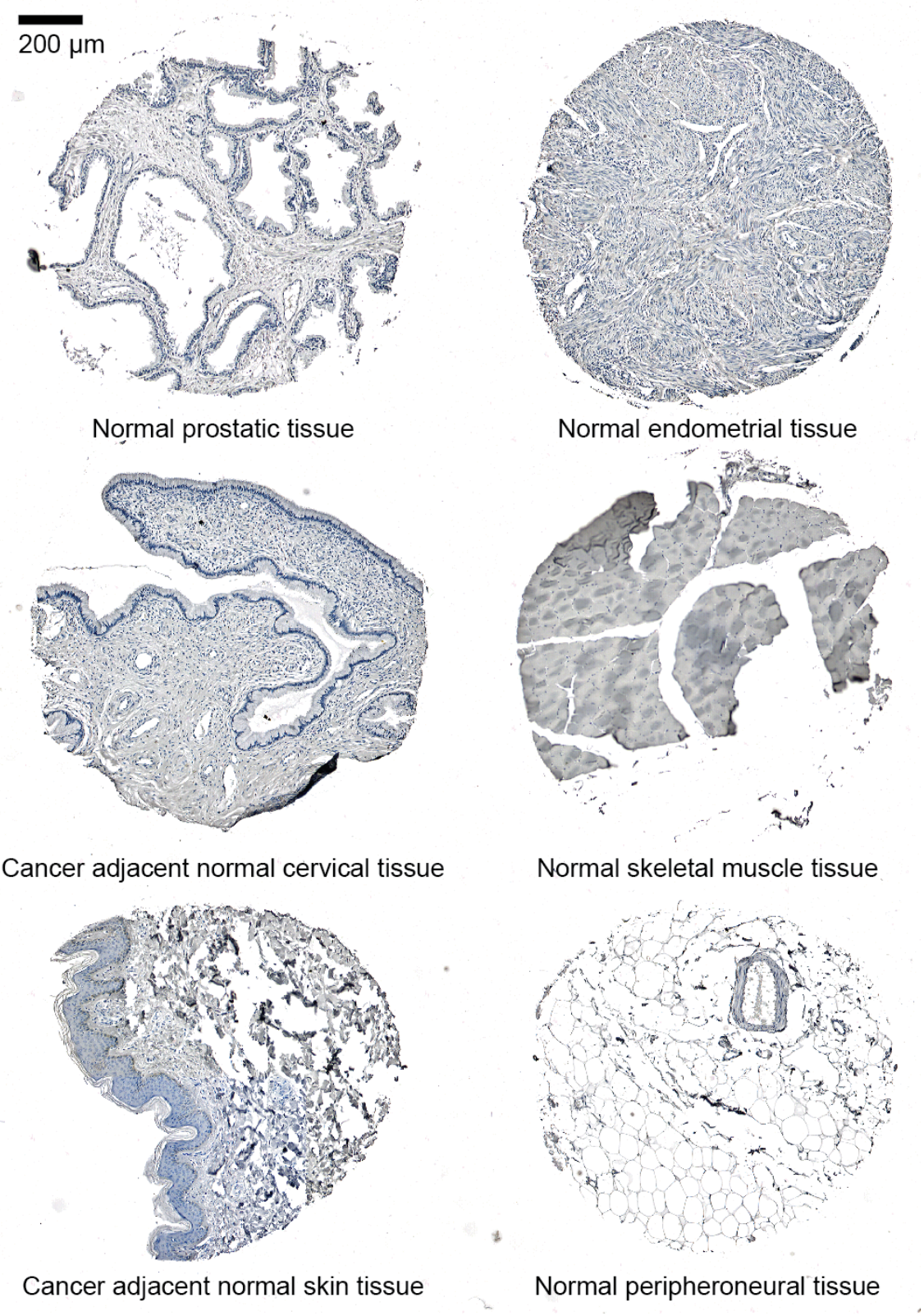



Figure **5.1.2.1** (page 5 of 6)

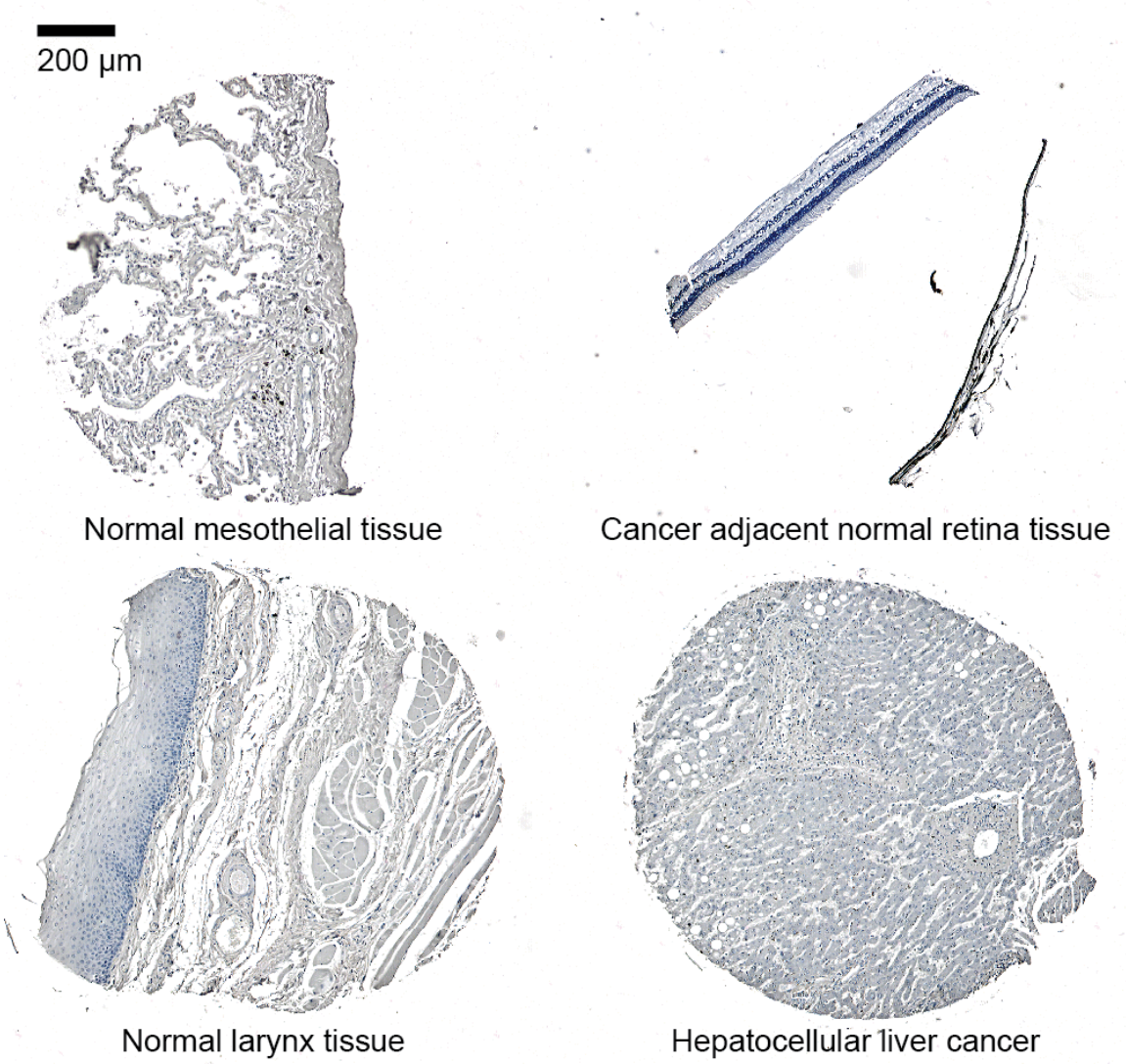



**Figure 5.1.2.1 (page 6 of 6): Immunostaining of multi-tissue antibody validation array – 39.10 mAb.** DAB-staining (brown) using mouse anti-human Endo180 mAb 39:10. Nuclei were counterstained with Mayer's haematoxylin (blue). Three cores from different individuals per tissue were assessed. One core of testis, breast and prostate and two cores of eye tissue were lost. One sample core is shown for each tissue. Scale bars = 200 µm.

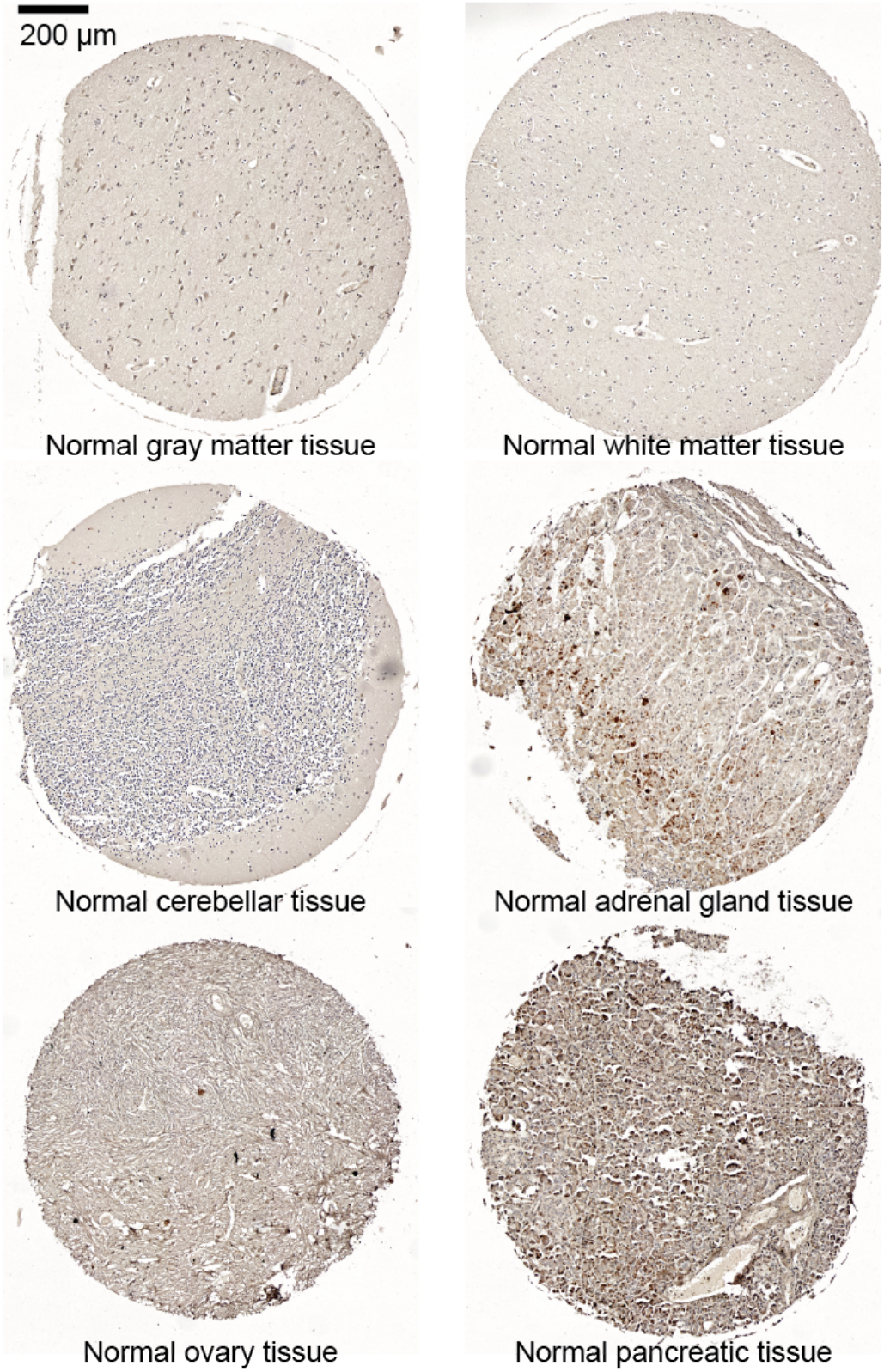



Figure **5.1.2.2** (page 1 of 6)

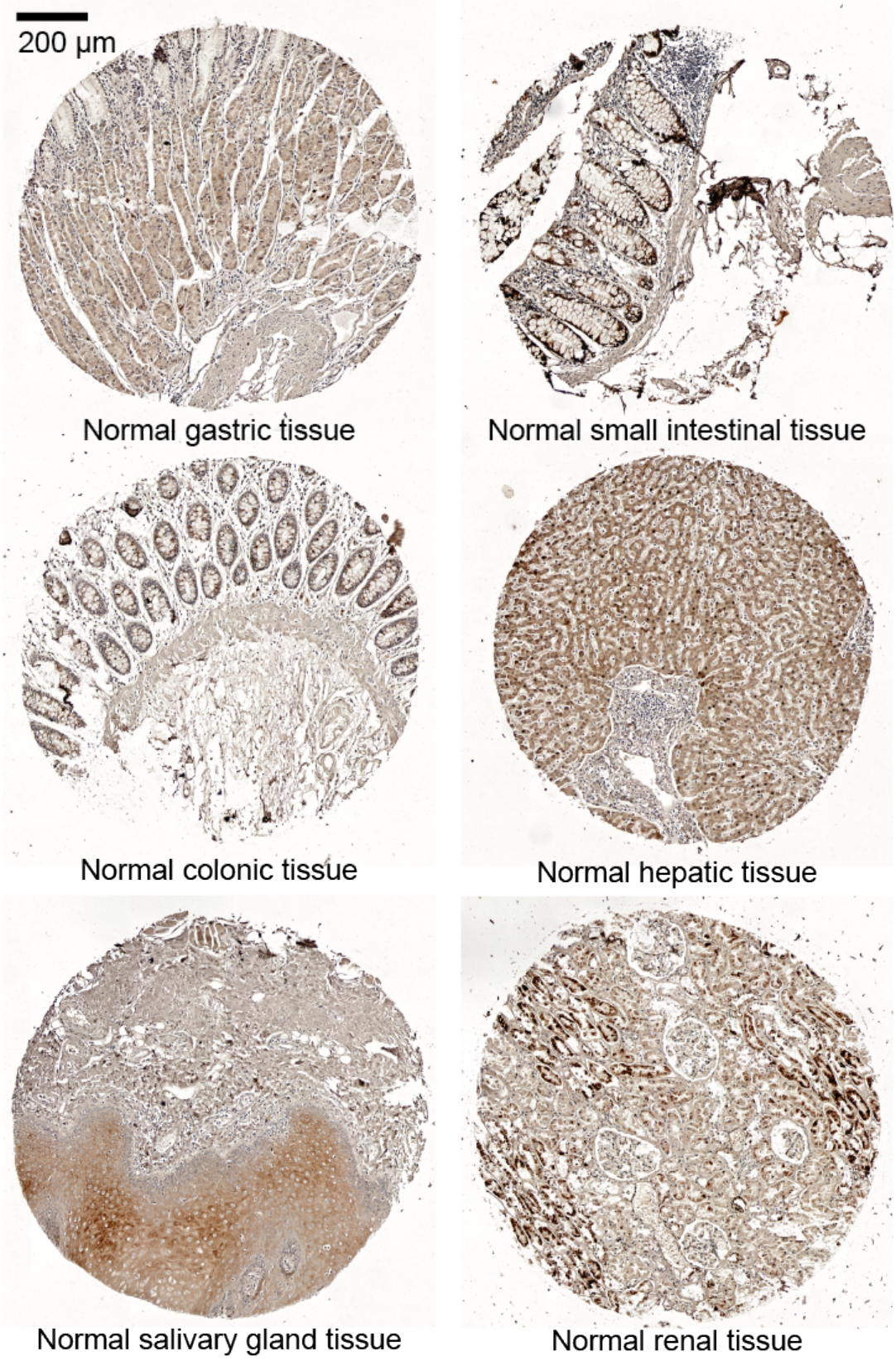



Figure **5.1.2.2** (page 2 of 6)

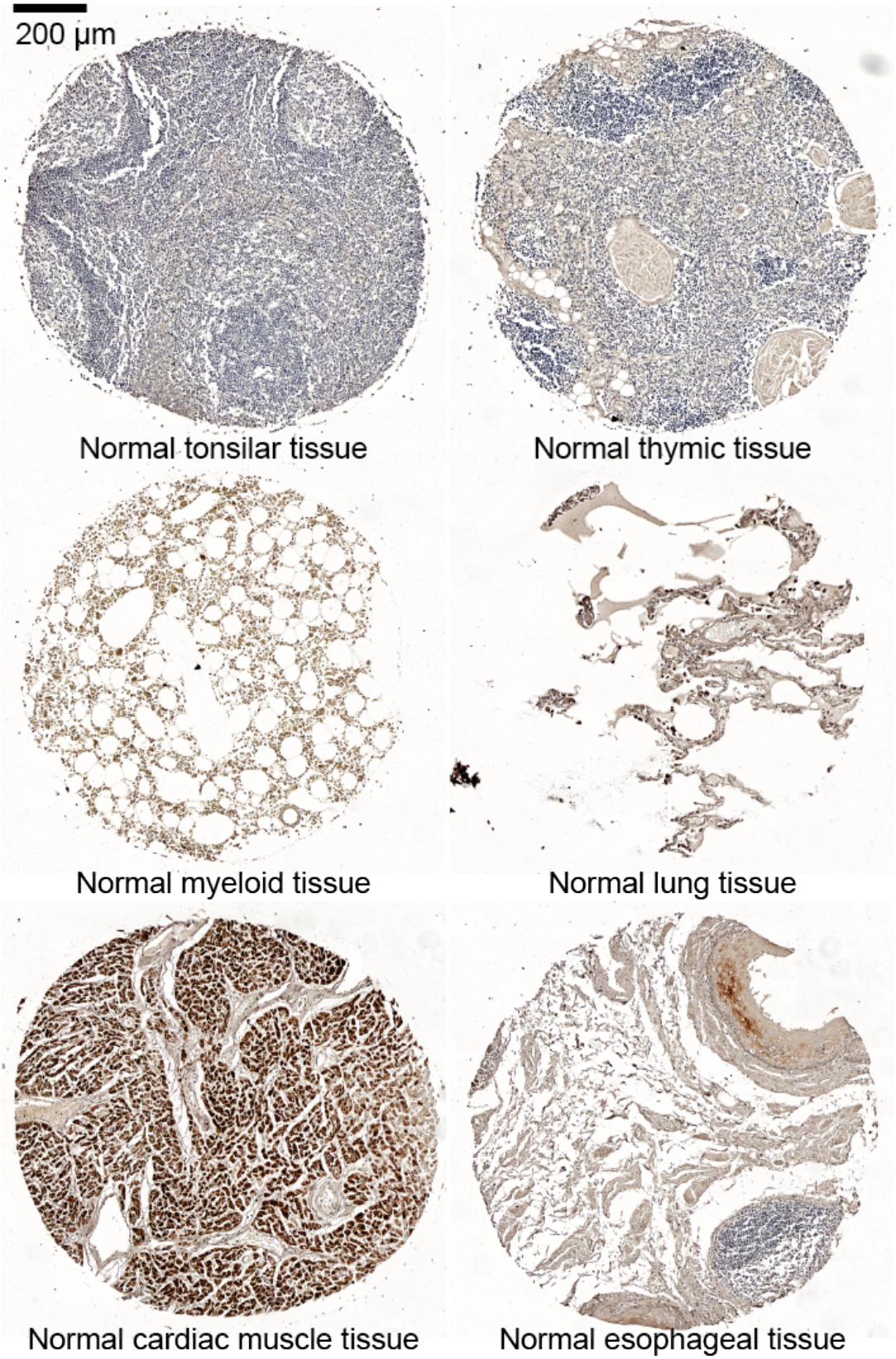



Figure **5.1.2.2** (page 3 of 6)

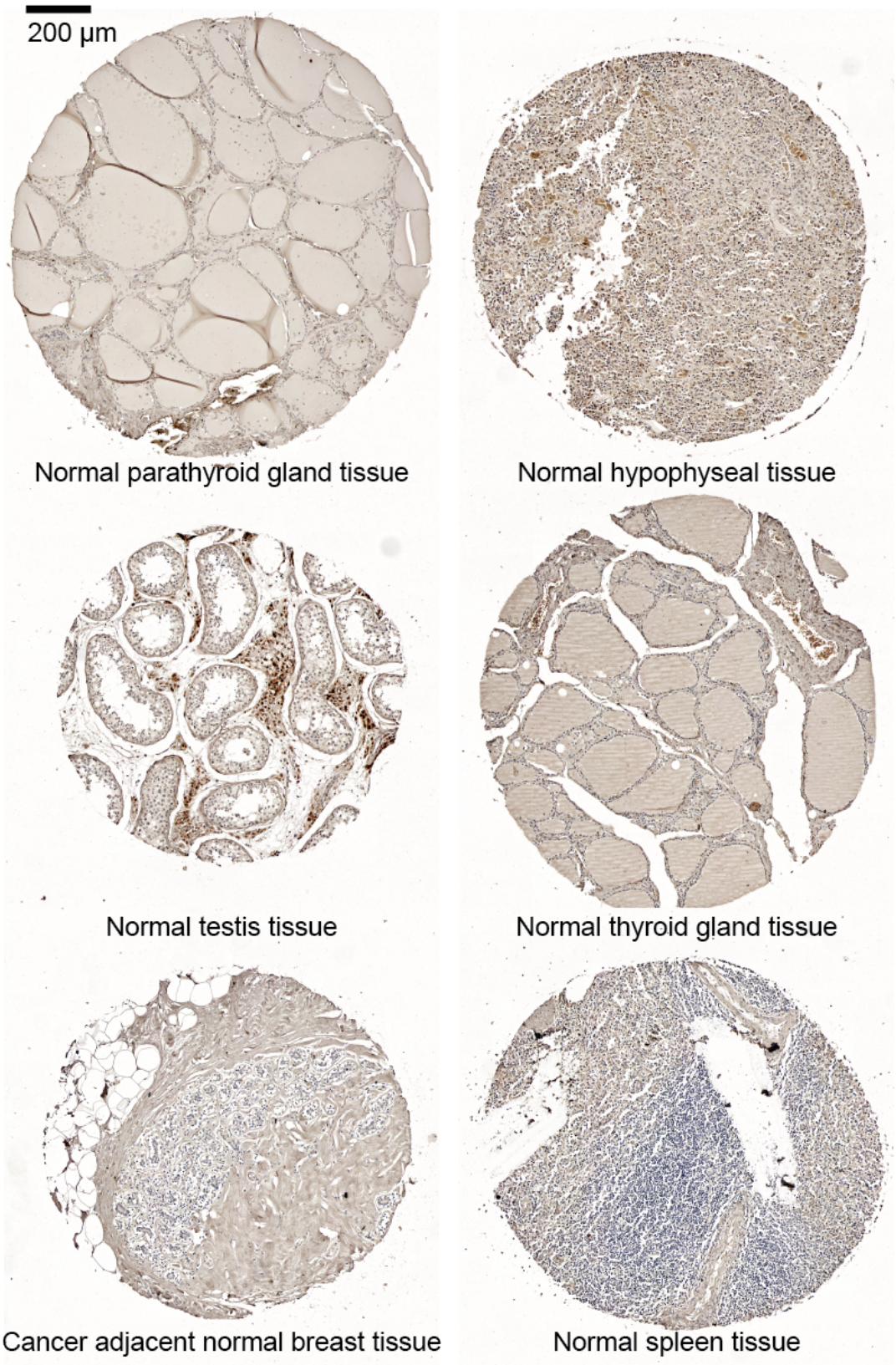



Figure **5.1.2.2** (page 4 of 6)

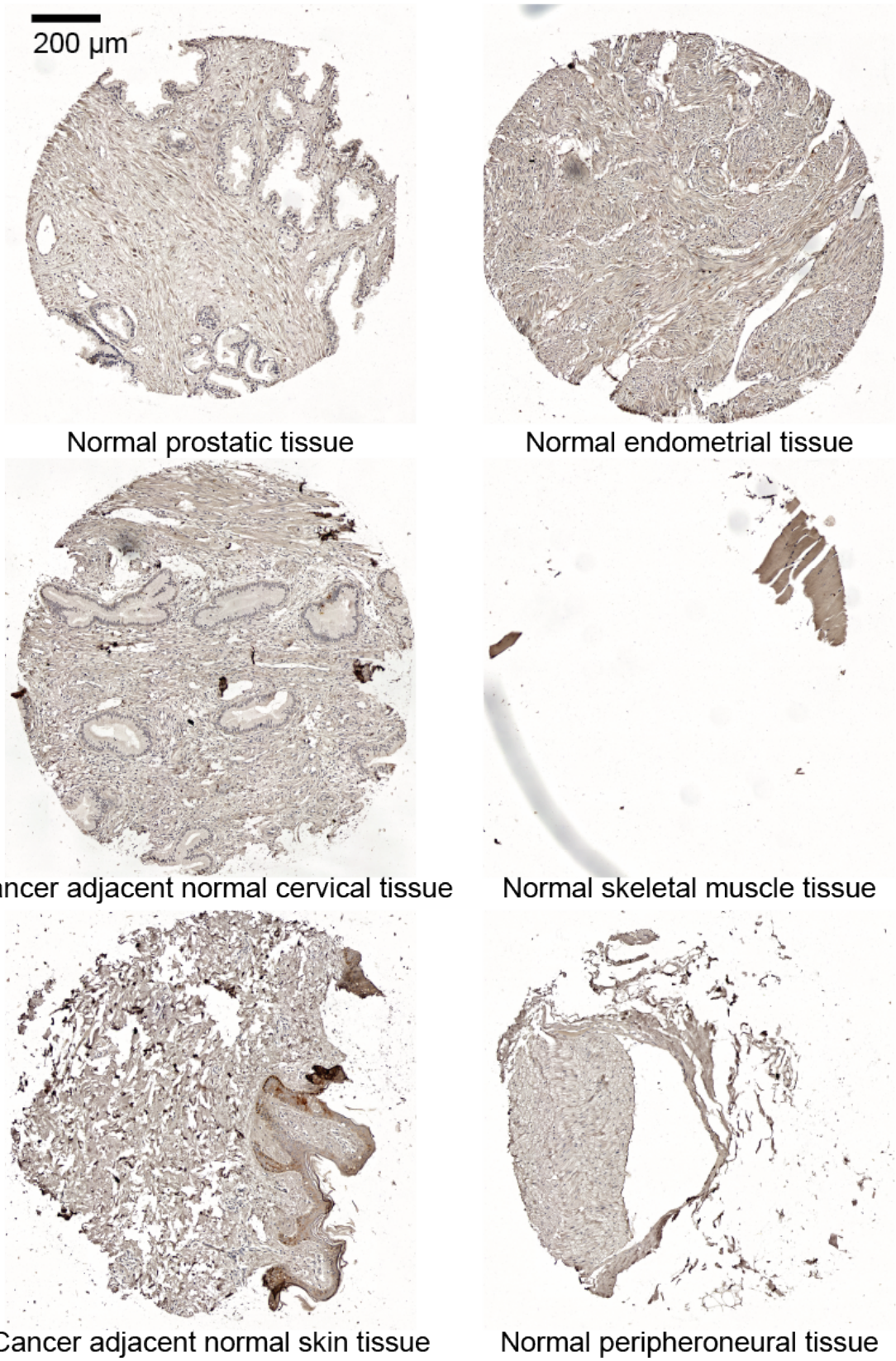



Figure **5.1.2.2** (page 5 of 6)

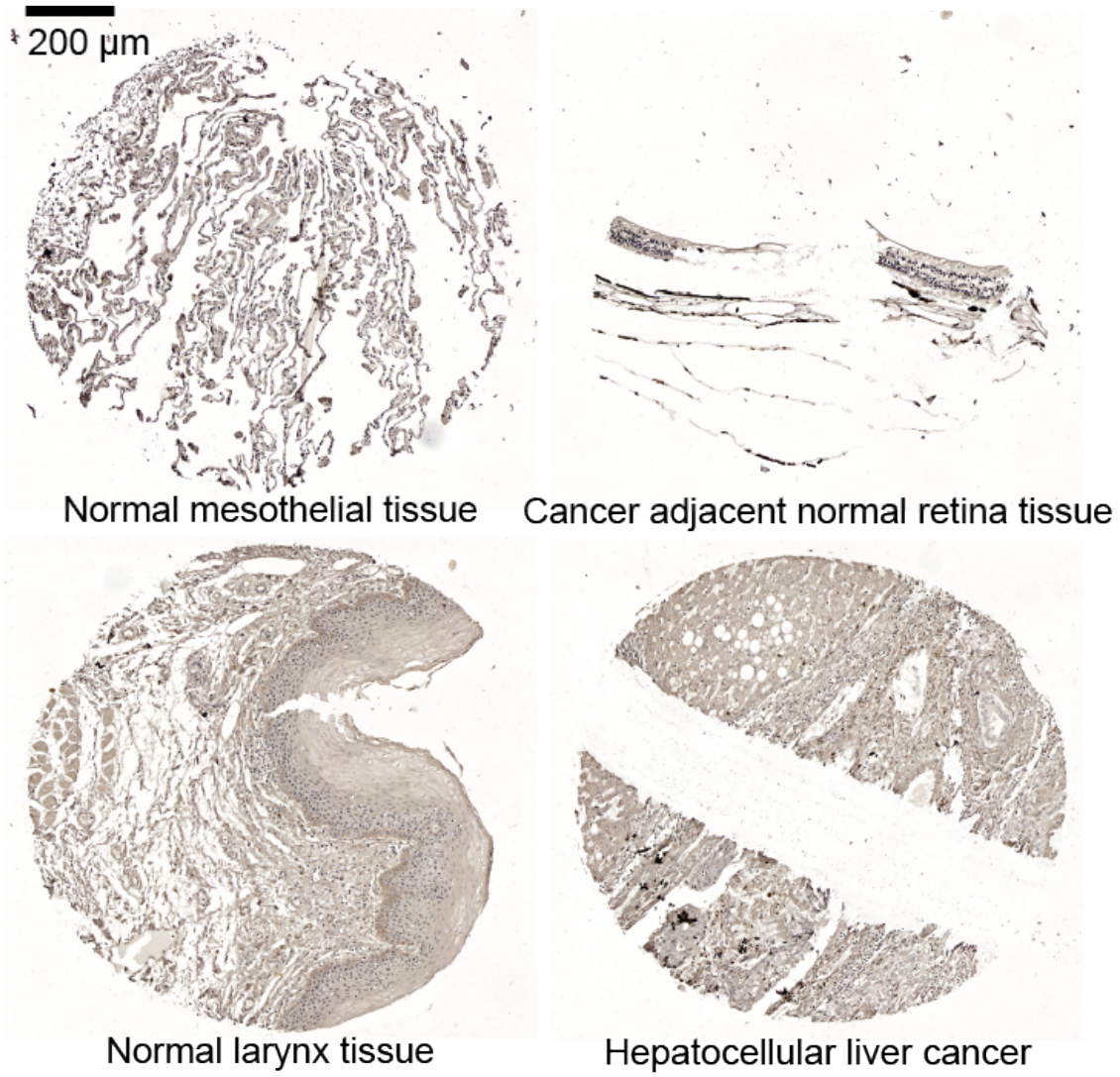



**Figure 5.1.2.2 (page 6 of 6): Immunostaining of multi-tissue antibody validation array – A5:158 mAb.** DAB-staining (brown) using mouse anti-human Endo180 mAb A5:158. Nuclei were counterstained with Mayer's haematoxylin (blue). Three cores from different individuals per tissue were assessed. One core of testis, breast and prostate and two cores of eye tissue were lost. One sample core is shown for each tissue. Scale bars = 200 µm.

| | | 39:10 | | A5:158 | | |
|---|---|---|---|---|---|---|
| Organ | Pathology diagnosis | Expression level [0-3] | localisation [% of cells] | Expression level [0-3] | localisation [% of cells] | comments |
| Cerebrum | Normal cerebral gray matter tissue | 1 | 20% (cytosol) | 1 | 15% (cytosol) | inconsistent |
| Cerebrum | Normal cerebral white matter tissue | 0 | 5% (nuclei) | 0 | 5% (nuclei) | inconsistent |
| Cerebellum | Normal cerebellar tissue | 0 | | 0 | | |
| Adrenal gland | Normal adrenal gland tissue | 1-2 | 10% (nuclei and cytosol) | 3 | 20-30% (nuclei and cytosol) | inconsistent |
| Ovary | Normal ovary tissue | 0 | | 2 | 5% (cytosol) | inconsistent |
| Pancreas | Normal pancreatic tissue | 0 | | 3 | 20% (cytosol) | |
| Parathyroid gland | Normal parathyroid gland tissue | 0 | 10 % (granular stain in cytosol) | 3 | 10% (cytosol) | inconsistent |
| Hypophysis | Normal hypophyseal tissue | 0 | staining in intercellular space | 2 | 5% (cytosol) | inconsistent |
| Testis | Normal testis tissue | 2 | 90% (cytosol of leydig cells only) | 3 | 90% (cytosol of leydig cells only) | |
| Thyroid gland | Normal thyroid gland tissue | 0 | staining in intercellular space | 0 | | inconsistent |
| Breast | Cancer adjacent normal breast tissue | 0 | | 0 | | |
| Spleen | Normal spleen tissue | 1 | 50% (nuclei) and intercellular space | 1 | 30% (nuclei) and intercellular space | |
| Tonsil | Normal tonsilar tissue | 1 | 50% (nuclei) and intercellular space | 2 | 50% (nuclei) and intercellular space | |
| Thymus gland | Normal thymic tissue | 1 | 60% (nuclei) | 1 | 60% (nuclei) | |
| Bone marrow | Normal myeloid tissue | 2 | 100% (nuclei and cytosol) | 3 | 100% (nuclei and cytosol) | |
| Lung | Normal lung tissue | 2 | 50% (cytosol) | 3 | 50% (cytosol) | inconsistent |
| Cardiac muscle | Normal cardiac muscle tissue | 1 | 30% (cytosol) | 2 | 30% (cytosol) | |
| Esophagus | Normal esophageal tissue | 0 | | 2 | 70% (cytosol of squamos and basal cells) | |
| Stomach | Normal gastric tissue | 1 | 30% (cytosol) | 2 | 80% (cytosol of parietal and chief cells) | |
| Small intestine | Normal small intestinal tissue | 0 | | 3 | 80% (apical site of epithelial and lamina propria cells) | |
| Colon | Normal colonic tissue | 0 | | 2 | 80% (cytosol of goblet cells) | |
| Liver | Normal hepatic tissue | 3 | 30% (nuclei and cytosol) cytosol weaker | 2 | Sinosoid cells | |
| Salivary gland | Normal salivary gland tissue | 0 | | 1 | 20% (cytosol) | |
| Kidney | Normal renal tissue | 2 | 20% (nuclei and cytosol) | 2 | 70% (cytosol of epithelial cells of tubules) | |
| Prostate | Normal prostatic tissue | 0 | | 0 | | |
| Endometrium | Normal endometrial tissue | 0 | | 0 | | |
| Uterine cervix | Cancer adjacent normal cervical tissue | 0 | | 0 | | |
| Skeletal muscle | Normal skeletal muscle tissue | 0 | | lost | | |
| Skin | Cancer adjacent normal skin tissue | 2 | cytosol of Stratum germinativum | 2 | cytosol of Stratum germinativum and some keratinocytes | |
| Peripheral nerves | Normal peripheroneural tissue | 0 | | 0 | | |
| Mesothelium | Normal mesothelial tissue | 1 | 80% (cytosol) mesothelial cells | lost | | inconsistent |
| Eye | Cancer adjacent normal retina tissue | 0 | | 0 | | |
| Larynx | Normal larynx tissue | 3 | 50% (nuclei) lamina propria only | 1 | 60% (cytosol) basal and luminal cells | |

**Table 5.1.2.3: An FDA approved multi-tissue antibody validation array – summary of Endo180 staining results.** Staining was carried out using mouse anti-human Endo180 mAbs 39:10 and A5:158. Expression localisation was analysed after slide digitalisation and cell populations were histologically identified. Staining is reported as inconsistent if it was not present in all three cores of the respective type of tissue. Endo180 expression was rated from 0-3.

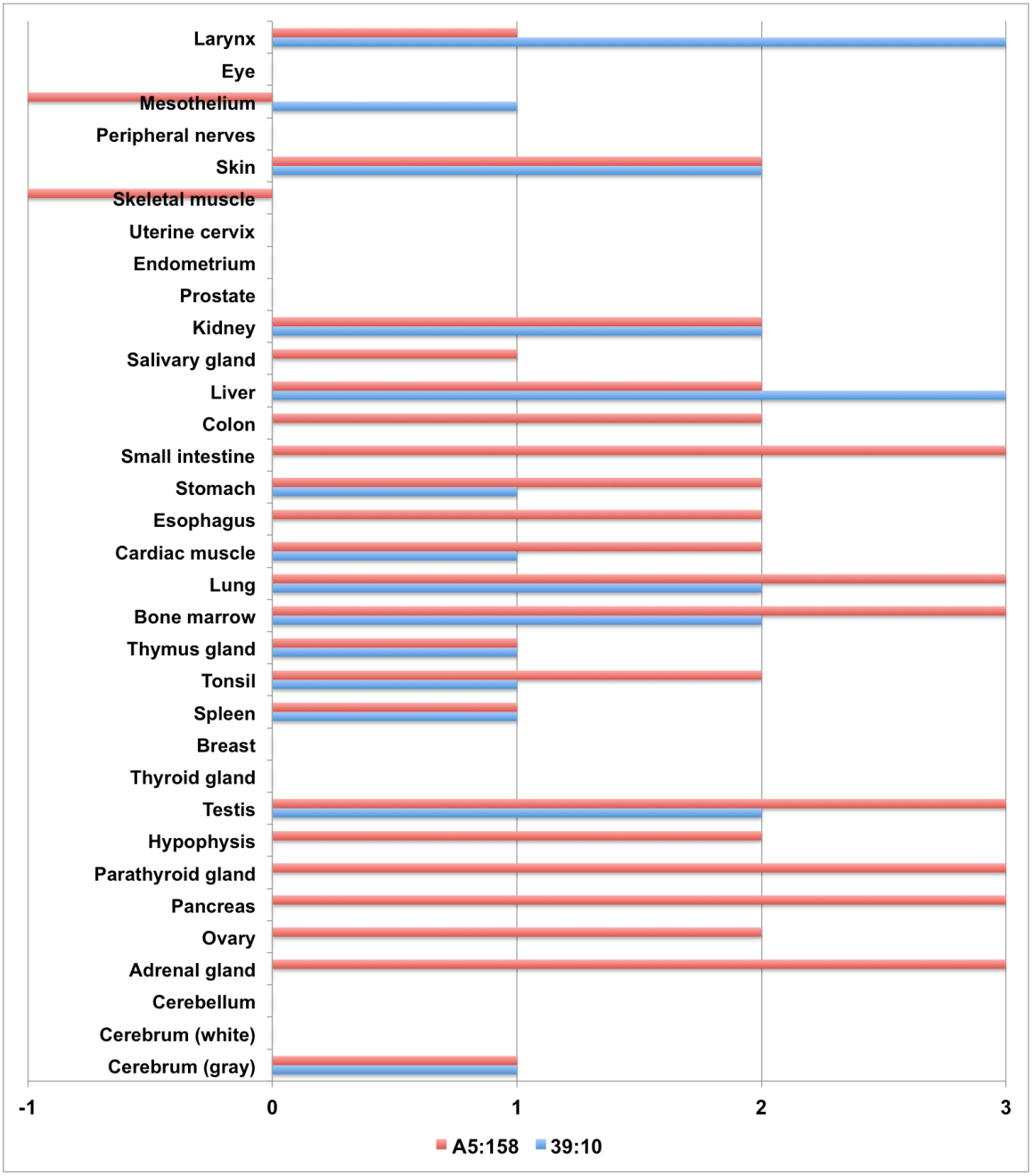



**Table 5.1.2.4: An FDA approved multi-tissue antibody validation array – summary of Endo180 staining results.** Comparative Visualisation of Endo180 expression rating between 39:10 and A5:158 staining.

### 5.1.2.1 Endo180 expression and localisation - 39:10

Although Endo180 was reported as a recycling endocytic receptor, positive staining in nuclei was detected in white matter, the adrenal gland, spleen, tonsil, thymus, bone marrow, liver, kidney and larynx (**Figure 5.1.2.1**). However, a consistent nuclear staining pattern over all three biopsies could only be observed in spleen, tonsil, bone marrow, thymus and larynx (**Table 5.1.2.3**).

Positive staining in the cytosol was observed in grey matter, adrenal gland, parathyroid gland, testis, bone marrow, lung, cardiac muscle, stomach, liver, kidney, skin, mesothelium and larynx (**Figure 5.1.2.2**). However, a consistent cytosolic staining pattern in all three biopsies was only observed in Leydig cells of the testis, the bone marrow and the stratum germinativum of the skin (**Table 5.1.2.3 and Figure 5.1.2.5**).

### 5.1.2.2 Endo180 expression and localisation - A5:158

The results obtained using the A5:158 mAb confirmed the findings obtained with the 39:10 mAb. However, the intensity of the staining was stronger and the A5:158 antibody stained tissue that showed no stain using the 39:10 mAb.

Similar to findings with the 39:10 mAb nuclear stain was observed in the same tissues (cerebral white matter, adrenal gland tissue and organs of the immune system).

Interestingly, in addition to findings with the 39:10 mAb, the A5:158 mAb stained distinct cell populations in the oesophagus, salivary gland, gastric, small intestine and colon tissue (**Figure 5.1.2.6**).

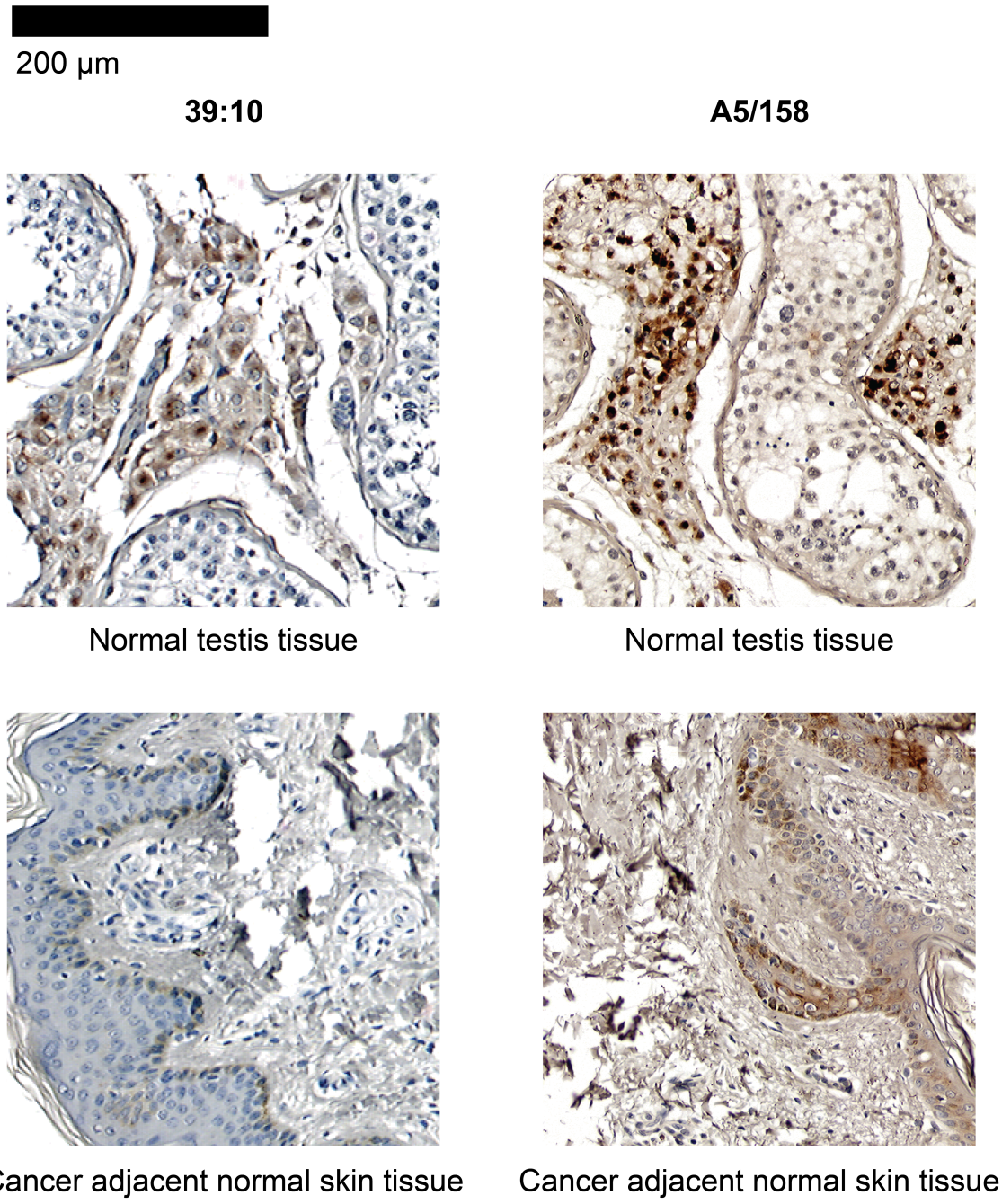



**Figure 5.1.2.5: An FDA approved multi-tissue antibody validation array – summary of Endo180 staining results.** Staining was carried out using mouse anti-human Endo180 mAbs 39:10 and A5:158. Expression localisation was analysed after slide digitalisation and cell populations were histologically identified. Staining is reported as inconsistent if it was not present in all three cores of the respective type of tissue.

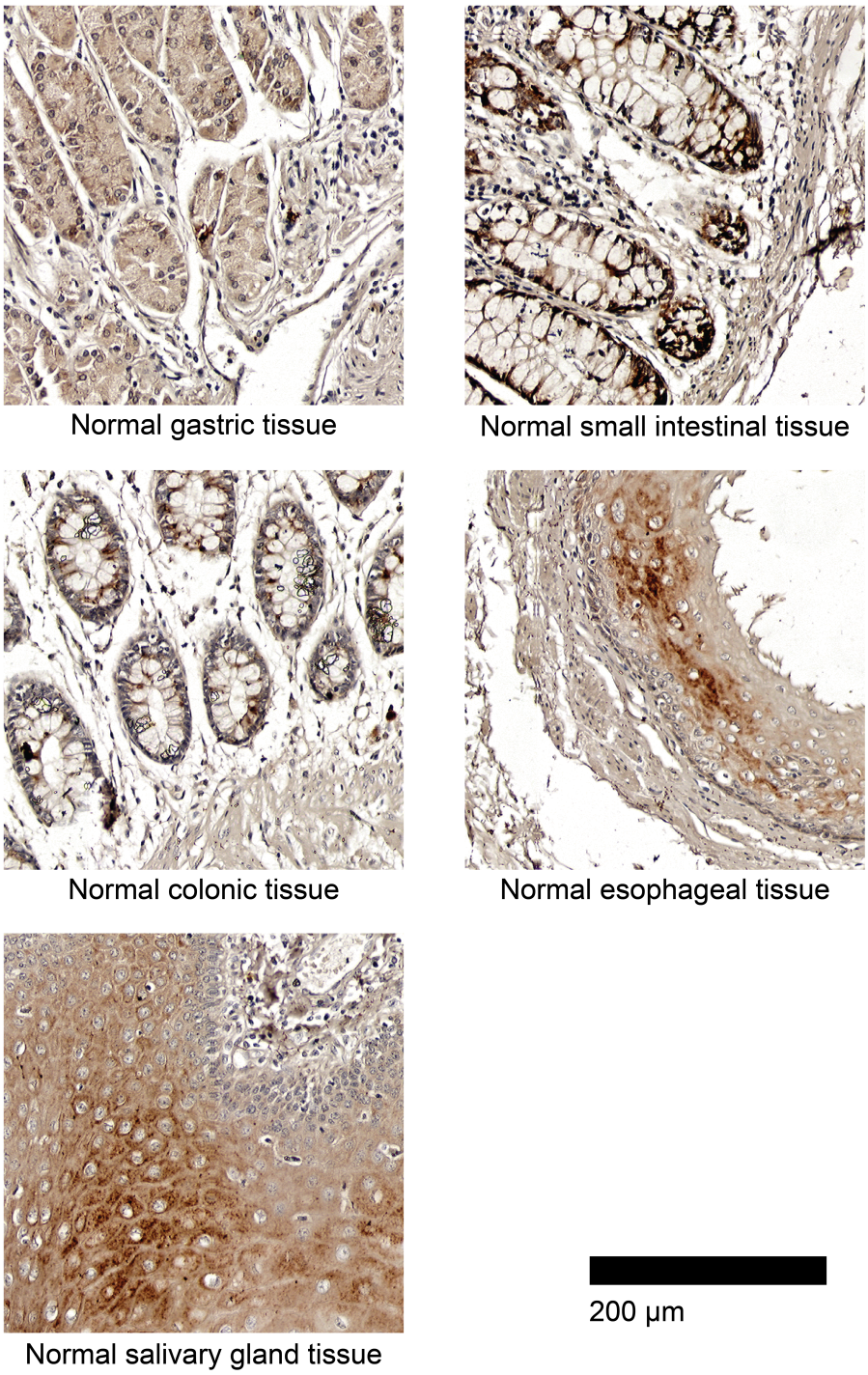



**Figure 5.1.2.6: An FDA approved multi-tissue antibody validation array – summary of Endo180 staining results.** Staining was carried out using mouse anti-human Endo180 mAbs 39:10 and A5:158. Expression localisation was analysed after slide digitalisation and cell populations were histologically identified. Staining is reported as inconsistent if it was not present in all three cores of the respective type of tissue.

In case of the small intestine, the staining was confined to only the apical site of epithelial cells and to cells in the lamina propria. In the oesophagus, squamous and basal cells displayed Endo180 expression. In gastric tissue parietal and chief cells and in the colon the goblet cells showed strong Endo180 expression (**Figure 5.1.2.6**). Additionally, the clearer staining allowed identification of Endo180 expression in the liver (restricted to sinosoid cells) and in the kidneys (epithelial cells of renal tubules).

### 5.1.3 Discussion

#### 5.1.3.1 Comparison to other studies

The findings were compared to earlier reports by Professor Isacke and the Genentech Corporation (Isacke et al., 1990; Wu et al., 1996) (**figure 5.1.3.1**). In their first report about the Endo180 protein Clare Isacke and co-workers analysed its expression in various tissues by Western Blot analysis of homogenised human and rat tissue (Isacke et al., 1990) (**figure 5.1.3.1**). The Genentech Corporation measured Endo180 transcript level by Northern Blot analysis of several human and rat tissues (Wu et al., 1996) (**figure 5.1.3.1**). The relative transcript levels amongst different tissues differ strongly between human and rat tissue. For example, whereas Endo180 transcript level is high in human testis, it is absent in rat testis. Whereas expression in the lung of rats is a magnitude higher than in the heart the situation is reversed in human tissue (Wu et al., 1996) (**figure 5.1.3.1**).

While Isacke's analysis of protein levels (in rat) aligns with Genentech's analysis of the transcript level (in rat) in testis, kidney, lung, liver and testis, the results differ in brain, spleen, heart muscle and skeletal muscle. The only tissue lysates of human origin that have been analysed by Isacke were taken from the skin and placenta. While Isacke reports high protein expression levels in the human placenta, Genentech reports low transcript levels (**figure 5.1.3.1**).

| | 39:10 | A5:158 | | | | |
|---|---|---|---|---|---|---|
| Organ | Expression level [0-3] | Expression level [0-3] | naming convention [Isacke] | Expression level [-,+,++] | naming convention [Genentech] | Expression level [0-100] |
| Cerebrum (gray) | 1 | 1 | Brain | - | Brain | 1 |
| Cerebrum (white) | 0 | 0 | | | | |
| Cerebellum | 0 | 0 | | | | |
| Adrenal gland | 1-2 | 3 | | | | |
| Ovary | 0 | 2 | | | Ovary | 100 |
| Pancreas | 0 | 3 | | | Pancreas | 20 |
| Parathyroid gland | 0 | 3 | | | | |
| Hypophysis | 0 | 2 | | | | |
| Testis | 2 | 3 | Testis | - | Testis | 67 |
| Thyroid gland | 0 | 0 | | | | |
| Breast | 0 | 0 | | | | |
| Spleen | 1 | 1 | Spleen | + | Spleen | 20 |
| Tonsil | 1 | 2 | | | | |
| Thymus gland | 1 | 1 | Thymus | - | Thymus | 11 |
| Bone marrow | 2 | 3 | | | | |
| Lung | 2 | 3 | Lung | ++ | Lung | 26 |
| Cardiac muscle | 1 | 2 | Heart muscle | - | Heart | 73 |
| Esophagus | 0 | 2 | | | | |
| Stomach | 1 | 2 | | | | |
| Small intestine | 0 | 3 | | | Intestine | 59 |
| Colon | 0 | 2 | | | Colon | 10 |
| Liver | 3 | 2 | Liver | - | Liver | 7 |
| Salivary gland | 0 | 1 | | | | |
| Kidney | 2 | 2 | Kidney | + | Kidney | 15 |
| Prostate | 0 | 0 | | | Prostate | 55 |
| Endometrium | 0 | 0 | | | | |
| Uterine cervix | 0 | 0 | | | | |
| Skeletal muscle | 0 | lost | Skeletal muscle | - | Muscle | 37 |
| Skin | 2 | 2 | Skin | + | | |
| Peripheral nerves | 0 | 0 | | | | |
| Mesothelium | 1 | lost | | | | |
| Eye | 0 | 0 | | | | |
| Larynx | 3 | 1 | | | | |
| | | | Bladder | + | | |
| | | | Placenta | ++ | Placenta | 12 |

**Figure 5.1.3.1: Comparison of multi-tissue TMA with previous studies.** (**columns 1 and 2)** the result obtain in this study using the FDA multi-tissue array. (**columns 3 and 4**) Clare Isacke analysed tissue lysates by Western Blot and reported expression level on a scale from negative (-) to positive (+) and a (++) value for very high expression. Please note that only skin and placenta were of human origin. All other tissues were from rat. (**columns 5 and 6**) The Genentech Corporation analysed Endo180 transcript level in human tissue by Northern Blot analysis. Their published results were quantified by densitometry and the expression level normalised on a scale from 0-100.

In summary, all thee studies, the TMA, Western Blot by Isacke and Northern Blot by Genentech agree on an absence of Endo180 expression in the healthy brain. Furthermore, there is no disagreement over the expression of Endo180 in the testis of humans and its absence in rats. According to the TMA, expression of Endo180 in the human testis is confined to Leydig cells. All studies found expression of Endo180 in the lungs and kidneys of rats and humans. In the TMA pictures, expression appeared to be dominant in the epithelial cells of renal tubes. There is no disagreement over the expression of Endo180 in the skin of humans. The expression was found to be mainly concentrated in the stratum germinativum. Northern Blot findings by Genentech concerning Endo180 expression in the colon and intestine were confirmed by the TMA results.

However, while Genentech reported high transcript levels in the ovaries and prostate of humans, no corresponding protein expression was apparent on the TMA. Positive staining of heart muscle cells on the TMA is in accordance with Genentech's findings, however, Genentech and Isacke disagree over the expression of Endo180 in the heart of rats. Genentech reported a splice variant of Endo180 in the liver of human foetal livers but no expression of Endo180 in the liver of adults. This is in disagreement with Endo180 staining on sinusoid liver cells on the TMA. Neither Genentech nor Isacke detected Endo180 expression in the liver of rats. The TMA results for Endo180 expression in skeletal muscles are inconclusive and therefore unable to shed light onto the contradicting findings by Genentech and Isacke. No human placenta tissue was included in the TMA, which is why no clarification for these contradicting reports was found.

Expression of Endo180 in organs of the immune system remains inconclusive. Several cell nuclei in these tissues appeared to be DAB stained on the TMA. Isacke and Genentech both agree on an absence of Endo180 transcript in the thymus of humans and rats. However, nuclear stain appeared on the TMA. Genentech reports transcription of Endo180 in the human spleen but no such transcription in the rat spleen, which is in disagreement with Isacke who reported protein in the rat spleen.

### 5.1.3.2 Discussion - multi tissue array

The finding that the A5:158 mAb at a concentration of 10 µg/ml gives a low signal in tissue is in accordance with finding of the co-operation partners at the University of Newcastle (see **Section 5.2** for a detailed discussion). Interestingly, by titrating the antibody from 10 µg/ml over 20 µg/ml to 50 µg/ml an incremental increase in tissue staining was observed. Even at the relatively high concentration of 50 µg/ml a clear cytosolic/peri-nuclear staining of distinct cell populations without any notable increase in background staining was achieved. This is in stark contrast to a strong background that appeared after increasing the 39:10 mAb concentration to 50 µg/ml.

Contrary to earlier studies about the cell biology of the Endo180 protein DAB staining was observed in cell nuclei in various tissues using both, the 39:10 and A5:158 mAbs (see **Figures 5.1.2.1 & 5.1.2.2**). However, similar observations have been made before and discarded as non-specific antibody interaction/artefact (Justin Sturge, personal communication). The 39:10 as well as the A5:158 antibody bind to FNII or CTLD domains (extracellular) of the Endo180 protein. Disulphide bonds, which are integral part of three-dimensional structure of these domains, will be reduced/dissolved in the reducing environment of cytosol and nucleus. Therefore, a presence of this domain of Endo180 in the nucleus is unlikely. No evidence has been shown or suggestion being made in literature or personal communications that the Endo180 protein has ever been associated with the nucleus. The majority of potential nuclear stain has been observed in immune cells. These cells are significantly smaller than epithelial cells or fibroblasts. It is very difficult to differentiate nuclear staining from staining of the peri-cellular recycling compartment in these cell types due to the small cell size. The Endo180 stain might appear to be nuclear while in fact it is peri-nuclear. Furthermore, the immunoprecipitation results revealed an assembly of nuclear proteins in mass spectroscopy analysis (**section 4**). For further analysis of US Biomax and Newcastle

prostate cancer TMAs any nuclear staining by the 39:10 or A5:158 mAb was treated as artefact.

Differences between findings in the TMA study and Clare Isacke's findings can be easily explained by the fact that Clare Isacke and co-workers used rat tissue for their Western Blot analysis while the TMA contains human tissue only. As reported in **Section 5.1.3.1** the Genentech Corporation showed that the Endo180 transcript level in different tissues differs significantly between rat and human tissue. Therefore it is very likely that the relative protein levels differ between humans and rat as well. Differences between Isacke's and Genentech's findings in rat might relate to the fact that Genentech looked at transcript levels whereas Isacke looked at protein level. Another explanation might be transient expression that only occurs at a certain age or breeding conditions.

The most striking differences between the Genentech study on the transcription level in humans and findings in the TMA study are apparent in the ovaries, skeletal muscle and prostate where no Endo180 protein can be detected on the TMA while Genentech detected Endo180 transcripts. On the other hand, Endo180 protein was detected in liver and kidney whereas Genentech reports low or zero transcript level. Endo180 expression in the liver and kidney has been reported and investigated in detail (Mousavi et al., 2009; Okamura et al., 2011). The tissue used to generate the sections of prostatic tissue on the TMA was retrieved from young men in their 20's. In later studies (**Section 5.2)** expression of Endo180 in non-malignant prostate of elder men was detected.

Endo180 protein level does not necessarily correlate to the amount of Endo180 transcript, as a post-transcriptional regulation of protein expression is possible. Another possible explanation for these discrepancies might be the observation that the expression of Endo180 seems to differ between the tissues of different individuals in some tissues (inconsistent staining). Genentech has used commercial multiple tissue Northern Blots manufactured by the Clontech Corporation. It was not possible to discover whether these Northern Blots have been produced from one individual human or represent a pool.

The biopsies on the TMA represent only a small fraction of the whole organ. In cases where the expression of Endo180 is restricted to specific areas within the organ, the analysis might overlook Endo180 protein, which would be present in whole tissue lysates. This might explain why Genentech detects Endo180 in tissues that appear negative on the TMA. This observation may explain the absence of Endo180 in ovary biopsies. The ovaries contain a cell population called hilum cells, which are similar to the Leydig cells of the testis and are capable of producing androgens. These cells are the likely source of Leydig cell carcinoma of the ovaries. Leydig cells are positive for Endo180, however, no hilum cells were present on the array. Expression of Endo180 by hilum cells due to their similarity to Leydig cells of the testis might explain the high Endo180 transcript levels detected by the Genentech Corporation in human ovaries.

The titration of A5:158 mAb revealed additional sites of Endo180 expression in comparison to the 39:10 mAb this observation may be due to differences in Endo180 expression levels. The expression of Endo180 might be significantly lower in the additional sites that were discovered in comparison to the sites that have been successfully stained with both antibodies. Unpublished work in our lab suggest that A5:158 demonstrates a preference for Endo180 localised on the cell surface while 39:10 mAb shows a preference for Endo180 located on intracellular membranes. This effect has only been observed in cells with significant epithelial characteristics but could explain the increased staining seen in the TMA. Such observations were made in DU145 in RWPE-1 acinar cultures. As discussed in the introduction (**Section 1.4.5**) a decrease in pH associated with internalisation of the receptor into endocytotic vesicles will most likely induce a conformational change. This conformational change might enhance the interaction with the 39:10 mAb while at the same time it might decrease the affinity towards binding to the A5:158 mAb.

The role of Endo180 in bone development has been addressed before (Engelholm et al., 2001b) but the role of Endo180 in healthy skin or testis has not been investigated to date. The stratum germinativum or basal layer of the skin is

mitotically active and gives rise to the outer cells of the skin (Gilbert, 2000). The basal layer is thought to be the location of the stem cells of the epidermis (Fuchs, 2009). Leydig cells are located in between the seminiferous tubes. These cells are rich in smooth endoplasmic reticulum and produce androgens, mainly testosterone which is necessary for spermatogenesis in the seminiferous tubes (Bruce Alberts, 2002; Whitehead, 2001).

For the purpose of validating the antibodies for use in a disease marker study, their performance was demonstrated in tissue from a wide range of organs and different individuals. For further studies, the role of Endo180 in Leydig cells of the human testis as well as in several tissues of the gut (intestine, colon, oesophagus) seems to be of the highest interest. The role of Endo180 in the development of bone and lungs as well as wound healing (skin) has been investigated previously (Engelholm et al., 2001b; Honardoust et al., 2006; Smith et al., 2008). Furthermore, the role of Endo180 in a mouse model of renal fibrosis as well as the liver of the rat has been investigated previously (Mousavi et al., 2009; Okamura et al., 2011).

## 5.2 Endo180 expression in prostate cancer

To examine the expression level and localisation of Endo180 in prostate cancer progression 39:10 and A5:158 mAbs were used to immunostain paraffin embedded biopsies from prostate cancer patients. In total six independent TMAs were analysed. The PR208 TMA was purchased from US Biomax Corporation. The five remaining TMAs (NCLPC1-5) were obtained through collaboration with Professor Craig Robson, Dr Luke Gaughan and Dr Stephen Darby at Newcastle University (**Table 5.2.1**).

The PR208 TMA only included the age of the patient and patient Gleason grade. NCLPC1 and NCLPC4 included biopsies from patients with low and high Gleason grade and survival data. NCLPC3 and NCLPC6 contained biopsies of patients diagnosed with low-grade disease with additional information about the nature of the localised disease. For example, whether: (a) one or both lobes of the prostate were affected by the disease; and (b) tumour cells had invaded the capsule of the gland. The data sheet for NCLPC5 contained tumour grading/disease staging systems that were inconsistent between patients. For example, patient "A" is classified using a numerical scale (Grade 1-4), patient "B" is classified using Gleason Score and patient "C" is given a descriptive classification (eg. poorly differentiated).

Endo180 immunostaining was scored by a qualified pathologist as follows:

(1) the intensity of staining ($x$) was scored (0 to 3); if intensity was scored 1+, 2+ or 3+ they were assumed to be 1.5, 2.5 and 3.5 respectively.

(2) the percentage ($y$) of tumour tissue area stained was estimated.

(3) the final Endo180 staining score was calculated using the simple formula ($xy$) to give a score of 0 to 300 (or 350 for 3+) (e.g. where **30%** of tumour area was stained with a staining intensity of **2.0** the score given was **60**.

(4) an average (mean) score was calculated from 2-3 cores for each patient.

Type I and IV collagen staining intensity in the tumour-associated stroma was graded from 0 to 3+ (staining area was 90-100% in all cases).

| TMA | PR208 | NCLPC1 | NCLPC3 | NCLPC4 | NCLPC5 | NCLPC6 |
|---|---|---|---|---|---|---|
| Source | US Biomax | New Castle | New Castle | New Castle | New Castle | New Castle |
| Pathologist | Dr Wang | Dr Mauri | Dr Mauri | Dr Mauri | Dr Mauri | Dr Mauri |
| 39:10 | Yes | Yes | Yes (intensity poor) | Yes | Yes (intensity poor) | Yes (intensity poor) |
| A5:158 | failed | failed | failed | failed | failed | failed |
| No. of Patients | 69 | 76 | 45 | 81 | 149 | 67 |
| Years of study | - | 1989-1995 | 1993-1998 | 1988-1997 | 1990-2002 | 1999-2003 |
| tumour cores/patient | 3 | 2 | 2 | 2 | 1-2 | 2 |
| BPH cores/patient | 0 | 0 | 2 | 0-2 | 0 | 0 |
| BPH/normal prostate | 27 | 0 | 0 | 0 | 8 | 0 |
| Sections/core | 1 | 1 | 1 | 1 | 1 | 1 |
| Age range | 26-83 | - | 39-70 | 55-89 | 44-85 | 48-70 |
| median Age | 69 | - | 64 | 72 | 73 | 62 |
| preop PSA | - | - | 27/45 | - | Yes | 30/67 |
| relapse PSA | - | 18/76 | 2/45 | 29/81 | Yes | - |
| nadir PSA | - | - | Yes | - | Yes | 5/67 |
| time to nadir | - | - | Yes | Yes | Yes | 5/67 |
| Gleason (core, pathologist) | Dr Wang | - | - | - | - | - |
| Gleason (core, datasheet) | No (different grading system) | Yes | - | Yes | - (inconsistent) | - |
| Gleason (patient, datasheet) | Yes | Yes | Yes | Yes | - (inconsistent) | Yes |
| Gleason range | 6-10 | 6-10 | 6-7 (other grades negligible) | 6-10 | - (inconsistent) | 6-7 |
| staging (e.g. T3a) | | Yes | Yes | - | - (inconsistent) | Yes |
| metastatic disease | - | Yes | - | Yes | Yes | - |
| Survival | - | Yes | - | Yes | Yes | - |
| cause of death | - | Yes | - | Yes | Yes | - |
| LND lymph node dissection | - | - | 22/45 | - | - | 62/67 |
| PNI (perineural invasion) | - | - | 36/45 | - | - | 56/67 |
| PIN (prostatic intraepithelial neoplasia) | - | - | 45/45 | - | - | 66/67 |
| capsular invasion | - | - | 21/45 | - | - | 20/63 |
| surgical margins positive | - | - | 25/45 | - | - | 31/67 |
| SV (seminal vesicle invasion) | - | - | 2/45 | - | - | 1/67 |

**Table 5.2.1 TMA details.** The table indicates the source of the different TMAs analysed and whether staining was successful or not. The name of the pathologist is indicated. The availability of accompanying patient data listed in column 1 is also indicated. Where data is indicated to be inconsistent the information is either incomplete or inconsistently recorded so cannot be included in any analysis.

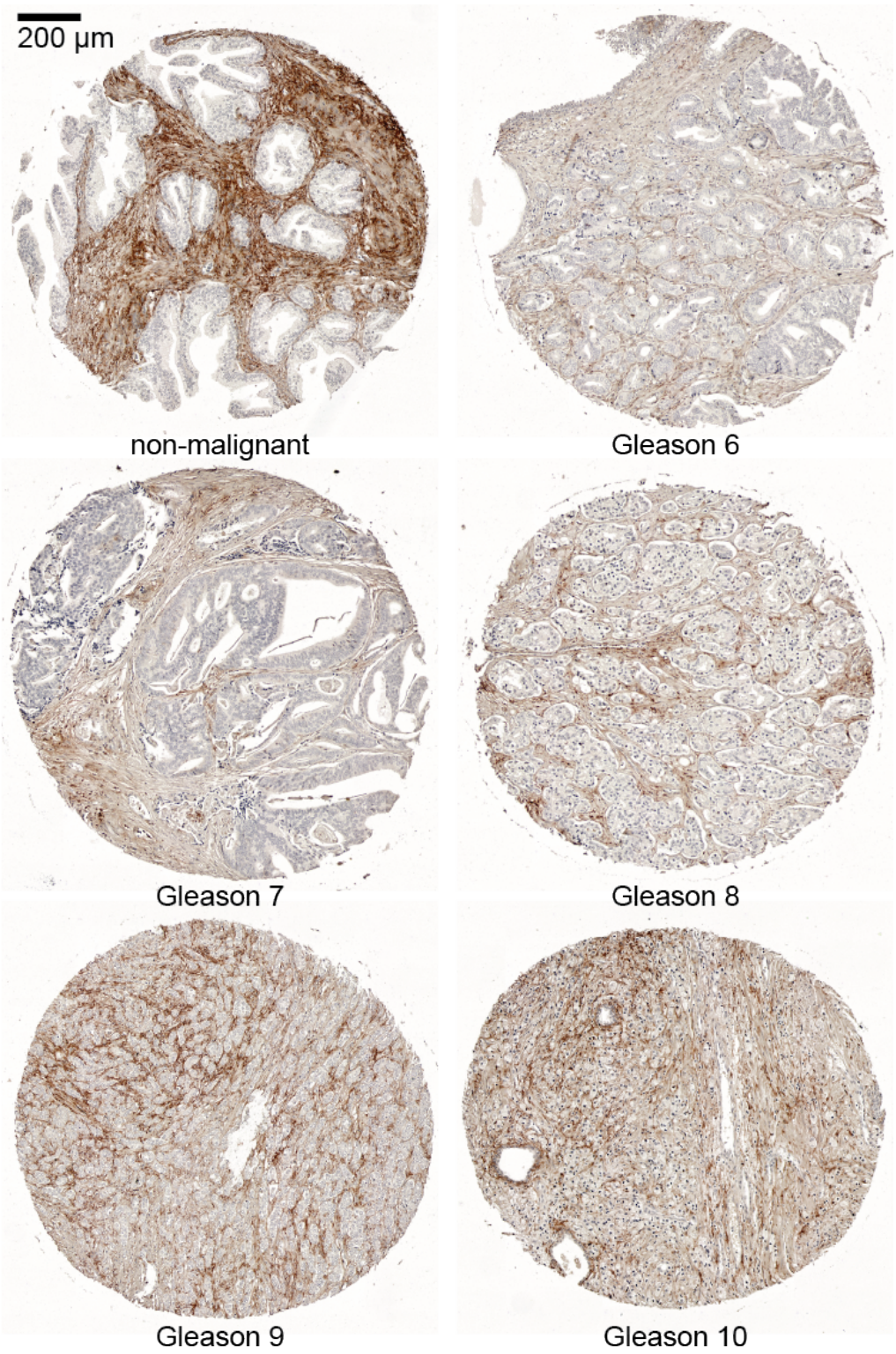



**Figure 5.2.2 PR208 – Endo180 staining.** DAB staining (brown) using mouse anti-human Endo180 39:10 mAb is shown. Nuclei were counterstained with Mayer's Haematoxylin (blue). Samples are categorised as non-malignant or by the Gleason grade of each biopsy. Scale bar = 200 µm.

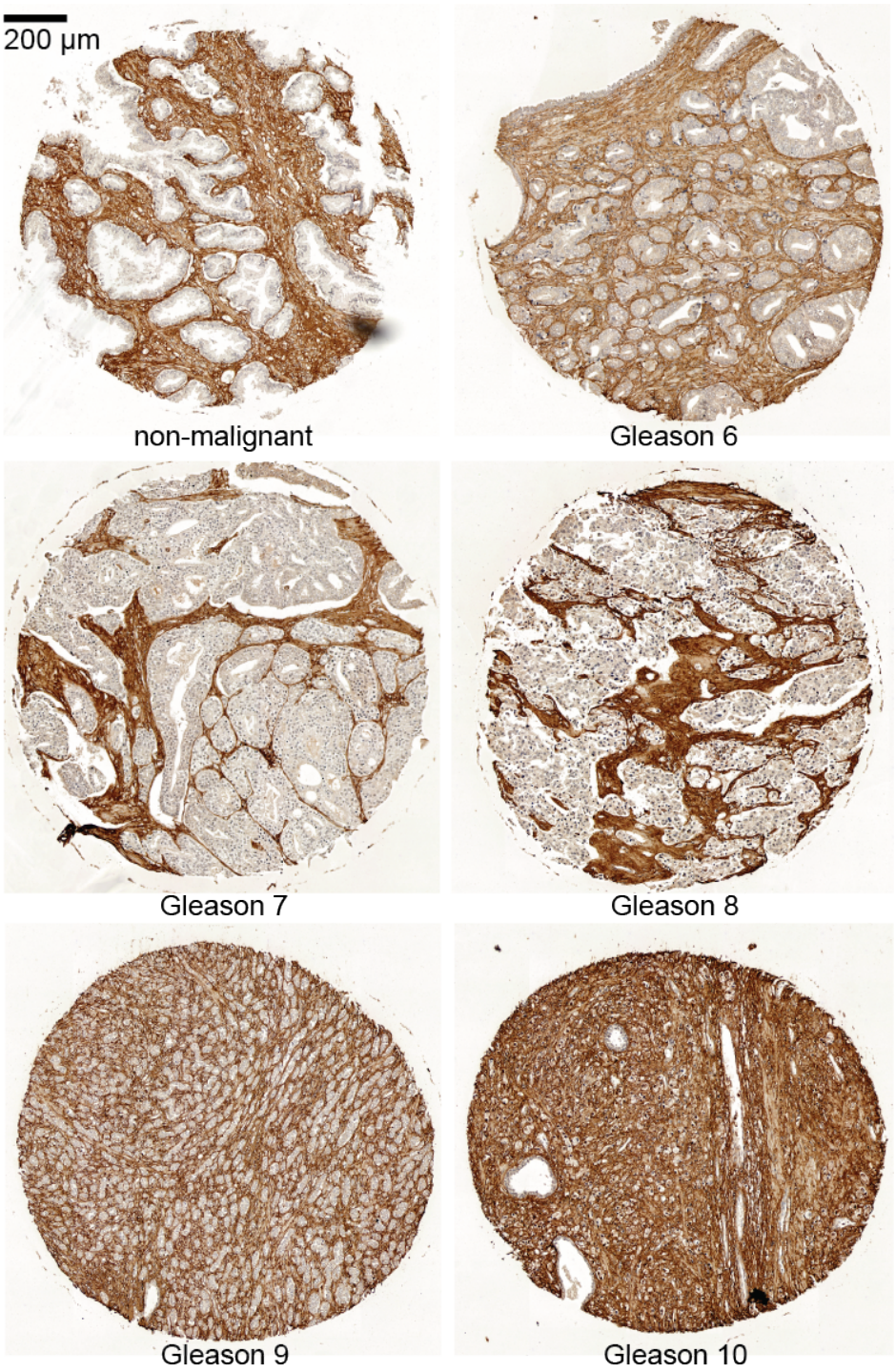



**Figure 5.2.3 PR208 – collagen I staining.** DAB-staining (brown) using rabbit anti collagen I is shown. Nuclei were counterstained with Mayer's Haematoxylin (blue). Samples are categorised as non-malignant or by the Gleason grade of each biopsy. Scale bar = 200 µm.




**Figure 5.2.4 PR208 – collagen IV staining.** DAB-staining (brown) using rabbit anti collagen IV is shown. Nuclei were counterstained with Mayer's haematoxylin (blue). Samples are categorised as non-malignant or by the Gleason grade of each biopsy. Scale bar = 200 µm.

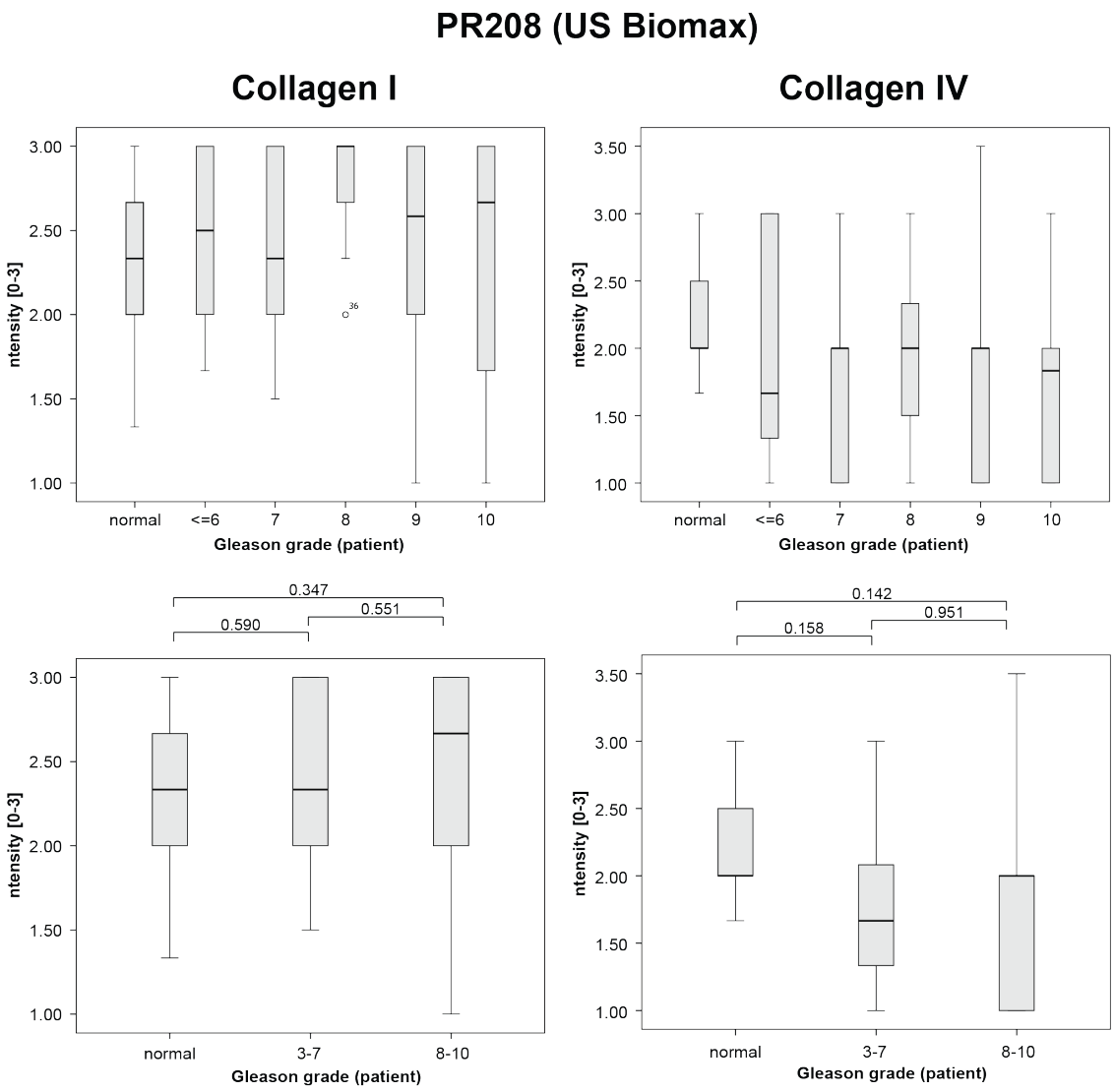



**Figure 5.2.5 PR208 – collagen I/IV – patient Gleason score.** The staining intensity of collagen types I and IV in tumour-associated stroma quantified on a scale of 0 to 3.5 (3+). Samples are categorised as non-malignant (normal) or by individual Gleason grade (3-10) or clinical Gleason grouping (3-7 or 8-10). Two biopsies were analysed per patient and the average (mean) intensity for each patient used in the analysis. Box plots show the total range (vertical lines), mean (horizontal line) and upper and lower quartiles (grey area). P-values were calculated using the Mann-Whitney Rank test.

### 5.2.1 The PR208 TMA

Consecutive sections of the PR208 TMA were stained for Endo180, type I collagen, and type IV collagen; and the possible Endo180 interaction partner AdamTS2 identified in **Section 4.7.** Additionally, the potential correlation of nicastrin expression in prostate cancer was intended as a follow on study from our earlier findings in breast cancer (Filipovic et al., 2011). Initially AdamTS2, nicastrin and Endo180 were stained using an established Proteinase K antigen retrieval method (Kogianni et al., 2009) (data not shown). As mentioned in Section 5.1 this antigen retrieval method resulted in the over digestion of tissue. Therefore, antigen retrieval was carried out by boiling the TMA slides in citrate buffer. Subsequently, three consecutive sections of the PR208 TMA were stained for Endo180 (39:10 mAb), collagens I and IV. Dr Francesco Mauri (Imperial College London) carried out histopathological analysis of the stained arrays (**Figures 5.2.2 - 5.2.4**).

#### 5.2.1.1 Endo180 - 39:10 mAb - staining

Staining with 10 μg/ml of 39:10 mAb resulted in undetectable staining by visual inspection under the microscope. The concentration was raised to 20 μg/ml and 50 μg/ml. Peri-nuclear staining of Endo180 was detectable in tumour cells in < 5/69 patients. In the TMA stained with 50 μg/ml the tumour-associated stroma displayed a positive staining pattern similar to collagen I/IV staining (compare **Figure 5.2.2** with **Figures 5.2.3** and **5.2.4**).

#### 5.2.1.2 Collagen I and collagen IV staining

Staining with collagen I/IV antibodies (Acris Organics) resulted in typical staining for collagen in the stroma (**Figures 5.2.3 and 5.2.4**). Positive staining within the tumour cells was observed in < 5/69 patients. There was no correlation between collagens I/IV in the tumour associated stroma and Gleason grade (**Figure 5.2.5**).

### 5.2.2 Newcastle arrays - Endo180 staining

Dr Luke Gaughan (Newcastle University) stained five prostate cancer TMAs (NCLPC1, NCLPC2, NCLPC3, NCLPC4, NCLPC5 and NCLPC6) using 39:10 and A5:158 mAbs. The slides were scanned for storage on the Aperio database located at Newcastle University and shipped to London. Endo180 staining was histopathological scored using the system described in **Section 5.2.1** by Dr Francesco Mauri (Imperial College London). A5:158 mAb produced a low level of staining that could not be quantified. 39:10 mAb staining was at a level that could be quantified on NCLPC1 and NCLPC4; but weak on NCLPC3, NCLPC5 and NCLPC6. 39:10 mAb staining on NCLPC1 and NCLPC4 was scored by a histopathologist (Dr Francesco Mauri, Imperial College London). The two TMAs were analysed individually and then pooled (**Figures 5.2.6 - 5.2.12**).

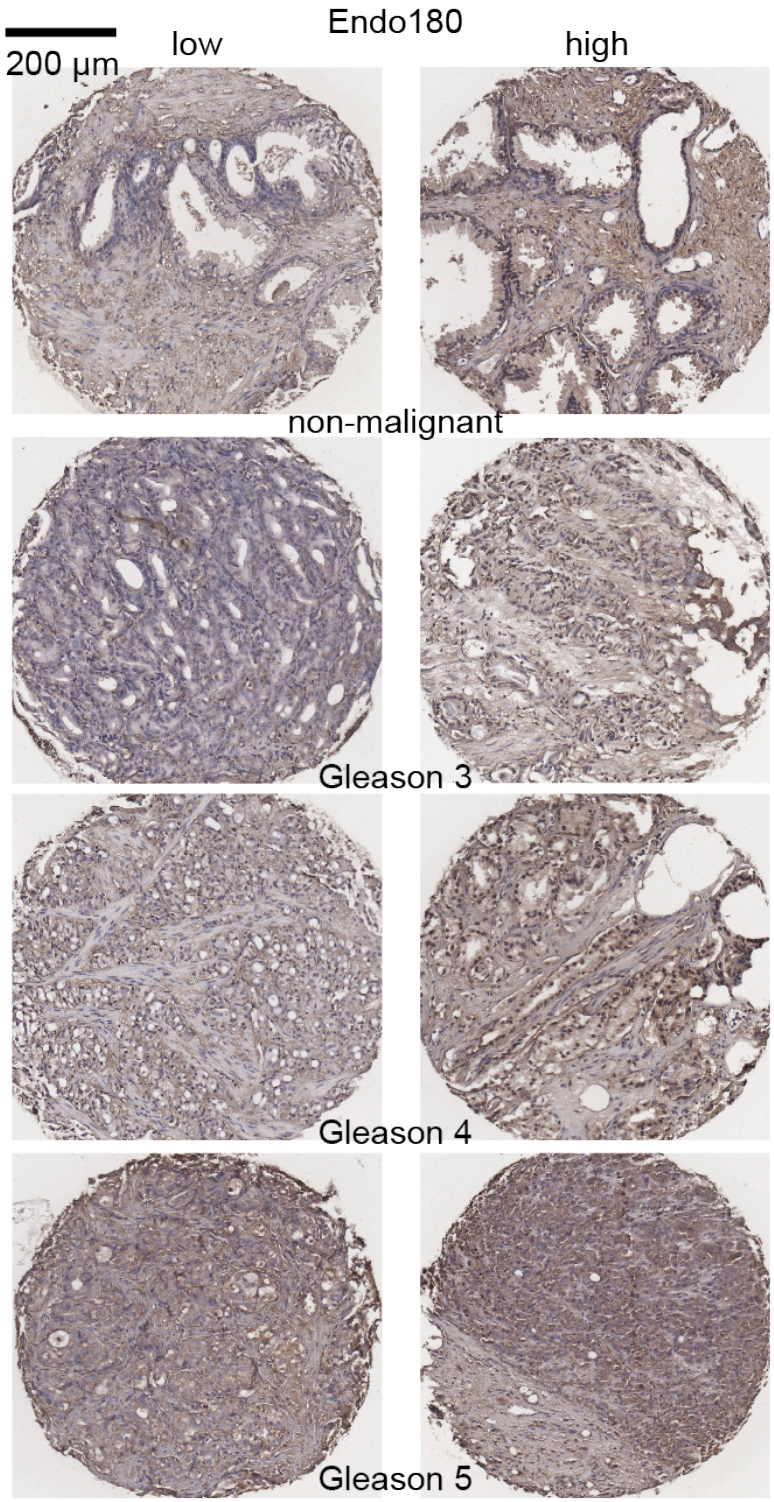



**Figure 5.2.6 NCLPC1 – Endo180 staining.** DAB staining (brown) with mouse anti-human Endo180 mAb 39:10 is shown. Nuclei were counterstained with Mayer's haematoxylin (blue). Samples are categorised as non-malignant or by the Gleason grade of each biopsy. Scale bar = 200 µm.

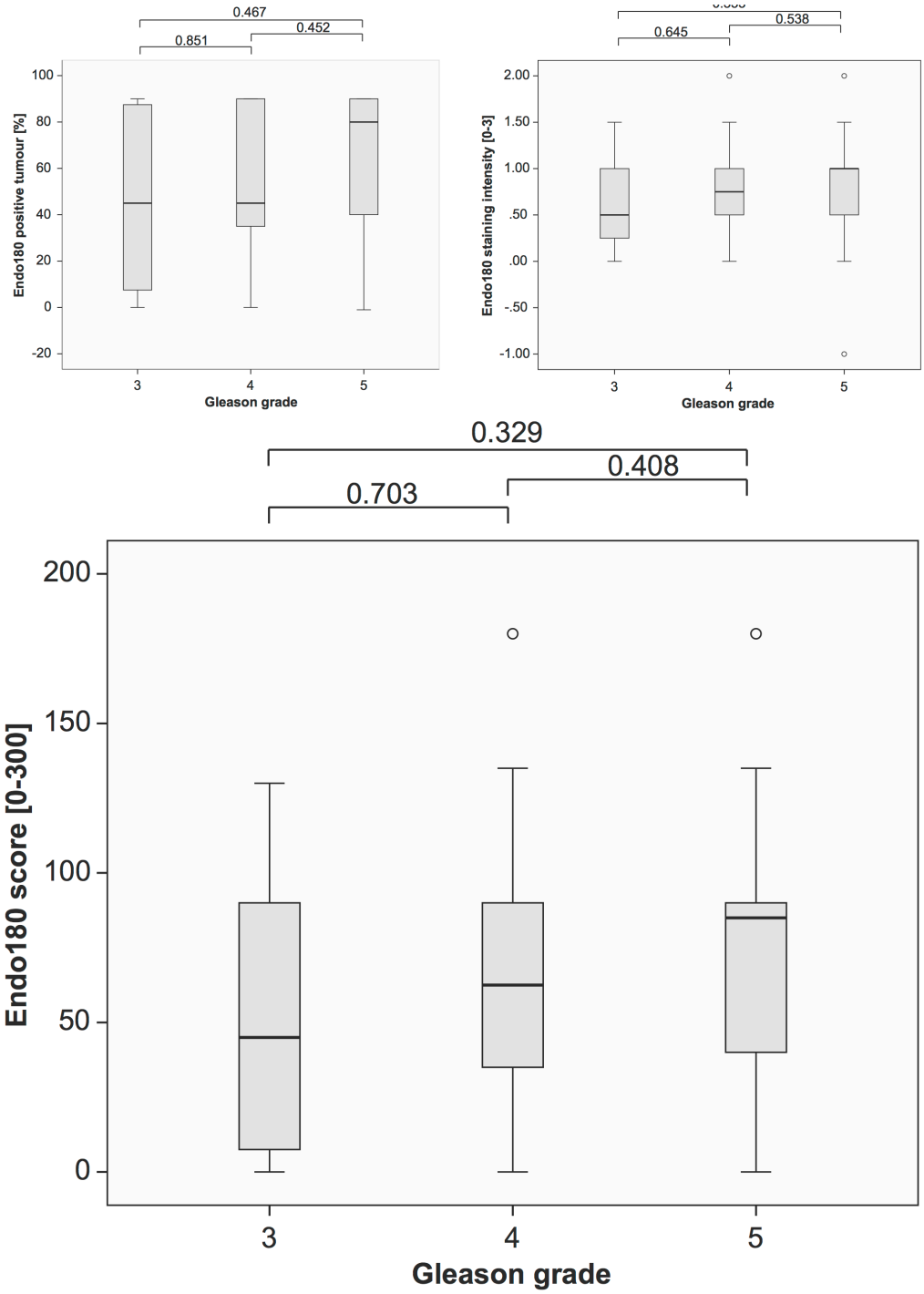



**Figure 5.2.7 NCLPC1 – Endo180 – core Gleason score.** Endo180 score was calculated by multiplying the positive tumour area with staining intensity (0-300). Samples were categorised by the Gleason grade of individual core biopsies. Two biopsies were analysed and the average (mean) value was used for the analysis. Box plots show the total range (vertical lines), mean (horizontal line) and upper and lower quartiles (grey area). P-values were calculated using the Mann-Whitney-Wilcoxon test.

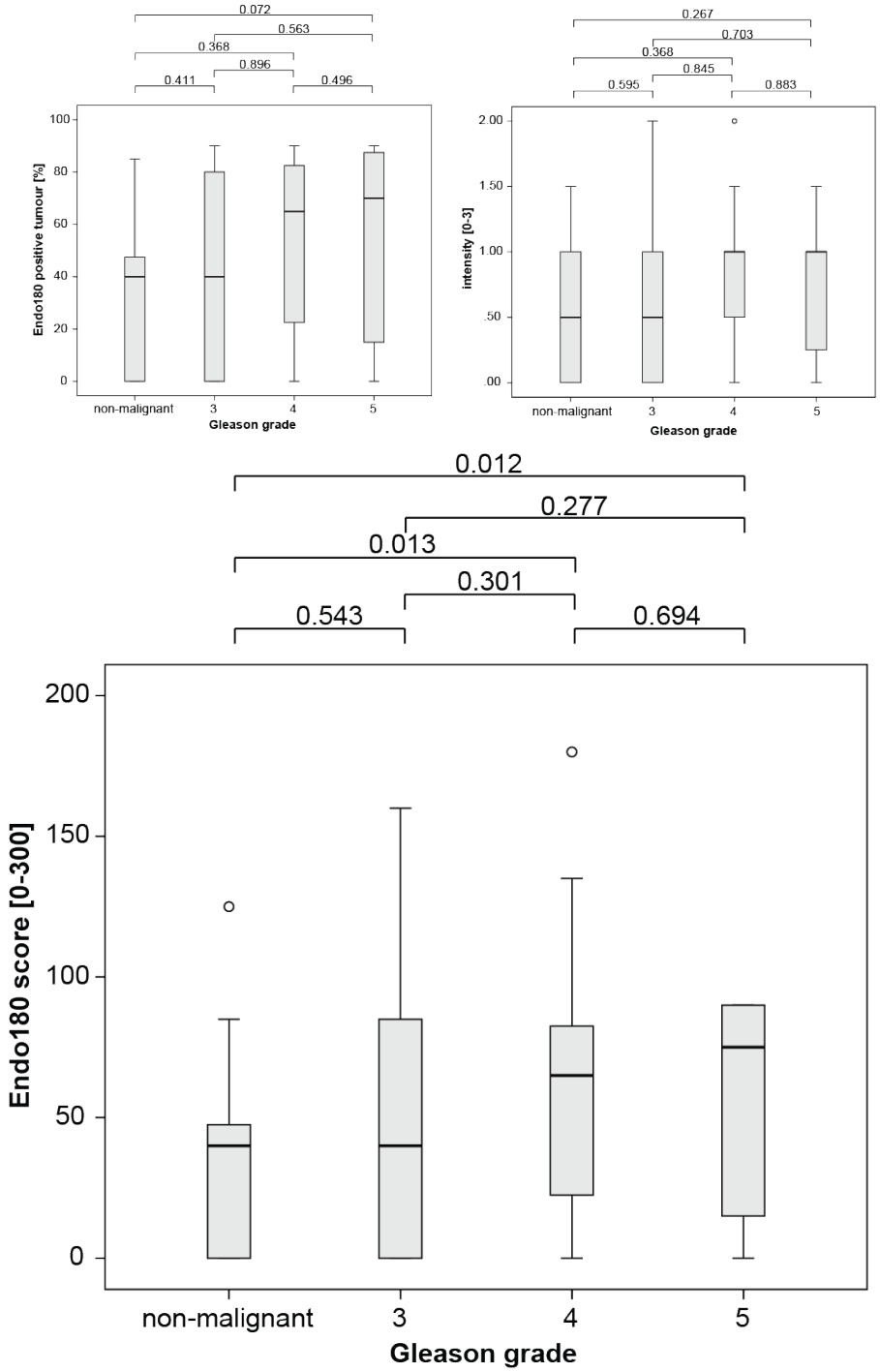



**Figure 5.2.8. NCLPC4 – Endo180 – core Gleason score.** Endo180 score was calculated by multiplying the positive tumour area with staining intensity (0-300). Samples are categorised as non-malignant or by the Gleason grade of individual core biopsies. Two biopsies were analysed and the average (mean) value was used for the analysis. Box plots show the total range (vertical lines), mean (horizontal line) and upper and lower quartiles (grey area). P-values were calculated using the Mann-Whitney-Wilcoxon test.

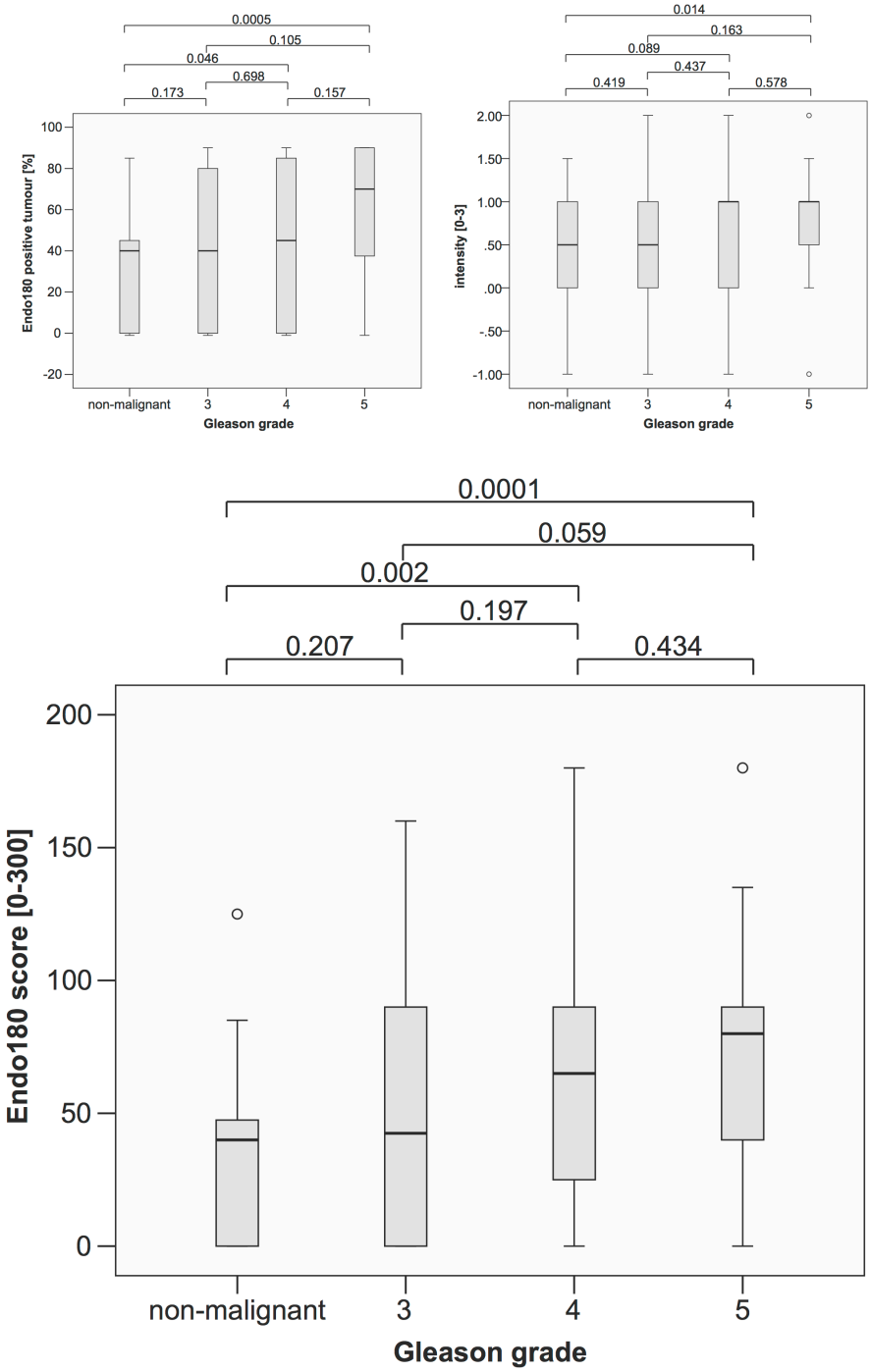



**Figure 5.2.9 TMA NCLPC1 and NCLPC4 pooled – core Gleason score.** Endo180 score was calculated by multiplying the positive area with the intensity (0-300). Samples are categorised as non-malignant or by the Gleason grade of the individual biopsy. Two biopsies were analysed and the average (mean) value was used in the analysis. Box plots show the total range (vertical lines), mean (horizontal line) and upper and lower quartiles (grey area). P-values were calculated using the Mann-Whitney-Wilcoxon test.

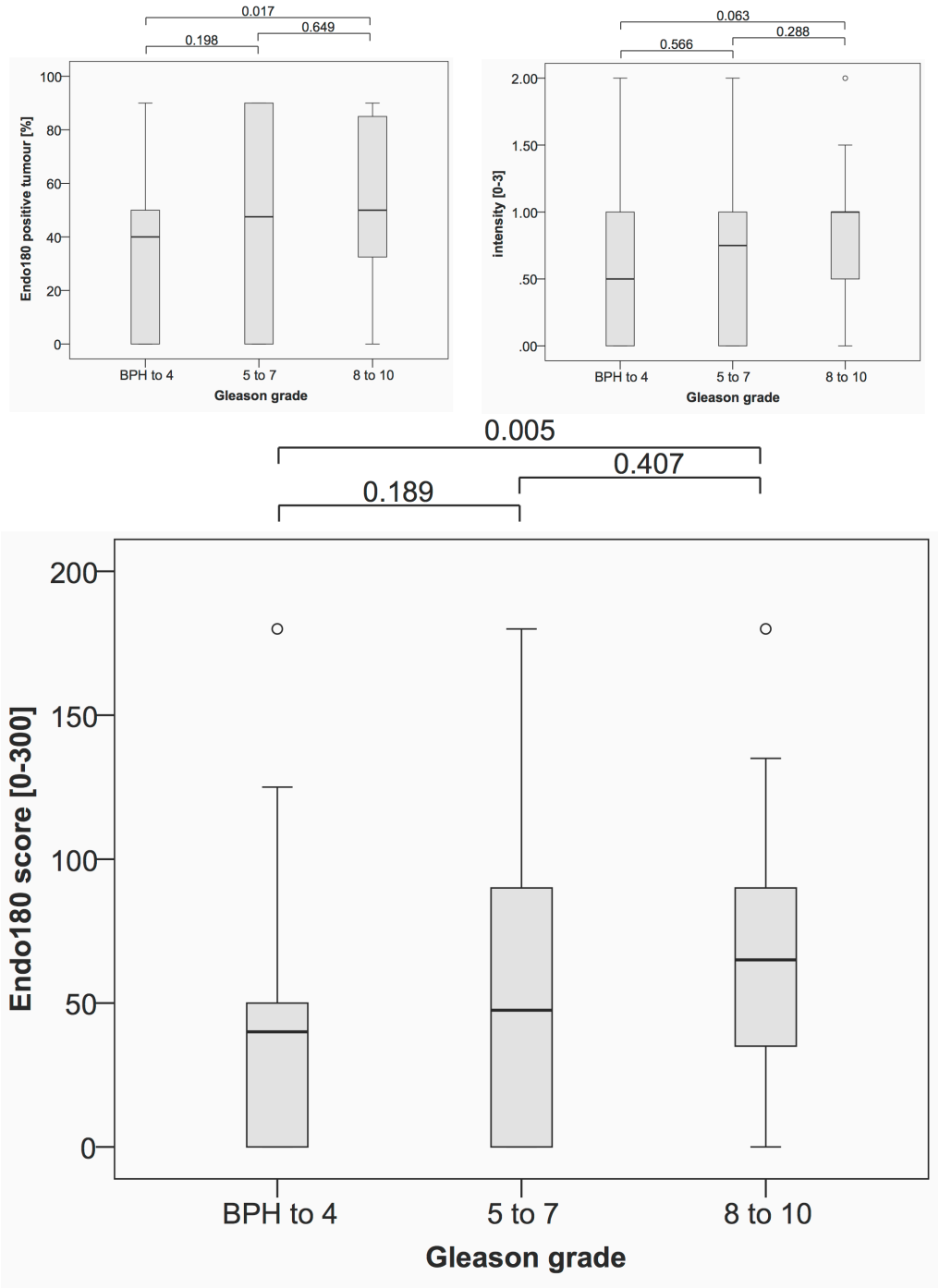
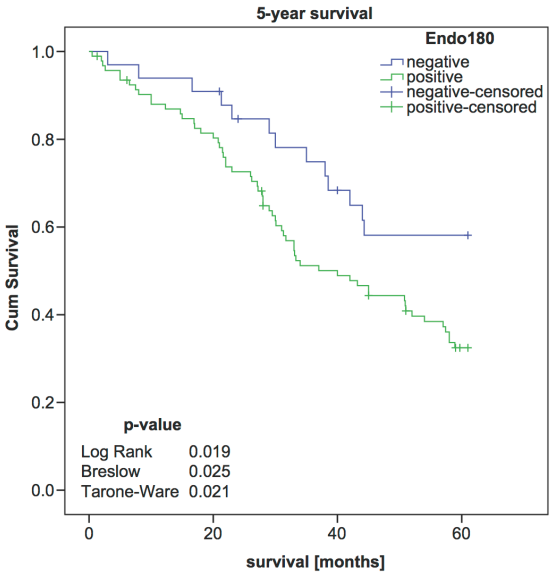
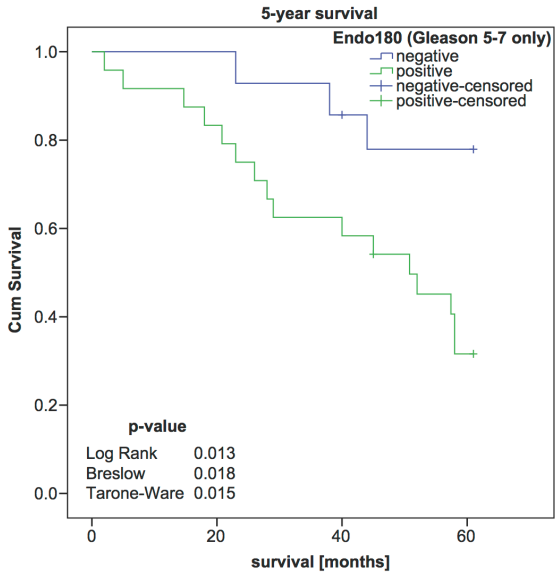


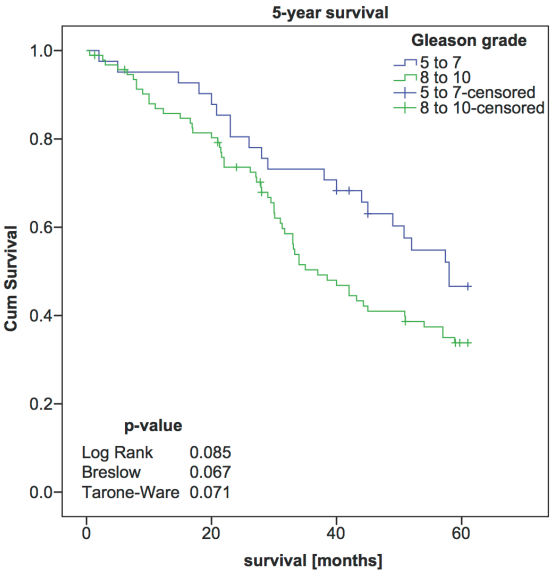

**Figure 5.2.10. NCLPC1 and NCLPC4 – patient Gleason score.** Endo180 score was calculated by multiplying the positive area with the intensity (0-300). Samples are categorised as benign hyperplasia (BPH) or by the Gleason grade of the individual biopsy. Two biopsies were analysed per patient and the average (mean) value per patient was used in the analysis. Box plots show the total range (vertical lines), mean (horizontal line) and upper and lower quartiles (grey area). P-values were calculated using the Mann-Whitney-Wilcoxon test.

| Patient characteristics | N | [%] |
|---|---|---|
| Total | 157 | |
| Age range | 55-89 | |
| Median age | 72 | |
| (known for 81 (52%) patients) | | |
| Years of study | 1988-1997 | |
| Gleason grade (core) | | |
| 3 | 38 | 24 |
| 4 | 65 | 42 |
| 5 | 52 | 34 |
| Gleason grade (patient) | | |
| 6 | 19 | 13 |
| 7 | 22 | 15 |
| 8 | 51 | 35 |
| 9 | 34 | 23 |
| 10 | 20 | 14 |
| Endo180 status | | |
| Negative (score ≤30) | 38 | 27 |
| Positive (score >30) | 104 | 73 |
| Metastasis at TURP | | |
| No | 61 | 45 |
| Yes | 40 | 30 |
| Subsequent | 34 | 25 |

**Figure 5.2.11 NCLPC1 and NCLPC4 pooled – patient characteristics.** Table shows patient characteristics of the pooled arrays: age range; median age; years of study; Gleason grade (per core and per patient); negative/positive Endo180 status (cut-off Endo180 score = 30); and metastatic status at TURP or subsequent metastasis. The number (N) and percentage of total patients (%) are shown.




| Groups | N [total] | N [dead after 3 years] | N [dead after 5 years] | N [dead after 7 years] | N [dead after 10 years] |
|---|---|---|---|---|---|
| Gleason grade 5-7 | 41 | 11 (27%) | 21 (51%) | 27 (66%) | 32 (78%) |
| Gleason grade 8-10 | 93 | 44 (47%) | 58 (62%) | 65 (70%) | 70 (75%) |
| Log Rank | | 0.028 | 0.085 | 0.188 | 0.443 |
| Breslow | | 0.047 | 0.067 | 0.091 | 0.121 |
| Tarone-Ware | | 0.036 | 0.071 | 0.118 | 0.202 |
| Endo180 negative | 33 | 8 (24%) | 13 (39%) | 18 (55%) | 23 (70%) |
| Endo180 positive | 93 | 44 (47%) | 60 (65%) | 69 (74%) | 74 (80%) |
| Log Rank | | 0.026 | 0.019 | 0.030 | 0.098 |
| Breslow | | 0.030 | 0.025 | 0.027 | 0.036 |
| Tarone-Ware | | 0.027 | 0.021 | 0.026 | 0.048 |
| Gleason grade 5-7 | | | | | |
| Endo180 negative | 14 | 1 (7%) | 3 (21%) | 6 (43%) | 9 (64%) |
| Endo180 positive | 24 | 9 (38%) | 16 (67%) | 19 (79%) | 21 (88%) |
| Log Rank | | 0.045 | 0.013 | 0.021 | 0.047 |
| Breslow | | 0.046 | 0.018 | 0.020 | 0.023 |
| Tarone-Ware | | 0.046 | 0.015 | 0.019 | 0.027 |

**Figure 5.2.12 NCLPC1 and NCLPC4 pooled – patient survival.** Kaplan Meier analysis of Endo180 negative versus positive patients, Endo180 negative versus positive patients in low Gleason patients and low versus high Gleason score. All graphs show five-year survival curves with Log Rank, Breslow and Tarone-Ware statistical analysis. Table shows statistical analysis of data for 3, 5, 7 and 10 year survival. $P > 0.05$ is considered significant.

Analysis of NCLPC1 indicated that the median percentage area of Endo180 positive tumour was increased by approximately 2-fold when cores classified as Gleason 3 or Gleason 4 were compared to cores classified as Gleason 5; however, this increase was not statistically significant: Gleason 3 versus Gleason 5 ($p = 0.467$); and Gleason 4 versus Gleason 5 ($p = 0.452$) (**Figure 5.2.7**). The median intensity of cores classified as Gleason 3 (0.5), Gleason 4 (0.75) and Gleason 5 (1.0) were not significantly different (**Figure 5.2.7**). The Endo180 scores were not significantly different between cores classified as Gleason 3, 4 and 5 (**Figure 5.2.7**).

NCLPC4 contained cores classified as non-malignant (tumour adjacent) tissue. There was a marginal difference between the median percentage areas of Endo180 positive staining in this non-malignant tissue (~40%) compared to cores classified as Gleason 5 (~70%) ($p = 0.072$) (**Figure 5.2.8**). Likewise, the median intensity of cores classified as non-malignant (0.5), Gleason 3 (0.5), Gleason 4 (1.0) and Gleason 5 (1.0) were not significantly different (**Figure 5.2.8**). Endo180 scores were significantly different between cores classified as non-malignant and Gleason 4 ($p = 0.013$) and Gleason 5 ($p = 0.012$) (**Figure 5.2.8**).

Due to the lack of non-malignant tissue on NCLPC1 the data from this TMA was pooled with the data from NCLPC4 as carried out in a recent study (Brooke et al., 2011) (**Figure 5.2.9**). NCLPC1 and NCLPC4 data pooling resulted in significant differences for all measured parameters (**Figure 5.2.10**). The percentage of positive tumour area alone was significantly different between cores classified as non-malignant and Gleason 4 ($p = 0.046$) or core Gleason 5 ($p = 0.0005$) (**Figure 5.2.10**). Endo180 staining intensity was significantly different between cores classified as non-malignant and Gleason 5 ($p = 0.014$) (**Figure 5.2.10**). Endo180 scores were significantly different between cores scored as non-malignant and Gleason 4 ($p = 0.002$) and core Gleason 5 ($p = 0.0001$) (**Figure 5.2.10**). These results suggest that Endo180 expression has diagnostic potential at the tissue level as reported by our group (Kogianni et al., 2009).

To determine whether Endo180 expression has diagnostic predictive value at the patient level the correlation between clinically used categories of Gleason score and

Endo180 staining intensity, area and score were tested using the NCPCL1 and NCLPC4 pooled dataset (**Figure 5.2.11**). Patients were classified to have BPH (non-malignant, tumour adjacent tissue) or Gleason score 1-4 (low-risk disease); Gleason score 5-7 (intermediate-risk disease); or Gleason score 8-10 (high-risk disease). The percentage of Endo180 positive tumour area was significantly different between patients classified as low-risk and high-risk disease ($p = 0.017$); differences in Endo180 intensity remained marginal ($p = 0.063$) (**Figure 5.2.11**). The significant difference between the Endo180 score between low-risk and high-risk disease was highly significant ($p = 0.005$) (**Figure 5.2.11**).

To assess the prognostic value of Endo180 Kaplan Meier analysis was conducted. A cut-off value (Endo180 score = 30) was applied to distinguish between Endo180 negative and Endo180 positive patients. This resulted in 38 (27%) patients being diagnosed as Endo180 negative and 104 (73%) patients being diagnosed as Endo180 positive (**Figure 5.2.9**). Kaplan-Meier analysis revealed that Endo180 positive patients were predicted to have shorter disease free survival. The difference in 5-year survival was found to be statistically significant using three highly stringent statistical tests (Log Rank: $p = 0.019$; Breslow: $p = 0.025$; and Tarone-Ware: $p = 0.021$) (**Figure 5.2.12**). Gleason grade alone was less powerful with the difference between intermediate-risk (Gleason grade 3-7) and high-risk (Gleason grade 8-10) disease displaying marginal differences with all three statistical tests (Log Rank: $p = 0.085$, Breslow: $p = 0.067$; Tarone-Ware: $p = 0.071$) (**Figure 5.2.12**). To test whether Endo180 can help to predict patient survival and provide a potential indication for adjuvant chemotherapy in low or intermediate risk disease patients were grouped according to their Endo180 status. Endo180 positive patients ($n = 24$) displayed statistically significant lower survival expectations than Endo180 negative patients ($n = 14$) in this low to intermediate risk patient group (Log Rank: $p = 0.013$; Breslow: $p = 0.018$; Tarone-Ware: $p = 0.015$) (**Figure 5.2.12**).

### 5.2.3 Discussion

Similar to the report by Kogianni et al, (2009) the expression of Endo180 was correlated to Gleason grade indicating its potential power as a diagnostic biomarker. The results reported in this thesis used statistical tests that allowed accurate analysis of datasets with skewed distributions and outliers and further reports that Endo180 expression is significantly correlated with patient survival. This is the first time that Endo180 has been validated to have prognostic value in a common human disease. In an earlier study prognostic value was determined in a rare subset of metaplastic basal breast cancer, which represents approximately 1.5 % of all breast cancers (Wienke et al., 2007). Other cancer studies have only reported that Endo180 expression is associated with tumour cells (Schnack Nielsen et al., 2002),or tumour grade (Huijbers et al., 2010; Kogianni et al., 2009; Sulek et al., 2007) but not clinicopathological outcome (see **Section 1.4.10.5**).

In prostate cancer patients with tumours that are negative for Endo180 there is significantly higher probability that they will survive longer after TURP than patients with Endo180 positive tumours. Even patients with tumours classified as low risk by the Gleason scoring system were found to have a significantly shorter survival if they had an Endo180 positive tumour. The significant differences in patient survival were independent of the statistical test used; all tests were balanced and favoured either early or late events.

The decrease in significance over time following TURP may be explained by the high median age of the affected population. The median age at TURP was 72 years for NCLPC4 and unknown for NCLPC1. However, taken into consideration, that both patient samples were collected in the 1980s before PSA screening for prostate cancer was introduced (circa 1992) there is no reason to assume that the demographic of NCLPC1 is significantly younger than the one of NCLPC4. At a median age of 72 years it would be expected that most patients will die within the next 10 years.

Although the results obtained with NCLPC1 and NCLPC4 appear promising there are several potential problems that may need to be considered. Firstly, the staining intensity for Endo180 in prostate tissue was weak in four out of six TMAs. Attempts to counteract this problem by increasing the 39:10 mAb concentration led to stromal staining similar in appearance to collagen staining. Interestingly, A5:158 mAb concentration could be increased up to 50 µg/ml to increase the signal on the FDA multi-tissue array without generating a similar background (in normal prostate tissue or any other tissue). Therefore, Endo180 staining by A5:158 mAb appears to be specific even at 50 µg/ml. A5:158 mAb staining was not tested on the commercial array and was only tested at a lower concentration (10 µg/ml) on the five Newcastle TMAs. Higher sensitivity with adequate specificity may be achievable by using the A5:158 antibody at a concentration of 50 µg/ml.

It is unlikely, that the inconsistent staining problems result out of the antigen-retrieval and staining process. The Newcastle arrays were stained in parallel with the two Endo180 antibodies using the same protocol. Likewise the commercial arrays were stained in parallel with at least one of the FDA approved multi-tissue arrays. The highest Endo180 scores were obtained for cores from high Gleason grade tumours on NCLPC1 and NCLPC4. It is of note that advanced cases of disease were not included in any of the other Newcastle arrays. Therefore, the lower overall Endo180 staining on NCLPC3 and NCLPC6 in comparison to NCLPC1 and NCLPC4 is expected.

However, to explain the low staining simply by an absence of high Gleason grade tumours is problematic for two reasons:

- low Gleason grade tumours were scored for Endo180 expression in NCLPC1 and NCLPC4 and equal grade tumours were present on NCLPC3 and NCLPC6 where the expression of Endo180 was barely detectable
- like NCLPC1 and NCLPC4 the commercial array contained a high number of high Gleason grade cores (8-10)

With respect to this last point the pattern of Gleason grading, categories used and the fact that the TMA is based in the USA altogether indicates that the cores were collected in the USA where tumours tend to be graded higher compared to the UK. This is apparent from the fact that the very common Gleason grades 3+4 and 4+3 were missing or underrepresented on this TMA.

An explanation for the discrepancy between TMA is the method of biopsy fixation and storage. It is clear from the results reported in this Section that antigen retrieval methods can improve the consistency of staining. It is clear that prior to its use as a as a marker for disease staging the source for these staining problems needs to be resolved and the protocol further optimised.

The function of Endo180 in prostate cancer has yet to be established. In breast, Endo180 expression in the tumour-associated stroma is linked to the suppression of tumour fibrosis. However, stromal Endo180 staining appears to be relatively weak in the prostate gland, with highest staining levels being on the epithelial tumour cells.

Endo180 overexpression in MCF-7 breast cancer cells resulted in their increased growth and a lower collagen content when these cells were used in mouse xenografts. MCF-7 cells that overexpress Endo180 were also endowed with the ability to detect a chemotactic gradient of uPA (Sturge et al., 2003). Interestingly, an internalisation defective mutant of Endo180 led to increased collagen content in the tumour stroma of xenografts (Wienke et al., 2007). The internalisation defective Endo180 mutant displays two significant differences in its function when compared to wild-type Endo180, including: (a) the inability to internalise collagen (Wienke et al., 2007); and (b) the inability to activate Rho-ROCK-MLC2 based cell contractility and random cell migration (Sturge et al., 2003; Sturge et al., 2006). Therefore, the role of Endo180 in prostate cancer cells and its impact on prostate cancer progression could equally be the result of its function in the promotion of collagen turnover or the increased random or chemotactic migration of tumour cells during metastatic dissemination.

## 5.3 A cell line model for prostate cancer progression

### 5.3.1 Introduction

A cell line based model of prostate cancer disease progression was designed in an attempt to best fit the EMT hypothesis (Yang and Weinberg 2008). The model included cells derived from: normal and/or BPH (RWPE1,, BPH1, RC170N and RC165N); low (RC92a) and intermediate (RC58T) grade primary prostate cancer; and three commonly used prostate cell lines derived from metastatic lesions in the lymph nodes (LNCaP), bone (PC3) and brain (DU145) (**Table 5.3.1**). Where appropriate, two widely used breast cancer cell lines with epithelioid (MCF7) and mesenchymal-like (MDA-MB-231) characteristics were employed as controls. Additional controls included cells of mesenchymal origin: the osteoblastic cell line, MG63, primary human osteoblasts (OBs) derived from femoral bone and HCA2, hTert immortalised human dermal fibroblasts.

| | Gleason score | Clinical stage | Pathological state | Assigned clinical risk status | Immortalisation method |
|---|---|---|---|---|---|
| RWPE-1 | n/a | normal/ benign | n/a | negligible | HPV-18 |
| RC170N | n/a | benign | n/a | negligible | hTert |
| RC165N | n/a | benign | n/a | negligible | hTert |
| RC92a | 3+3 | B0 | T2C | low | hTert |
| RC58T | 3+4 | B1 | T2C | intermediate | hTert |
| LNCaP | unknown | D | N1 M0 | high | n/a |
| PC3 | unknown | D | M1b | high | n/a |
| DU145 | unknown | D | M1c | high | n/a |

**Table 5.3.1 Prostate cell line characteristics.** Clinical stage = Whitmore-Jewett staging: B = tumour can be felt, D = tumour has spread to distant organs; Pathological state = TNM staging: T2C = primary tumour, N1 M0 = tumour only spread to lymph nodes, M1 = tumour spread to distant organs; n/a = not applicable

### 5.3.2 Androgen-receptor expression during prostate cancer EMT

The initial responsiveness to anti-androgen therapy is frequently followed by subsequent progression to androgen-independent growth and eventual disease relapse. The development of this androgen-independence is one of the most studied phenomena in prostate cancer pathology and the LNCaP cell line provides the most widely used model due to their androgen-dependent growth and overexpression of androgen-receptor (AR). The two other most commonly used prostate cancer cell lines, PC3 and DU145, are widely reported to be AR-negative and display androgen-independent growth so are not used as models to study androgen signalling in the progression of prostate cancer. For this reason some researchers have suggested that PC3 and DU145 cells do not have a prostate-like cell phenotype. However, recent evidence has revealed that relatively low expression of AR exists in PC3 and DU145 cells, which can facilitate their androgen-responsiveness and optimal cell growth (Martinez et al., 2008).

For this reason we have investigated how the expression levels of AR are aligned within the proposed cell line-based EMT model of prostate cancer progression. To do this AR expression was measured by immunoblotting whole cell lysates from the panel of prostate cells, together with MCF-7, MDA-MB-231, MG-63 cells, HCA2 cells and primary OBs as controls (**Figure 5.3.2**).

In contradiction to published findings (Martinez et al., 2008) PC3 and DU145-cells displayed no detectable levels of AR expression compared to LNCaP cells (**Figure 5.3.2**). The BPH and primary prostate cancer cells as well as MDA-MB-231 cells and osteoblastic cells display a very low but detectable level of expression. It is apparent that LNCaP cells display least fit within the panel of cell lines tested here since their expression of AR is several fold higher than in the other cell types tested.

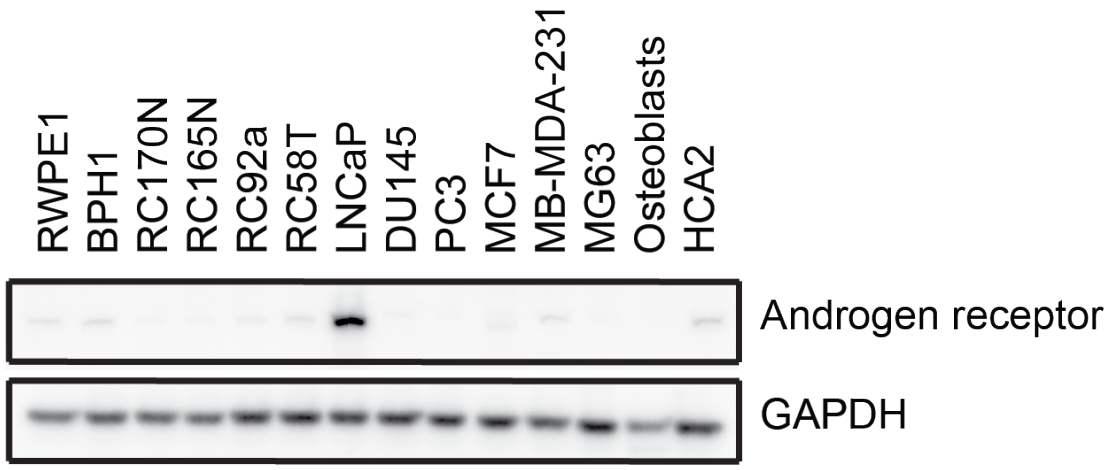



**Figure 5.3.2 Expression of androgen receptor (AR) during prostate cancer EMT.** RC165N, RC92a, RC58T, LNCaP, PC3, DU145, MCF7, MB-MDA-231, MG63 cells and primary human OBs were seeded on tissue culture plastic and grown under their normal growth conditions for four days. Whole cell lysates were prepared and subjected to SDS-PAGE using a 4-20% acrylamide gradient gel under reducing conditions. The upper panel shows AR protein migrating as a 99 kDa band detected by incubation with Dako mouse anti-human mAb followed by anti-mouse HRP-conjugated IgG. The bottom panel shows the loading control GAPDH migrating as an 36 kDa band detected by immunoblotting with rabbit anti-human pAb followed by anti-rabbit HRP-conjugated IgG. For all blots visualisation of immunoreactive bands was carried out using chemiluminesence. Chemiluminescent signal was recorded using a GE Lifesciences ImageQuant LAS 4000. Molecular weight markers (kDa) and proteins of interest are indicated for each blot: (n=2 for all lines except BPH1, RC170N and HCA2 cells; n =1).

### 5.3.3 Changes in cell morphology during prostate cancer EMT

As reviewed recently cells change their morphology during EMT (Thiery et al., 2009; Thiery and Sleeman, 2006). Typically, the epithelial cell monolayer loses its basal-apical-polarity and displays a triangular shape with front-back polarity in the horizontal plane, which is indicative of an increased migratory phenotype. To investigate the morphology of cells used in the proposed EMT-model of prostate cancer progression all cells were grown to similar densities, fixed and immunostained for α-tubulin and F-actin. MDA-MB-231 and MG63 cells were used as positive controls for cells with typical mesenchymal characteristics. The results of this morphological characterisation are shown in **Figure 5.3.3.**

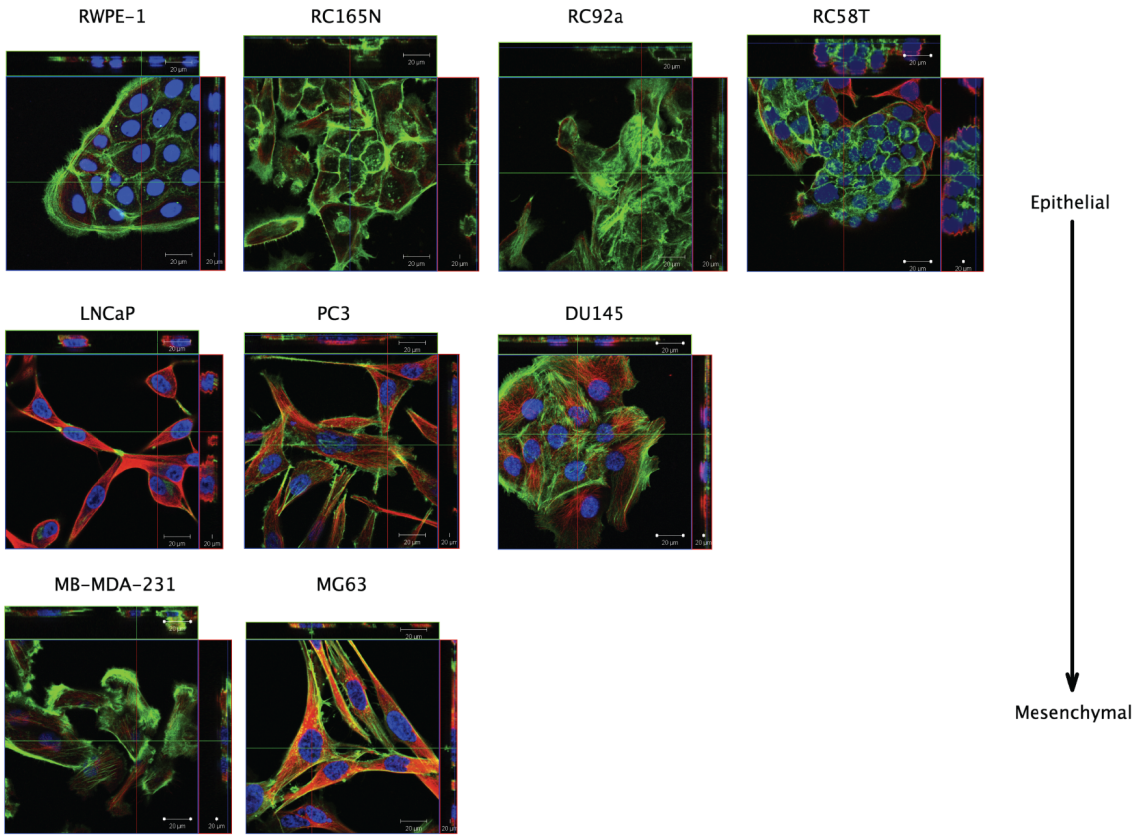



**Figure 5.3.3 Alterations in α-tubulin network and actin-cytoskeleton during prostate cancer EMT:** RC165N, RC92a, RC58T, LNCaP, PC3, DU145, MB-MDA-231 and MG63 cells were seeded on to sterile acid treated glass coverslips and grown under their normal growth conditions for four days. The cells were fixed in 4% w/v PFA diluted in PBS for 10 minutes at 37°C. Fixed cells were subsequently permeabilised in 0.3 % v/v Triton-X-100 and α-tubulin protein was fluorescently labelled with DM1A mouse anti-human mAb. Actin was fluorescently labelled with AlexaFluor-conjugated phalloidin. The images were acquired by confocal microscopy. For all cell lines a z-section with 2 µm depth is shown. Scale bar = 10 µm. Prostate cancer cell lines are arranged in order of the advance of disease. MB-MDA-231 and MG63 cells are shown as mesenchymal-like and true mesenchymal controls (n = 1).

As can be seen in **Figure 5.3.3** RWPE-1 cells were the most representative of a normal epithelium, having a well-defined monolayer with cells of equal size and/or spread. The BPH cell line, RC165N, also formed an epithelial monolayer but these were slightly more heterogeneous with regards to their individual cell shape, size and/or spread. Strong cortical F-actin rings were most apparent at the outer edge of RWPE-1 compared to RC165N colonies, however F-actin was seen to equally localise to the well organised cell-cell junctions in the monolayers of both cell types.

In comparison to normal/BPH cell lines, the primary-tumour derived cell lines, RC92a and RC58T, form much tighter monolayers and display a higher degree of heterogeneity with respect to their individual cell shape and size and/or spread (**Figure 5.3.3**). In both cell lines there was less F-actin localised to the cortical areas and cell-cell junctions, instead it was localised to stress fibre-like structures in the central regions of the cell. Additionally, there was a considerable amount of colony-growth into the third dimension. This was determined by the construction of z-stacks from serial z-sections of cell monolayers obtained by confocal microscopy (**Figure 5.3.3**). This phenomenon resembles the 'multi-layering' that can be observed in epithelial tissue during cancer progression was most pronounced in the intermediate clinical risk cell line, RC58T. It was also noted that the RC58T cells located at the colony-borders show a loss in their basal-apical polarity compared to cells located within the central region of the colony. Instead these peripheral cells displayed a clear front-back polarity in the horizontal plane, an increase in alpha-tubulin-rich microtubules and a decrease in F-actin.

Confocal images in **Figure 5.3.3** generated from z-stacks confirm that the metastatic cell lines do not display basal-apical-polarity and have an extensive network of alpha-tubulin-rich microtubules.

In comparison to the other prostate cell-types LNCaP cells have an atypical actin and microtubule cytoskeleton. In this cell type F-actin is localised solely at the tips of short protrusive structures. Typically 1-2 of these structures were localised at either end of the elongated cell body.

PC3-cells share a similar morphology with MB-MDA-231 and MG63 cells, having a triangular shape with F-actin-rich lamellipodial protrusions and stress-fibres that are a good indication that these cells display firm cell-substratum adhesions and a more contractile, migratory phenotype.

Although DU145-cells grow in colonies that in part resemble epithelial monolayers their actin cytoskeleton clearly displays distinct mesenchymal characteristics, such as, the formation of F-actin-rich stress-fibres that are also clearly observed in mesenchymal-like MDA-MB-231 and MG63 cells and indicate the formation of basal cell-substratum adhesions. Accordingly DU145 monolayers were very flattened indicating that this cell type is more spread and adherent than the normal/BPH and primary prostate cell monolayers.

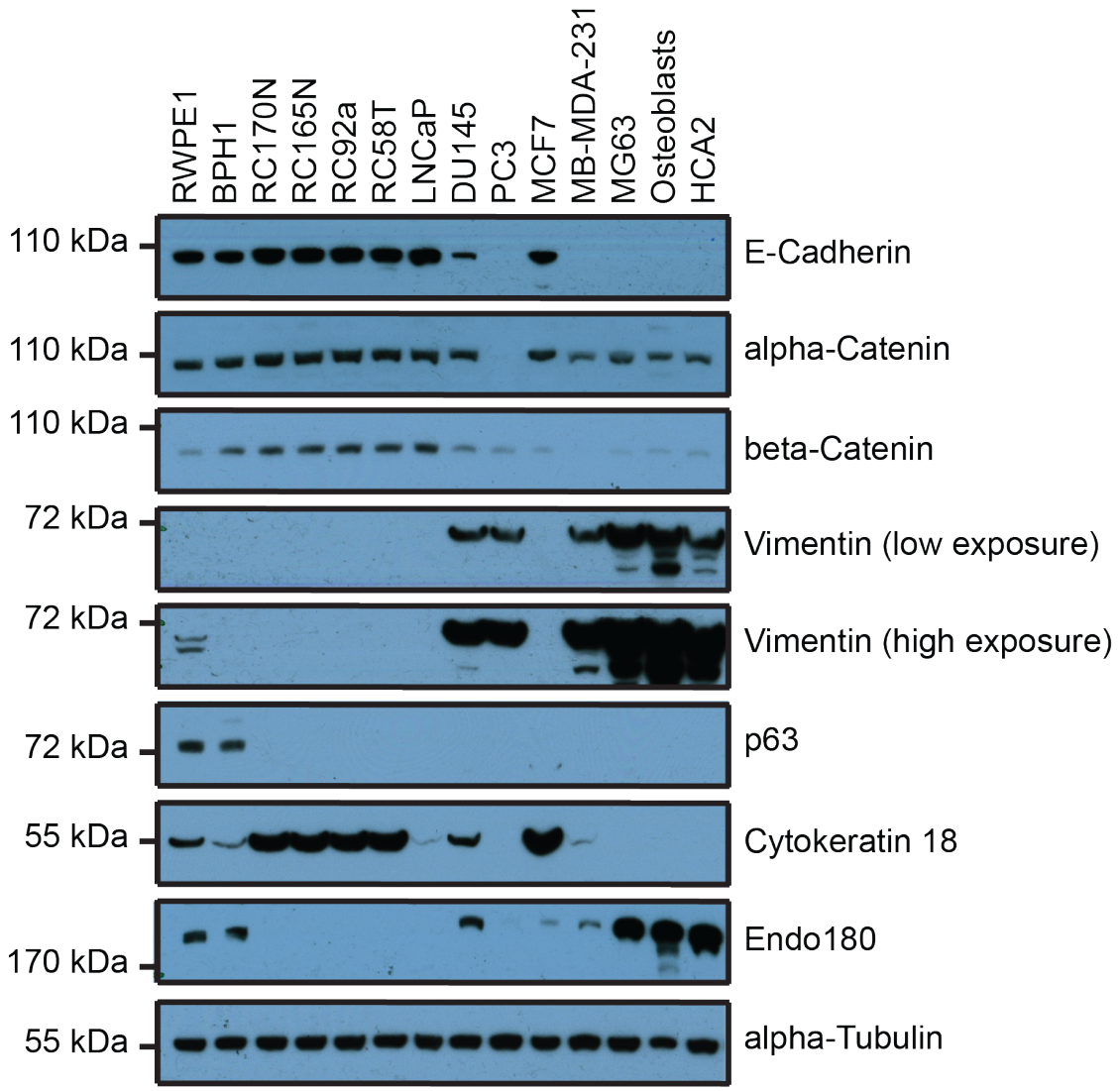



**Figure 5.3.4 Expression of EMT-markers during prostate cancer EMT.** RWPE-1, BPH1, RC170N, RC165N, RC92a, RC58T, LNCaP, PC3, DU145, MCF-7, MB-MDA-231, MG63, HCA2 cells and primary human osteoblasts were seeded on tissue culture plastic and grown under their normal growth conditions for four days. Whole cell lysates were prepared and subjected to SDS-PAGE using a 4-20% acrylamide gradient gel. The panels show immunoblots obtained using the primary antibody concentrations listed in **Table 2.1** followed by the appropriate HRP-conjugated secondary antibody: E-Cadherin (MW = 97 kDa); α/β-catenin (MW = 100/85 kDa); vimentin (MW = 54 kDa); p63 (MW = 77 kDa); Ck18 (MW = 48 kDa); Endo180 (MW = 180 kDa) and α-Tubulin (MW = 55 kDa). For all blots visualisation of immunoreactive bands was carried out using chemiluminesence. Molecular weight (MW) markers (kDa) and proteins of interest are indicated for each blot: ($n \geq 3$ for all markers with the exception of p63 and Ck18; BPH1, RC170N and HCA2 cells; n n= 2).

### 5.3.4 Expression profile of epithelial- and mesenchymal-associated cytoskeletal markers during prostate cancer EMT

The expression of the epithelial intermediate filament, cytokeratin (Ck), is normally downregulated during EMT, whereas the mesenchymal intermediate filament, vimentin, is normally upregulated (Kokkinos et al., 2007; van Dorst et al., 1998). To assess this status in the proposed EMT-model of prostate cancer progression quantifiation of vimentin in the panel of prostate and control cells was carried out using immunoblotting (**Figure 5.3.4**). A major feature of EMT is the loss of cell-cell adherens junctions, which are formed via homotypic interaction between cell surface E-cadherin molecules located on adjacent cells (Thiery et al., 2009; Thiery and Sleeman, 2006). E-cadherin junctions are stabilised by α–catenin, which regulates actin-filament assembly through the formation of a complex with E-cadherin and β-catenin (Drees et al., 2005).

Immunoblot analysis of RWPE-1, BPH-1, RC170N, RC165N, RC92a, RC58T and LNCaP cell lines revealed low to negligible levels of vimentin but high levels of E-cadherin, α-catenin and β-catenin (**Figure 5.3.4**). LNCaP cells were akin to the BPH and primary tumour cell lines in their adhesion molecule expression profile: they expressed no detectable level of vimentin and high levels of E-cadherin α-catenin and β-catenin (**Figure 5.3.4**). The striking similarity between LNCaP-cells and the BPH/primary tumour cell lines with respect to their expression of cell-cell and cell-matrix adhesion markers indicates that an EMT-like phenotype (apparent EMT) was not adopted by this cell-type during prostate cancer progression.

Primary human OBs expressed both α-catenin and low levels of β-catenin, but not E-cadherin. Similar levels of β-catenin and absence of E-cadherin was also found to be the case for PC3 cells (**Figure 5.3.4**), which indicates they have a mesenchymal-like adhesion phenotype. It was observed that DU145 cells have E-cadherin negative and positive populations (**data not shown**); this observation may explain the low total protein expression levels determined by immunoblot analysis (**Figure 5.3.4**). This

reduced level of E-cadherin-expression in DU145 cells is in accordance with the current EMT-models proposed for cancer cell metastasis and could be indicative of the commonly observed phenomenon of group-cell-invasion and/or mesenchymal-to-epithelial (MET) transition at a secondary tumour site (Chaffer and Weinberg, 2011; Hanahan and Weinberg, 2011; Yang and Weinberg, 2008).

### 5.3.5 Endo180 expression during prostate cancer EMT

In **Section 5.2** it was demonstrated that expression of Endo180 strongly correlates with prostate cancer progression and serves as a potential marker of clincopathological outcome and may be a potential therapeutic target. In an earlier study, increases in Endo180 expression were closely correlated with increases in its cooperative partner for chemotactic cell migration, uPA; and its cell surface receptor uPAR (Kogianni et al., 2009). To establish whether these pathological findings can be extrapolated to an *in vitro* model, the proposed cell line was used to evaluate the expression profile of Endo180, uPA and uPAR. To confirm whether Endo180-expression correlates with the adoption of an apparent EMT phenotype, Endo180 expression levels in the different cell lines were determined by immunoblotting with four antibodies targeting different epitopes in the receptor (**Figure 5.3.5**). MCF7 and MB-MDA-231 cells were included as controls since the Endo180-uPA-uPAR chemotactic cell migration axis has been well characterised in this pair of breast cancer cell lines (Sturge et al., 2003). The osteoblastic MG63 cell line and primary human osteoblasts were used as mesenchymal controls.

All prostate cell lines with the exception of LNCaP cells expressed Endo180. The absence of Endo180 expression in LNCaP cells is yet further evidence that this cell line does not have molecular or functional characteristics of mesenchymal cells. For the other cell lines, which express Endo180, levels were low for both hTert immortalised BPH lines (RC170N and RC165N). Similar expression levels were observed in the primary cancer cell lines: RC92a (low grade) and RC58T (intermediate grade); and the invasive metastatic PC3 cell line. Surprisingly, both

RWPE-1 (**Figure 5.3.5**) and BPH-1 (**Figure 5.3.4**) express comparatively high amounts of Endo180

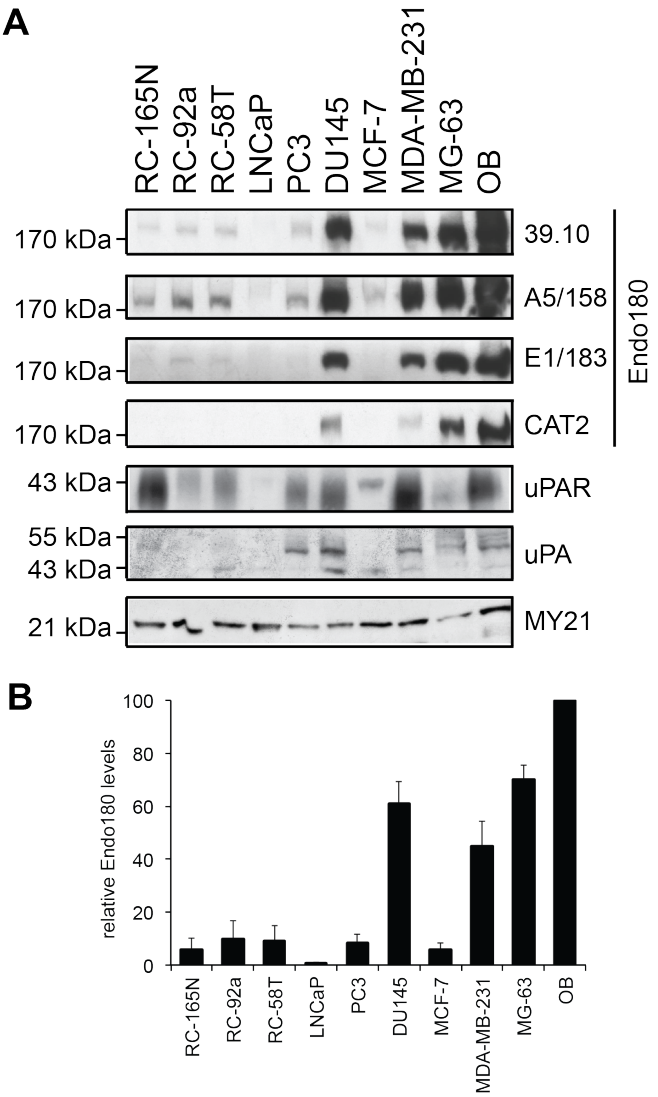



**Figure 5.3.5 Expression of Endo180 and its interaction partners uPA and uPAR during prostate cancer EMT.** RC165N, RC92a, RC58T, LNCaP, PC3, DU145, MCF7, MB-MDA-231, MG63 cells and primary human osteoblasts were seeded on tissue culture plastic and grown under their normal growth conditions for four days. Whole cell lysates were prepared and subjected to SDS-PAGE using a 4-20% acrylamide gradient gel under reducing (uPA, MLC, Endo180: CAT2) and non-reducing (uPAR, Endo180: A5:158, E1:183 and 39.10) conditions. The upper panels show Endo180 migrating as a 180 kDa protein band detected by immunoblotting with the four different Endo180 antibodies listed in **Table 2.2**: CAT2, 39.10, A5:158 and E1:183; followed by anti-rabbit (CAT1, CAT2) or anti-mouse (39.10, A5:158 and E1:183) HRP-conjugated IgG. The next panels show uPAR migrating as a 37 kDa protein band detected by immunoblotting with 399R pAb; and uPA migrating as a 52/54 kDa protein band detected by immunoblotting with ab24121 pAb (**Table 2.2**). The bottom panel shows the loading control MLC migrating as an 18 kDa band detected by immunoblotting with MY21 mAb followed by anti-mouse HRP-conjugated IgG. All immunoreactive bands were visualised by chemiluminesence. Molecular weight markers (kDa) and proteins of interest are indicated for each blot: ($n \geq 3$ for CAT2, A5:158 and 39:10; excluding osteoblasts (n = 1); and n=2 for uPA and uPAR)..

The high expression levels in DU145 cells were similar to those observed in the highly invasive MB-MDA-231 breast cancer cell line, which display Endo180-dependent random cell migration and chemotaxis in a uPA gradient (Sturge et al., 2003). Although Endo180 expression in mesenchymal fibroblasts and mesenchymal-like tumour cells with a singular cell phenotype is known to promote collagen uptake and cell migration the predominant function(s) of low endogenous Endo180 expression in epithelial cell monolayers and/or tumour cells with an epithelial phenotype has not been investigated.

An unexpected finding was the relatively low expression level of Endo180 in PC3 cells which expressed similar levels as the low and intermediate grade primary prostate cancer cell lines, RC92a and RC58T. This relatively low expression of Endo180 in PC3 cells does not directly fit with an *in vitro* model for the progressive upregulation of Endo180. However, another project in the laboratory has confirmed that there is a substantial upregulation of Endo180 in PC3 cells co-cultured with primary osteoblasts that coincides with dramatic changes in bone matrix formation and collagen remodelling (Caley et al., accepted for publication). The microenivironment of bone-matrix forming osteoblasts closely resembles the metastatic bone lesion from which PC3 cells were originally derived and therefore is representative of their normal *in vivo* phenotype.

### 5.3.6 uPAR and uPA expression during prostate cancer EMT

GPI-anchored uPAR requires Endo180 in order to promote chemotaxis towards uPA-gradients (Sturge et al., 2003), however it is not yet known whether Endo180 requires uPAR to promote chemotaxis towards uPA or whether Endo180 can act alone as a functional uPA receptor. To identify suitable *in vitro* model(s) to investigate whether this potential cooperativity during chemotactic migration exists during prostate cancer progression, uPA and uPAR expression was determined by immunoblot analysis of the prostate cell line panel (**Figure 5.3.5**). As previously, MCF7 and MB-MDA-231 cells were included as negative and positive controls for

the Endo180-uPA-uPAR chemotactic axis (Sturge et al., 2003); and the osteoblastic MG63 cell line and primary human osteoblasts were used as mesenchymal controls.

uPAR was expressed by all prostate cell lines with the exception of LNCaP cells. Surprisingly there was no clear correlation between cancer progression and uPAR-expression: the BPH cell line RC165N expressed the highest amount of uPAR, at levels, which were most comparable to MB-MDA-231-cells and primary osteoblasts. Low grade RC92a expressed low levels of uPAR similar to those observed in MG63 cells. The intermediate grade RC58T cells expressed similar levels to PC3 cells. In keeping with recent histopathological data (Kogianni, Walker et al. 2008), uPA-expression was not detected in cell lines derived from BPH and low-grade primary cancer cell lines: RC165N and RC92a; and LNCaP cells. A low level of low molecular weight uPA was detectable in the intermediate grade primary prostate cancer cell line RC58T as well as in DU145, MCF7, MDA-MB-231 and primary human osteoblasts. PC3 and DU145 cells were the only prostate cancer cell types to express a higher molecular weight form of uPA like the other mesenchymal-like and mesenchymal cell types: MDA-MB-231, MG63 and primary human osteoblasts. These results confirm that both PC3 and DU145 cells express all three components of the Endo180-uPA-uPAR chemotactic axis, making them suitable models for functional studies using the Dunn chemotaxis chamber that was used to identify this pathway in MDA-MB-231 cells (Sturge et al., 2003).

### 5.3.7 Differential modes of migration & invasion during prostate cancer EMT

The acquisition of a more mesenchymal phenotype during cancer progression is commonly associated with an increased migratory and invasive behaviour. Mesenchymal-like cell migration and invasion involves contraction of the actin cytoskeleton via direct engagement of phosphorylated myosin-light chain-2 (MLC2) (Ridley et al., 2004). To establish whether the model of prostate cancer EMT being characterised here had progressive migratory and invasive potential the phosphorylation of MLC2 was quantified in the different prostate cells by immunoblot analysis (**Figure 5.3.7**). Cells with low (MCF7) and high (MDA-MB-231)

migratory and invasive behaviour were used as reference controls (Sturge, Wienke et al. 2003). Functional assays for cell migration (**Figure 5.3.9**) and stromal invasion (**Figure 5.3.10**) were also carried out to directly compare the behaviour of the complete prostate cancer cell line model: BPH1, RWPE-1, RC170N, RC165N, RC92a, RC58T, LNCaP, PC3 and DU145.

Several EMT inducing growth factors were previously tested for their potential to induce Endo180 expression in MCF7 breast cancer cells (Wienke et al., 2007). The primary cell lines provided by Rhim et al, RWPE-1, RC170N, RC165N, RC92a, RC58T, were screened for their responsiveness to the same EMT inducing stimuli (**figure 5.3.6**). The percentage of RWPE-1 and RC92a that stained positive for Vimentin doubled upon stimulation with TGF-beta1 (**figure 5.3.6)**. Interestingly, under normal growth conditions both cell lines displayed a Vimentin positive side population. Under TGF-beta1 stimulation the percentage of Vimentin positive cells increased. Vimentin expression under normal growth conditions was confirmed for RWPE-1 cells by Western Blot analysis (**figure 5.3.4**). However, RC92a cells appeared Vimentin negative in Western Blot analysis under normal growth conditions. It was attempted to analyse Endo180 expression levels upon growth factor stimulation but screening microscopy was unable to detect Endo180 expression prior or post stimulation in these five cell lines. However, endogenous Endo180 expression is very low in these cell lines (**figure 5.3.5**). The expression level presented by DU145 and MDA-MB-231 cells represented the lower limit of what can be detected by immunofluorescence.

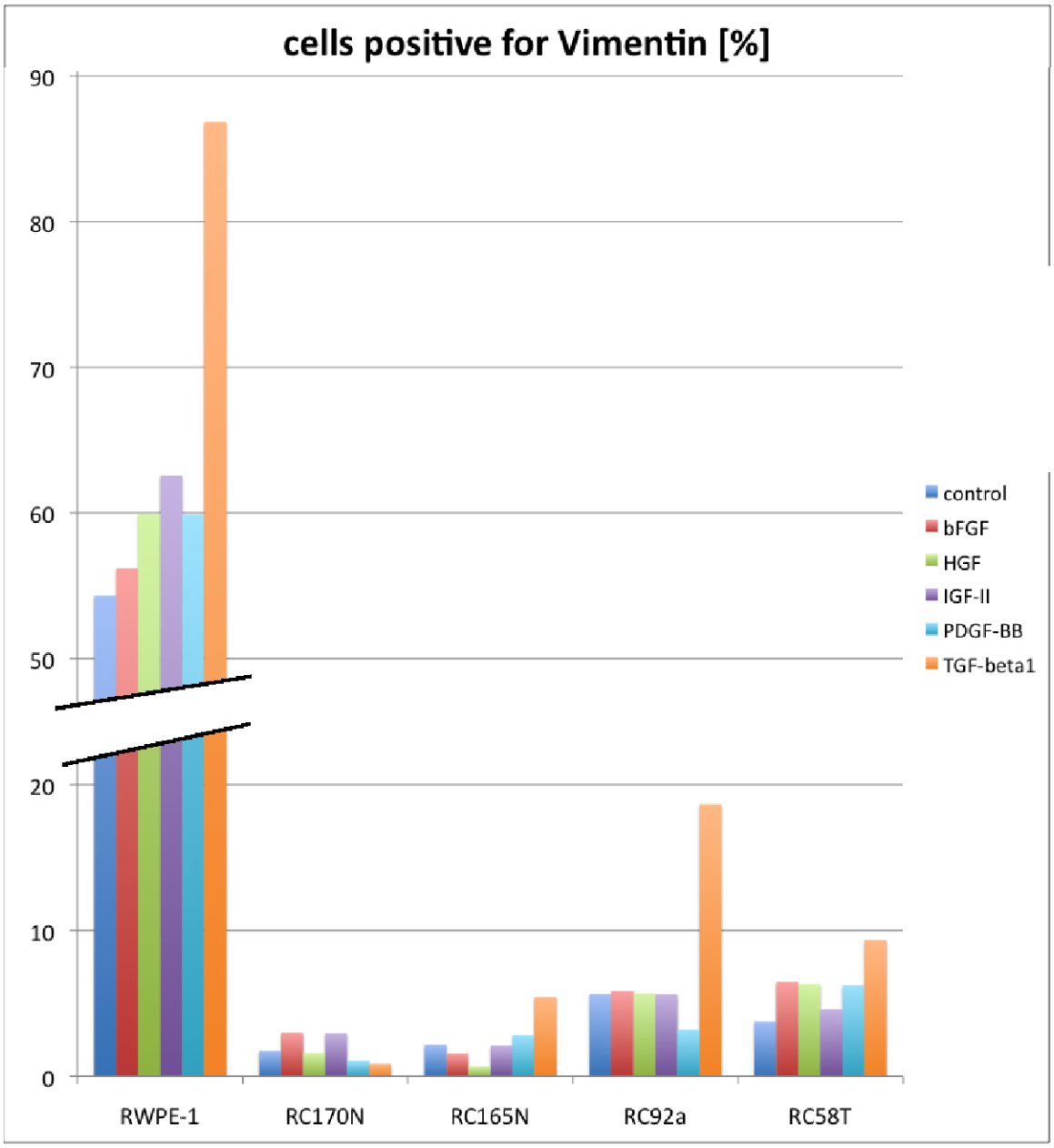



**Figure 5.3.6 EMT inducing factors:** RWPE-1, RC170N, RC165N, RC92a and RC58T cells were seeded on tissue culture plastic, grown under normal growth conditions for two days and subsequently incubated for 72h with 50ng/ml PDGF-BB/IGF-II or 5ng/ml HGF/bFGF/TGF-beta1. Response to EMT inducing growth factors was measured by immunofluorescent staining for Vimentin/Cytokeratin and quantified by MetaXpress 2.0 pattern recognition software. (n=1)

Similar to the low migratory/invasive reference MCF7 cell line MLC2 phosphorylation was comparatively low in BPH and intermediate grade prostate cells (**Figure 5.3.7**) and this was also the case for LNCaP cells. In accordance with their high migratory/invasive properties, MDA-MB-231 cells had a high level of MLC2 phosphorylation. PC3 and DU145 cells also had a significant amount of MLC2 phosphorylation but at a lower level than MDA-MB-231 cells. This correlates with the observed morphological differences between these three cells types: (a) PC3 and MDA-MB-231 cells display horizontal front-end polarity but the latter have more protrusions and actin stress fibers; (b) DU145 cells have a dual epithelioid and mesenchymal phenotype and phosphorylation of MLC2 indicates that this functional component is most likely associated with the mesenchymal-like phenotype.

To confirm whether the differential MLC2-signalling phenotypes observed in the three metastatic prostate cancer cell lines correlate with functional differences in their migratory potential video time-lapse microscopy was used (**Figure 5.3.9**).

Both singular and grouped LNCaP-cells displayed small back and forth movements of the cell body without detachment of their actin-rich anchors and no evidence of any cell translocation being achieved. In contrast, PC3-cells displayed a very typical mesenchymal-like cell migration with substantial cell body translocation achieved by the formation of lamellipodial protrusions at the leading edge and contraction at the cell rear. This was similar, in part, to the migratory phenotype of MDA-MB-231 cells (Sturge et al., 2003). Since DU145-cells grow in colonies most cells were observed as stationary but with a substantial number of cells at the colony borders displaying single cell migration and cell body translocation until the they form contact with another part of the same colony or a different colony and reform cell-cell adhesions.

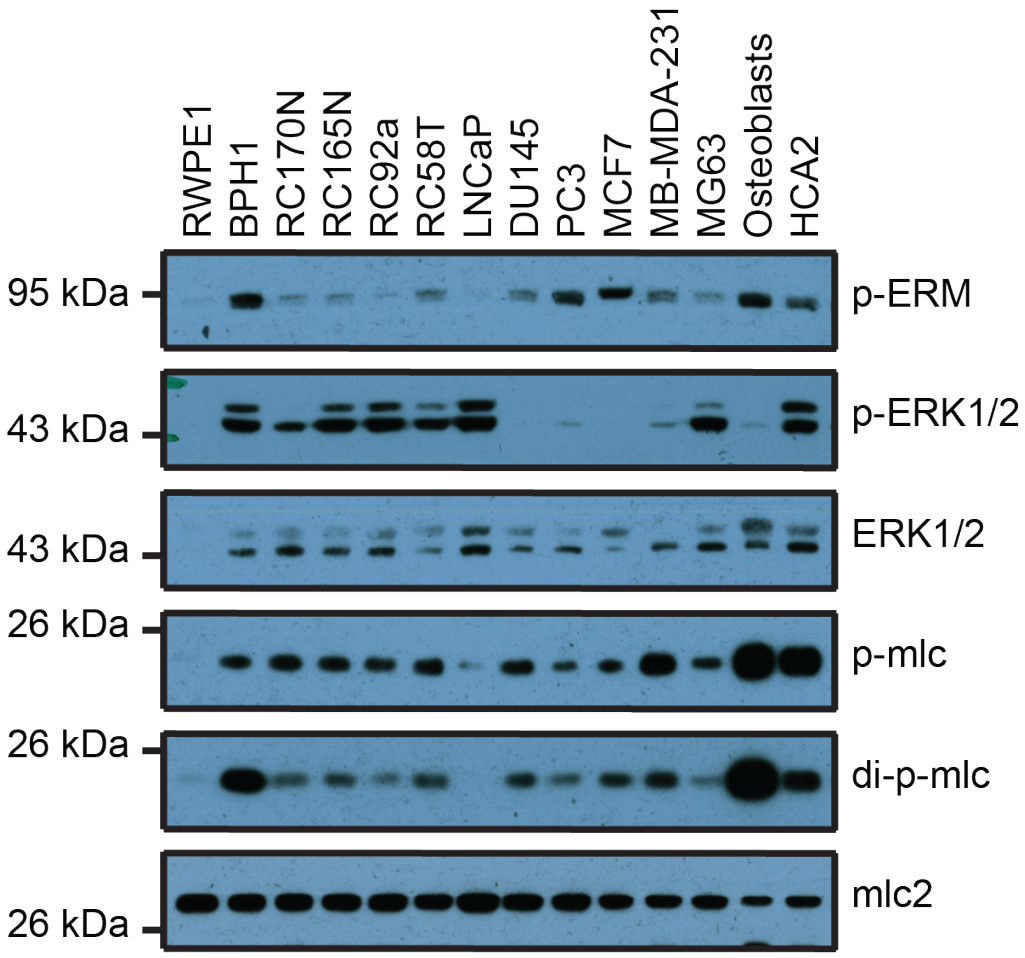



**Figure 5.3.7 Phosphorylation status of MLC2 as an indicator of migratory and invasive potential.** RWPE-1, BPH1, RC170N, RC165N, RC92a, RC58T, LNCaP, PC3, DU145, MCF-7, MB-MDA231, MG63, HCA2 cells and primary human osteoblasts were seeded on tissue culture plastic and grown under their normal growth conditions for four days. Whole cell lysates were prepared and subjected to SDS-PAGE using a 4-20% acrylamide gradient gel under reducing conditions. The panels show immunoblots obtained using the primary antibody concentrations listed in **Table 2.1** followed by the appropriate HRP-conjugated secondary antibody: phosphorylated Ezrin/Radixin/Moesin (MW = 69 kDa); ERK and phosphorylated ERK (MW = 43 kDa) MLC2 phosphorylated at Serine 19 (MW = 18 kDa); MLC2 phosphorylated at Threonine 18 and Serine 19 (MW = 18 kDa) and total MLC2 (MW = 18 kDa). For all blots visualisation of immunoreactive bands was carried out using chemiluminesence. Molecular weight (MW) markers (kDa) and proteins of interest are indicated for each blot: ($n \geq 3$ for all markers and cell lines with the exception of p-ERK; BPH1, RC170N and HCA2 cells; $n = 2$).

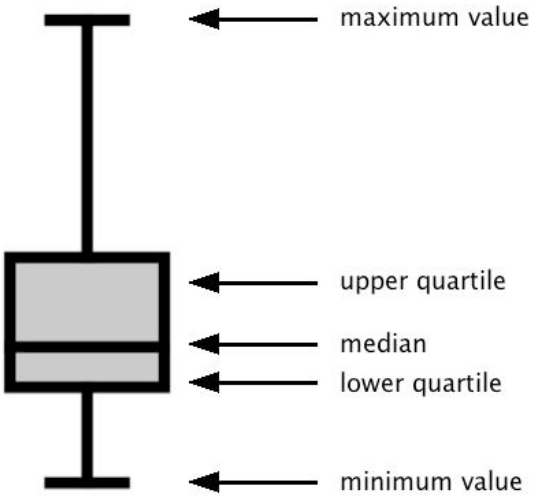



**Figure 5.3.8 Box and Whiskers.** The migratory speed in μm/h is represented in a Box and Whiskers Plot. The Whiskers represent the fastest (maximum value) and slowest (minimum value) migrating cell. The two grey boxes above and below the median represent upper and lower quartile. The upper quartile extends from the median over 25% of cells that migrate faster than the median while the lower quartile extends over the 25% of cells that migrate slower than the median. The whole box extends over 50% of cells centered around the median.

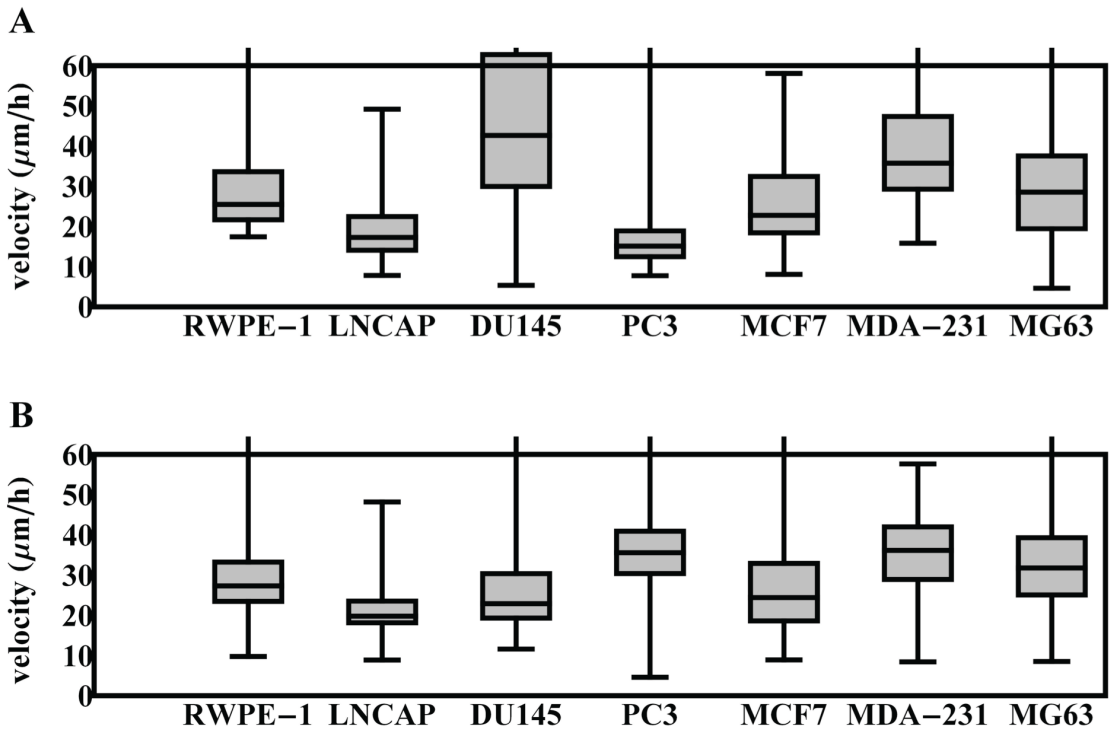
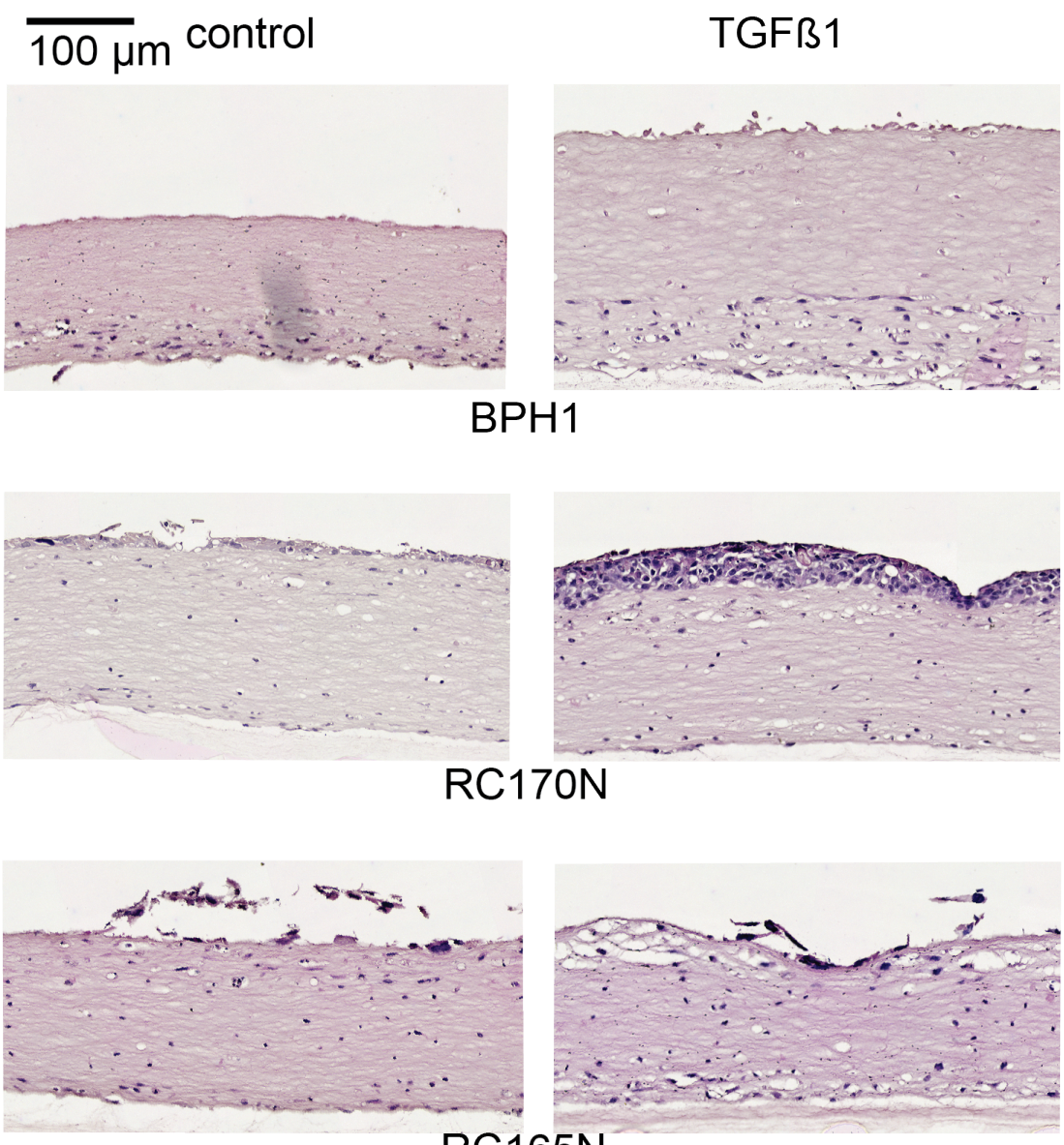


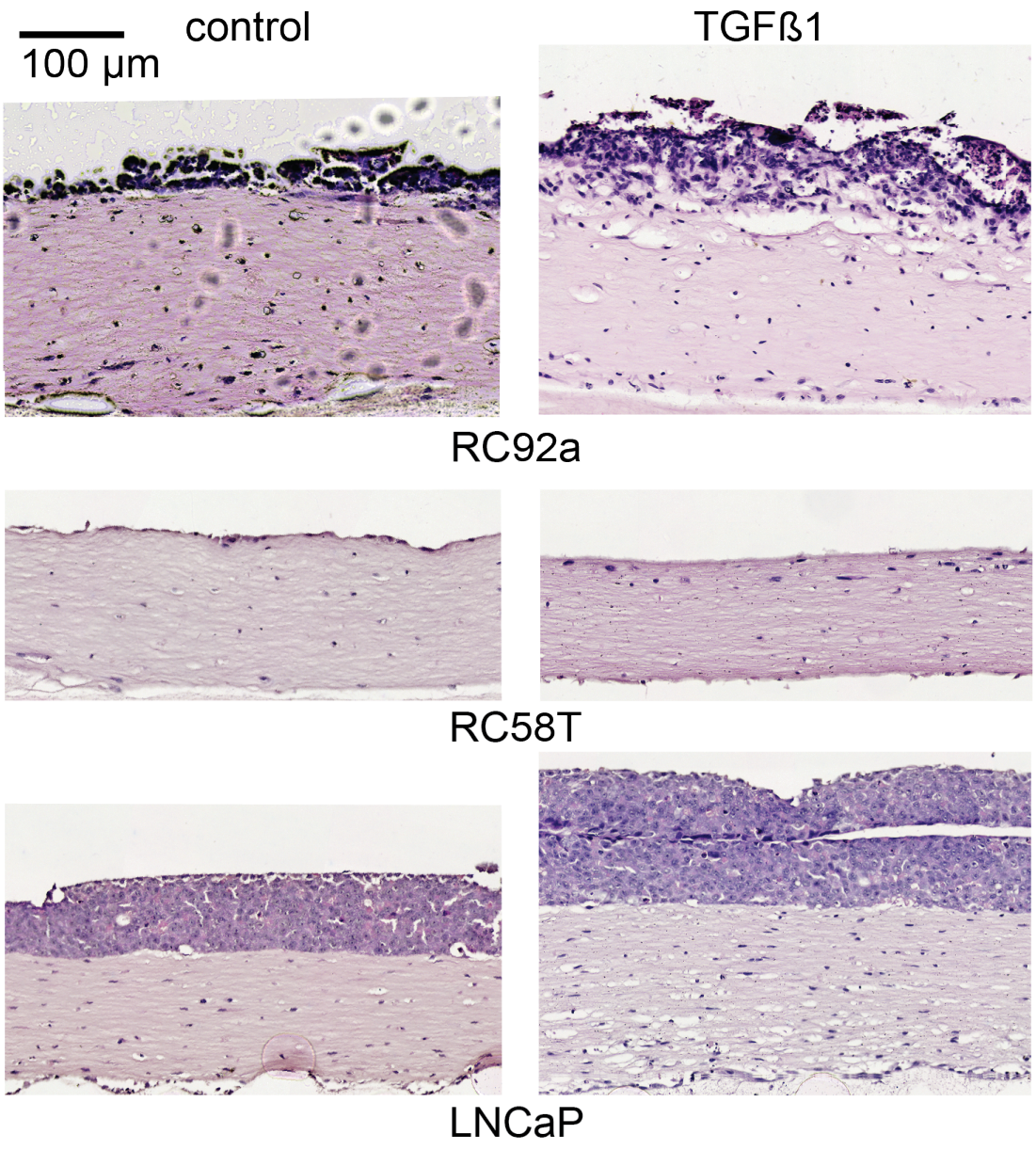

**Figure 5.3.9 Migratory behaviour of metastatic prostate cancer cell lines.** RWPE-1, LNCaP, DU145, PC3, MCF7, MDA-231 and MG63 cells were seeded on tissue culture plastic and grown under their normal growth conditions for (A) 2 or (B) 24 hours. The cells were subjected to video time-lapse microscopy (1 frame/minute) for 12 hours in an incubation chamber under normal growth conditions. The videos were analysed with the object tracker function of the Metamorph software (Molecular Devices). Cell tracks were exported to Mathematica (Wolfram Research) in order to calculate the mean cell velocity (μm/h) (n=1).

The invasive potential of the three metastatic prostate cancer cell lines was investigated using an organotypic model (**Figure 5.3.10**). In this model fibroblasts are implanted into Matrigel-collagen-gels to mimic the same matrix remodelling processes and generation of migratory/invasive cues generated by stromal tissue. Similar to the *in vivo* situation the prostate cancer cells were seeded and maintained as an epithelial layer on top of the reconstituted stroma for two weeks. After this time the whole organotypic culture was fixed, dissected and H&E stained to assess the level and nature of cellular invasion.

In normal tissue culture the comparative growth rates of the three metastatic lines is: PC3 > DU145 > LNCaP. However, in the organotypic cultures the apparent growth rates were reversed as was evident from the formation of multilayers of LNCaP cells on the surface of the organotypic cultures. However, there was no evidence of LNCaP cellular invasion into the stromal collagen gel. Both PC3 and DU145 were able to penetrate the stromal collagen gel. In accordance with their singular cell morphology clusters of PC3-cells were not observed in the stromal matrix. DU145-cells displayed the greatest invasive potential and did so as part of multiple multicellular groups. On the other hand the majority of BPH1 and RC165N cells disappeared over the course of the 14 days of organotypic culture. Similar results were observed with RC58T cells.

In a screen for EMT inducing growth factors TGF-$\beta_1$ was found to be capable of inducing rapid vimentin expression and and E-cadherin internalisation in RC92a cells. This was the rationale for supplementing the growth medium of the chemotaxis invasion assays with TGF-$\beta_1$ over the 14-day incubation period. RC92a cells started to invade the organotypic matrix in the presence of TGF-$\beta_1$ but not under normal growth conditions (keratinocyte growth medium). RC170N cells, which disappeared under normal growth conditions displayed strong three-dimensional growth and invagination into the organotypic matrix with TGF-$\beta_1$ treatment. Similar results were also observed when keratinocyte growth medium was replaced with DMEM 10% FCS.


100 µm
control
TGFß1
BPH1
RC170N
RC165N


100 µm
control
TGFß1
RC92a
RC58T
LNCaP

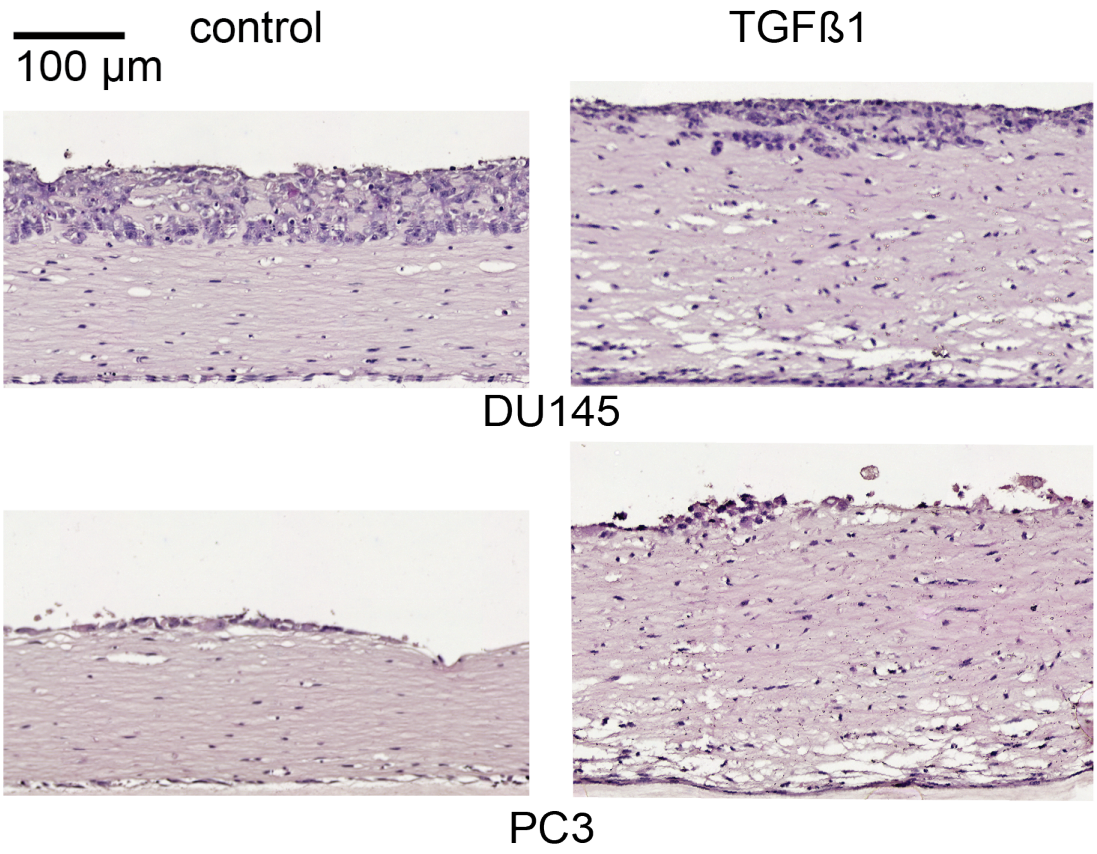



**Figure 5.3.10 Invasive behaviour of BPH, RWPE-1, RC170N, RC165N, RC92a, RC58T, LNCaP, DU145 and PC3 cell lines:** hTert immortalised human dermal fibroblasts (HCA2) were embedded into a 50/50 Matrigel/collagen gel mix and allowed to equilibrate for 24 hours in order to form an organotypic matrix. Normal prostate and cancer cells were subsequently seeded on top of the organotypic matrix to form an epithelial layer. After 3 days the gels were raised onto grids and the cells allowed 14 days to invade. Medium was changed every four days and supplemented with 5 ng/ml TGF-$\beta_1$ (R& Systems) where indicated until the organotypic cultures were fixed, bisected and embedded in paraffin wax. 10 µm sections stained with haematoxylin and eosin (H&E) are shown (n=3).

### 5.3.8 Discussion

Others have developed 3-D models of prostate cancer (Chu et al., 2009; Harma et al., 2010; Yates et al., 2007). Here we establish and characterise an unbiased cell line based model of prostate cancer for progressive differences in morphology, cytoskeletal proteins, cell-cell and cell-matrix adhesions together with their migratory signalling cues, migratory behaviour and invasive capacity in an stromal "organotypic" matrix. From the findings of this study it can be hypothesised that it is the transition to adopt mesenchymal characteristics rather than the loss of epithelial characteristics that is sufficient to enable prostate cancer cell invasion and metastasis. Evidence for this lies in the very divergent invasive behaviours of LNCaP and DU145 cells, which both retain epithelial characteristics. Only the DU145 cells have adopted mesenchymal characteristics and can undergo efficient group cell invasion into stromal matrix. The group cell invasion by DU145 cells appeared to be more efficient than the single cell mode of invasion used by PC3-cells.

It is not surprising that LNCaP cells are unable to undergo efficient stromal tissue invasion since they lack many key cytoskeletal and adhesion proteins and are devoid of important contractile signalling cues. The concomitant overexpression of $\alpha$–tubulin in LNCaP cells may represent their origin being from a rare neuroendocrine-derived prostate tumour (Yuan et al., 2007), rather than the common EMT phenotypes adopted by PC3 and DU145 cells.

The use of a relevant cell line model systems to correctly evaluate the molecular mechanisms underlying the biological response of specific prostate carcinoma subtypes is essential because they display major differences in their clinical behaviour, prognosis, and treatment (Grignon, 2004). From the studies carried out in this Section it can be concluded that PC3 and DU145 cells, but not LNCaP cells, are suitable for the study of *bona fide* mesenchymal properties involved in prostate cancer invasion and metastasis.

The absence of invasion by LNCaP cells may result from the retention of their epithelial characteristics. This possibility was tested by evaluated by considering

whether BPH, low or intermediate grade primary prostate cancer cell lines could undergo stromal invasion into an organotypic stroma. In these experiments one of the BPH cell lines (RC170N) and the low-grade primary prostate cancer cell line (RC92a) were induced to invade the organotypic stroma in response to TGF-$\beta_1$.

This provides a new tool for the study of early prostate cancer and progression via an EMT-like event. The role of Endo180 is this model was not determined. However, it is pertinent to take into account the fact that TGF-$\beta_1$ is the only EMT-associated factor to induce Endo180 expression in invasive breast cancer and glioma tumour cell lines. Results of other projects in the lab have confirmed that TGF-$\beta_1$-SMAD2/3 dependent signalling is a major regulatory axis for the control of Endo180 expression in PC3 cells cultured within a bone stromal-derived matrix. It can be speculated that the same signalling axis is active during the invasive processes observed in these two experimental settings. This can be confirmed in future work by targeting the different components of the TGF-$\beta_1$-SMAD2/3-Endo180 signalling axis in this newly established model of EMT-like event driving prostate cancer stromal invasion. By manipulating the functionality of Endo180 in the collagen remodelling, Rho-ROCK-MLC2-based migration or uPA-uPAR-dependent chemotaxis proposed as a mechanistic

# 6 Final Discussion

The goal of this study was to investigate a potential role for Endo180 in prostate cancer. The rationale for this interest was an earlier study, not yet published at the time that showed a positive correlation between Endo180 expression and Gleason grade on a small prostate cancer tissue microarray (Kogianni et al., 2009).

The chosen approach was to contribute knowledge and to develop tools to study the cellular function of Endo180, to investigate a potential correlation between Endo180 expression and patient survival in prostate cancer, as well as to define a suitable cell line model for further studies of Endo180 in prostate cancer progression.

The study was structured into three main parts: (a) in silico structural and evolutionary analysis of Endo180; (b) functional studies of Endo180; and (c) the role of Endo180 in prostate cancer progression.

## 6.1 Structural analysis of Endo180 *in silico*

Prior to this work, Endo180 has only been described in the genomes of mice, humans and Belgian blue cattle. Here, it was established for the first time that Endo180 encoding genes are present throughout the whole vertebrate kingdom. It was also discovered that the interaction partners of Endo180, uPA and uPAR as well as other members of the Mannose receptor family are co-conserved alongside Endo180 throughout the whole vertebrate kingdom. Furthermore, the functional amino acid residues, responsible for proper receptor shuttling were found to be conserved in Endo180 sequences for all inventoried species. The group-based phosphorylation scoring system, GPS, predicted potential kinase substrates juxta-positioned to these functional amino acid residues. Complex phosphorylation regulation of the cytoplasmic tail of Endo180 might be caused by potential involvement of the PKC regulator 14-3-3. Additionally, these potential kinase substrates as well as the potential 14-3-3 binding sites are evolutionary conserved.

Interestingly, the conservation of functional amino acid residues was not limited to the dihydrophobic motif but extended to the LDL receptor endocytosis motif although mutation of this motif only resulted in mild alterations to receptor sorting.

A potential uPA interacting motif, RxxSSxR, was previously found within the Endo180 amino acid sequence in a large screening study (Liang et al., 2003). However, no further analysis was undertaken at the time (Liang et al., 2003).

Here, supporting evidence was gathered concerning the validity of the predicted uPA interacting motif. It was discovered that the motif is located within the CTLD4 domain of the Endo180 protein. Structural modelling of the CTLD4 domain revealed that the site is located accessible on the surface of the complex quartery structure of the Endo180 ectodomains.

Additionally, it was found that the potential interaction motif is evolutionary conserved in all mammals but not in Endo180 sequences of any other vertebra sequenced to date: fish, amphibia and reptiles. In support of these findings, the kringle domain of uPA, which binds to the RxxSSxR motif, is only conserved within mammals but not in other vertebrates. The RxxSSxR motif within the CTLD4 domain of Endo180 as well as its potential interaction partner, the kringle domain of uPA, are evolutionarily co-conserved and their common presence appears to be restricted to mammals.

While the RxxSSxR motif binds to the kringle domain of uPA, the uPA receptor, uPAR binds to the amino-terminal fragment, ATF, of uPA (Liang et al., 2003). uPAR lacks a cytosolic domain and is dependent on receptor clustering to initiate intracellular signalling (Smith and Marshall, 2010). A possible working hypothesis is that Endo180 forms a tri-molecular cell surface cluster with uPA-uPAR via direct interaction with the RxxSSxR motif to form a signalling platform that can direct cell migration towards chemotactic cues within the stromal microenvironment. Endo180 antibodies have been characterised for their ability to abrogate chemotaxis towards uPA gradients. Potentially, Endo180 antibodies prevent complex formation and in consequence signalling by steric hindrance. Based on

these findings, co-workers in the Sturge group have established a CTLD4-GST fusion protein as blocking agent for Endo180 function in acinar formation assays using CTLD2-GST as control (Rodriguez publication in preparation).

For future studies, Endo180 mutants were created that lack the RxxSSxR motif. Overexpression of those mutants in established cell line models for Endo180 signalling, will allow to verify if mutant Endo180 is unable to induce Rho GTPase signalling upon uPA stimulation. Another important remaining question is the dependence on uPAR for Endo180 mediated Rho GTPase activation upon uPA stimulation. While we have postulated the formation of a tri-molecular complex, previous studies have shown that uPA can activate integrin signalling independently of uPAR by means of a direct interaction between integrins and the kringle domain of uPA (Tarui et al., 2006). It is possible that Endo180 can act independently of uPAR in the same manner. This could be investigated in the future by silencing uPAR expression in a suitable cell line model.

A thorough understanding of the precise interplay of the uPA-uPAR-Endo180 axis may offer the possibility for discovery of advanced treatments for disease processes associated with Endo180 protein function through direct targeting of the functional subdomains.

## 6.2 Functional studies of Endo180

This part of the study concentrated on phosphorylation of Endo180 as well as subcellular localisation of Endo180 in epithelial cells. Additionally, several preliminary characterisations of PC3 prostate cancer cells overexpressing Endo180 were discussed.

On the outset, a potential phosphorylation of Endo180 was only addressed in the earliest study of the protein using radioactive labelling (East and Isacke, 2002; Isacke et al., 1990). At least one further attempt to investigate the phosphorylation status of Endo180 using generic phospho-Serine/Threonine/Tyronsine antibodies had failed (Sturge/Yarwood – personal communication).

Although it was possible to predict potential Endo180 phosphorylation sites *in silico* (**section 4**), it was impossible with the methods applied to detect any phosphorylated Endo180 *in vivo*. These findings were in stark contrasts to the earlier report (East and Isacke, 2002; Isacke et al., 1990). However, the methods applied in the other study were far more sensitive than those applied here (East and Isacke, 2002; Isacke et al., 1990). Several other possible reasons and alternative approaches were discussed (**section 4**). In summary, the change in cell line as well as the different experimental approach, both, have the potential to be causal for the negative outcome. There is the possibility that only a small subpopulation of Endo180 is being phosphorylated *in vivo*, which might explain the experimental difficulties.

The initial cloning of the human Endo180 encoding gene by the Isacke lab proved to be very challenging (Sturge personal communication). Prior to this study, co-workers and other groups struggled to amplify the Endo180 encoding sequence by PCR. Molecular cloning had to be based on restriction digests only (Sturge personal communication). Surprisingly, it was possible to perform site-directed mutagenesis on an Endo180 expression vector (**section 3**). As a result, PCR of Endo180 expression vectors was revisited and it was discovered for the first time that PCR of the full-length human Endo180 encoding sequence is possible by the addition of DMSO to the PCR reaction. This discovery implies that the Endo180 encoding sequence is forming stable secondary structures potentially based on stem loops in GC-rich regions (Kang et al., 2005). Surprisingly, amplification of the sequence encoding murine Endo180 was possible under standard conditions.

This discovery was exploited to clone the Endo180 encoding sequence into a fluorescent expression vector. Prior to this study, Endo180 was cloned into a pEGFP-C1 vector in the Isacke lab. However, protein expression in human cells was problematic and stable cell lines could not be derived (Sturge personal communication). Usage of the pEGFP-C1 vector implies that EGFP and Endo180 were fused at the c-terminal end of the Endo180 protein.

Conversely, in this study it was decided to fuse a fluorescent protein, hmKO2, and Endo180 at the N-terminal end of the Endo180 protein to avoid interference with the formation of the quartery structure of the Endo180 receptor. While it was possible to transiently express the Endo180-hmKO2 fusion protein in DU145 prostate cancer cells, creation of stable Endo180-hmKO2 expressing DU145 cell lines failed.

In fluorescent live cell microscopy the protein appeared to be expressed and sorted correctly in transiently transfected DU145 cells. In 3D confocal images, Endo180-hmKO2 fusion protein appeared to be restricted to vesicular compartments of DU145 prostate cancer cells. This construct might offer new ways of studying Endo180 receptor internalisation and trafficking. The failure of producing stable Endo180-hmKO2 expressing DU145 cells gives rise to concerns about a potential impairment of receptor function/stability by the fused fluorescent protein. For future studies, Endo180-hmKO2 fusion protein should be characterised for correct receptor function in the established model systems for RhoGTPase signalling and collagen internalisation. Conventional lipid based transfection proved to be very challenging in conjunction with DU145 cells on growth surfaces other than tissue culture plastics. For future studies, switching to a lentiviral vector is highly recommended (Wells et al., 2010).

Interestingly, immunofluorescent staining of untransfected DU145 cells with the Endo180 antibody A5/158 revealed co-localisation of Endo180 with E-Cadherin at cell-cell junctions. Surprisingly, only the A5/158 antibody was able to bind to Endo180 co-located with E-Cadherin, the 39:10 antibody was not able to display the same characteristics. Localisation to cell-cell junctions might be associated with a new role for Endo180 in epithelial cells. No role has been described for Endo180 in epithelial cells to date. However, based on these findings as well as the finding that Endo180 is expressed in early stage prostate cancer cells (**section 6**), co-workers have investigated a role for Endo180 in acinar formation. 3D-cultures of early stage prostate cancer cells for acinar structures but addition of different Endo180 antibodies as well as CTLD4-GST protein abrogates acinar formation or alters acinar

shape and dimension (Rodriguez-Teja et al., publication in preparation). As outlined in section 1.4, Endo180 preferentially interacts with specific Collagens, amongst them Collagen IV, which is almost exclusively restricted to the basal lamina (Khoshnoodi et al., 2008). It is possible that Endo180 is involved in interactions between epithelial cells and the basal lamina through which it might perform a role in prostate development/homeostasis. Interestingly, co-workers have identified differences in Collagen IV structure in sections from wild type and partial Endo180 knockout mice (Rodriguez-Teja et al., publication in preparation). .

## 6.3 Endo180 as biomarker and prostate cancer model

Prior to this study, it had been established that Endo180 expression correlates with Gleason grade on a small prostate cancer tissue microarray.

Here, the predictive value of Endo180 expression in malignant prostate tissue was analysed in a large tissue microarray study. The correlation of Endo180 expression with Gleason grade was confirmed. Additionally, for the first time it was discovered that patients with tumours negative for Endo180 expression displayed a highly significant increase in overall survival after TURP. Furthermore, Endo180 was able to predict disease outcome for patients diagnosed with low or intermediate risk prostate cancer. This is the first study that investigated a correlation between Endo180 expression in tumour samples and clinicopathological outcome. However, the procedure for staining for Endo180 expression in paraffin embedded tissue is not yet ready for deployment in a clinical environment. The reliability of antigen staining needs to be addressed. All available antibodies are targeting functional domains. A better understanding of the conformational changes of Endo180 associated with receptor function (**section 3 and 4**) might lead to the discovery of more robust staining techniques or the development of Endo180-based *in vivo* imaging tools.

In order to establish Endo180 as a potential clinical marker, FDA approved multi-tissue areas were stained for Endo180 expression with both, the 39:10 and A5:158 antibodies. In addition to well-established sites of Endo180 expression such as the skin, it was discovered, that Endo180 is expressed in the Leydig cells of the testis as

well as throughout most of the gastrointestinal-tract. The function of Endo180 in these tissues as well as a potential involvement in disease processes in those tissues needs to be addressed. Furthermore, the exact mechanism through which Endo180 promotes prostate cancer progression has yet to be established. Earlier studies showed that Endo180 could act both as an activator of the Rho GTPase signalling axis as well as Collagen uptake receptor in breast cancer cells. Therefore, Endo180 could act as a mediator of cell migration and chemotaxis as well as promoter of Collagen turnover in prostate cancer.

The Rhim lab provided early stage prostate cancer cell lines. Those cell lines together with the commonly used LNCaP, PC3 and DU145 cells were defined as multi cell line model to study prostate cancer progressions. This panel of cell lines represented earliest up to late stage of the disease. Endo180 was expressed in low but detectable amounts in early stage prostate cancer cells. While expression was relatively low in E-Cadherin negative PC3 cells, E-Cadherin positive DU145 cells expressed the highest amount of Endo180 amongst the members of the panel. Therefore, within this novel cell line model, expression of Endo180 does not correlate with tumourigenicity. However, the model was found to be well suited to study the concept of EMT in a prostate cancer setting. Especially two cell lines, a hTert-immortalised benign prostate hyperplasia cell line, RC170N and a hTert-immortalised low risk (Gleason grade 6) prostate cancer cell line, RC92a showed TGF-ß$_1$ dependent invasive behaviour in an organotypic model.

At the outset of this thesis it was mentioned that the prostate cancer field relied on only three cell lines, mainly LNCaP, DU145 and PC3 cells. We have discovered that these cells do not align well in a staged disease progression model. LNCaP cells appeared to be atypical within our multi-cell line model. The more recently developed cell lines included in this study are promising additions to the repertoire of available cell lines. These cell lines can be used to develop new models to study the crucial process of early prostate cancer progression and metastasis.

## 6.4 Final remarks

In conclusion, it was discovered that Endo180, its interaction partners and other members of the same receptor family are evolutionary conserved throughout the vertebrate kingdom. Functionally characterised amino acid residues are evolutionary conserved such as a potential interaction site with the kringle domain of uPA. Localisation to cell-cell junctions indicates a potential novel role for Endo180 in epithelial cells.

For the first time, a correlation between Endo180 and clinicopathological outcome was investigated. It was demonstrated that expression of Endo180 is highly correlated with patient survival in prostate cancer progression. A multi cell line model was defined to study prostate cancer disease progression *in vitro*. Member cell lines represent different stages of the disease, beginning with BPH up to metastasised disease. The multi cell line model was tested in the organotypic invasion assay developed by the Marshall lab (Queen Mary's University London). Interestingly, early stage prostate cancer cells become invasive upon stimulation with TGF-ß$_1$. Several cell lines within this panel were found to express Endo180. However, no correlation between disease stage represented by the cell line and Endo180 expression level was detected. Further studies should be aimed at linking TGF-ß$_1$-dependent regulation of Endo180 with the invasive behaviour of prostate cancer cells from early disease stages as a potential therapeutic target for the prevention of tumour progression.

# 7 Bibliography

Bibliography

Alberts, B. 2002. Molecular biology of the cell. Garland Science, New York ; London. xxxiv, 1463 p. pp.

Allen, W.E., G.E. Jones, J.W. Pollard, and A.J. Ridley. 1997. Rho, Rac and Cdc42 regulate actin organization and cell adhesion in macrophages. *J Cell Sci*. 110 ( Pt 6):707-720.

Alsaid, B., I. Karam, T. Bessede, I. Abdlsamad, J.F. Uhl, V. Delmas, G. Benoit, and S. Droupy. 2010. Tridimensional computer-assisted anatomic dissection of posterolateral prostatic neurovascular bundles. *European urology*. 58:281-287.

Arias-Romero, L.E., and J. Chernoff. 2008. A tale of two Paks. *Biology of the cell / under the auspices of the European Cell Biology Organization*. 100:97-108.

Bae, S.N., G. Arand, H. Azzam, P. Pavasant, J. Torri, T.L. Frandsen, and E.W. Thompson. 1993. Molecular and cellular analysis of basement membrane invasion by human breast cancer cells in Matrigel-based in vitro assays. *Breast cancer research and treatment*. 24:241-255.

Bailey, L., D. Wienke, M. Howard, V. Knauper, C.M. Isacke, and G. Murphy. 2002. Investigation of the role of Endo180/urokinase-type plasminogen activator receptor-associated protein as a collagenase 3 (matrix metalloproteinase 13) receptor. *Biochem J*. 363:67-72.

Barnett, D.H., H.Y. Huang, X.R. Wu, R. Laciak, E. Shapiro, and W. Bushman. 2002. The human prostate expresses sonic hedgehog during fetal development. *J Urol*. 168:2206-2210.

Barry, M., S. Perner, F. Demichelis, and M.A. Rubin. 2007. TMPRSS2-ERG fusion heterogeneity in multifocal prostate cancer: clinical and biologic implications. *Urology*. 70:630-633.

Begnami, M.D., M. Quezado, P. Pinto, W.M. Linehan, and M. Merino. 2007. Adenoid cystic/basal cell carcinoma of the prostate: review and update. *Archives of pathology & laboratory medicine*. 131:637-640.

Behrendt, N. 2004. The urokinase receptor (uPAR) and the uPAR-associated protein (uPARAP/Endo180): membrane proteins engaged in matrix turnover during tissue remodeling. *Biol Chem*. 385:103-136.

Behrendt, N., O.N. Jensen, L.H. Engelholm, E. Mortz, M. Mann, and K. Dano. 2000. A urokinase receptor-associated protein with specific collagen binding properties. *J Biol Chem*. 275:1993-2002.

Bello, D., M.M. Webber, H.K. Kleinman, D.D. Wartinger, and J.S. Rhim. 1997. Androgen responsive adult human prostatic epithelial cell lines immortalized by human papillomavirus 18. *Carcinogenesis*. 18:1215-1223.

Berman, D.M., N. Desai, X. Wang, S.S. Karhadkar, M. Reynon, C. Abate-Shen, P.A. Beachy, and M.M. Shen. 2004. Roles for Hedgehog signaling in androgen production and prostate ductal morphogenesis. *Dev Biol*. 267:387-398.

Bhatia-Gaur, R., A.A. Donjacour, P.J. Sciavolino, M. Kim, N. Desai, P. Young, C.R. Norton, T. Gridley, R.D. Cardiff, G.R. Cunha, C. Abate-Shen, and M.M. Shen.

1999. Roles for Nkx3.1 in prostate development and cancer. *Genes & development*. 13:966-977.
Bianchetti, L., M. Barczyk, J. Cardoso, M. Schmidt, A. Bellini, and S. Mattoli. 2011. Extracellular matrix remodelling properties of human fibrocytes. *Journal of cellular and molecular medicine*.
Bieberich, C.J., K. Fujita, W.W. He, and G. Jay. 1996. Prostate-specific and androgen-dependent expression of a novel homeobox gene. *J Biol Chem*. 271:31779-31782.
Bierie, B., M. Nozawa, J.P. Renou, J.M. Shillingford, F. Morgan, T. Oka, M.M. Taketo, R.D. Cardiff, K. Miyoshi, K.U. Wagner, G.W. Robinson, and L. Hennighausen. 2003. Activation of beta-catenin in prostate epithelium induces hyperplasias and squamous transdifferentiation. *Oncogene*. 22:3875-3887.
Boskovic, J., J.N. Arnold, R. Stilion, S. Gordon, R.B. Sim, A. Rivera-Calzada, D. Wienke, C.M. Isacke, L. Martinez-Pomares, and O. Llorca. 2006. Structural model for the mannose receptor family uncovered by electron microscopy of Endo180 and the mannose receptor. *J Biol Chem*. 281:8780-8787.
Boyer, B., and J.P. Thiery. 1993. Epithelium-mesenchyme interconversion as example of epithelial plasticity. *APMIS*. 101:257-268.
Brooke, G.N., R.L. Culley, D.A. Dart, D.J. Mann, L. Gaughan, S.R. McCracken, C.N. Robson, B. Spencer-Dene, S.C. Gamble, S.M. Powell, R. Wait, J. Waxman, M.M. Walker, and C.L. Bevan. 2011. FUS/TLS is a novel mediator of androgen-dependent cell-cycle progression and prostate cancer growth. *Cancer Res*. 71:914-924.
Bruce Alberts, A.J., Julian Lewis, Martin Raff, Keith Roberts, and Peter Walter. 2002. Molecular Biology of the Cell. New York: Garland Science.
Bussemakers, M.J., A. van Bokhoven, G.W. Verhaegh, F.P. Smit, H.F. Karthaus, J.A. Schalken, F.M. Debruyne, N. Ru, and W.B. Isaacs. 1999. DD3: a new prostate-specific gene, highly overexpressed in prostate cancer. *Cancer Res*. 59:5975-5979.
Caballero, I., I. Parrilla, C. Alminana, D. del Olmo, J. Roca, E.A. Martinez, and J.M. Vazquez. 2012. Seminal plasma proteins as modulators of the sperm function and their application in sperm biotechnologies. *Reproduction in domestic animals = Zuchthygiene*. 47 Suppl 3:12-21.
Caley, M.P., G. Kogianni, A. Adamarek, J.H. Gronau, M. Rodriguez-Teja, A.V. Fonseca, F. Mauri, A. Sandison, J.S. Rhim, C. Palmieri, J.P. Cobb, J. Waxman, and J. Sturge. 2012. TGFbeta1-Endo180-dependent collagen deposition is dysregulated at the tumour-stromal interface in bone metastasis. *J Pathol*. 226:775-783.
Cancilla, B., R.A. Jarred, H. Wang, S.L. Mellor, G.R. Cunha, and G.P. Risbridger. 2001. Regulation of prostate branching morphogenesis by activin A and follistatin. *Dev Biol*. 237:145-158.
Chaffer, C.L., and R.A. Weinberg. 2011. A perspective on cancer cell metastasis. *Science*. 331:1559-1564.
Chang, W.Y., L. Birch, C. Woodham, L.I. Gold, and G.S. Prins. 1999. Neonatal estrogen exposure alters the transforming growth factor-beta signaling system in the

developing rat prostate and blocks the transient p21(cip1/waf1) expression associated with epithelial differentiation. *Endocrinology*. 140:2801-2813.
Choi, Y.J., J.K. Kim, N. Kim, K.W. Kim, E.K. Choi, and K.S. Cho. 2007. Functional MR imaging of prostate cancer. *Radiographics : a review publication of the Radiological Society of North America, Inc*. 27:63-75; discussion 75-67.
Chu, J.H., S. Yu, S.W. Hayward, and F.L. Chan. 2009. Development of a three-dimensional culture model of prostatic epithelial cells and its use for the study of epithelial-mesenchymal transition and inhibition of PI3K pathway in prostate cancer. *The Prostate*. 69:428-442.
Curino, A.C., L.H. Engelholm, S.S. Yamada, K. Holmbeck, L.R. Lund, A.A. Molinolo, N. Behrendt, B.S. Nielsen, and T.H. Bugge. 2005. Intracellular collagen degradation mediated by uPARAP/Endo180 is a major pathway of extracellular matrix turnover during malignancy. *J Cell Biol*. 169:977-985.
de Kok, J.B., G.W. Verhaegh, R.W. Roelofs, D. Hessels, L.A. Kiemeney, T.W. Aalders, D.W. Swinkels, and J.A. Schalken. 2002. DD3(PCA3), a very sensitive and specific marker to detect prostate tumors. *Cancer Res*. 62:2695-2698.
Demichelis, F., K. Fall, S. Perner, O. Andren, F. Schmidt, S.R. Setlur, Y. Hoshida, J.M. Mosquera, Y. Pawitan, C. Lee, H.O. Adami, L.A. Mucci, P.W. Kantoff, S.O. Andersson, A.M. Chinnaiyan, J.E. Johansson, and M.A. Rubin. 2007. TMPRSS2:ERG gene fusion associated with lethal prostate cancer in a watchful waiting cohort. *Oncogene*. 26:4596-4599.
Demichelis, F., and M.A. Rubin. 2007. TMPRSS2-ETS fusion prostate cancer: biological and clinical implications. *J Clin Pathol*. 60:1185-1186.
Denoix, P. 1946. Enquete permanent dans les centres anticancereaux. *Bull Inst Natl Hyg*. 1:12-17.
Deras, I.L., S.M. Aubin, A. Blase, J.R. Day, S. Koo, A.W. Partin, W.J. Ellis, L.S. Marks, Y. Fradet, H. Rittenhouse, and J. Groskopf. 2008. PCA3: a molecular urine assay for predicting prostate biopsy outcome. *J Urol*. 179:1587-1592.
Donjacour, A.A., A.A. Thomson, and G.R. Cunha. 2003. FGF-10 plays an essential role in the growth of the fetal prostate. *Dev Biol*. 261:39-54.
Drake, R.L., W. Vogl, A.W.M. Mitchell, and H. Gray. 2005. Gray's anatomy for students. Elsevier Churchill Livingstone, Edinburgh; London. xxv, 1058 p. pp.
Drees, F., S. Pokutta, S. Yamada, W.J. Nelson, and W.I. Weis. 2005. Alpha-catenin is a molecular switch that binds E-cadherin-beta-catenin and regulates actin-filament assembly. *Cell*. 123:903-915.
Duband, J.L., F. Monier, M. Delannet, and D. Newgreen. 1995. Epithelium-mesenchyme transition during neural crest development. *Acta Anat (Basel)*. 154:63-78.
East, L., and C.M. Isacke. 2002. The mannose receptor family. *Biochim Biophys Acta*. 1572:364-386.
East, L., A. McCarthy, D. Wienke, J. Sturge, A. Ashworth, and C.M. Isacke. 2003. A targeted deletion in the endocytic receptor gene Endo180 results in a defect in collagen uptake. *EMBO Rep*. 4:710-716.
East, L., S. Rushton, M.E. Taylor, and C.M. Isacke. 2002. Characterization of sugar binding by the mannose receptor family member, Endo180. *J Biol Chem*. 277:50469-50475.

Economides, K.D., and M.R. Capecchi. 2003. Hoxb13 is required for normal differentiation and secretory function of the ventral prostate. *Development*. 130:2061-2069.

Edwards, S., C. Campbell, P. Flohr, J. Shipley, I. Giddings, R. Te-Poele, A. Dodson, C. Foster, J. Clark, S. Jhavar, G. Kovacs, and C.S. Cooper. 2005. Expression analysis onto microarrays of randomly selected cDNA clones highlights HOXB13 as a marker of human prostate cancer. *British journal of cancer*. 92:376-381.

Engelholm, L.H., S. Ingvarsen, H.J. Jurgensen, T. Hillig, D.H. Madsen, B.S. Nielsen, and N. Behrendt. 2009. The collagen receptor uPARAP/Endo180. *Front Biosci*. 14:2103-2114.

Engelholm, L.H., K. List, S. Netzel-Arnett, E. Cukierman, D.J. Mitola, H. Aaronson, L. Kjoller, J.K. Larsen, K.M. Yamada, D.K. Strickland, K. Holmbeck, K. Dano, H. Birkedal-Hansen, N. Behrendt, and T.H. Bugge. 2003. uPARAP/Endo180 is essential for cellular uptake of collagen and promotes fibroblast collagen adhesion. *J Cell Biol*. 160:1009-1015.

Engelholm, L.H., B.S. Nielsen, K. Dano, and N. Behrendt. 2001a. The urokinase receptor associated protein (uPARAP/endo180): a novel internalization receptor connected to the plasminogen activation system. *Trends Cardiovasc Med*. 11:7-13.

Engelholm, L.H., B.S. Nielsen, S. Netzel-Arnett, H. Solberg, X.D. Chen, J.M. Lopez Garcia, C. Lopez-Otin, M.F. Young, H. Birkedal-Hansen, K. Dano, L.R. Lund, N. Behrendt, and T.H. Bugge. 2001b. The urokinase plasminogen activator receptor-associated protein/endo180 is coexpressed with its interaction partners urokinase plasminogen activator receptor and matrix metalloprotease-13 during osteogenesis. *Lab Invest*. 81:1403-1414.

Epstein, J.I., W.C. Allsbrook, Jr., M.B. Amin, and L.L. Egevad. 2005. The 2005 International Society of Urological Pathology (ISUP) Consensus Conference on Gleason Grading of Prostatic Carcinoma. *The American journal of surgical pathology*. 29:1228-1242.

Fasquelle, C., A. Sartelet, W. Li, M. Dive, N. Tamma, C. Michaux, T. Druet, I.J. Huijbers, C.M. Isacke, W. Coppieters, M. Georges, and C. Charlier. 2009. Balancing selection of a frame-shift mutation in the MRC2 gene accounts for the outbreak of the Crooked Tail Syndrome in Belgian Blue Cattle. *PLoS Genet*. 5:e1000666.

Fernandez, N., S. Alonso, I. Valera, A.G. Vigo, M. Renedo, L. Barbolla, and M.S. Crespo. 2005. Mannose-containing molecular patterns are strong inducers of cyclooxygenase-2 expression and prostaglandin E2 production in human macrophages. *J Immunol*. 174:8154-8162.

Filipovic, A., J.H. Gronau, A.R. Green, J. Wang, S. Vallath, D. Shao, S. Rasul, I.O. Ellis, E. Yague, J. Sturge, and R.C. Coombes. 2011. Biological and clinical implications of nicastrin expression in invasive breast cancer. *Breast cancer research and treatment*. 125:43-53.

Fine, S.W., H.A. Al-Ahmadie, A. Gopalan, S.K. Tickoo, P.T. Scardino, and V.E. Reuter. 2007. Anatomy of the anterior prostate and extraprostatic space: a

contemporary surgical pathology analysis. *Advances in anatomic pathology*. 14:401-407.
Fine, S.W., and V.E. Reuter. 2012. Anatomy of the prostate revisited: implications for prostate biopsy and zonal origins of prostate cancer. *Histopathology*. 60:142-152.
Fizazi, K., and N.M. Navone. 2005. [Preclinical models of prostate cancer]. *Bulletin du cancer*. 92:129-141.
Frick, J., and W. Aulitzky. 1991. Physiology of the prostate. *Infection*. 19 Suppl 3:S115-118.
Fuchs, E. 2009. Finding one's niche in the skin. *Cell stem cell*. 4:499-502.
Gao, N., K. Ishii, J. Mirosevich, S. Kuwajima, S.R. Oppenheimer, R.L. Roberts, M. Jiang, X. Yu, S.B. Shappell, R.M. Caprioli, M. Stoffel, S.W. Hayward, and R.J. Matusik. 2005. Forkhead box A1 regulates prostate ductal morphogenesis and promotes epithelial cell maturation. *Development*. 132:3431-3443.
Gilbert, S.F. 2000. Developmental Biology. Swarthmore College
Sunderland (MA): Sinauer Associates.
Gleason, D.F. 1966. Classification of prostatic carcinomas. *Cancer chemotherapy reports. Part 1*. 50:125-128.
Gleason, D.F. 1992. Histologic grading of prostate cancer: a perspective. *Human pathology*. 23:273-279.
Gleason, D.F., and G.T. Mellinger. 1974. Prediction of prognosis for prostatic adenocarcinoma by combined histological grading and clinical staging. *J Urol*. 111:58-64.
Grignon, D.J. 2004. Unusual subtypes of prostate cancer. *Mod Pathol*. 17:316-327.
Grishina, I.B., S.Y. Kim, C. Ferrara, H.P. Makarenkova, and P.D. Walden. 2005. BMP7 inhibits branching morphogenesis in the prostate gland and interferes with Notch signaling. *Dev Biol*. 288:334-347.
Groskopf, J., S.M. Aubin, I.L. Deras, A. Blase, S. Bodrug, C. Clark, S. Brentano, J. Mathis, J. Pham, T. Meyer, M. Cass, P. Hodge, M.L. Macairan, L.S. Marks, and H. Rittenhouse. 2006. APTIMA PCA3 molecular urine test: development of a method to aid in the diagnosis of prostate cancer. *Clinical chemistry*. 52:1089-1095.
Gu, Y., H. Li, J. Miki, K.H. Kim, B. Furusato, I.A. Sesterhenn, W.S. Chu, D.G. McLeod, S. Srivastava, C.M. Ewing, W.B. Isaacs, and J.S. Rhim. 2006. Phenotypic characterization of telomerase-immortalized primary non-malignant and malignant tumor-derived human prostate epithelial cell lines. *Exp Cell Res*. 312:831-843.
Hall, A. 1998. Rho GTPases and the actin cytoskeleton. *Science*. 279:509-514.
Hanahan, D., and R.A. Weinberg. 2011. Hallmarks of cancer: the next generation. *Cell*. 144:646-674.
Harma, V., J. Virtanen, R. Makela, A. Happonen, J.P. Mpindi, M. Knuuttila, P. Kohonen, J. Lotjonen, O. Kallioniemi, and M. Nees. 2010. A comprehensive panel of three-dimensional models for studies of prostate cancer growth, invasion and drug responses. *PLoS One*. 5:e10431.
Hay, E.D. 1995. An overview of epithelio-mesenchymal transformation. *Acta Anat (Basel)*. 154:8-20.

Hessels, D., J.M. Klein Gunnewiek, I. van Oort, H.F. Karthaus, G.J. van Leenders, B. van Balken, L.A. Kiemeney, J.A. Witjes, and J.A. Schalken. 2003. DD3(PCA3)-based molecular urine analysis for the diagnosis of prostate cancer. *European urology*. 44:8-15; discussion 15-16.

Honardoust, H.A., G. Jiang, L. Koivisto, D. Wienke, C.M. Isacke, H. Larjava, and L. Hakkinen. 2006. Expression of Endo180 is spatially and temporally regulated during wound healing. *Histopathology*. 49:634-648.

Horoszewicz, J.S., S.S. Leong, T.M. Chu, Z.L. Wajsman, M. Friedman, L. Papsidero, U. Kim, L.S. Chai, S. Kakati, S.K. Arya, and A.A. Sandberg. 1980. The LNCaP cell line--a new model for studies on human prostatic carcinoma. *Progress in clinical and biological research*. 37:115-132.

Horoszewicz, J.S., S.S. Leong, E. Kawinski, J.P. Karr, H. Rosenthal, T.M. Chu, E.A. Mirand, and G.P. Murphy. 1983. LNCaP model of human prostatic carcinoma. *Cancer Res*. 43:1809-1818.

Horwich, A., and C. Parker. 2007. Prostate cancer: ESMO clinical recommendations for diagnosis, treatment and follow-up. *Annals of oncology : official journal of the European Society for Medical Oncology / ESMO*. 18 Suppl 2:ii36-37.

Howard, M.J., M.G. Chambers, R.M. Mason, and C.M. Isacke. 2004. Distribution of Endo180 receptor and ligand in developing articular cartilage. *Osteoarthritis Cartilage*. 12:74-82.

Howard, M.J., and C.M. Isacke. 2002. The C-type lectin receptor Endo180 displays internalization and recycling properties distinct from other members of the mannose receptor family. *J Biol Chem*. 277:32320-32331.

Huang, L., Y. Pu, D. Hepps, D. Danielpour, and G.S. Prins. 2007. Posterior Hox gene expression and differential androgen regulation in the developing and adult rat prostate lobes. *Endocrinology*. 148:1235-1245.

Huang, L., Y. Pu, W.Y. Hu, L. Birch, D. Luccio-Camelo, T. Yamaguchi, and G.S. Prins. 2009. The role of Wnt5a in prostate gland development. *Dev Biol*. 328:188-199.

Huber, M.A., N. Kraut, and H. Beug. 2005. Molecular requirements for epithelial-mesenchymal transition during tumor progression. *Curr Opin Cell Biol*. 17:548-558.

Hudson, D.L. 2004. Epithelial stem cells in human prostate growth and disease. *Prostate cancer and prostatic diseases*. 7:188-194.

Hudson, D.L., A.T. Guy, P. Fry, M.J. O'Hare, F.M. Watt, and J.R. Masters. 2001. Epithelial cell differentiation pathways in the human prostate: identification of intermediate phenotypes by keratin expression. *J Histochem Cytochem*. 49:271-278.

Huijbers, I.J., M. Iravani, S. Popov, D. Robertson, S. Al-Sarraj, C. Jones, and C.M. Isacke. 2010. A role for fibrillar collagen deposition and the collagen internalization receptor endo180 in glioma invasion. *PLoS One*. 5:e9808.

Isacke, C.M., P. van der Geer, T. Hunter, and I.S. Trowbridge. 1990. p180, a novel recycling transmembrane glycoprotein with restricted cell type expression. *Mol Cell Biol*. 10:2606-2618.

Itoh, N., U. Patel, A.S. Cupp, and M.K. Skinner. 1998. Developmental and hormonal regulation of transforming growth factor-beta1 (TGFbeta1), -2, and -3 gene

expression in isolated prostatic epithelial and stromal cells: epidermal growth factor and TGFbeta interactions. *Endocrinology*. 139:1378-1388.
Ivetic, A., and A.J. Ridley. 2004. Ezrin/radixin/moesin proteins and Rho GTPase signalling in leucocytes. *Immunology*. 112:165-176.
Jaffe, A.B., and A. Hall. 2005. Rho GTPases: biochemistry and biology. *Annual review of cell and developmental biology*. 21:247-269.
Joesting, M.S., S. Perrin, B. Elenbaas, S.E. Fawell, J.S. Rubin, O.E. Franco, S.W. Hayward, G.R. Cunha, and P.C. Marker. 2005. Identification of SFRP1 as a candidate mediator of stromal-to-epithelial signaling in prostate cancer. *Cancer Res*. 65:10423-10430.
Johansson, K.A., and A. Grapin-Botton. 2002. Development and diseases of the pancreas. *Clinical genetics*. 62:14-23.
Jones, G.E., W.E. Allen, and A.J. Ridley. 1998. The Rho GTPases in macrophage motility and chemotaxis. *Cell adhesion and communication*. 6:237-245.
Jurgensen, H.J., D.H. Madsen, S. Ingvarsen, M.C. Melander, H. Gardsvoll, L. Patthy, L.H. Engelholm, and N. Behrendt. 2011. A novel functional role of collagen glycosylation: Interaction with the endocytic receptor uPARAP/Endo180. *J Biol Chem*.
Juyena, N.S., and C. Stelletta. 2012. Seminal plasma: an essential attribute to spermatozoa. *Journal of andrology*. 33:536-551.
Kaighn, M.E., K.S. Narayan, Y. Ohnuki, J.F. Lechner, and L.W. Jones. 1979. Establishment and characterization of a human prostatic carcinoma cell line (PC-3). *Investigative urology*. 17:16-23.
Kalluri, R., and R.A. Weinberg. 2009. The basics of epithelial-mesenchymal transition. *The Journal of clinical investigation*. 119:1420-1428.
Kang, J., M.S. Lee, and D.G. Gorenstein. 2005. The enhancement of PCR amplification of a random sequence DNA library by DMSO and betaine: application to in vitro combinatorial selection of aptamers. *Journal of biochemical and biophysical methods*. 64:147-151.
Kareskoski, M., and T. Katila. 2008. Components of stallion seminal plasma and the effects of seminal plasma on sperm longevity. *Animal reproduction science*. 107:249-256.
Khoshnoodi, J., V. Pedchenko, and B.G. Hudson. 2008. Mammalian collagen IV. *Microscopy research and technique*. 71:357-370.
Kim, M.J., R. Bhatia-Gaur, W.A. Banach-Petrosky, N. Desai, Y. Wang, S.W. Hayward, G.R. Cunha, R.D. Cardiff, M.M. Shen, and C. Abate-Shen. 2002. Nkx3.1 mutant mice recapitulate early stages of prostate carcinogenesis. *Cancer Res*. 62:2999-3004.
Kimelman, D. 2006. Mesoderm induction: from caps to chips. *Nat Rev Genet*. 7:360-372.
Kinoshita, E., E. Kinoshita-Kikuta, and T. Koike. 2009. Separation and detection of large phosphoproteins using Phos-tag SDS-PAGE. *Nature protocols*. 4:1513-1521.
Kjoller, L., L.H. Engelholm, M. Hoyer-Hansen, K. Dano, T.H. Bugge, and N. Behrendt. 2004. uPARAP/endo180 directs lysosomal delivery and degradation of collagen IV. *Exp Cell Res*. 293:106-116.

Kogianni, G., M.M. Walker, J. Waxman, and J. Sturge. 2009. Endo180 expression with cofunctional partners MT1-MMP and uPAR-uPA is correlated with prostate cancer progression. *Eur J Cancer*. 45:685-693.

Kokkinos, M.I., R. Wafai, M.K. Wong, D.F. Newgreen, E.W. Thompson, and M. Waltham. 2007. Vimentin and epithelial-mesenchymal transition in human breast cancer--observations in vitro and in vivo. *Cells Tissues Organs*. 185:191-203.

Komura, K., T. Inamoto, M. Tsuji, N. Ibuki, K. Koyama, T. Ubai, H. Azuma, and Y. Katsuoka. 2010. Basal cell carcinoma of the prostate: unusual subtype of prostatic carcinoma. *International journal of clinical oncology / Japan Society of Clinical Oncology*. 15:594-600.

Kopachik, W., S.W. Hayward, and G.R. Cunha. 1998. Expression of hepatocyte nuclear factor-3alpha in rat prostate, seminal vesicle, and bladder. *Developmental dynamics : an official publication of the American Association of Anatomists*. 211:131-140.

Kozma, R., S. Ahmed, A. Best, and L. Lim. 1995. The Ras-related protein Cdc42Hs and bradykinin promote formation of peripheral actin microspikes and filopodia in Swiss 3T3 fibroblasts. *Mol Cell Biol*. 15:1942-1952.

Kumar, V.L., and P.K. Majumder. 1995. Prostate gland: structure, functions and regulation. *International urology and nephrology*. 27:231-243.

Kuslak, S.L., and P.C. Marker. 2007. Fibroblast growth factor receptor signaling through MEK-ERK is required for prostate bud induction. *Differentiation; research in biological diversity*. 75:638-651.

Lamm, M.L., W.S. Catbagan, R.J. Laciak, D.H. Barnett, C.M. Hebner, W. Gaffield, D. Walterhouse, P. Iannaccone, and W. Bushman. 2002. Sonic hedgehog activates mesenchymal Gli1 expression during prostate ductal bud formation. *Dev Biol*. 249:349-366.

Lee, C.H., O. Akin-Olugbade, and A. Kirschenbaum. 2011. Overview of prostate anatomy, histology, and pathology. *Endocrinology and metabolism clinics of North America*. 40:565-575, viii-ix.

Lee, J.M., S. Dedhar, R. Kalluri, and E.W. Thompson. 2006. The epithelial-mesenchymal transition: new insights in signaling, development, and disease. *J Cell Biol*. 172:973-981.

Leman, E.S., G.W. Cannon, B.J. Trock, L.J. Sokoll, D.W. Chan, L. Mangold, A.W. Partin, and R.H. Getzenberg. 2007. EPCA-2: a highly specific serum marker for prostate cancer. *Urology*. 69:714-720.

Li, H., A. Kapur, J.X. Yang, S. Srivastava, D.G. McLeod, J.F. Paredes-Guzman, A. Daugsch, Y.K. Park, and J.S. Rhim. 2007. Antiproliferation of human prostate cancer cells by ethanolic extracts of Brazilian propolis and its botanical origin. *International journal of oncology*. 31:601-606.

Li, H., J. Zhou, J. Miki, B. Furusato, Y. Gu, S. Srivastava, D.G. McLeod, J.C. Vogel, and J.S. Rhim. 2008. Telomerase-immortalized non-malignant human prostate epithelial cells retain the properties of multipotent stem cells. *Exp Cell Res*. 314:92-102.

Liang, O.D., T. Chavakis, M. Linder, K. Bdeir, A. Kuo, and K.T. Preissner. 2003. Binding of urokinase plasminogen activator to gp130 via a putative urokinase-binding consensus sequence. *Biol Chem*. 384:229-236.

Llorca, O. 2008. Extended and bent conformations of the mannose receptor family. *Cell Mol Life Sci*. 65:1302-1310.

Long, R.M., C. Morrissey, J.M. Fitzpatrick, and R.W. Watson. 2005. Prostate epithelial cell differentiation and its relevance to the understanding of prostate cancer therapies. *Clin Sci (Lond)*. 108:1-11.

Madsen, D.H., L.H. Engelholm, S. Ingvarsen, T. Hillig, R.A. Wagenaar-Miller, L. Kjoller, H. Gardsvoll, G. Hoyer-Hansen, K. Holmbeck, T.H. Bugge, and N. Behrendt. 2007. Extracellular collagenases and the endocytic receptor, urokinase plasminogen activator receptor-associated protein/Endo180, cooperate in fibroblast-mediated collagen degradation. *J Biol Chem*. 282:27037-27045.

Madsen, D.H., S. Ingvarsen, H.J. Jurgensen, M.C. Melander, L. Kjoller, A. Moyer, C. Honore, C.A. Madsen, P. Garred, S. Burgdorf, T.H. Bugge, N. Behrendt, and L.H. Engelholm. 2011. The Non-phagocytic Route of Collagen Uptake: A DISTINCT DEGRADATION PATHWAY. *J Biol Chem*. 286:26996-27010.

Makarov, D.V., S. Loeb, R.H. Getzenberg, and A.W. Partin. 2009. Biomarkers for prostate cancer. *Annual review of medicine*. 60:139-151.

Martinez, H.D., R.J. Jasavala, I. Hinkson, L.D. Fitzgerald, J.S. Trimmer, H.J. Kung, and M.E. Wright. 2008. RNA editing of androgen receptor gene transcripts in prostate cancer cells. *J Biol Chem*. 283:29938-29949.

Martinez-Pomares, L., D. Wienke, R. Stillion, E.J. McKenzie, J.N. Arnold, J. Harris, E. McGreal, R.B. Sim, C.M. Isacke, and S. Gordon. 2006. Carbohydrate-independent recognition of collagens by the macrophage mannose receptor. *Eur J Immunol*. 36:1074-1082.

Martini, F., and W.C. Ober. 2006. Fundamentals of anatomy and physiology. Pearson/Benjamin Cummings, San Francisco. 1 vol. (various pagings) pp.

McNeal, J.E. 1981. The zonal anatomy of the prostate. *The Prostate*. 2:35-49.

Meeks, J.J., and E.M. Schaeffer. 2011. Genetic regulation of prostate development. *Journal of andrology*. 32:210-217.

Menoret, M. 2002. The genesis of the notion of stages in oncology: the French Permanent Cancer Survey (1943-1952). *Social history of medicine : the journal of the Society for the Social History of Medicine / SSHM*. 15:291-302.

Messaritou, G., L. East, C. Roghi, C.M. Isacke, and H. Yarwood. 2009. Membrane type-1 matrix metalloproteinase activity is regulated by the endocytic collagen receptor Endo180. *J Cell Sci*. 122:4042-4048.

Mickey, D.D., K.R. Stone, H. Wunderli, G.H. Mickey, and D.F. Paulson. 1980. Characterization of a human prostate adenocarcinoma cell line (DU 145) as a monolayer culture and as a solid tumor in athymic mice. *Progress in clinical and biological research*. 37:67-84.

Miki, J., B. Furusato, H. Li, Y. Gu, H. Takahashi, S. Egawa, I.A. Sesterhenn, D.G. McLeod, S. Srivastava, and J.S. Rhim. 2007. Identification of putative stem cell markers, CD133 and CXCR4, in hTERT-immortalized primary nonmalignant and malignant tumor-derived human prostate epithelial cell lines and in prostate cancer specimens. *Cancer Res*. 67:3153-3161.

Miller, D.C., K.S. Hafez, A. Stewart, J.E. Montie, and J.T. Wei. 2003. Prostate carcinoma presentation, diagnosis, and staging: an update form the National Cancer Data Base. *Cancer*. 98:1169-1178.

Mirosevich, J., N. Gao, and R.J. Matusik. 2005. Expression of Foxa transcription factors in the developing and adult murine prostate. *The Prostate*. 62:339-352.

Montironi, R., R. Mazzucchelli, D. Stramazzotti, M. Scarpelli, A. Lopez Beltran, and D.G. Bostwick. 2005. Basal cell hyperplasia and basal cell carcinoma of the prostate: a comprehensive review and discussion of a case with c-erbB-2 expression. *J Clin Pathol*. 58:290-296.

Mousavi, S.A., M.S. Fonhus, and T. Berg. 2009. Up-regulation of uPARAP/Endo180 during culture activation of rat hepatic stellate cells and its presence in hepatic stellate cell lines from different species. *BMC Cell Biol*. 10:39.

Mousavi, S.A., M. Sato, M. Sporstol, B. Smedsrod, T. Berg, N. Kojima, and H. Senoo. 2005. Uptake of denatured collagen into hepatic stellate cells: evidence for the involvement of urokinase plasminogen activator receptor-associated protein/Endo180. *Biochem J*. 387:39-46.

Muino-Blanco, T., R. Perez-Pe, and J.A. Cebrian-Perez. 2008. Seminal plasma proteins and sperm resistance to stress. *Reproduction in domestic animals = Zuchthygiene*. 43 Suppl 4:18-31.

Nakajima, Y., T. Yamagishi, S. Hokari, and H. Nakamura. 2000. Mechanisms involved in valvuloseptal endocardial cushion formation in early cardiogenesis: roles of transforming growth factor (TGF)-beta and bone morphogenetic protein (BMP). *The Anatomical record*. 258:119-127.

Nauseef, J.T., and M.D. Henry. 2011. Epithelial-to-mesenchymal transition in prostate cancer: paradigm or puzzle? *Nature reviews. Urology*. 8:428-439.

Nobes, C.D., and A. Hall. 1995. Rho, rac, and cdc42 GTPases regulate the assembly of multimolecular focal complexes associated with actin stress fibers, lamellipodia, and filopodia. *Cell*. 81:53-62.

Nystrom, M.L., G.J. Thomas, M. Stone, I.C. Mackenzie, I.R. Hart, and J.F. Marshall. 2005. Development of a quantitative method to analyse tumour cell invasion in organotypic culture. *J Pathol*. 205:468-475.

Oefelein, M., C. Chin-Chance, and W. Bushman. 1996. Expression of the homeotic gene Hox-d13 in the developing and adult mouse prostate. *J Urol*. 155:342-346.

Ohori, M., T.M. Wheeler, and P.T. Scardino. 1994. The New American Joint Committee on Cancer and International Union Against Cancer TNM classification of prostate cancer. Clinicopathologic correlations. *Cancer*. 74:104-114.

Okamura, D.M., K. Pasichnyk, J.M. Lopez-Guisa, S. Collins, D.K. Hsu, F.T. Liu, and A.A. Eddy. 2011. Galectin-3 preserves renal tubules and modulates extracellular matrix remodeling in progressive fibrosis. *American journal of physiology. Renal physiology*. 300:F245-253.

Osunkoya, A.O. 2012. Update on prostate pathology. *Pathology*. 44:391-406.

Palmieri, C., M.P. Caley, K. Purshouse, A.V. Fonseca, M. Rodriguez-Teja, G. Kogianni, L. Woodley, J. Odendaal, K. Elliott, J. Waxman, and J. Sturge. 2013. Endo180

modulation by bisphosphonates and diagnostic accuracy in metastatic breast cancer. *British journal of cancer*. 108:163-169.
Podlasek, C.A., D.H. Barnett, J.Q. Clemens, P.M. Bak, and W. Bushman. 1999a. Prostate development requires Sonic hedgehog expressed by the urogenital sinus epithelium. *Dev Biol*. 209:28-39.
Podlasek, C.A., J.Q. Clemens, and W. Bushman. 1999b. Hoxa-13 gene mutation results in abnormal seminal vesicle and prostate development. *J Urol*. 161:1655-1661.
Podlasek, C.A., D. Duboule, and W. Bushman. 1997. Male accessory sex organ morphogenesis is altered by loss of function of Hoxd-13. *Developmental dynamics : an official publication of the American Association of Anatomists*. 208:454-465.
Polascik, T.J., J.E. Oesterling, and A.W. Partin. 1999. Prostate specific antigen: a decade of discovery--what we have learned and where we are going. *J Urol*. 162:293-306.
Prins, G.S., L. Huang, L. Birch, and Y. Pu. 2006. The role of estrogens in normal and abnormal development of the prostate gland. *Annals of the New York Academy of Sciences*. 1089:1-13.
Prins, G.S., and O. Putz. 2008. Molecular signaling pathways that regulate prostate gland development. *Differentiation; research in biological diversity*. 76:641-659.
Pu, Y., L. Huang, L. Birch, and G.S. Prins. 2007. Androgen regulation of prostate morphoregulatory gene expression: Fgf10-dependent and -independent pathways. *Endocrinology*. 148:1697-1706.
Pu, Y., L. Huang, and G.S. Prins. 2004. Sonic hedgehog-patched Gli signaling in the developing rat prostate gland: lobe-specific suppression by neonatal estrogens reduces ductal growth and branching. *Dev Biol*. 273:257-275.
Raghow, S., E. Shapiro, and M.S. Steiner. 1999. Immunohistochemical localization of transforming growth factor-alpha and transforming growth factor-beta during early human fetal prostate development. *J Urol*. 162:509-513.
Ridley, A., M. Peckham, and C. P. 2004. Cell Motility. Wiley.
Ridley, A.J., and A. Hall. 1992. The small GTP-binding protein rho regulates the assembly of focal adhesions and actin stress fibers in response to growth factors. *Cell*. 70:389-399.
Ridley, A.J., H.F. Paterson, C.L. Johnston, D. Diekmann, and A. Hall. 1992. The small GTP-binding protein rac regulates growth factor-induced membrane ruffling. *Cell*. 70:401-410.
Rivera-Calzada, A., D. Robertson, J.R. MacFadyen, J. Boskovic, C.M. Isacke, and O. Llorca. 2003. Three-dimensional interplay among the ligand-binding domains of the urokinase-plasminogen-activator-receptor-associated protein, Endo180. *EMBO Rep*. 4:807-812.
Robinson, E.J., D.E. Neal, and A.T. Collins. 1998. Basal cells are progenitors of luminal cells in primary cultures of differentiating human prostatic epithelium. *The Prostate*. 37:149-160.

Rodriguez-Martinez, H., U. Kvist, J. Ernerudh, L. Sanz, and J.J. Calvete. 2011. Seminal plasma proteins: what role do they play? *Am J Reprod Immunol*. 66 Suppl 1:11-22.
Sahadevan, K., S. Darby, H.Y. Leung, M.E. Mathers, C.N. Robson, and V.J. Gnanapragasam. 2007. Selective over-expression of fibroblast growth factor receptors 1 and 4 in clinical prostate cancer. *J Pathol*. 213:82-90.
Schnack Nielsen, B., F. Rank, L.H. Engelholm, A. Holm, K. Dano, and N. Behrendt. 2002. Urokinase receptor-associated protein (uPARAP) is expressed in connection with malignant as well as benign lesions of the human breast and occurs in specific populations of stromal cells. *Int J Cancer*. 98:656-664.
Schneider, A., T. Brand, R. Zweigerdt, and H. Arnold. 2000. Targeted disruption of the Nkx3.1 gene in mice results in morphogenetic defects of minor salivary glands: parallels to glandular duct morphogenesis in prostate. *Mechanisms of development*. 95:163-174.
Sciavolino, P.J., E.W. Abrams, L. Yang, L.P. Austenberg, M.M. Shen, and C. Abate-Shen. 1997. Tissue-specific expression of murine Nkx3.1 in the male urogenital system. *Developmental dynamics : an official publication of the American Association of Anatomists*. 209:127-138.
Sheikh, H., H. Yarwood, A. Ashworth, and C.M. Isacke. 2000. Endo180, an endocytic recycling glycoprotein related to the macrophage mannose receptor is expressed on fibroblasts, endothelial cells and macrophages and functions as a lectin receptor. *J Cell Sci*. 113 ( Pt 6):1021-1032.
Sherwood, L. 2013. Human physiology : from cells to systems. Brooks/Cole Cengage Learning, Belmont, Calif. 1 v. (various pagings) pp.
Shi, F., J. Harman, K. Fujiwara, and J. Sottile. 2010. Collagen I matrix turnover is regulated by fibronectin polymerization. *Am J Physiol Cell Physiol*. 298:C1265-1275.
Shidaifat, F., B. Al-Trad, and R. Al-Omari. 2007. Testosterone effect on immature prostate gland development associated with suppression of transforming growth factor-beta. *Life sciences*. 80:829-834.
Shou, J., S. Ross, H. Koeppen, F.J. de Sauvage, and W.Q. Gao. 2001. Dynamics of notch expression during murine prostate development and tumorigenesis. *Cancer Res*. 61:7291-7297.
Singer, E.A., D.J. Golijanin, H. Miyamoto, and E.M. Messing. 2008. Androgen deprivation therapy for prostate cancer. *Expert opinion on pharmacotherapy*. 9:211-228.
Sinha, A.A., and M.D. Bentley. 1984. The relationship of epithelial cell types in the ventral prostate glands of castrated mice treated with testosterone. *The Anatomical record*. 208:533-544.
Slabakova, E., Z. Pernicova, E. Slavickova, A. Starsichova, A. Kozubik, and K. Soucek. 2011. TGF-beta1-induced EMT of non-transformed prostate hyperplasia cells is characterized by early induction of SNAI2/Slug. *The Prostate*. 71:1332-1343.
Smith, H.W., and C.J. Marshall. 2010. Regulation of cell signalling by uPAR. *Nat Rev Mol Cell Biol*. 11:23-36.

Smith, L., T.E. Wagner, I. Huizar, and L.M. Schnapp. 2008. uPARAP expression during murine lung development. *Gene expression patterns : GEP*. 8:486-493.
Sobin, L.H., M.K. Gospodarowicz, and C. Wittekind. 2009. TNM Classification of Malignant Tumours. Wiley-Blackwell.
Sokoll, L.J., W. Ellis, P. Lange, J. Noteboom, D.J. Elliott, I.L. Deras, A. Blase, S. Koo, M. Sarno, H. Rittenhouse, J. Groskopf, and R.L. Vessella. 2008. A multicenter evaluation of the PCA3 molecular urine test: pre-analytical effects, analytical performance, and diagnostic accuracy. *Clinica chimica acta; international journal of clinical chemistry*. 389:1-6.
Soller, M.J., M. Isaksson, P. Elfving, W. Soller, R. Lundgren, and I. Panagopoulos. 2006. Confirmation of the high frequency of the TMPRSS2/ERG fusion gene in prostate cancer. *Genes, chromosomes & cancer*. 45:717-719.
Sreenath, T., A. Orosz, K. Fujita, and C.J. Bieberich. 1999. Androgen-independent expression of hoxb-13 in the mouse prostate. *The Prostate*. 41:203-207.
Standring, S., and H. Gray. 2008. Gray's anatomy : the anatomical basis of clinical practice. Churchill Livingstone, Edinburgh. xxiv, 1551 p. pp.
Sturge, J., S.K. Todd, G. Kogianni, A. McCarthy, and C.M. Isacke. 2007. Mannose receptor regulation of macrophage cell migration. *J Leukoc Biol*. 82:585-593.
Sturge, J., D. Wienke, L. East, G.E. Jones, and C.M. Isacke. 2003. GPI-anchored uPAR requires Endo180 for rapid directional sensing during chemotaxis. *J Cell Biol*. 162:789-794.
Sturge, J., D. Wienke, and C.M. Isacke. 2006. Endosomes generate localized Rho-ROCK-MLC2-based contractile signals via Endo180 to promote adhesion disassembly. *J Cell Biol*. 175:337-347.
Sulek, J., R.A. Wagenaar-Miller, J. Shireman, A. Molinolo, D.H. Madsen, L.H. Engelholm, N. Behrendt, and T.H. Bugge. 2007. Increased expression of the collagen internalization receptor uPARAP/Endo180 in the stroma of head and neck cancer. *J Histochem Cytochem*. 55:347-353.
Takahashi, S., H. Yamada-Okabe, K. Hamada, S. Ohta, T. Kawase, K. Yoshida, and M. Toda. 2011. Downregulation of uPARAP mediates cytoskeletal rearrangements and decreases invasion and migration properties in glioma cells. *Journal of neuro-oncology*. 103:267-276.
Takahashi, Y., J. Hamada, K. Murakawa, M. Takada, M. Tada, I. Nogami, N. Hayashi, S. Nakamori, M. Monden, M. Miyamoto, H. Katoh, and T. Moriuchi. 2004. Expression profiles of 39 HOX genes in normal human adult organs and anaplastic thyroid cancer cell lines by quantitative real-time RT-PCR system. *Exp Cell Res*. 293:144-153.
Tanaka, M., I. Komuro, H. Inagaki, N.A. Jenkins, N.G. Copeland, and S. Izumo. 2000. Nkx3.1, a murine homolog of Ddrosophila bagpipe, regulates epithelial ductal branching and proliferation of the prostate and palatine glands. *Developmental dynamics : an official publication of the American Association of Anatomists*. 219:248-260.
Tanji, N., M. Tsuji, N. Terada, M. Takeuchi, and G.R. Cunha. 1994. Inhibitory effects of transforming growth factor-beta 1 on androgen-induced development of neonatal mouse seminal vesicles in vitro. *Endocrinology*. 134:1155-1162.

Taplin, M.E. 2007. Drug insight: role of the androgen receptor in the development and progression of prostate cancer. *Nature clinical practice. Oncology*. 4:236-244.

Tarin, D., E.W. Thompson, and D.F. Newgreen. 2005. The fallacy of epithelial mesenchymal transition in neoplasia. *Cancer Res*. 65:5996-6000; discussion 6000-5991.

Tarui, T., N. Akakura, M. Majumdar, N. Andronicos, J. Takagi, A.P. Mazar, K. Bdeir, A. Kuo, S.V. Yarovoi, D.B. Cines, and Y. Takada. 2006. Direct interaction of the kringle domain of urokinase-type plasminogen activator (uPA) and integrin alpha v beta 3 induces signal transduction and enhances plasminogen activation. *Thrombosis and haemostasis*. 95:524-534.

Thibodeau, G.A., and K.T. Patton. 1999. Anatomy & physiology. Mosby, St. Louis London. xxxiii, 1083 p pp.

Thiery, J.P. 1984. Mechanisms of cell migration in the vertebrate embryo. *Cell differentiation*. 15:1-15.

Thiery, J.P. 2002. Epithelial-mesenchymal transitions in tumour progression. *Nat Rev Cancer*. 2:442-454.

Thiery, J.P., H. Acloque, R.Y. Huang, and M.A. Nieto. 2009. Epithelial-mesenchymal transitions in development and disease. *Cell*. 139:871-890.

Thiery, J.P., and J.P. Sleeman. 2006. Complex networks orchestrate epithelial-mesenchymal transitions. *Nat Rev Mol Cell Biol*. 7:131-142.

Thomas, E.K., M. Nakamura, D. Wienke, C.M. Isacke, A. Pozzi, and P. Liang. 2005. Endo180 binds to the C-terminal region of type I collagen. *J Biol Chem*. 280:22596-22605.

Thompson, I.M., D.K. Pauler, P.J. Goodman, C.M. Tangen, M.S. Lucia, H.L. Parnes, L.M. Minasian, L.G. Ford, S.M. Lippman, E.D. Crawford, J.J. Crowley, and C.A. Coltman, Jr. 2004. Prevalence of prostate cancer among men with a prostate-specific antigen level < or =4.0 ng per milliliter. *The New England journal of medicine*. 350:2239-2246.

Thomson, A.A., and P.C. Marker. 2006. Branching morphogenesis in the prostate gland and seminal vesicles. *Differentiation; research in biological diversity*. 74:382-392.

Timme, T.L., L.D. Truong, V.W. Merz, T. Krebs, D. Kadmon, K.C. Flanders, S.H. Park, and T.C. Thompson. 1994. Mesenchymal-epithelial interactions and transforming growth factor-beta expression during mouse prostate morphogenesis. *Endocrinology*. 134:1039-1045.

Tomida, J., H. Kitao, E. Kinoshita, and M. Takata. 2008. Detection of phosphorylation on large proteins by western blotting using Phos-tag containing gel. *Protocol Exchange*.

Tomlins, S.A., D.R. Rhodes, S. Perner, S.M. Dhanasekaran, R. Mehra, X.W. Sun, S. Varambally, X. Cao, J. Tchinda, R. Kuefer, C. Lee, J.E. Montie, R.B. Shah, K.J. Pienta, M.A. Rubin, and A.M. Chinnaiyan. 2005. Recurrent fusion of TMPRSS2 and ETS transcription factor genes in prostate cancer. *Science*. 310:644-648.

Tomlinson, D.C., S.H. Freestone, O.C. Grace, and A.A. Thomson. 2004. Differential effects of transforming growth factor-beta1 on cellular proliferation in the developing prostate. *Endocrinology*. 145:4292-4300.

Van Aelst, L., and C. D'Souza-Schorey. 1997. Rho GTPases and signaling networks. *Genes & development*. 11:2295-2322.
van der Cruijsen-Koeter, I.W., A.N. Vis, M.J. Roobol, M.F. Wildhagen, H.J. de Koning, T.H. van der Kwast, and F.H. Schroder. 2005. Comparison of screen detected and clinically diagnosed prostate cancer in the European randomized study of screening for prostate cancer, section rotterdam. *J Urol*. 174:121-125.
van Dorst, E.B., G.N. van Muijen, S.V. Litvinov, and G.J. Fleuren. 1998. The limited difference between keratin patterns of squamous cell carcinomas and adenocarcinomas is explicable by both cell lineage and state of differentiation of tumour cells. *J Clin Pathol*. 51:679-684.
van Gils, M.P., D. Hessels, O. van Hooij, S.A. Jannink, W.P. Peelen, S.L. Hanssen, J.A. Witjes, E.B. Cornel, H.F. Karthaus, G.A. Smits, G.A. Dijkman, P.F. Mulders, and J.A. Schalken. 2007. The time-resolved fluorescence-based PCA3 test on urinary sediments after digital rectal examination; a Dutch multicenter validation of the diagnostic performance. *Clinical cancer research : an official journal of the American Association for Cancer Research*. 13:939-943.
van Leenders, G., H. Dijkman, C. Hulsbergen-van de Kaa, D. Ruiter, and J. Schalken. 2000. Demonstration of intermediate cells during human prostate epithelial differentiation in situ and in vitro using triple-staining confocal scanning microscopy. *Lab Invest*. 80:1251-1258.
van Leenders, G.J., and J.A. Schalken. 2003. Epithelial cell differentiation in the human prostate epithelium: implications for the pathogenesis and therapy of prostate cancer. *Crit Rev Oncol Hematol*. 46 Suppl:S3-10.
Verhagen, A.P., T.W. Aalders, F.C. Ramaekers, F.M. Debruyne, and J.A. Schalken. 1988. Differential expression of keratins in the basal and luminal compartments of rat prostatic epithelium during degeneration and regeneration. *The Prostate*. 13:25-38.
Viebahn, C. 1995. Epithelio-mesenchymal transformation during formation of the mesoderm in the mammalian embryo. *Acta Anat (Basel)*. 154:79-97.
Vincent-Salomon, A., and J.P. Thiery. 2003. Host microenvironment in breast cancer development: epithelial-mesenchymal transition in breast cancer development. *Breast Cancer Res*. 5:101-106.
Wagenaar-Miller, R.A., L.H. Engelholm, J. Gavard, S.S. Yamada, J.S. Gutkind, N. Behrendt, T.H. Bugge, and K. Holmbeck. 2007. Complementary roles of intracellular and pericellular collagen degradation pathways in vivo. *Mol Cell Biol*. 27:6309-6322.
Walker, M.M., S.M. Ellis, M.J. Auza, A. Patel, and P. Clark. 2008. The intercellular adhesion molecule, cadherin-10, is a marker for human prostate luminal epithelial cells that is not expressed in prostate cancer. *Mod Pathol*. 21:85-95.
Walsh, P.C., and P.J. Donker. 1982. Impotence following radical prostatectomy: insight into etiology and prevention. *J Urol*. 128:492-497.
Walz, J., M. Graefen, and H. Huland. 2011. Surgical anatomy of the prostate in the era of radical robotic prostatectomy. *Current opinion in urology*. 21:173-178.
Wang, X.D., C.C. Leow, J. Zha, Z. Tang, Z. Modrusan, F. Radtke, M. Aguet, F.J. de Sauvage, and W.Q. Gao. 2006. Notch signaling is required for normal prostatic epithelial cell proliferation and differentiation. *Dev Biol*. 290:66-80.

Wang, X.D., J. Shou, P. Wong, D.M. French, and W.Q. Gao. 2004. Notch1-expressing cells are indispensable for prostatic branching morphogenesis during development and re-growth following castration and androgen replacement. *J Biol Chem*. 279:24733-24744.

Warot, X., C. Fromental-Ramain, V. Fraulob, P. Chambon, and P. Dolle. 1997. Gene dosage-dependent effects of the Hoxa-13 and Hoxd-13 mutations on morphogenesis of the terminal parts of the digestive and urogenital tracts. *Development*. 124:4781-4791.

Weinberg, R.A. 2007. The Biology of Cancer. Garland Science, Taylor & Francis Group, LLC.

Wells, C.M., A. Abo, and A.J. Ridley. 2002. PAK4 is activated via PI3K in HGF-stimulated epithelial cells. *J Cell Sci*. 115:3947-3956.

Wells, C.M., and G.E. Jones. 2010. The emerging importance of group II PAKs. *Biochem J*. 425:465-473.

Wells, C.M., M. Walmsley, S. Ooi, V. Tybulewicz, and A.J. Ridley. 2004. Rac1-deficient macrophages exhibit defects in cell spreading and membrane ruffling but not migration. *J Cell Sci*. 117:1259-1268.

Wells, C.M., A.D. Whale, M. Parsons, J.R. Masters, and G.E. Jones. 2010. PAK4: a pluripotent kinase that regulates prostate cancer cell adhesion. *J Cell Sci*. 123:1663-1673.

Whitehead, S.N.a.S. 2001. Endocrinology: An Integrated Approach. St. George's Hospital Medical School, London, UK, Oxford: BIOS Scientific Publishers.

Wienke, D., G.C. Davies, D.A. Johnson, J. Sturge, M.B. Lambros, K. Savage, S.E. Elsheikh, A.R. Green, I.O. Ellis, D. Robertson, J.S. Reis-Filho, and C.M. Isacke. 2007. The collagen receptor Endo180 (CD280) Is expressed on basal-like breast tumor cells and promotes tumor growth in vivo. *Cancer Res*. 67:10230-10240.

Wienke, D., J.R. MacFadyen, and C.M. Isacke. 2003. Identification and characterization of the endocytic transmembrane glycoprotein Endo180 as a novel collagen receptor. *Mol Biol Cell*. 14:3592-3604.

Wu, K., J. Yuan, and L.A. Lasky. 1996. Characterization of a novel member of the macrophage mannose receptor type C lectin family. *J Biol Chem*. 271:21323-21330.

Xue, Y., J. Ren, X. Gao, C. Jin, L. Wen, and X. Yao. 2008. GPS 2.0, a tool to predict kinase-specific phosphorylation sites in hierarchy. *Molecular & cellular proteomics : MCP*. 7:1598-1608.

Yang, J., and R.A. Weinberg. 2008. Epithelial-mesenchymal transition: at the crossroads of development and tumor metastasis. *Dev Cell*. 14:818-829.

Yates, C.C., C.R. Shepard, D.B. Stolz, and A. Wells. 2007. Co-culturing human prostate carcinoma cells with hepatocytes leads to increased expression of E-cadherin. *British journal of cancer*. 96:1246-1252.

Ye, Q., M.C. Harmsen, Y. Ren, and R.A. Bank. 2011. The role of collagen receptors Endo180 and DDR-2 in the foreign body reaction against non-crosslinked collagen and gelatin. *Biomaterials*. 32:1339-1350.

Ye, Q., Q. Xing, Y. Ren, M.C. Harmsen, and R.A. Bank. 2010. Endo180 and MT1-MMP are involved in the phagocytosis of collagen scaffolds by macrophages and is regulated by interferon-gamma. *European cells & materials*. 20:197-209.

Yuan, T.C., S. Veeramani, and M.F. Lin. 2007. Neuroendocrine-like prostate cancer cells: neuroendocrine transdifferentiation of prostate adenocarcinoma cells. *Endocr Relat Cancer*. 14:531-547.

Zagars, G.K., F.B. Geara, A. Pollack, and A.C. von Eschenbach. 1994. The T classification of clinically localized prostate cancer. An appraisal based on disease outcome after radiation therapy. *Cancer*. 73:1904-1912.

Zhang, T.J., B.G. Hoffman, T. Ruiz de Algara, and C.D. Helgason. 2006. SAGE reveals expression of Wnt signalling pathway members during mouse prostate development. *Gene expression patterns : GEP*. 6:310-324.

Zhou, J.C., G.D. Zhu, K.J. Wu, J. Zeng, D. Zhang, Y. Xue, Y.L. Chen, X.Y. Wang, and D.L. He. 2011. [Epithelial-mesenchymal transition and human fetal prostate development]. *Zhonghua nan ke xue = National journal of andrology*. 17:146-150.

Zhu, G., H.E. Zhau, H. He, L. Zhang, B. Shehata, X. Wang, W.H. Cerwinka, J. Elmore, and D. He. 2007. Sonic and desert hedgehog signaling in human fetal prostate development. *The Prostate*. 67:674-684.

Bibliography

# 8 Appendix

## 8.1 Evolutionary conservation of Endo180 ecto-domains (non-modified figure)

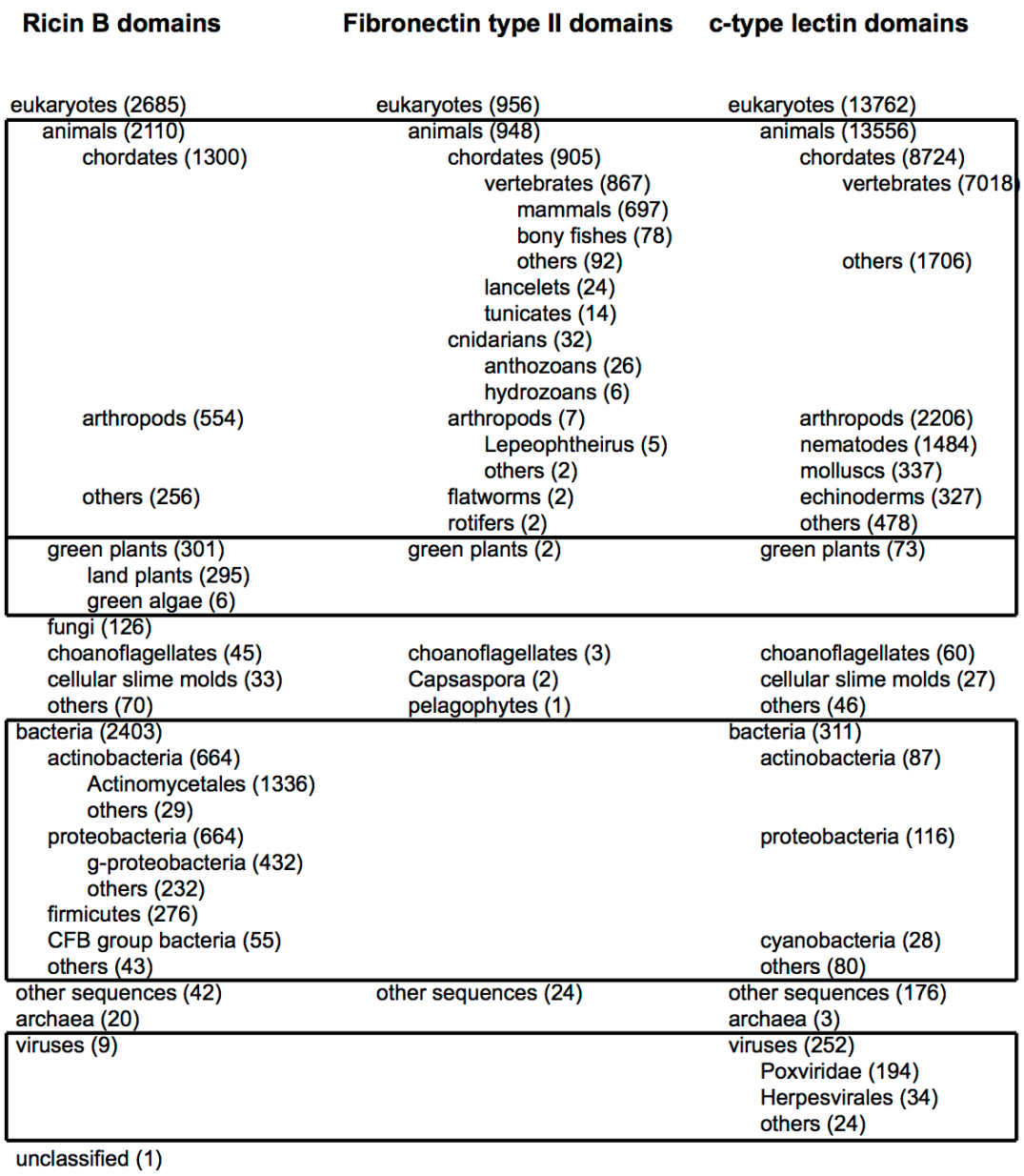



**Figure 8.1 Evolutionary conservation of Endo180 ectodomains.** Taxonomy trees were generated using the conserved domain database of NCBI. The number of open reading frames stored in the NCBI database, which contain one or more receptor domains is indicated in brackets after each class. Classes were broke out for more details if domains were significantly enriched in one particular subclass. The analysis includes evaluation of the: Ricin B domain; Fibronectin type II (FNII) domain; and C-type lectin like domains (CTLD's); of Endo180.